QCD

Jan M. Pawlowski[1] and Tilman Plehn[1]

[1] *Institut für Theoretische Physik, Universität Heidelberg*

CONTENTS

I. BASICS

The theory of strong interactions, quantum chromodynamics (QCD), has been developed on the basis of scattering experiments that showed an internal $SU(3)$-symmetry and related charges much the same way quantum-electrodynamics (QED) shows the $U(1)$-symmetry related to the electric charge. The corresponding gauge theory, $SU(3)$ Yang-Mills theory, is non-Abelian and hence self-interacting, i.e. the (quantized) pure gauge theory is already non-trivial, in contrast to the $U(1)$-based QED.

A. Yang-Mills theory

1. Classical action

We start by constructing the pure gauge part or Yang-Mills part of QCD as an $SU(3)$ gauge theory, fixing our conventions and repeating the main features known from the QFT II lecture. The weak $SU(2)$-theory turns out to have the same qualitative features as QCD (asymptotic freedom and confinement), but is technically simpler. On the other hand, the $SU(2)$ gauge bosons in the Standard Model are massive, leading to a major modification of this theory. Instead, we will assume massless gauge bosons throughout this lecture. As for QED, the classical action of QCD can be derived from the gauge-invariant (minimal) extension of the action of a free spin-one particle. The requirement of invariance of physics under local $SU(N_c)$ or color rotations with $\mathcal{U} \in SU(N_c)$, combined with a minimal coupling, leads us from partial to covariant derivatives,

$$\partial_\mu \to D_\mu(A) = \partial_\mu - i\, g\, A_\mu \,. \tag{I.1}$$

The gauge field A_μ in the adjoint representation is Lie-algebra–valued,

$$A_\mu = A_\mu^a\, t^a \,, \qquad \text{with} \qquad a = 1, ..., N_c^2 - 1 \,. \tag{I.2}$$

The matrices t^a are the generators of $SU(N_c)$. In physical QCD the gauge group has eight generators, $a = 1, ..., 8$, the Gell-Mann matrices. They are defined through

$$[t^a, t^b] = i\, f^{abc} t^c \,, \qquad\qquad \mathrm{tr}_{\mathrm{f}}(t^a t^b) = \frac{1}{2}\delta^{ab} \,, \tag{I.3}$$

where the coefficients f^{abc} are the structure constants of the Lie algebra. and tr_{f} is the trace in the fundamental representation. The covariant derivative (I.1) does not carry any indices. In the adjoint representation it links to $SU(N_c)$ indices and reads

$$D_\mu^{ab}(A) = \partial_\mu \delta^{ab} - g\, f^{abc} A_\mu^c \,. \qquad \text{with} \qquad (t^c_{\mathrm{ad}})^{ab} = -i\, f^{abc}. \tag{I.4}$$

The covariant derivative D_μ with its two color indices then has to transform as a tensor under gauge transformations,

$$D_\mu(A) \to D_\mu(A^{\mathcal{U}}) = \mathcal{U}\, D_\mu\, \mathcal{U}^\dagger \,, \qquad \text{with} \qquad \mathcal{U} = e^{i\omega} \in SU(N_c) \,, \tag{I.5}$$

where $\omega \in su(N_c)$ is the corresponding Lie algebra element. The covariance of D under gauge transformations in (I.5) implies

$$A_\mu \to A_\mu^{\mathcal{U}} = \frac{i}{g} U\, (D_\mu U^\dagger) = \mathcal{U}\, A_\mu\, \mathcal{U}^\dagger + \frac{i}{g} \mathcal{U}\, (\partial_\mu \mathcal{U}^\dagger) \,. \tag{I.6}$$

From the first term we confirm that in a non-Abelian gauge theory the gauge boson A_μ carries the corresponding color charge. There are various notations on the market leading to factors i and $-$ in the Lie algebra relations above. In the present lecture notes we have chosen hermitian generators which leads to the factor $+1/2$ for the trace in (I.3). It also entails real structure constants f^{abc} in the Lie-algebra in (I.3).

In analogy to QED the field strength tensor is defined through the commutator of covariant derivatives, it is the curvature tensor of the gauge theory. Based on the definitions in (I.1) and (I.3) we find

$$F_{\mu\nu} = \frac{i}{g}[D_\mu \,,\, D_\nu] = F_{\mu\nu}^a t^a \qquad \text{with} \qquad F_{\mu\nu}^a = \partial_\mu A_\nu^a - \partial_\nu A_\mu^a + g\, f^{abc} A_\mu^b\, A_\nu^c. \tag{I.7}$$

$S_{\mathrm{YM}}[A] \propto$ 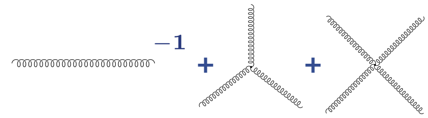

FIG. 1: Diagrammatic depiction of the Yang-Mills action.

Defined as in (I.7) the field strength $F_{\mu\nu}$ also transforms covariantly (as a tensor) under gauge transformations,

$$\begin{aligned}F_{\mu\nu}(A^{\mathcal{U}}) &= \frac{i}{g}\,[D_\mu(A^{\mathcal{U}}), D_\nu(A^{\mathcal{U}})] \\ &= \frac{i}{g}\,\mathcal{U}\,[D_\mu(A_\mu), D_\nu(A_\nu)]\,\mathcal{U}^\dagger = \mathcal{U}\,F_{\mu\nu}(A)\,\mathcal{U}^\dagger\ .\end{aligned} \tag{I.8}$$

This allows us to define a gauge-invariant Yang-Mills (YM) action,

$$S_{\mathrm{YM}}[A] = \frac{1}{2}\int_x \mathrm{tr_f}\ (F_{\mu\nu}\,F_{\mu\nu}) = \frac{1}{4}\int_x F^a_{\mu\nu}\,F^a_{\mu\nu}\,, \tag{I.9}$$

with $\int_x = \int d^dx$. Its gauge invariance follows from (I.8),

$$S_{\mathrm{YM}}[A^{\mathcal{U}}] = \frac{1}{2}\int_x \mathrm{tr_f}\ \left(\mathcal{U}\,F_{\mu\nu}(A)F_{\mu\nu}(A)\,\mathcal{U}^\dagger\right) = S_{\mathrm{YM}}[A]\,, \tag{I.10}$$

where the last equality holds due to cyclicity of the trace in color space. Clearly, the action (I.9) with the field strength (I.7) is a self-interacting theory with coupling constant g. It has a quadratic kinetic term and three-gluon and four-gluon vertices. This is illustrated diagrammatically as Figure 1.
This allows us to read off the Feynman rules for the purely gluonic vertices. The full Feynman rules of QCD in the general covariant gauge are summarized in Appendix A. As in QED we can identify color-electric and color-magnetic fields as the components in the field strength tensor,

$$\begin{aligned}E_i^a &= F^a_{0i} \\ B_i^a &= \frac{1}{2}\epsilon_{ijk}F^a_{jk}.\end{aligned} \tag{I.11}$$

In contrast to QED these color-electric and magnetic fields are no observables, they change under gauge transformations. Only $\mathrm{tr}\,\vec{E}^2, \mathrm{tr}\,\vec{B}^2$ are observables.

A Yang-Mills theory can most easily be quantized through the path integral. Naively, the generating functional of pure YM-theory would read

$$Z[J] = \int dA\ \exp\left(-S_{\mathrm{YM}}[A] + \int_x J^a_\mu\,A^a_\mu\right)\,. \tag{I.12}$$

The fundamental problem is that it contains redundant integrations due to gauge invariance of the action, see I A 1. These redundant integrations are usually removed by introducing a gauge fixing condition

$$\mathcal{F}[A_{\mathrm{gf}}] = 0 \tag{I.13}$$

Commonly used gauge fixings are

$$\begin{aligned}\partial_\mu A_\mu &= 0\,, &&\text{covariant or Lorenz gauge}\,,\\ \partial_i A_i &= 0\,, &&\text{Coulomb gauge}\,,\\ n_\mu A_\mu &= 0\,, &&\text{axial gauge}\,.\end{aligned} \tag{I.14}$$

The general covariant gauge has the technical advantage that it does not single out a space-time direction. This property reduces the possible tensor structure of correlation functions and hence simplifies computations. The Coulomb gauge and the axial gauge single out specific frames. At finite temperature (and density) this might be useful as the temperature singles out the thermal rest frame. In that case the Coulomb gauge and the temporal or Weyl gauge ($n_\mu = \delta_{\mu 0}$) are used often.

Gauge fields that are connected by gauge transformations are physically equivalent, i.e. their actions agree. They lie in so-called gauge orbits, $\{A^{\mathcal{U}}, \mathcal{U} \in SU(N)\}$, and fixing a gauge is equivalent to choosing a representative of such an orbit $A \to A_{\mathrm{gf}}$, up to potential (Gribov) copies. The occurrence of Gribov copies and how to handle them is discussed in Appendix B. To keep things simple we ignore them for the time being and continue with the construction of the QCD Lagrangian.

The path integral measure $\mathrm{d}A$ introduced in I A 1 can be split into an integration over physically inequivalent configurations A_{gf} and the gauge transformations $\mathcal{U}$,

$$\mathrm{d}A = J \, \mathrm{d}A_{\mathrm{gf}} \, \mathrm{d}\mathcal{U} \tag{I.15}$$

In (I.15) J denotes the Jacobian of the transformation $A \to (A_{\mathrm{gf}}, \mathcal{U})$, and we include $\mathrm{d}\mathcal{U}$ as the Haar measure of the gauge group, see e.g. [1]. The coordinate transformation (I.15) and the computation of the Jacobian J are done using the Faddeev-Popov quantization, [2]. To separate the integral I A 1 into the two parts shown in (I.15) we insert a very convoluted unity into the path integral,

$$1 = \int \mathrm{d}\mathcal{U} \, \delta\left[\mathcal{F}[A^{\mathcal{U}}]\right] \, \Delta_{\mathcal{F}}[A] = \Delta_{\mathcal{F}}[A] \int \mathrm{d}\mathcal{U} \, \delta\left[\mathcal{F}[A^{\mathcal{U}}]\right] \quad \Leftrightarrow \quad \Delta_{\mathcal{F}}[A] = \left(\int \mathrm{d}\mathcal{U} \, \delta\left[\mathcal{F}[A^{\mathcal{U}}]\right]\right)^{-1}, \tag{I.16}$$

where $\Delta_{\mathcal{F}}[A]$ is gauge-invariant due to the property $\mathrm{d}(\mathcal{U}\mathcal{V}) = \mathrm{d}\mathcal{U}$ of the Haar measure. For the path integral this gives us

$$\int \mathrm{d}A \, e^{-S_{\mathrm{YM}}[A]} = \int \mathrm{d}A \, \mathrm{d}\mathcal{U} \, \delta\left[\mathcal{F}[A^{\mathcal{U}}]\right] \, \Delta_{\mathcal{F}}[A] \, e^{-S_{\mathrm{YM}}[A]} \, . \tag{I.17}$$

Let us now consider a general observable $\mathcal{O}$, like *e.g.* $\mathrm{tr}F^2(x) \, \mathrm{tr}F^2(0)$. Observables are necessarily gauge invariant and local. The expectation value of $\mathcal{O}$ is defined as

$$\langle \mathcal{O} \rangle = \frac{\int \mathrm{d}A \, \mathcal{O}[A] \, e^{-S_{\mathrm{YM}}[A]}}{\int \mathrm{d}A \, e^{-S_{\mathrm{YM}}[A]}} = \frac{\int \mathrm{d}A \, \mathrm{d}\mathcal{U} \, \delta\left[\mathcal{F}[A^{\mathcal{U}}]\right] \, \Delta_{\mathcal{F}}[A] \, \mathcal{O}[A] \, e^{-S_{\mathrm{YM}}[A]}}{\int \mathrm{d}A \, \mathrm{d}\mathcal{U} \, \delta\left[\mathcal{F}[A^{\mathcal{U}}]\right] \, \Delta_{\mathcal{F}}[A] \, e^{-S_{\mathrm{YM}}[A]}} \, , \tag{I.18}$$

where we have simply inserted (I.16) into the path integral. In (I.18) all terms are gauge invariant except for the δ-function. Hence we can absorb the $\mathcal{U}$-dependence via $A \to A^{\mathcal{U}^\dagger}$. Then the (infinite) integral over the Haar measure decouples in numerator and denominator, and we arrive at

$$\langle \mathcal{O} \rangle = \frac{\int \mathrm{d}A \, \delta\left[\mathcal{F}[A]\right] \, \Delta_{\mathcal{F}}[A] \, \mathcal{O}[A] \, e^{-S_{\mathrm{YM}}[A_{\mathrm{gf}}]}}{\int \mathrm{d}A \, \delta\left[\mathcal{F}[A]\right] \, \Delta_{\mathcal{F}}[A] \, e^{-S_{\mathrm{YM}}[A_{\mathrm{gf}}]}} \, . \tag{I.19}$$

To compute the Jacobian $\Delta_{\mathcal{F}}[A]$ we apply a coordinate transformation to the δ-distribution

$$\delta[\mathcal{F}[A^{\mathcal{U}}]] = \frac{\delta[\omega - \omega_1]}{|\det \frac{\delta \mathcal{F}}{\delta \omega}|} \equiv \frac{\delta[\omega - \omega_1]}{|\det \mathcal{M}_{\mathcal{F}}[A]|} \quad \text{with} \quad \mathcal{U} = e^{i\omega} \, , \tag{I.20}$$

combined with a gauge fixing condition in the form (I.13)

$$\mathcal{F}[A_{\mathrm{gf}} = A^{\mathcal{U}(\omega_1)}] = 0 \, . \tag{I.21}$$

Using the definition (I.16) this leads to

$$\Delta_{\mathcal{F}}[A] = |\det \mathcal{M}_{\mathcal{F}}[A_{\mathrm{gf}}]| \qquad \text{with} \qquad \mathcal{M}_{\mathcal{F}}[A] = \left.\frac{\delta \mathcal{F}}{\delta \omega}\right|_{\omega=0} [A] \, . \tag{I.22}$$

Here A_{gf} is the solution with the minimal distance to $A = 0$. The inverse Jacobian $\det \mathcal{M}_{\mathcal{F}}$ of the ansatz (I.15) is called the Faddeev-Popov determinant. For its computation we consider an infinitesimal gauge transformation $\mathcal{U} = 1 + i \, g \, \omega$ where we have rescaled the transformation with the strong coupling g for convenience. Such a rescaling gives global factors of powers of $1/g$ that drop out in normalized expectation values. Then, the infinitesimal variation of the covariant gauge $\partial_\mu A_\mu = 0$ follows as

$$\mathcal{F}[A^{\mathcal{U}}] = \partial_\mu A^{\mathcal{U}}_\mu = \partial_\mu A_\mu - \partial_\mu D_\mu \omega + O(\omega^2) \stackrel{!}{=} 0\,. \tag{I.23}$$

This gives us the Faddeev-Popov matrix

$$\mathcal{M}_{\mathcal{F}}[A] = -\frac{\delta \partial_\mu D_\mu \omega}{\delta\omega} = -\partial_\mu D_\mu \frac{\delta\omega}{\delta\omega} = -\partial_\mu D_\mu \mathbb{1}. \tag{I.24}$$

We assume that $-\partial^\mu D_\mu$ is a positive definite operator and we arrive at

$$\Delta_{\mathcal{F}}[A] = \det \mathcal{M}[A] = \det\left(-\partial_\mu D_\mu\right)\,. \tag{I.25}$$

A useful observation is that determinants can be represented by a Gaussian integral. In regular space such a Gaussian integral reads

$$\int_x e^{-\frac{1}{2}x^T M x} = \frac{(2\pi)^n}{\sqrt{\det M}}\,. \tag{I.26}$$

We want to use this relation to replace the Faddeev-Popov determinant (I.25) in the Lagrangian. It turns out that the usual form does not give a useful action or Lagrangian. However, we can instead use two anti-commuting Grassmann fields C and switch the sign in the exponent to

$$\det \mathcal{M}_{\mathcal{F}}[A] = \int \mathrm{d}c\, \mathrm{d}\bar{c}\, \exp\left\{\int d^d x\, d^d y\, \bar{c}^a(x) \mathcal{M}^{ab}_{\mathcal{F}}(x,y) c^b(y)\right\}\,. \tag{I.27}$$

Finally we slightly modify the gauge by introducing a Gaußian average over the gauges

$$\delta[\mathcal{F}[A^{\mathcal{U}}]] \to \int \mathrm{d}\mathcal{C}\, \delta[\mathcal{F}[A^{\mathcal{U}} - \mathcal{C}]] \exp\left\{-\frac{1}{2\xi}\int_x \mathcal{C}^a \mathcal{C}^a\right\}\,. \tag{I.28}$$

In summary, and restricting ourselves to the covariant gauge we then arrive at the generating functional for our Yang-Mills theory

$$Z[J_A, J_c, \bar{J}_c] = \int \mathrm{d}A\, \mathrm{d}c\, \mathrm{d}\bar{c}\, e^{-S_A[A,c,\bar{c}] + \int_x \left(J_A \cdot A + \bar{J}_c \cdot c - \bar{c}\cdot J_c\right)}\,. \tag{I.29}$$

The action including a general gauge fixing term and the Faddeev-Popov ghosts c^a is

$$S_A[A,c,\bar{c}] = \frac{1}{4}\int_x F^a_{\mu\nu} F^a_{\mu\nu} + \frac{1}{2\xi}\int_x \left(\partial_\mu A^a_\mu\right)^2 + \int_x \bar{c}^a \partial_\mu D^{ab}_\mu c^b\,, \tag{I.30}$$

where $\int_x = \int d^d x$ and the Landau gauge is achieved for $\xi = 0$. Note that the ghost action implies a negative dispersion for the ghost, related to the determinant of the positive operator $\mathcal{M}_{\mathcal{F}} = -\partial_\mu D_\mu$. However, this is a matter of convention, we might as well use a positive dispersion, the minus sign drops out for all correlation functions which do not involve ghosts, and only those are related to scattering amplitudes. The source term with all indices reads

$$\int_x \left(J_A \cdot A + \bar{J}_c \cdot c - \bar{c}\cdot J_c\right) \equiv \int_x \left(J^a_{A,\mu} A^a_\mu + \bar{J}^a_c c^a - \bar{c}^a J^a_c\right)\,. \tag{I.31}$$

The Feynman rules derived from (I.30) are summarized in Appendix A.

B. QCD

1. Classical action of the matter sector

After briefly sketching the gauge part of QCD we now add fermionic matter fields. As before we start with the classical action, now given by the Dirac action of a quark doublet,

$$S_{\rm Dirac}[\psi,\bar\psi,A] = \int_x \bar\psi\ (\not{D} + m_\psi - \gamma_0\,\mu)\ \psi\,, \tag{I.32}$$

where the Dirac matrices are defined through

$$\{\gamma_\mu\,,\,\gamma_\nu\} = 2\,\delta_{\mu\nu} \qquad \text{and} \qquad \not{D} = \gamma_\mu D_\mu\,. \tag{I.33}$$

In (VI.28), the fermions carry a Dirac index defining the 4-component spinor, gauge group indices in the fundamental representation of $SU(3)$, as well flavor indices. The latter we will ignore as long as we only talk about QCD and neglect the doublet nature of the matter fields in the Standard Model. The Dirac operator $\not{D}$ is diagonal in the flavor space as is the chemical potential term. The mass term depends on the current quark masses related to spontaneous symmetry breaking of the Higgs sector of the Standard Model. The up and down current quark masses are of the order $2-5$ MeV whereas the current quark mass of the strange quark is of the order 10^2 MeV. The other quark masses are of order $1-200$ GeV. In low energy QCD this has to be compared with the scale of strong chiral symmetry breaking $\Delta m \approx 300$ MeV. This mass scales are summarized in Table I.

Generation	first	second	third	Charge
Mass [MeV]	1.5-4	1150-1350	170×10^3	
Quark	u	c	t	$\frac{2}{3}$
Quark	d	s	b	$-\frac{1}{3}$
Mass [MeV]	4-8	80-130	$(4.1\text{-}4.4)\times10^3$	

TABLE I: Quark masses and charges. The scale of strong chiral symmetry breaking is $\Delta m \approx 300$ MeV as is $\Lambda_{\rm QCD}$. This entails that only $2+1$ flavours have to be considered for most applications to the phase diagram of QCD.

Evidently, for most applications of the QCD phase diagram we only have to consider the three lightest quark flavors, that is up, down and strange quark, to be dynamical. The current quark masses of up and down quarks are two order of magnitude smaller than all QCD infrared scales related to $\Lambda_{\rm QCD}$. Hence, the up and down quarks can be considered to be massless. This leads to the important observation that the physical masses of neutrons and protons — and hence the masses of the world around us — comes about from strong chiral symmetry breaking and has nothing to do with the Higgs sector.

In turn, the mass of the strange quark is of the order of $\Lambda_{\rm QCD}$ and has to be considered heavy for application in low energy QCD. The three heavier flavors, charm, bottom and top, are essentially static they do not contribute to the QCD dynamics relevant for its phase structure even though in particular the c-quark properties and bound states are much influenced by the infrared dynamics of QCD. In summary we will consider the $N_f = 2$ and $N_f = 2+1$ flavor cases for the phase structure of QCD, while for LHC physics all flavors are relevant.

2. Generating functional of QCD and perturbation theory

Again in analogy to the Yang-Mills action we describe the quantized theory using its generating functional. The full generating functional of QCD is the straightforward extension of the Yang-Mills version in I A 1. The quark fields are Grassmann fields because of their fermionic nature and we are led to the generating functional

$$Z[J] = \int \mathrm{d}\Phi\, e^{-S_{\rm QCD}[\Phi]+\int_x\, J\cdot\phi}\,, \tag{I.34}$$

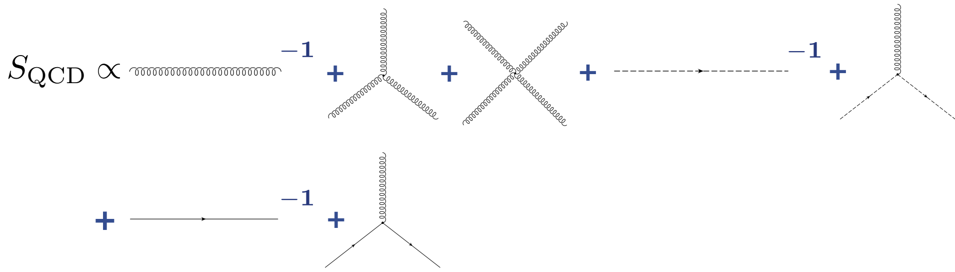

FIG. 2: Diagrammatic depiction of the gauge fixed QCD action.

As a notation we have introduced super-fields and super-currents

$$
\begin{aligned}
\Phi &= (A, c, \bar{c}, \psi, \bar{\psi}) & J &= (J_A, J_c, \bar{J}_c, J_\psi, \bar{J}_\psi) \\
\mathrm{d}\Phi &= \int \mathrm{d}A\, \mathrm{d}c\, \mathrm{d}\bar{c}\, \mathrm{d}\psi\, \mathrm{d}\bar{\psi} & J \cdot \Phi &= J_A \cdot A + \bar{J}_c \cdot c - \bar{c} \cdot J_c + \bar{J}_\psi \cdot \psi - \bar{\psi} \cdot J_\psi \,.
\end{aligned} \tag{I.35}
$$

The gauge-fixed action $S_{\rm QCD}$ in (I.34) in the Landau gauge is given by

$$
S_{\rm QCD}[\Phi] = \frac{1}{4} \int_x F^a_{\mu\nu} F^a_{\mu\nu} + \frac{1}{2\xi} \int_x \left(\partial_\mu A^a_\mu\right)^2 + \int_x \bar{c}^a \partial_\mu D^{ab}_\mu c^b + \int_x \bar{\psi} \left(\not{D} + m_\psi - \gamma_0\, \mu \right) \psi \,. \tag{I.36}
$$

The action in (I.36) is illustrated diagrammatically in Figure 2. For physical observables the gauge dependence entering through the last two graphs in the first line, the ghost terms, is cancelled by the hidden gauge fixing dependence of the inverse gluon propagator. The Feynman rules are summarized in Appendix A.

The two equations (I.34), (I.36) define the fundamental quantum theory of strong interactions and have, apart from the mass matrix m_q of the quarks one input parameter, the strong coupling. In the full quantum theory we have a running coupling

$$
\alpha_s(p) = \frac{g^2}{4\pi} \,, \tag{I.37}
$$

where p is the relevant momentum/energy scale of a given process. The scale-dependence of $\alpha_s(p)$ is inflicted by quantum corrections. For perturbation theory being applicable the expansion parameter $\alpha_s/(4\pi)$ should be small. Moreover, the perturbative expansion is an asymptotic series (with convergence radius $\alpha_{s,\rm max} = 0$). The gluon self-coupling in QCD, depicted in Figure 2 leads to a running coupling which decreases with the momentum scale, i.e. ,

$$
\beta_g = \frac{1}{2} p \partial_p \alpha_s = -\beta_0 \alpha^2 + O(\alpha_s^3) \qquad \text{with} \qquad \beta_0 = \frac{\alpha_s^2}{12\pi} \left(11 N_c + 2 N_f\right) \,. \tag{I.38}
$$

Integrating the β-function (I.38) at one loop leads to the running coupling

$$
\alpha_s(p) = \frac{\alpha_s(\mu)}{1 + \beta_0 \alpha_s(\mu) \log \frac{p^2}{\mu^2}} + O(\alpha_s^2) \,, \tag{I.39}
$$

with some reference (momentum) scale μ^2. The running coupling in (I.39) tends to zero logarithmically for $p \to \infty$. This property is called asymptotic freedom (Nobel prize 2004) and guarantees the existence of the the perturbative expansion of QCD. Its validity for large energies and momenta is by now impressively proven in various scattering experiments, see e.g. [3]. These experiments can also be used to define a running coupling (which is not unique beyond two loop, see e.g. [4]) and the related plot of $\alpha_s(p^2)$ in Figure 3 has been taken from [3].

In turn, in the infrared regime of QCD at low momentum scales, perturbation theory is not applicable any more. The coupling grows and the failure of perturbation theory is finally signaled by the so-called Landau pole with $\alpha_s(\Lambda_{\rm QCD}) = \infty$. We emphasise that a large or diverging coupling does *not* imply confinement, the theory could still be QEDsS-like showing a Coulomb-potential with a large coupling. The latter would not lead to the absence of colored asymptotic states but rather to so-called color charge superselection sectors as in QED. There, we have asymptotic charged states and no physics process can change the charge.

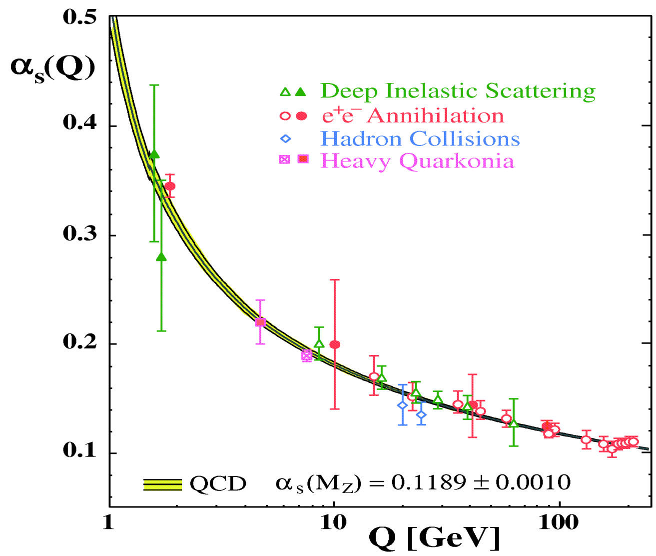

FIG. 3: Experimental tests of the running coupling, figure taken from [3].

II. DIVERGENCES

A. Ultraviolet divergences

From general field theory we know that when we are interested for example in cross section prediction with higher precision we need to compute further terms in its perturbative series in α_s. This computation will lead to ultraviolet divergences which can be absorbed into counter terms for any parameter in the Lagrangian. The crucial feature is that for a renormalizable theory like our Standard Model the number of counter terms is finite, which means once we know all parameters including their counter terms our theory becomes predictive.

In Section II B we will see that in QCD processes we also encounter another kind of divergences. They arise from the infrared momentum regime. Infrared divergences is what this lecture is really going to be about, but before dealing with them it is very instructive to see what happens to the much better understood ultraviolet divergences. In Section II A 1 we will review how such ultraviolet divergences arise and how they are removed. In Section II A 2 we will review how running parameters appear in this procedure, *i.e.* how scale dependence is linked to the appearance of divergences. Finally, in Section II A 3 we will interpret the use of running parameters physically and see that in perturbation theory they resum classes of logarithms to all orders in perturbation theory. Later in Section II B we will follow exactly the same steps for infrared divergences and develop some crucial features of hadron collider physics.

1. Counter terms

Renormalization as the proper treatment of ultraviolet divergences is one of the most important things to understand about field theories; you can find more detailed discussions in any book on advanced field theory. The particular aspect of renormalization which will guide us through this section is the appearance of the renormalization scale.

In perturbation theory, scales automatically arise from the regularization of infrared or ultraviolet divergences. We can see this by writing down a simple scalar loop integral, with to two virtual scalar propagators with masses $m_{1,2}$ and an external momentum p flowing through a diagram,

$$B(p^2; m_1, m_2) \equiv \int \frac{d^4q}{16\pi^2} \, \frac{1}{q^2 - m_1^2} \, \frac{1}{(q+p)^2 - m_2^2} \; . \tag{II.1}$$

Such two-point functions appear for example in the gluon self energy with virtual gluons, with massless ghost scalars, with a Dirac trace in the numerator for quarks, and with massive scalars for supersymmetric scalar quarks. In those cases the two masses are identical $m_1 = m_2$. The integration measure $1/(16\pi^2)$ is dictated by the Feynman rule for the integration over loop momenta. Counting powers of q in Eq.(II.1) we see that the integrand is not suppressed by powers of $1/q$ in the ultraviolet, so it is logarithmically divergent and we have to regularize it. Regularizing means expressing the divergence in a well–defined manner or scheme, allowing us to get rid of it by renormalization.

One regularization scheme is to introduce a cutoff into the momentum integral Λ, for example through the so-called Pauli—Villars regularization. Because the ultraviolet behavior of the integrand or integral cannot depend on any parameter living at a small energy scales, the parameterization of the ultraviolet divergence in Eq.(II.1) cannot involve the mass m or the external momentum p^2. The scalar two-point function has mass dimension zero, so its divergence has to be proportional to $\log(\Lambda/\mu_R)$ with a dimensionless prefactor and some scale μ_R^2 which is an artifact of the regularization of such a Feynman diagram. Because it is an artifact, this scale μ_R has to eventually vanish from our theory prediction.

A more elegant regularization scheme is dimensional regularization. It is designed not to break gauge invariance and naively seems to not introduce a mass scale μ_R. When we shift the momentum integration from 4 to $4-2\epsilon$ dimensions and use analytic continuation in the number of space–time dimensions to renormalize the theory, a renormalization scale μ_R nevertheless appears once we ensure the two-point function and with it observables like cross sections keep their correct mass dimension

$$\int \frac{d^4q}{16\pi^2} \cdots \longrightarrow \mu_R^{2\epsilon} \int \frac{d^{4-2\epsilon}q}{16\pi^2} \cdots = \frac{i\mu_R^{2\epsilon}}{(4\pi)^2} \left[\frac{C_{-1}}{\epsilon} + C_0 + C_1\,\epsilon + \mathcal{O}(\epsilon^2) \right] . \tag{II.2}$$

At the end, the scale μ_R might drop out after renormalization and analytic continuation, but to be on the safe side we keep it. The constants C_i in the series in $1/\epsilon$ depend on the loop integral we are considering. To regularize the ultraviolet divergence we have to assume $\epsilon > 0$, to find mathematically well defined poles $1/\epsilon$. Defining scalar integrals with the integration measure $1/(i\pi^2)$ will make for example C_{-1} come out as of the order $\mathcal{O}(1)$. This is the reason we usually find factors $1/(4\pi)^2 = \pi^2/(2\pi)^4$ in front of the loop integrals.

The poles in $1/\epsilon$ will cancel with the universal counter terms once we renormalize the theory. Counter terms we include by shifting parameters in the Lagrangian and the leading order matrix element. They cancel the poles in the combined leading order and virtual one-loop prediction

$$\begin{aligned} |\mathcal{M}_{\rm LO}(g) + \mathcal{M}_{\rm virt}|^2 &= |\mathcal{M}_{\rm LO}(g)|^2 + 2\,\mathrm{Re}\,\mathcal{M}_{\rm LO}(g)\mathcal{M}_{\rm virt} + \cdots \\ &\to |\mathcal{M}_{\rm LO}(g+\delta g)|^2 + 2\,\mathrm{Re}\,\mathcal{M}_{\rm LO}(g)\mathcal{M}_{\rm virt} + \cdots \\ \text{with} \qquad g \to g^{\rm bare} &= g + \delta g \qquad \text{and} \quad \delta g \propto \alpha_s/\epsilon \, . \end{aligned} \tag{II.3}$$

The dots indicate higher orders in α_s, for example absorbing the δg corrections in the leading order and virtual interference. As we can see in Eq.(II.3) the counter terms do not come with a factor $\mu_R^{2\epsilon}$ in front. Therefore, while the poles $1/\epsilon$ cancel just fine, the scale factor $\mu_R^{2\epsilon}$ will not be matched between the actual ultraviolet divergence and the counter term.

We can keep track of the renormalization scale best by expanding the prefactor of the regularized but not yet renormalized integral in Eq.(II.2) in a Taylor series in ϵ, no question asked about convergence radii

$$\begin{aligned} \mu_R^{2\epsilon} \left[\frac{C_{-1}}{\epsilon} + C_0 + \mathcal{O}(\epsilon) \right] &= e^{2\epsilon \log \mu_R} \left[\frac{C_{-1}}{\epsilon} + C_0 + \mathcal{O}(\epsilon) \right] \\ &= \left[1 + 2\epsilon \log \mu_R + \mathcal{O}(\epsilon^2) \right] \left[\frac{C_{-1}}{\epsilon} + C_0 + \mathcal{O}(\epsilon) \right] \\ &= \frac{C_{-1}}{\epsilon} + C_0 + C_{-1}\,\log \mu_R^2 + \mathcal{O}(\epsilon) \\ &\to \frac{C_{-1}}{\epsilon} + C_0 + C_{-1}\,\log \frac{\mu_R^2}{M^2} + \mathcal{O}(\epsilon) \, . \end{aligned} \tag{II.4}$$

In the last step we correct by hand for the fact that $\log \mu_R^2$ with a mass dimension inside the logarithm cannot appear in our calculations. From somewhere else in our calculation the logarithm will be matched with a $\log M^2$ where M^2 is the typical mass or energy scale in our process. This little argument shows that also in dimensional regularization we introduce a mass scale μ_R which appears as $\log(\mu_R^2/M^2)$ in the renormalized expression for our observables. There is no way of removing ultraviolet divergences without introducing some kind of renormalization scale.

In Eq.(II.4) there appear two finite contributions to a given observable, the expected C_0 and the renormalization–induced C_{-1}. Because the factors C_{-1} are linked to the counter terms in the theory we can often guess them without actually computing the complete loop integral, which is very useful in cases where they numerically dominate.

Counter terms as they schematically appear in Eq.(II.3) are not uniquely defined. They need to include a given divergence to return finite observables, but we are free to add any finite contribution we want. This opens many ways to define a counter term for example based on physical processes where counter terms do not only cancel the pole but also finite contributions at a given order in perturbation theory. Needless to say, such schemes do not automatically work universally. An example for such a physical renormalization scheme is the on–shell scheme for masses, where we define a counter term such that external on–shell particles do not receive any corrections to their masses. For the top mass this means that we replace the leading order mass with the bare mass, for which we then insert the expression in terms of the renormalized mass and the counter term

$$\begin{aligned} m_t^{\text{bare}} &= m_t + \delta m_t \\ &= m_t + m_t \frac{\alpha_s C_F}{4\pi} \left(3 \left(-\frac{1}{\epsilon} + \gamma_E - \log(4\pi) - \log \frac{\mu_R^2}{M^2} \right) - 4 + 3 \log \frac{m_t^2}{M^2} \right) \\ &\equiv m_t + m_t \frac{\alpha_s C_F}{4\pi} \left(-\frac{3}{\tilde{\epsilon}} - 4 + 3 \log \frac{m_t^2}{M^2} \right) \qquad \Leftrightarrow \qquad \frac{1}{\tilde{\epsilon}\left(\frac{\mu_R}{M}\right)} \equiv \frac{1}{\epsilon} - \gamma_E + \log \frac{4\pi\mu_R^2}{M^2} \; , \end{aligned} \tag{II.5}$$

with the color factor $C_F = (N^2-1)/(2N)$ and the Euler constant $\gamma_E \approx 0.577$ coming from the evaluation of the Gamma function $\Gamma(\epsilon) = 1/\epsilon + \gamma_E + \mathcal{O}(\epsilon)$. The convenient scale dependent pole $1/\tilde{\epsilon}$ includes the universal additional terms like the Euler gamma function and the scaling logarithm. This logarithm is the big problem in this universality argument, since we need to introduce the arbitrary energy scale M to separate the universal logarithm of the renormalization scale and the parameter-dependent logarithm of the physical process.

A theoretical problem with this on–shell renormalization scheme is that it is not gauge invariant. On the other hand, it describes for example the kinematic features of top pair production at hadron colliders in a stable perturbation series. This means that once we define a more appropriate scheme for heavy particle masses in collider production mechanisms it better be numerically close to the pole mass. For the computation of total cross sections at hadron colliders or the production thresholds at e^+e^- colliders the pole mass is not well suited at all, but since this is not where we expect to measure particle masses at the LHC we should do fine with something very similar to the pole mass.

Another example for a process dependent renormalization scheme is the mixing of γ and Z propagators. There we choose the counter term of the weak mixing angle such that an on–shell Z boson cannot oscillate into a photon, and vice versa. We can generalize this scheme for mixing scalars as they for example appear in supersymmetry, but it is not gauge invariant with respect to the weak gauge symmetries of the Standard Model either. For QCD corrections, on the other hand, it is the most convenient scheme keeping all exchange symmetries of the two scalars.

To finalize this discussion of process dependent mass renormalization we quote the result for a scalar supersymmetric quark, a squark, where in the on–shell scheme we find

$$\begin{aligned} m_{\tilde{q}}^{\text{bare}} &= m_{\tilde{q}} + \delta m_{\tilde{q}} \\ &= m_{\tilde{q}} + m_{\tilde{q}} \frac{\alpha_s C_F}{4\pi} \left(-\frac{2r}{\tilde{\epsilon}} - 1 - 3r - (1-2r)\log r - (1-r)^2 \log \left| \frac{1}{r} - 1 \right| - 2r \log \frac{m_{\tilde{q}}^2}{M^2} \right) \; . \end{aligned} \tag{II.6}$$

with $r = m_{\tilde{g}}^2/m_{\tilde{q}}^2$. The interesting aspect of this squark mass counter term is that it also depends on the gluino mass, not just the squark mass itself. The reason why QCD counter terms tend to depend only on the renormalized quantity itself is that the gluon is massless. In the limit of vanishing gluino contribution the squark mass counter term is again only proportional to the squark mass itself

$$m_{\tilde{q}}^{\text{bare}} \Bigg|_{m_{\tilde{g}}=0} = m_{\tilde{q}} + \delta m_{\tilde{q}} = m_{\tilde{q}} + m_{\tilde{q}} \frac{\alpha_s C_F}{4\pi} \left(-\frac{1}{\tilde{\epsilon}} - 3 + \log \frac{m_{\tilde{q}}^2}{M^2} \right) \; . \tag{II.7}$$

Taking the limit of Eq.(II.6) to derive Eq.(II.7) is computationally not trivial, though.

One common feature of all mass counter terms listed above is $\delta m \propto m$, which means that our renormalization is actually multiplicative,

$$m^{\text{bare}} = Z_m \, m = (1 + \delta Z_m) \, m = \left(1 + \frac{\delta m}{m} \right) m = m + \delta m \qquad \text{with} \qquad \delta Z_m = \frac{\delta m}{m} \; , \tag{II.8}$$

linking the two ways of writing the mass counter term. This form implies that particles with zero mass will not obtain a finite mass through renormalization. If we remember that chiral symmetry protects a Lagrangian from acquiring fermion masses this means that on–shell renormalization does not break this symmetry. A massless theory cannot become massive by mass renormalization. Regularization and renormalization schemes which do not break symmetries of the Lagrangian are ideal.

When we introduce counter terms in general field theory we usually choose a slightly more model independent scheme — we define a renormalization point. This is the energy scale at which the counter terms cancels all higher order contributions, divergent as well as finite. The best known example is the electric charge which we renormalize in the Thomson limit of zero momentum transfer through the photon propagator

$$e \to e^{\text{bare}} = e + \delta e \; . \tag{II.9}$$

Looking back at δm_t as defined in Eq.(II.5) we also see a way to define a completely general counter term: if dimensional regularization, *i.e.* the introduction of $4-2\epsilon$ dimensions does not break any of the symmetries of our Lagrangian, like Lorentz symmetry or gauge symmetries, we can simply subtract the ultraviolet pole and nothing else. The only question is: do we subtract $1/\epsilon$ in the MS scheme or do we subtract $1/\tilde{\epsilon}$ in the $\overline{\text{MS}}$ scheme. In the $\overline{\text{MS}}$ scheme the counter term is then scale dependent.

Carefully counting, there are three scales present in such a scheme. First, there is the physical scale in the process. In our case of a top self energy this is for example the top mass m_t appearing in the matrix element for the process $pp \to t\bar{t}$. Next, there is the renormalization scale μ_R, a reference scale which is part of the definition of any counter term. And last but not least, there is the scale M separating the counter term from the process dependent result, which we can choose however we want, but which as we will see implies a running of the counter term. The role of this scale M will become clear when we go through the example of the running strong coupling α_s. Of course, we would prefer to choose all three scales the same, but in a complex physical process this might not always be possible. For example, any massive $(2 \to 3)$ production process naturally involves several external physical scales.

Just a side remark for completeness: a one loop integral which has no intrinsic mass scale is the two-point function with zero mass in the loop and zero momentum flowing through the integral: $B(p^2 = 0; 0, 0)$. It appears for example in the self energy corrections of external quarks and gluons. Based on dimensional arguments this integral has to vanish altogether. On the other hand, we know that like any massive two-point function it has to be ultraviolet divergent $B \sim 1/\epsilon_{\text{UV}}$ because setting all internal and external mass scales to zero is nothing special from an ultraviolet point of view. This can only work if the scalar integral also has an infrared divergence appearing in dimensional regularization. We can then write the entire massless two-point function as

$$B(p^2 = 0; 0, 0) = \int \frac{d^4q}{16\pi^2} \, \frac{1}{q^2} \, \frac{1}{(q+p)^2} = \frac{i\pi^2}{16\pi^2} \left(\frac{1}{\epsilon_{\text{UV}}} - \frac{1}{\epsilon_{\text{IR}}} \right) \; , \tag{II.10}$$

keeping track of the divergent contributions from the infrared and the ultraviolet regimes. For this particular integral they precisely cancel, so the result for $B(0; 0, 0)$ is zero, but setting it to zero too early will spoil any ultraviolet and infrared finiteness test. Treating the two divergences strictly separately and dealing with them one after the other also ensures that for ultraviolet divergences we can choose $\epsilon > 0$ while for infrared divergences we require $\epsilon < 0$.

2. Running coupling

To get an idea what these different scales which appear in the process of renormalization mean let us compute such a scale dependent parameter, namely the running strong coupling $\alpha_s(\mu_R^2)$. The Drell–Yan process is one of the very few relevant processes at hadron colliders where the strong coupling does not appear at tree level, so we cannot use it as our toy process this time. Another simple process where we can study this coupling is bottom pair production at the LHC, where at some energy range we will be dominated by valence quarks: $q\bar{q} \to b\bar{b}$. The only Feynman diagram is an s-channel off–shell gluon with a momentum flow $p^2 \equiv s$.

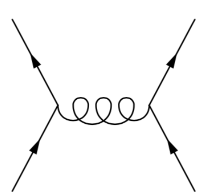

At next–to–leading order this gluon propagator will be corrected by self energy loops, where the gluon splits into two quarks or gluons and re-combines before it produces the two final–state bottoms. Let us for now assume that all quarks are massless. The Feynman diagrams for the gluon self energy include a quark look, a gluon loop, and the ghost loop which removes the unphysical degrees of freedom of the gluon inside the loop.

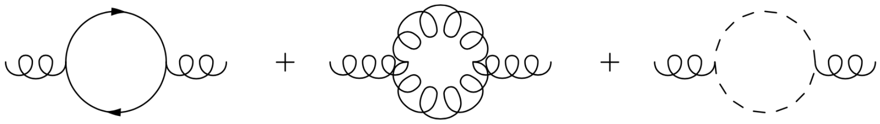

The gluon self energy correction or vacuum polarization, as propagator corrections to gauge bosons are usually labelled, will be a scalar. This way, all fermion lines close in the Feynman diagram and the Dirac trace is computed inside the loop. In color space the self energy will (hopefully) be diagonal, just like the gluon propagator itself, so we can ignore the color indices for now. In unitary gauge the gluon propagator is proportional to the transverse tensor $T^{\mu\nu} = g^{\mu\nu} - p^\nu p^\mu / p^2$. As mentioned in the context of the effective gluon–Higgs coupling, the same should be true for the gluon self energy, which we therefore write as $\Pi^{\mu\nu} \equiv \Pi \, T^{\mu\nu}$. The case with only one external momentum gives us the useful simple relations

$$\begin{aligned} T^{\mu\nu} g_\nu^\rho &= \left(g^{\mu\nu} - \frac{p^\mu p^\nu}{p^2} \right) g_\nu^\rho = T^{\mu\rho} \\ T^{\mu\nu} T_\nu^\rho &= \left(g^{\mu\nu} - \frac{p^\mu p^\nu}{p^2} \right) \left(g_\nu^\rho - \frac{p_\nu p^\rho}{p^2} \right) = g^{\mu\rho} - 2 \frac{p^\mu p^\rho}{p^2} + p^2 \frac{p^\mu p^\rho}{p^4} = T^{\mu\rho} \; . \end{aligned} \tag{II.11}$$

Including the gluon, quark, and ghost loops the regularized gluon self energy with a momentum flow p^2 through the propagator reads

$$\begin{aligned} -\frac{1}{p^2} \, \Pi \left(\frac{\mu_R^2}{p^2} \right) &= \frac{\alpha_s}{4\pi} \left(-\frac{1}{\tilde{\epsilon}} + \log \frac{p^2}{M^2} \right) \left(\frac{13}{6} N_c - \frac{2}{3} n_f \right) + \mathcal{O}(\log m_t^2) \\ &\equiv \alpha_s \left(-\frac{1}{\tilde{\epsilon}} + \log \frac{p^2}{M^2} \right) b_0 + \mathcal{O}(\log m_t^2) \\ &\text{with} \qquad b_0 = \frac{1}{4\pi} \left(\frac{13}{6} N_c - \frac{2}{3} n_f \right) \\ &\text{and better} \qquad \boxed{ b_0 = \frac{1}{4\pi} \left(\frac{11}{3} N_c - \frac{2}{3} n_f \right) \stackrel{\text{SM}}{>} 0 } \; . \end{aligned} \tag{II.12}$$

The minus sign arises from the factors i in the propagators. The number of fermions coupling to the gluons is n_f. From the comments on $B(p^2; 0, 0)$ we understand how the loop integrals will give a logarithm $\log p^2$ which is then matched by a process-dependent logarithm $\log M^2$ implicitly included in the definition of $\tilde{\epsilon}$.

The factor b_0 arises from one-loop corrections, *i.e.* from diagrams which include one additional power of α_s. Strictly speaking, it gives the first term in a perturbative series in the strong coupling $\alpha_s = g_s^2/(4\pi)$. Later on, we will indicate where additional higher order corrections would enter.

In the last step of Eq.(II.12) we have snuck in additional contributions to the renormalization of the strong coupling from the other one-loop diagrams in the process, replacing the factor 13/6 by a factor 11/3. This is related to the fact that there are actually three types of divergent virtual gluon diagrams in the physical process $q\bar{q} \to b\bar{b}$: the external quark self energies with renormalization factors $Z_f^{1/2}$, the internal gluon self energy Z_A, and the vertex corrections Z_{Aff}. The only physical parameters we can renormalize in this process are the strong coupling and, if finite, the bottom mass. Wave function renormalization constants are not physical, but vertex renormalization terms are. The entire divergence in our $q\bar{q} \to b\bar{b}$ process which needs to be absorbed in the strong coupling Z_g is given by the combination

$$Z_{Aff} = Z_g Z_A^{1/2} Z_f \qquad \Leftrightarrow \qquad \frac{Z_{Aff}}{Z_A^{1/2} Z_f} \equiv Z_g \; . \tag{II.13}$$

The additional contributions change the above factor from 13/6 to 11/3 in the running of the strong coupling.

We can check this definition of Z_g by comparing all vertices in which the strong coupling g_s appears, namely the gluon coupling to quarks and ghosts, as well as the triple and quartic gluon vertex. All of them need to have the same divergence structure

$$\frac{Z_{Aff}}{Z_A^{1/2} Z_f} \stackrel{!}{=} \frac{Z_{A\eta\eta}}{Z_A^{1/2} Z_\eta} \stackrel{!}{=} \frac{Z_{3A}}{Z_A^{3/2}} \stackrel{!}{=} \sqrt{\frac{Z_{4A}}{Z_A^2}} \; . \tag{II.14}$$

If we had done the same calculation in QED and looked for a running electric charge, we would have found that the vacuum polarization diagrams for the photon do account for the entire counter term of the electric charge. The other two renormalization constants Z_{Aff} and Z_f cancel because of gauge invariance.

In contrast to QED, the strong coupling diverges in the Thomson limit because QCD is confined towards large distances and weakly coupled at small distances. Lacking a well enough motivated reference point we are lead to renormalize α_s in the $\overline{\text{MS}}$ scheme. From Eq.(II.12) we know that the ultraviolet pole which needs to be cancelled by the counter term is proportional to the function b_0

$$\begin{aligned} & g_s^{\text{bare}} = Z_g g_s = (1+\delta Z_g)\, g_s = \left(1 + \frac{\delta g_s}{g_s}\right) g_s \\ \Rightarrow \qquad & (g_s^2)^{\text{bare}} = (Z_g g_s)^2 = \left(1 + \frac{\delta g_s}{g_s}\right)^2 g_s^2 = \left(1 + 2\frac{\delta g_s}{g_s} + \cdots\right) g_s^2 = \left(1 + \frac{\delta(g_s^2)}{g_s^2}\right) g_s^2 \\ \Rightarrow \qquad & \alpha_s^{\text{bare}} = \left(1 + \frac{\delta\alpha_s}{\alpha_s}\right)\alpha_s \stackrel{\overline{\text{MS}}}{=} \left(1 - \left.\frac{\Pi}{p^2}\right|_{\text{pole}}\right)\alpha_s(M^2) \stackrel{\text{Eq.(II.12)}}{=} \left(1 - \frac{\alpha_s}{\tilde{\epsilon}\left(\dfrac{\mu_R}{M}\right)}\, b_0\right)\alpha_s(M^2) \; . \end{aligned} \tag{II.15}$$

In the last step we have explicitly included the scale dependence of the counter term. Because the bare coupling does not depend on any scales, this means that α_s depends on the unphysical scale M. Similar to the top mass renormalization scheme we can switch to a more physical scheme for the strong coupling as well: we can absorb also the finite contributions of $\Pi(\mu_R^2/p^2)$ into the strong coupling by simply identifying $M^2 = p^2$. Based again on Eq.(II.12) this implies

$$\alpha_s^{\text{bare}} = \alpha_s(p^2)\left(1 - \frac{\alpha_s(p^2) b_0}{\tilde{\epsilon}} + \alpha_s(p^2) b_0 \log\frac{p^2}{M^2}\right) \; . \tag{II.16}$$

On the right hand side α_s is consistently evaluated as a function of the physical scale p^2. The lograrithm just shifts the argument of $\tilde{\epsilon}$ from M^2 to p^2. This formula defines a running coupling $\alpha_s(p^2)$, because the definition of the coupling now has to account for a possible shift between the original argument p^2 and the scale M^2 coming out of the $\overline{\text{MS}}$ scheme. Combining Eqs.(II.15) and (II.16) the bare strong coupling can be expressed in terms of $\alpha_s(M^2)$ or in terms of $\alpha_s(p^2)$, and we can link the two scales through

$$\begin{aligned} & \alpha_s(M^2) = \alpha_s(p^2) + \alpha_s^2(p^2) b_0 \log\frac{p^2}{M^2} = \alpha_s(p^2)\left(1 + \alpha_s(p^2) b_0 \log\frac{p^2}{M^2}\right) \\ \Leftrightarrow \qquad & \frac{d\alpha_s(p^2)}{d\log p^2} = -\alpha_s^2(p^2) b_0 + \mathcal{O}(\alpha_s^3) \; . \end{aligned} \tag{II.17}$$

To the given loop order the argument of the strong coupling squared on the right side can be neglected — its effect is of higher order. We nevertheless keep the argument as a higher order effect to later distinguish different approaches to the running coupling. From Eq.(II.12) we know that $b_0 > 0$, which means that towards larger scales the strong coupling has a negative slope. The ultraviolet limit of the strong coupling is zero. This makes QCD an asymptotically free theory. We can compute the function b_0 in general models by simply adding all contributions of strongly interacting particles in this loop

$$b_0 = -\frac{1}{12\pi} \sum_{\text{colored states}} D_j \, T_{R,j} \; , \tag{II.18}$$

where we need to know some kind of counting factor D_j which is -11 for a vector boson (gluon), +4 for a Dirac fermion (quark), +2 for a Majorana fermion (gluino), +1 for a complex scalar (squark) and +1/2 for a real scalar. Note that this sign is not given by the fermionic or bosonic nature of the particle in the loop. The color charges are $T_R = 1/2$ for the fundamental representation of $SU(3)$ and $C_A = N_c$ for the adjoint representation. The masses of the loop particles are not relevant in this approximation because we are only interested in the ultraviolet regime of QCD where all particles can be regarded massless. When we really model the running of α_s we need to take into account threshold effects of heavy particles, because particles can only contribute to the running of α_s at scales above their mass scale.

We can do even better than this fixed order in perturbation theory: while the correction to α_s in Eq.(II.16) is perturbatively suppressed by the usual factor $\alpha_s/(4\pi)$ it includes a logarithm of a ratio of scales which does not need to be small. Instead of simply including these gluon self energy corrections at a given order in perturbation theory we can instead include chains of one-loop diagrams with Π appearing many times in the off–shell gluon propagator. It means we replace the off–shell gluon propagator by

$$\begin{aligned}\frac{T^{\mu\nu}}{p^2} \to & \frac{T^{\mu\nu}}{p^2} + \left(\frac{T}{p^2} \cdot (-T\,\Pi) \cdot \frac{T}{p^2} \right)^{\mu\nu} \\ & + \left(\frac{T}{p^2} \cdot (-T\,\Pi) \cdot \frac{T}{p^2} \cdot (-T\,\Pi) \cdot \frac{T}{p^2} \right)^{\mu\nu} + \cdots \\ = & \frac{T^{\mu\nu}}{p^2} \sum_{j=0}^{\infty} \left(-\frac{\Pi}{p^2} \right)^j = \frac{T^{\mu\nu}}{p^2} \frac{1}{1+\Pi/p^2} \; , \end{aligned} \tag{II.19}$$

schematically written without the factors i. To avoid indices we abbreviate $T^{\mu\nu}T_\nu^\rho = T \cdot T$ which make sense because according to Eq.(II.11)

$$(T \cdot T \cdot T)^{\mu\nu} = T^{\mu\rho} T_\rho^\sigma T_\sigma^\nu = T^{\mu\sigma} T_\sigma^\nu = T^{\mu\nu} \; . \tag{II.20}$$

This resummation of the logarithm which appears in the next–to–leading order corrections to α_s moves the finite shift in α_s shown in Eqs.(II.12) and (II.16) into the denominator, while we assume that the pole will be properly taken care off in any of the schemes we discuss

$$\alpha_s^{\text{bare}} = \alpha_s(M^2) - \frac{\alpha_s^2 b_0}{\tilde{\epsilon}} \equiv \frac{\alpha_s(p^2)}{1 - \alpha_s(p^2)\; b_0\; \log \dfrac{p^2}{M^2}} - \frac{\alpha_s^2 b_0}{\tilde{\epsilon}} \; . \tag{II.21}$$

Just as in the case without resummation, we can use this complete formula to relate the values of α_s at two reference points, *i.e.* we consider it a renormalization group equation (RGE) which evolves physical parameters from one scale to another in analogy to the fixed order version in Eq.(II.17)

$$\frac{1}{\alpha_s(M^2)} = \frac{1}{\alpha_s(p^2)} \left(1 - \alpha_s(p^2)\; b_0\; \log \frac{p^2}{M^2} \right) = \frac{1}{\alpha_s(p^2)} - b_0\; \log \frac{p^2}{M^2} + \mathcal{O}(\alpha_s) \; . \tag{II.22}$$

The factor α_s inside the parentheses we can again evaluate at either of the two scales, the difference is a higher order effect. If we keep it at p^2 we see that the expression in Eq.(II.22) is different from the un-resummed version in Eq.(II.16). If we ignore this higher order effect the two formulas become equivalent after switching p^2 and M^2. Resumming the vacuum expectation bubbles only differs from the un-resummed result once we include some next–to–leading order contribution. When we differentiate $\alpha_s(p^2)$ with respect to the momentum transfer p^2 we find, using the relation $d/dx(1/\alpha_s) = -1/\alpha_s^2\; d\alpha_s/dx$

$$\frac{1}{\alpha_s} \frac{d\alpha_s}{d\log p^2} = -\alpha_s \frac{d}{d\log p^2} \frac{1}{\alpha_s} = -\alpha_s\, b_0 + \mathcal{O}(\alpha_s^2) \qquad \text{or} \qquad \boxed{p^2 \frac{d\alpha_s}{dp^2} \equiv \frac{d\alpha_s}{d\log p^2} = \beta = -\alpha_s^2 \sum_{n=0} b_n \alpha_s^n} \; . \tag{II.23}$$

This is the famous running of the strong coupling constant including all higher order terms b_n.

In the running of the strong coupling constant we relate the different values of α_s through multiplicative factors of the kind

$$\left(1 \pm \alpha_s b_0 \log \frac{p^2}{M^2} \right) \; . \tag{II.24}$$

Such factors appear in the un-resummed computation of Eq.(II.17) as well as in Eq.(II.21) after resummation. Because they are multiplicative, these factors can move into the denominator, where we need to ensure that they do not vanish. Dependent on the sign of b_0 this becomes a problem for large scale ratios $|\alpha_s \log p^2/M^2| > 1$, where it leads to the Landau pole. For $b_0 > 0$ and large coupling values at small scales $p^2 \ll M^2$ the combination $(1 + \alpha_s b_0 \log p^2/M^2)$ can indeed vanish and become a problem.

It is customary to replace the renormalization point of α_s in Eq.(II.21) with a reference scale defined by the Landau pole. At one loop order we first define the reference scale Λ_{QCD}

$$1+\alpha_s(M^2)\, b_0\, \log\frac{\Lambda^2_{\text{QCD}}}{M^2} \stackrel{!}{=} 0 \qquad \Leftrightarrow \qquad \log\frac{\Lambda^2_{\text{QCD}}}{M^2} = -\frac{1}{\alpha_s(M^2) b_0} \qquad \Leftrightarrow \qquad \log\frac{p^2}{M^2} = \log\frac{p^2}{\Lambda^2_{\text{QCD}}} - \frac{1}{\alpha_s(M^2) b_0}\,, \tag{II.25}$$

and then include it in the running

$$\begin{aligned} \frac{1}{\alpha_s(p^2)} &\stackrel{\text{Eq.(II.22)}}{=} \frac{1}{\alpha_s(M^2)} + b_0\, \log\frac{p^2}{M^2} \\ &= \frac{1}{\alpha_s(M^2)} + b_0 \log\frac{p^2}{\Lambda^2_{\text{QCD}}} - \frac{1}{\alpha_s(M^2)} = b_0 \log\frac{p^2}{\Lambda^2_{\text{QCD}}} \qquad \Leftrightarrow \qquad \boxed{\alpha_s(p^2) = \frac{1}{b_0 \log\dfrac{p^2}{\Lambda^2_{\text{QCD}}}}}\,. \end{aligned} \tag{II.26}$$

This scheme can be generalized to any order in perturbative QCD and is not that different from the Thomson limit renormalization scheme of QED, except that with the introduction of Λ_{QCD} we are choosing a reference point which is particularly hard to compute perturbatively. One thing that is interesting in the way we introduce Λ_{QCD} is the fact that we introduce a scale into our theory without ever setting it. All we did was renormalize a coupling which becomes strong at large energies and search for the mass scale of this strong interaction. This trick is called <u>dimensional transmutation</u>.

In terms of language, there is a little bit of <u>confusion</u> between field theorists and phenomenologists: up to now we have introduced the renormalization scale μ_R as the renormalization point, for example of the strong coupling constant. In the $\overline{\text{MS}}$ scheme, the subtraction of $1/\tilde{\epsilon}$ shifts the scale dependence of the strong coupling to M^2 and moves the logarithm $\log M^2/\Lambda^2_{\text{QCD}}$ into the definition of the renormalized parameter. This is what we will from now on call the renormalization scale in the phenomenological sense, *i.e.* the argument we evaluate α_s at. Throughout this section we will keep the symbol M for this renormalization scale in the $\overline{\text{MS}}$ scheme, but from Section II B on we will shift back to μ_R instead of M as the argument of the running coupling, to be consistent with the literature.

3. Resumming scaling logarithms

In the last Section II A 2 we have introduced the running strong coupling in a fairly abstract manner. For example, we did not link the resummation of diagrams and the running of α_s in Eqs.(II.17) and (II.23) to physics. In what way does the resummation of the one-loop diagrams for the s-channel gluon improve our prediction of the bottom pair production rate at the LHC?

To illustrate those effects we best look at a simple observable which depends on just one physical energy scale p^2. The first observable coming to mind is again the Drell–Yan cross section $\sigma(q\bar{q} \to \mu^+\mu^-)$, but since we are not really sure what to do with the parton densities which are included in the actual hadronic observable, we better use an observable at an e^+e^- collider. Something that will work and includes α_s at least in the one-loop corrections is the R parameter

$$R = \frac{\sigma(e^+e^- \to \text{hadrons})}{\sigma(e^+e^- \to \mu^+\mu^-)} = N_c \sum_{\text{quarks}} Q_q^2 = \frac{11 N_c}{9}\,. \tag{II.27}$$

The numerical value at leading order assumes five quarks. Including higher order corrections we can express the result in a power series in the renormalized strong coupling α_s. In the $\overline{\text{MS}}$ scheme we subtract $1/\tilde{\epsilon}(\mu_R/M)$ and in general include an unphysical scale dependence on M in the individual prefactors r_n

$$R\left(\frac{p^2}{M^2}, \alpha_s\right) = \sum_{n=0} r_n \left(\frac{p^2}{M^2}\right)\, \alpha_s^n(M^2) \qquad\qquad r_0 = \frac{11 N_c}{9}\,. \tag{II.28}$$

The r_n we can assume to be dimensionless — if they are not, we can scale R appropriately using p^2. This implies that the r_n only depend on ratios of two scales, the externally fixed p^2 on the one hand and the artificial M^2 on the other.

At the same time we know that R is an observable, which means that including all orders in perturbation theory it cannot depend on any artificial scale choice M. Writing this dependence as a total derivative and setting it to zero we find an equation which would be called a Callan–Symanzik equation if instead of the running coupling we had included a running mass

$$\begin{aligned}
0 &\stackrel{!}{=} M^2 \frac{d}{dM^2} R\left(\frac{p^2}{M^2}, \alpha_s(M^2)\right) \\
&= \left[M^2 \frac{\partial}{\partial M^2} + \beta \frac{\partial}{\partial \alpha_s} \right] \sum_{n=0} r_n \left(\frac{p^2}{M^2}\right) \alpha_s^n \\
&= \sum_{n=1} M^2 \frac{\partial r_n}{\partial M^2} \alpha_s^n + \sum_{n=1} \beta\, r_n\, n \alpha_s^{n-1} & \text{with} \quad r_0 = \frac{11 N_c}{9} = \text{const} \\
&= M^2 \sum_{n=1} \frac{\partial r_n}{\partial M^2} \alpha_s^n - \sum_{n=1} \sum_{m=0} n r_n \, \alpha_s^{n+m+1}\, b_m & \text{with} \quad \beta = -\alpha_s^2 \sum_{m=0} b_m \alpha_s^m \\
&= M^2 \frac{\partial r_1}{\partial M^2} \alpha_s + \left(M^2 \frac{\partial r_2}{\partial M^2} - r_1 b_0 \right) \alpha_s^2 + \left(M^2 \frac{\partial r_3}{\partial M^2} - 2 r_2 b_0 - r_1 b_1 \right) \alpha_s^3 + \mathcal{O}(\alpha_s^4) \; .
\end{aligned} \tag{II.29}$$

In the second line we have to remember that the M dependence of α_s is already included in the appearance of β, so α_s should be considered a variable by itself. This perturbative series in α_s has to vanish in each order of perturbation theory. Our kind–of–Callan–Symanzik equation requires

$$\begin{aligned}
\frac{\partial r_1}{\partial \log M^2} &= 0 \\
\frac{\partial r_2}{\partial \log M^2} &= r_1 b_0 \\
\frac{\partial r_3}{\partial \log M^2} &= r_1 b_1 + 2 r_2(M^2) b_0 \\
&\vdots
\end{aligned} \tag{II.30}$$

The mix of r_n derivatives and the perturbative terms in the β function we can read off the α_s^3 term: first, we have the appropriate NNNLO corrections r_3; next, we have one loop in the gluon propagator b_0 and two loops for example in the vertex r_2; and finally, we need the two-loop diagram for the gluon propagator b_1 and a one-loop vertex correction r_1. The dependence on the argument M^2 vanishes for r_0 and r_1. Keeping in mind that there will be integration constants c_n and that another, in our case, unique momentum scale p^2 has to cancel the mass units inside $\log M^2$ we find

$$\begin{aligned}
r_0 &= c_0 = \frac{11 N_c}{9} \\
r_1 &= c_1 \\
r_2 &= c_2 + r_1 b_0 \log \frac{M^2}{p^2} = c_2 + c_1 b_0 \log \frac{M^2}{p^2} \\
r_3 &= \int d \log \frac{M'^2}{p^2} \left(c_1 b_1 + 2 \left(c_2 + c_1 b_0 \log \frac{M'^2}{p^2} \right) b_0 \right) = c_3 + (c_1 b_1 + 2 c_2 b_0) \log \frac{M^2}{p^2} + c_1 b_0^2 \log^2 \frac{M^2}{p^2} \\
&\vdots
\end{aligned} \tag{II.31}$$

This chain of r_n values looks like we should interpret the apparent fixed-order perturbative series for R in Eq.(II.28) as a series which implicitly includes terms of the order $\log^{n-1} M^2/p^2$ in each r_n. They can become problematic if this logarithm becomes large enough to spoil the fast convergence in terms of $\alpha_s \sim 0.1$, evaluating the observable R at scales far away from the scale choice for the strong coupling constant M.

Instead of the series in r_n we can use Eq.(II.31) to express R in terms of the c_n and collect the logarithms appearing with each c_n,

$$R = \sum_n r_n \left(\frac{p^2}{M^2} \right) \alpha_s^n(M^2) = c_0 + c_1 \left(1 + \alpha_s(M^2) b_0 \log \frac{M^2}{p^2} + \alpha_s^2(M^2) b_0^2 \log^2 \frac{M^2}{p^2} + \cdots \right) \alpha_s(M^2)$$
$$+ c_2 \left(1 + 2\alpha_s(M^2) b_0 \log \frac{M^2}{p^2} + \cdots \right) \alpha_s^2(M^2) + \cdots \tag{II.32}$$

We encounter geometric series, which we resum as

$$R = c_0 + c_1 \frac{\alpha_s(M^2)}{1 - \alpha_s(M^2) b_0 \log \dfrac{M^2}{p^2}} + c_2 \left(\frac{\alpha_s(M^2)}{1 - \alpha_s(M^2) b_0 \log \dfrac{M^2}{p^2}} \right)^2 + \cdots \equiv \sum c_n \; \alpha_s^n(p^2) \; . \tag{II.33}$$

In the original ansatz α_s is always evaluated at the scale M^2. In the last step we use Eq.(II.22) with flipped arguments p^2 and M^2, derived from the resummation of the vacuum polarization bubbles. In contrast to the r_n integration constants the c_n are by definition independent of p^2/M^2 and therefore more suitable as a perturbative series in the presence of potentially large logarithms. Note that the un-resummed version of the running coupling in Eq.(II.16) would not give the correct result, so Eq.(II.33) only holds for resummed vacuum polarization bubbles.

This re-organization of the perturbation series for R can be interpreted as resumming all logarithms of the kind $\log M^2/p^2$ in the new organization of the perturbative series and absorbing them into the running strong coupling evaluated at the scale p^2. All scale dependence in the perturbative series for the dimensionless observable R is moved into α_s, so possibly large logarithms $\log M^2/p^2$ have disappeared. In Eq.(II.33) we also see that this series in c_n will never lead to a scale-invariant result when we include a finite order in perturbation theory. Some higher–order factors c_n are known, for example inserting $N_c = 3$ and five quark flavors just as we assume in Eq.(II.27)

$$R = \frac{11}{3} \left(1 + \frac{\alpha_s(p^2)}{\pi} + 1.4 \left(\frac{\alpha_s(p^2)}{\pi} \right)^2 - 12 \left(\frac{\alpha_s(p^2)}{\pi} \right)^3 + \mathcal{O} \left(\frac{\alpha_s(p^2)}{\pi} \right)^4 \right) \; . \tag{II.34}$$

This alternating series with increasing perturbative prefactors seems to indicate the asymptotic instead of convergent behavior of perturbative QCD. At the bottom mass scale the relevant coupling factor is only $\alpha_s(m_b^2)/\pi \sim 1/14$, so a further increase of the c_n would become dangerous. However, a detailed look into the calculation shows that the dominant contributions to c_n arise from the analytic continuation of logarithms, which are large finite terms for example from $\mathrm{Re}(\log^2(-E^2)) = \log^2 E^2 + \pi^2$. In the literature such π^2 terms arising from the analytic continuation of loop integrals are often phrased in terms of $\zeta_2 = \pi^2/6$.

Before moving on we collect the logic of the argument given in this section: when we regularize an ultraviolet divergence we automatically introduce a reference scale μ_R. Naively, this could be an ultraviolet cutoff scale, but even the seemingly scale invariant dimensional regularization in the conformal limit of our field theory cannot avoid the introduction of a scale. There are several ways of dealing with such a scale: first, we can renormalize our parameter at a reference point. Secondly, we can define a running parameter and this way absorb the scale logarithm into the $\overline{\text{MS}}$ counter term. In that case introducing Λ_{QCD} leaves us with a compact form of the running coupling $\alpha_s(M^2; \Lambda_{\text{QCD}})$.

Strictly speaking, at each order in perturbation theory the scale dependence should vanish together with the ultraviolet poles, as long as there is only one scale affecting a given observable. However, defining the running strong coupling we sum one-loop vacuum polarization graphs. Even when we compute an observable at a given loop order, we implicitly include higher order contributions. They lead to a dependence of our perturbative result on the artificial scale M^2, which phenomenologists refer to as renormalization scale dependence.

Using the R ratio we see what our definition of the running coupling means in terms of resumming logarithms: reorganizing our perturbative series to get rid of the ultraviolet divergence $\alpha_s(p^2)$ resums the scale logarithms $\log p^2/M^2$ to all orders in perturbation theory. We will need this picture once we introduce infrared divergences in the following section.

B. Infrared divergences

After this brief excursion into ultraviolet divergences and renormalization we can return to the original example, the Drell–Yan process, written in the low-energy QED limit as

$$\sigma(pp \to \ell^+\ell^-)\Bigg|_{\text{QED}} = \frac{4\pi\alpha^2 Q_\ell^2}{3N_c} \int_0^1 dx_1 dx_2 \sum_j Q_j^2 \, f_j(x_1) \, f_{\bar{j}}(x_2) \, \frac{1}{q^2} \,, \tag{II.35}$$

At this stage the parton distributions (pdfs) $f_j(x)$ in the proton are only functions of the collinear momentum fraction of the partons inside the proton about which from a theory point of view we only know a set of sum rules.

The perturbative question we need to ask for $\mu^+\mu^-$ production at the LHC is: what happens if together with the two leptons we produce additional jets which for one reason or another we do not observe in the detector. Such jets could for example come from the radiation of a gluon from the initial–state quarks. In Section II B 1 we will study the kinematics of radiating such jets and specify the infrared divergences this leads to. In Sections II B 2 and IV A we will show that these divergences have a generic structure and can be absorbed into a re-definition of the parton densities, similar to an ultraviolet renormalization of a Lagrangian parameter. In Sections IV B and IV C we will again follow the example of the ultraviolet divergences and specify what absorbing these divergences means in terms logarithms appearing in QCD calculations.

Throughout this writeup we will use the terms jets and final state partons synonymously. This is not really correct once we include jet algorithms and hadronization. On the other hand, the purpose of a jet algorithm is to take us from some kind of energy deposition in the calorimeter to the parton radiated in the hard process. The two should therefore be closely related.

1. *Single jet radiation*

Let us look at the radiation of additional partons in the Drell–Yan process. We can start for example by computing the cross section for the partonic process $q\bar{q} \to Zg$. However, this partonic process involves renormalization of ultraviolet divergences as well as loop diagrams which we have to include before we can say anything reasonable, *i.e.* ultraviolet and infrared finite.

To make life easier and still learn about the structure of collinear infrared divergences we instead look at the crossed process

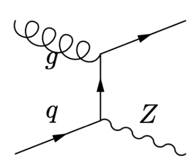

It should behave similar to any other $(2 \to 2)$ jet radiation, except that it has a different incoming state than the leading order Drell–Yan process and hence does not involve virtual corrections. This means we do not have to deal with ultraviolet divergences and renormalization, and can concentrate on parton or jet radiation from the initial state. Moreover, let us go back to Z production instead of a photon, to avoid confusion with additional massless particles in the final state.

The amplitude for this $(2 \to 2)$ process is — modulo charges and averaging factors, but including all Mandelstam variables

$$|\mathcal{M}|^2 \sim -\frac{t}{s} - \frac{s^2 - 2m_Z^2(s + t - m_Z^2)}{st} \,. \tag{II.36}$$

The Mandelstam variable t for one massless final–state particle can be expressed in terms of the rescaled gluon emission angle

$$t = -s(1-\tau)y \qquad \text{with} \qquad y = \frac{1-\cos\theta}{2} \qquad \text{and} \qquad \tau = \frac{m_Z^2}{s} \,. \tag{II.37}$$

Similarly, we obtain $u = -s(1-\tau)(1-y)$, so as a first check we can confirm that $t + u = -s(1-\tau) = -s + m_Z^2$. The collinear limit when the gluon is radiated in the beam direction is given by

$$
\begin{aligned}
& y \to 0 \qquad \Leftrightarrow \qquad t \to 0 \qquad \Leftrightarrow \qquad u = -s + m_Z^2 < 0 \\
& |\mathcal{M}|^2 \to \frac{s^2 - 2sm_Z^2 + 2m_Z^4}{s(s-m_Z^2)} \, \frac{1}{y} + \mathcal{O}(y^0) \; . \qquad \text{(II.38)}
\end{aligned}
$$

This expression is divergent for collinear gluon radiation or gluon splitting, *i.e.* for small angles y. We can translate this $1/y$ divergence for example into the transverse momentum of the gluon or Z

$$
sp_T^2 = tu = s^2(1-\tau)^2 \, y(1-y) = (s-m_Z^2)^2 y + \mathcal{O}(y^2) \qquad \text{(II.39)}
$$

In terms of p_T, the collinear limit our matrix element squared in Eq.(II.38) becomes

$$
|\mathcal{M}|^2 \sim \frac{s^2 - 2sm_Z^2 + 2m_Z^4}{s^2} \, \frac{s-m_Z^2}{p_T^2} + \mathcal{O}(p_T^0) \; . \qquad \text{(II.40)}
$$

The matrix element for the tree level process $qg \to Zq$ has a leading divergence proportional to $1/p_T^2$. To compute the total cross section for this process we need to integrate the matrix element over the entire two-particle phase space. Approximating the matrix element as C'/y or C/p_T^2, we then integrate

$$
\int_{y^{\min}}^{y^{\max}} dy \frac{C'}{y} = \int_{p_T^{\min}}^{p_T^{\max}} dp_T^2 \frac{C}{p_T^2} = 2 \int_{p_T^{\min}}^{p_T^{\max}} dp_T \; p_T \; \frac{C}{p_T^2} \simeq 2C \int_{p_T^{\min}}^{p_T^{\max}} dp_T \frac{1}{p_T} = 2C \; \log \frac{p_T^{\max}}{p_T^{\min}} \qquad \text{(II.41)}
$$

The form C/p_T^2 for the matrix element is of course only valid in the collinear limit; in the non–collinear phase space C is not a constant.

Next, we follow the same strategy as for the ultraviolet divergence. First, we regularize the divergence for example using dimensional regularization. Then, we find a well–defined way to get rid of it. Dimensional regularization means writing the two-particle phase space in $n = 4 - 2\epsilon$ dimensions. Just for reference, the complete formula for the y-distribuion reads

$$
s \, \frac{d\sigma}{dy} = \frac{\pi (4\pi)^{-2+\epsilon}}{\Gamma(1-\epsilon)} \left(\frac{\mu_F^2}{m_Z^2} \right)^\epsilon \frac{\tau^\epsilon (1-\tau)^{1-2\epsilon}}{y^\epsilon (1-y)^\epsilon} \, |\mathcal{M}|^2 \sim \left(\frac{\mu_F^2}{m_Z^2} \right)^\epsilon \; \frac{|\mathcal{M}|^2}{y^\epsilon (1-y)^\epsilon} \; . \qquad \text{(II.42)}
$$

In the second step we only keep the factors we are interested in. The additional factor $1/y^\epsilon$ regularizes the integral at $y \to 0$, as long as $\epsilon < 0$ by slightly increasing the suppression of the integrand in the infrared regime. This means that for infrared divergences we can as well choose $n = 4 + 2\epsilon$ space–time dimensions with $\epsilon > 0$. After integrating the leading collinear divergence $1/y^{1+\epsilon}$ we are left with a pole $1/(-\epsilon)$. This regularization procedure is symmetric in $y \leftrightarrow (1-y)$. What is important to notice is again the appearance of a scale $\mu_F^{2\epsilon}$ with the n-dimensional integral. This scale arises from the infrared regularization of the phase space integral and is referred to as factorization scale. The actual removal of the infrared pole — corresponding to the renormalization in the ultraviolet case — is called mass factorization and works exactly the same way as renormalizing a parameter: in a well–defined scheme we simply subtract the pole from the fixed-order matrix element squared.

2. Parton splitting

In this section we will show that we can indeed write all collinear divergences in a universal form, independent of the hard process which we choose as the Drell–Yan process. In the collinear limit, the radiation of additional partons or the splitting into additional partons will be described by universal splitting functions.

Infrared divergences occur for massless particles in the initial or final state, so we need to go through all ways incoming or outgoing gluons and quark can split into each other. The description of the factorized phase space, with which we will start, is common to all these different channels. The first and at the LHC most important case is the splitting of one gluon into two, shown in Figure 4. The two daughter gluons are close to mass shell while the mother has to have a finite positive invariant mass $p_a^2 \gg p_b^2, p_c^2$. We again assign the direction of the momenta as $p_a = -p_b - p_c$, which means we have to take care of minus signs in the particle energies. We can describe the

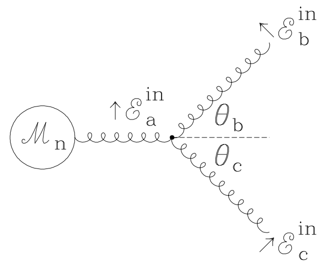

FIG. 4: Splitting of one gluon into two gluons. Figure from Ref. [5].

kinematics of this approximately collinear process in terms of the energy fractions z and $1-z$ defined as

$$z = \frac{|E_b|}{|E_a|} = 1 - \frac{|E_c|}{|E_a|} \qquad p_a^2 = (-p_b - p_c)^2 = 2(p_b p_c) = 2z(1-z)(1-\cos\theta)E_a^2 = z(1-z)E_a^2\theta^2 + \mathcal{O}(\theta^4)$$
$$\Leftrightarrow \qquad \theta \equiv \theta_b + \theta_c \simeq \frac{1}{|E_a|}\sqrt{\frac{p_a^2}{z(1-z)}} \; , \tag{II.43}$$

in the collinear limit and in terms of the opening angle θ between $\vec{p}_b$ and $\vec{p}_c$. Because $p_a^2 > 0$ we call this final–state splitting configuration time–like branching. For this configuration we can write down the so-called Sudakov decomposition of the four-momenta

$$-p_a = p_b + p_c = (-z p_a + \beta n + p_T) \; + \; (-(1-z)p_a - \beta n - p_T) \; . \tag{II.44}$$

It defines an arbitrary unit four-vector n, a p_T component orthogonal to the mother momentum and to n and p_a,

$$(p_a p_T) = 0 = (n p_T) \; , \tag{II.45}$$

and a free factor β. We can specify n such that it defines the direction of the p_b–p_c decay plane. In this decomposition we can set only one invariant mass to zero, for example that of a radiated gluon $p_c^2 = 0$. The second final state will have a finite invariant mass $p_b^2 \neq 0$.

As specific choice for the three reference four-vectors is

$$p_a = \begin{pmatrix} |E_a| \\ 0 \\ 0 \\ p_{a,3} \end{pmatrix} = |E_a| \begin{pmatrix} 1 \\ 0 \\ 0 \\ 1 + \mathcal{O}(\theta) \end{pmatrix} \qquad n = \begin{pmatrix} 1 \\ 0 \\ 0 \\ -1 \end{pmatrix} \qquad p_T = \begin{pmatrix} 0 \\ p_{T,1} \\ p_{T,2} \\ 0 \end{pmatrix} \; . \tag{II.46}$$

Relative to $\vec{p}_a$ we can split the opening angle θ for massless partons according to Figure 4

$$\theta = \theta_b + \theta_c \qquad \text{and} \qquad \frac{\theta_b}{\theta_c} = \frac{\dfrac{p_T}{|E_b|}}{\dfrac{p_T}{|E_c|}} = \frac{1-z}{z} \qquad \Leftrightarrow \qquad \theta = \frac{\theta_b}{1-z} = \frac{\theta_c}{z} \; . \tag{II.47}$$

The momentum choice in Eq.(II.46) has the additional feature that $n^2 = 0$, which allows us to extract β from the momentum parameterization shown in Eq.(II.44) and the additional condition $p_c^2 = 0$

$$\begin{aligned} p_c^2 &= (-(1-z)p_a - \beta n - p_T)^2 \\ &= (1-z)^2 p_a^2 + p_T^2 + 2\beta(1-z)(n p_a) \\ &= (1-z)^2 p_a^2 + p_T^2 + 4\beta(1-z)|E_a|(1+\mathcal{O}(\theta)) \stackrel{!}{=} 0 \qquad \Leftrightarrow \qquad \beta \simeq -\frac{p_T^2 + (1-z)^2 p_a^2}{4(1-z)|E_a|} \; . \end{aligned} \tag{II.48}$$

Using this phase space parameterization we divide an $(n+1)$-particle process into an n-particle process and a splitting process of quarks and gluons. First, this requires us to split the $(n+1)$-particle phase space alone into an n-particle phase space and the collinear splitting. The general $(n+1)$-particle phase space separating off the n-particle contribution

$$\begin{aligned}
d\Phi_{n+1} &= \cdots \frac{d^3\vec{p}_b}{2(2\pi)^3|E_b|}\,\frac{d^3\vec{p}_c}{2(2\pi)^3|E_c|} = \cdots \frac{d^3\vec{p}_a}{2(2\pi)^3|E_a|}\,\frac{d^3\vec{p}_c}{2(2\pi)^3|E_c|}\,\frac{|E_a|}{|E_b|} \\
&\equiv d\Phi_n\,\frac{dp_{c,3}dp_T p_T d\phi}{2(2\pi)^3|E_c|}\,\frac{1}{z} \\
&= d\Phi_n\,\frac{dp_{c,3}dp_T^2 d\phi}{4(2\pi)^3|E_c|}\,\frac{1}{z}
\end{aligned} \tag{II.49}$$

azimuthal angle ϕ. In other words, separating the $(n+1)$-particle space into an n-particle phase space and a $(1\to 2)$ splitting phase space is possible without any approximation, and all we have to take care of is the correct prefactors in the new parameterization.

Our next task is to translate $p_{c,3}$ and p_T^2 into z and p_a^2. Starting from Eq.(II.44) for $p_{c,3}$ with the third components of p_a and p_T given by Eq.(II.46) we insert β from Eq.(II.48) and obtain

$$\begin{aligned}
\frac{dp_{c,3}}{dz} &= \frac{d}{dz}\left[-(1-z)|E_a|(1+\mathcal{O}(\theta))+\beta\right] = \frac{d}{dz}\left[-(1-z)|E_a|(1+\mathcal{O}(\theta)) - \frac{p_T^2+(1-z)^2p_a^2}{4(1-z)|E_a|}\right] \\
&= |E_a|(1+\mathcal{O}(\theta)) - \frac{p_T^2}{4(1-z)^2E_a} + \frac{p_a^2}{4|E_a|} \\
&= \frac{|E_c|}{1-z}(1+\mathcal{O}(\theta)) - \frac{\theta^2z^2E_c^2}{4(1-z)^2E_a} + \frac{z(1-z)E_a^2\theta^2+\mathcal{O}(\theta^4)}{4|E_a|} \qquad \text{using Eq.(II.43) and Eq.(II.47)} \\
&= \frac{|E_c|}{1-z} + \mathcal{O}(\theta) \qquad \Leftrightarrow \qquad \frac{dp_{c,3}}{|E_c|} \simeq \frac{dz}{1-z}\,.
\end{aligned} \tag{II.50}$$

Next, we replace dp_T^2 with dp_a^2 according to

$$\frac{p_T^2}{p_a^2} = \frac{E_b^2\theta_b^2}{z(1-z)E_a^2\theta^2} = \frac{z^2E_a^2\,(1-z)^2\theta^2}{z(1-z)E_a^2\theta^2} = z(1-z) \qquad \Leftrightarrow \qquad dp_T^2 = z(1-z)dp_a^2\,. \tag{II.51}$$

This gives us the final result for the separated collinear phase space

$$\boxed{d\Phi_{n+1} = d\Phi_n\,\frac{dz\,dp_a^2\,d\phi}{4(2\pi)^3} = d\Phi_n\,\frac{dz\,dp_a^2}{4(2\pi)^2}}\,, \tag{II.52}$$

where in the second step we assume an azimuthal symmetry.

Adding the transition matrix elements to this factorization of the phase space and ignoring the initial–state flux factor which is common to both processes we can now postulate a full factorization for one emission and in the collinear approximation

$$\begin{aligned}
d\sigma_{n+1} &= \overline{|\mathcal{M}_{n+1}|^2}\,d\Phi_{n+1} \\
&= \overline{|\mathcal{M}_{n+1}|^2}\,d\Phi_n\frac{dp_a^2\,dz}{4(2\pi)^2}\,\,(1+\mathcal{O}(\theta)) \\
&\simeq \frac{2g_s^2}{p_a^2}\,\hat{P}(z)\,\overline{|\mathcal{M}_n|^2}\,d\Phi_n\frac{dp_a^2\,dz}{16\pi^2} \qquad \text{assuming} \quad \boxed{\overline{|\mathcal{M}_{n+1}|^2} \simeq \frac{2g_s^2}{p_a^2}\,\hat{P}(z)\,\overline{|\mathcal{M}_n|^2}}\,.
\end{aligned} \tag{II.53}$$

This last step is an assumption. We will proceed to show it step by step by constructing the appropriate splitting kernels $\hat{P}(z)$ for all different quark and gluon configurations. If Eq.(II.53) holds true this means that we can compute the $(n+1)$ particle amplitude squared from the n-particle case convoluted with the appropriate splitting kernel. Using $d\sigma_n \sim \overline{|\mathcal{M}_n|^2}\,d\Phi_n$ and $g_s^2 = 4\pi\alpha_s$ we can write this relation in its most common form

$$\sigma_{n+1} \simeq \int \sigma_n\,\frac{dp_a^2}{p_a^2}dz\,\frac{\alpha_s}{2\pi}\,\hat{P}(z)\,. \tag{II.54}$$

Reminding ourselves that relations of the kind $\overline{|\mathcal{M}_{n+1}|^2} = p\overline{|\mathcal{M}_n|^2}$ can typically be summed, for example for the case of successive soft photon radiation in QED, we see that Eq.(II.54) is not the final answer. It does not include the necessary phase space factor $1/n!$ from identical bosons in the final state which leads to the simple exponentiation.

As the first parton splitting in QCD we study a gluon splitting into two gluons, shown in Figure 4. To compute its transition amplitude we need to write down all gluon momenta and polarizations in a specific frame. We skip the derivation and just quote the result

$$\begin{aligned}
\overline{|\mathcal{M}_{n+1}|^2} &= \frac{2g_s^2}{p_a^2}\,\frac{N_c}{2}\,2\left[\frac{z}{1-z} + z(1-z) + \frac{1-z}{z}\right]\,\overline{|\mathcal{M}_n|^2} \\
&\equiv \frac{2g_s^2}{p_a^2}\,\hat{P}_{g\leftarrow g}(z)\,\overline{|\mathcal{M}_n|^2} \\
\Leftrightarrow \qquad & \hat{P}_{g\leftarrow g}(z) = C_A\left[\frac{z}{1-z} + \frac{1-z}{z} + z(1-z)\right] \; ,
\end{aligned} \tag{II.55}$$

using $C_A = N_c$. The form of the splitting kernel is symmetric when we exchange the two gluons z and $(1-z)$. It diverges if either of the gluons become soft. The notation $\hat{P}_{i\leftarrow j} \sim \hat{P}_{ij}$ is inspired by a matrix notation which we can use to multiply the splitting matrix from the right with the incoming parton vector to get the final parton vector. Following the logic described above, with this calculation we prove that the factorized form of the $(n+1)$-particle matrix element squared in Eq.(II.53) holds for gluons only.

The same kind of splitting kernel we can compute for the splitting of a gluon into two quarks and the splitting of a quark into a quark and a gluon

$$g(p_a) \to q(p_b) + \bar{q}(p_c) \qquad\qquad \text{and} \qquad\qquad q(p_a) \to q(p_b) + g(p_c) \; . \tag{II.56}$$

Both splittings include the quark–quark–gluon vertex, coupling the gluon current to the quark and antiquark spinors. Again, we omit the calculation and quote the result

$$\begin{aligned}
\overline{|\mathcal{M}_{n+1}|^2} &= \frac{2g_s^2}{p_a^2}\,T_R\,\left[z^2 + (1-z)^2\right]\,\overline{|\mathcal{M}_n|^2} \\
&\equiv \frac{2g_s^2}{p_a^2}\hat{P}_{q\leftarrow g}(z)\,\overline{|\mathcal{M}_n|^2} \\
\Leftrightarrow \qquad & \hat{P}_{q\leftarrow g}(z) = T_R\left[z^2 + (1-z)^2\right] \; ,
\end{aligned} \tag{II.57}$$

with $T_R = 1/2$. In the first line we implicitly assume that the internal quark propagator can be written as something like $u\bar{u}/p_a^2$ and we only need to consider the denominator. This splitting kernel is again symmetric in z and $(1-z)$ because QCD does not distinguish between the outgoing quark and the outgoing antiquark.

The third splitting we compute is gluon radiation off a quark,

$$q(p_a) \to q(p_b) + g(p_c) \; , \tag{II.58}$$

sandwiching the qqg vertex between an outgoing quark $\bar{u}_\pm(p_b)$ and an incoming quark $u_\pm(p_a)$. The result is

$$\begin{aligned}
\overline{|\mathcal{M}_{n+1}|^2} &= \frac{2g_s^2}{p_a^2}\,C_F\,\frac{1+z^2}{1-z}\,\overline{|\mathcal{M}_n|^2} \\
&\equiv \frac{2g_s^2}{p_a^2}\hat{P}_{q\leftarrow g}(z)\,\overline{|\mathcal{M}_n|^2} \\
\Leftrightarrow \qquad & \hat{P}_{q\leftarrow q}(z) = C_F\frac{1+z^2}{1-z} \; .
\end{aligned} \tag{II.59}$$

The color factor for gluon radiation off a quark is $C_F = (N^2-1)/(2N)$. The averaging factor $1/N_a = 2$ now is the number of quark spins in the intermediate state. Just switching $z \leftrightarrow (1-z)$ we can read off the kernel for a quark splitting written in terms of the final–state gluon

$$\hat{P}_{g\leftarrow q}(z) = C_F\frac{1+(1-z)^2}{z} \; . \tag{II.60}$$

This result finalizes our calculation of all QCD splitting kernels $\hat{P}_{i\leftarrow j}(z)$ between quarks and gluons. As alluded to earlier, similar to ultraviolet divergences which get removed by counter terms these splitting kernels are universal. They do not depend on the hard n-particle matrix element which is part of the original $(n+1)$-particle process. In Eqs.(II.55), (II.57), (II.59), and (II.60) we have shown by construction that the collinear factorization Eq.(II.54) holds at this level in perturbation theory.

Before using this splitting property to describe QCD effects at the LHC we need to look at the splitting of partons in the initial state, meaning $|p_a^2|, p_c^2 \ll |p_b^2|$ where p_b is the momentum entering the hard interaction. The difference to the final–state splitting is that now we can consider the split parton momentum $p_b = p_a - p_c$ as a t-channel diagram, so we already know $p_b^2 = t < 0$ from our usual Mandelstam variables argument. This space–like splitting version of Eq.(II.44) for p_b^2 gives us

$$\begin{aligned} t \equiv p_b^2 &= (-zp_a + \beta n + p_T)^2 \\ &= p_T^2 - 2z\beta(p_a n) && \text{with } p_a^2 = n^2 = (p_a p_T) = (n p_T) = 0 \\ &= p_T^2 + \frac{p_T^2 z}{1-z} && \text{using Eq.(II.48)} \\ &= \frac{p_T^2}{1-z} = -\frac{p_{T,1}^2 + p_{T,2}^2}{1-z} < 0 \; . \end{aligned} \tag{II.61}$$

The calculation of the splitting kernels and matrix elements is the same as for the time–like case, with the one exception that for splitting in the initial state the flow factor has to be evaluated at the reduced partonic energy $E_b = zE_a$ and that the energy fraction entering the parton density needs to be replaced by $x_b \to z x_b$. The factorized matrix element for initial–state splitting then reads just like Eq.(II.54)

$$\sigma_{n+1} = \int \sigma_n \, \frac{dt}{t} dz \, \frac{\alpha_s}{2\pi} \, \hat{P}(z) \; . \tag{II.62}$$

What we are missing for the infrared or better collinear divergences is the description of the scale dependence and the interpretation in terms of perturbation theory. That will lead us to the DGLAP equations in Sec. IV.

III. STRONG CHIRAL SYMMETRY BREAKING

In the previous sections we discussed the ultraviolet renomalisation of QCD and its relation to the scale dependence of physics. This scale dependence is apparent in the momentum dependence of the strong running coupling $\alpha_s(p^2) = g^2(p^2)/(4\pi)$ defined in (I.39) and (II.23). Here p is the relevant momentum/energy scale of a given process. The running coupling in (I.39) tends to zero logarithmically for $p \to \infty$. This property is called asymptotic freedom (Nobel prize 2004) and guarantees the existence of the the perturbative expansion of QCD. Its validity for large energies and momenta is by now impressively proven in various scattering experiments, see e.g. Figure 3 from [3]. These experiments can also be used to define a running coupling (which is not unique beyond two loop, see e.g. [4]).

In turn, in the infrared regime of QCD at low momentum scales, perturbation theory is not applicable any more. The coupling grows and the failure of perturbation theory is finally signaled by the so-called Landau pole with $\alpha_s(\Lambda_{\text{QCD}}) = \infty$. We infer from (I.39) that at one loop, Λ_{QCD} is given by

$$\Lambda_{\text{QCD}} = \mu \, e^{-\frac{1}{2\beta_0 \alpha_s(\mu)}} \, , \qquad \text{with} \qquad \mu \frac{d\Lambda_{\text{QCD}}}{d\mu} = 0 \, . \tag{III.1}$$

The RG-invariance of Λ_{QCD} is readily proven with the β-function (I.38) up to two-loop terms. This implies that Λ_{QCD} may be related to a physical scale and indeed it is (non-trivially) related to the mass gap in QCD. However, we emphasise that a large or diverging coupling does *not* imply confinement, the theory could still be QED-like showing a Coulomb-potential with a large coupling. The latter would not lead to the absence of coloured asymptotic states but rather to so-called color charge superselection sectors as in QED. There, we have asymptotic charged states and no physics process can change the charge. For more details see e.g. [6].

A. Spontaneous symmetry breaking and the Goldstone theorem

In the Standard Model we have two phenomena involving spontaneous symmetry breaking. The first is the spontaneous symmetry breaking in the Higgs sector (Englert-Brout-Higgs-Guralnik-Hagen-Kibble) which provides (current) masses for the quarks and leptons as well as for the W, Z vector bosons, the gauge bosons of the weak interactions. The corresponding Goldstone boson manifest itself as the third polarisation of the massive vector bosons (Higgs-Kibble dinner).

The second phenomena is strong chiral symmetry breaking in the quark sector with a mass scale of ≈ 300 MeV. This mechanism, loosely speaking, lifts the current quark masses to constituent quark masses. For the up and down quarks the current quark mass is negligible, see Table I. The corresponding (pseudo-) Goldstone bosons, the pions $\vec{\pi}$, are composite (quark–anti-quark) states and do not appear in the QCD action.

In the following we discuss similarities of and differences between these two phenomena. Before we come to the Standard Model, let us recall some basic facts about spontaneous symmetry breaking. Further details can be found in the literature. As a basic, but important, example we consider a simple scalar field theory with N real scalars and action

$$S[\phi] = \frac{1}{2}\int_x (\partial_\mu \phi^a)^2 + \int_x V(\rho)\,, \qquad \text{with} \qquad a = 1, ..., N\,, \qquad \text{and} \qquad \rho = \frac{1}{2}\phi^a\phi^a\,, \tag{III.2}$$

and the ϕ^4-potential

$$V(\rho) = -\frac{1}{2}\mu_\phi^2(\phi^a\phi^a) + \frac{\lambda_\phi}{8}(\phi^a\phi^a)^2 = -\mu_\phi\rho + \frac{\lambda_\phi}{2}\rho^2\,. \tag{III.3}$$

In the following considerations we shall not need the specific form (III.3) but only its symmetries. Still, the simple potential (III.3) serves as a good showcase. The action (III.2) with the potential (III.3) has $O(N)$-symmetry. Moreover, the potential (III.3) has a manifold of non-trivial minima, each of which breaks $O(N)$-symmetry. This leads us to the vacuum manifold

$$V'(\rho_0) = 0\,, \qquad \text{with} \qquad \rho_0 = \frac{\mu_\phi^2}{\lambda_\phi}\,, \tag{III.4}$$

where the prime stands for the derivative w.r.t. ρ. In Figure 5 the potential is depicted for the $O(2)$-case with $N = 2$.

Without loss of generality we pick a specific point on the vacuum manifold (III.4), to wit

$$\phi_0 = \begin{pmatrix} 0 \\ \vdots \\ 0 \\ \sqrt{2\rho_0} \end{pmatrix}\,. \tag{III.5}$$

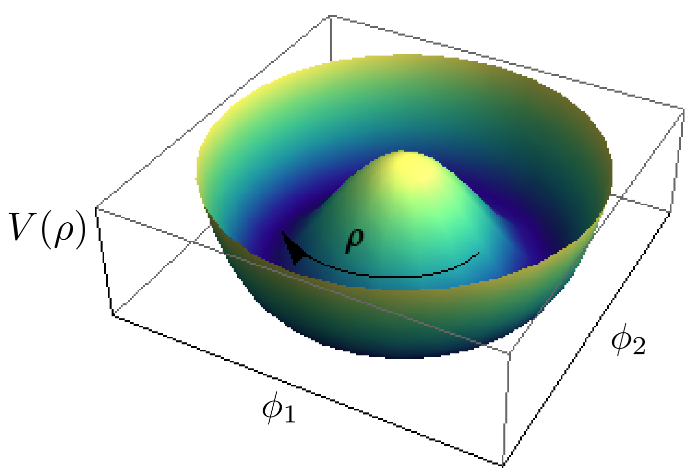

FIG. 5: Illustration of the Mexican hat potential for N = 2. The radial massive mode ρ is indicated by the arrow. The angular mode is the Goldstone mode.

The vacuum vector ϕ_0 in (III.5) is invariant under the subgroup (little group) $O(N-1)$ with the generators t^a, $a = N, N+1, ...N(N-1)/2$ of $O(N)$ that acts trivially on the Nth component field ϕ^N. This subgroup rotates the first $N-1$ component fields into each other. It leaves us with $N-1$ generators t^a, $a = 1, ..., N-1$ (of the quotient $O(N)/O(N-1)$) of the $N(N-1)/2$ generators of the group $O(N)$. In turn, a rotation of the vacuum vector within this quotient generates the full vacuum manifold. Applied to a vector $\phi^a = \delta^{Na}\sqrt{2\rho}$ with length it generates all fields,

$$\phi = e^{\frac{\theta^a}{\sqrt{2\rho_0}} t^a} \begin{pmatrix} 0 \\ \vdots \\ 0 \\ \sigma \end{pmatrix} , \tag{III.6}$$

where the denominator $1/\sqrt{2\rho_0}$ is chosen for convenience. Commonly, the Nth component field ϕ^N is expanded about the minimum $\sigma_0 = \sqrt{2\rho_0}$.

In the present lecture we choose a slightly different approach and stick to the Cartesian fields ϕ which we split into the radial mode σ and the rest, $\vec{\pi}$, i.e.

$$\phi = \begin{pmatrix} \vec{\pi} \\ \sigma \end{pmatrix} , \qquad \text{with} \qquad \phi_0 = \begin{pmatrix} 0 \\ \sigma \end{pmatrix} . \tag{III.7}$$

Note that in an expansion about the minimum ϕ_0 in the fields $\vec{\theta}$ and $\vec{\pi}$ agree in leading order. Using the representation (III.7) in the kinetic term in the action (III.2) we are led to

$$S_{\text{kinetic}}[\phi] = \frac{1}{2} \int_x \left[(\partial_\mu \sigma)^2 + (\partial_\mu \vec{\pi})^2 \right] . \tag{III.8}$$

The mass term of the model is given by the quadratic term of the potential in an expansion about the minimum. It reads generally

$$\frac{1}{2} \int_x m^{2\,ab}(\phi_0) \phi^a \, \phi^b \,, \qquad \text{with} \qquad m^{2\,ab}(\phi_0) = \partial_{\phi^a} \partial_{\phi^b} V(\rho_0) = \delta^{ab}\, V'(\rho_0) + \phi_0^a \phi_0^b \, V''(\rho_0) \,. \tag{III.9}$$

Using the expansion point (III.5) leads to the mass matrix

$$m^{2\,ab}(\phi_0) = \delta^{ab}\, V'(\rho_0) + 2\,\delta^{Na}\delta^{Nb} \rho_0 V''(\rho_0) = \delta^{Na}\delta^{Nb} \rho_0 \, \lambda \,. \tag{III.10}$$

Equation (III.10) entails that in the symmetry-broken phase of the model we have $N-1$ massless fields, the Goldstone fields. Note that we have not used the specific form (III.3) of the potential for this derivation.

The occurrence of the massless modes in (III.10) is a specific case/manifestation of the Goldstone theorem. It entails in general that in the case of a spontaneous symmetry breaking of a continuous symmetry massless modes, the Goldstone modes, occur. Their number is related to the number of generators in the Quotient G/H, where G is the symmetry group and H is the subgroup (little group) which leaves the vacuum invariant.

B. Spontaneous symmetry breaking, quantum fluctuations and masses*

The classical analysis done in chapter Section III A suffices to uncover the occurrence of massless modes in spontaneous symmetry breaking. However, it does not unravel the mechanism. The stability of the chosen vacuum, e.g. (III.5), necessitates, that an infinitesimal rotation on the vacuum manifold costs an infinite amount of energy. This does only happen (for continuous symmetries) in dimensions $d > 2$. In $d \leq 2$ no spontaneous symmetry breaking of a continuous symmetry occurs, which is covered by the Mermin-Wagner theorem (Mermin-Wagner-Hohenberg-Coleman). In $d = 2$ dimensions theories with discrete symmetry can exhibit spontaneous symmetry breaking, e.g. the Ising model.

Hence, the full analysis has to be done on the quantum level. A convenient way to address these questions is the quantum analogue of the classical action, the (quantum) effective action. Formally it is defined as the Legendre transform of the Schwinger functional, $W[J] = \log Z[J]$. In the present case this is

$$\Gamma[\phi] = \sup_J \left\{ \int_x J(x)\phi(x) - \log Z[J] \right\} , \qquad \text{where} \qquad Z[J] = \int D\varphi \, e^{-S[\varphi] + \int_x J\varphi} . \tag{III.11}$$

In the following we simply assume that (III.11) has a maximum and is differentiable w.r.t. J. Then the definition in (III.11) leads to

$$\phi = \frac{1}{Z[J]}\frac{\delta Z[J]}{\delta J} = \langle\varphi\rangle\,, \qquad \text{and} \qquad J = \frac{\delta\Gamma}{\delta\phi}\,. \tag{III.12}$$

The effective action also has a closed path integral representation in terms of a functional integro-differential equation, which we also quote for later use. For the derivation we substitute the current in (III.11) with (III.12) and use that $Z = \exp\{-\Gamma + \int_x J\phi\}$. This leads us to

$$e^{-\Gamma[\phi]} = \int D\varphi'\, e^{-S[\phi+\varphi']+\int_x \frac{\delta\Gamma}{\delta\phi}\varphi'}\,, \qquad \text{with} \qquad \langle\varphi'\rangle_c = 0\,, \tag{III.13}$$

where we also shifted the integration variable $\varphi = \varphi' + \varphi$. Equation (III.13) leads us immediately to the quantum equations of motion in general backgrounds ϕ, the Dyson-Schwinger equations. We simply take the ϕ-derivatives on both sides and arrive at

$$\frac{\delta\Gamma}{\delta\phi} = \left\langle\frac{\delta S}{\delta\varphi}\right\rangle\,, \tag{III.14}$$

the quantum eqautions of motion (EoM) in a given background $\phi = \langle\varphi\rangle$ triggered by the current J. Evaluated on the EoM with $J = 0$,

$$\left.\frac{\delta\Gamma}{\delta\phi}\right|_{\phi=\phi_{\rm EoM}} = 0\,, \tag{III.15}$$

The effective action $\Gamma[\phi_{\rm EoM}] = -\log Z[0]$ it is the free energy of the theory and implies $J[\phi_{\rm EoM}] = 0$. It is also a generating functional and generates the one-particle-irreducible (1PI) diagrams of the theory. As all diagrams can be constructed from 1PI diagrams, it contains the full information about the correlation functions of the theory. In the present context, the interesting feature is its relation to the free energy. It allows us to define the effective potential

$$V_{\rm eff}[\phi_c] = \Gamma[\phi_c]/{\rm vol}_4\,, \tag{III.16}$$

with constant fields ϕ_c and the four-volume ${\rm vol}_4 = \int d^4x$. If the effective potential shows the vacuum structure discussed above in the classical case, the theory exhibits spontaneous symmetry breaking. The Mermin-Wagner theorem simply entails that in lower dimensions the longe range nature of the quantum fluctuations washes out the non-trivial vacua.

The rôle of the effective action as the quantum analogue of the classical action is also very apparent in its relation to the propagator of the theory,

$$\langle\phi(p)\phi(-p)\rangle_c = \left.\frac{\delta^2\log Z[J]}{\delta J(p)\delta J(-P)}\right|_{J=0} = \left.\frac{1}{Z[0]}\frac{\delta^2 Z}{\delta J(p)\delta J(-P)}\right|_{J=0} - \langle\phi(p)\rangle\langle\phi(-p)\rangle\,, \qquad \text{with} \qquad \langle\phi\rangle = \frac{1}{Z[0]}\frac{\delta Z}{\delta J}\,, \tag{III.17}$$

where the subscript $_c$ stands for connected. Now we use the relation of $\log Z$ to the effective action defined in (III.11). We have

$$\delta(p-q) = \frac{\delta J(q)}{\delta J(p)} = \int_l \frac{\delta\phi(l)}{\delta J(p)}\cdot\frac{\delta J(q)}{\delta\phi(l)} = \int_l \frac{\delta^2\log Z}{\delta J(l)\delta J(p)}\cdot\frac{\delta^2\Gamma[\phi]}{\delta\phi(l)\delta(q)} \quad\Rightarrow\quad \langle\phi(p)\phi(q)\rangle_c = \frac{1}{\Gamma^{(2)}}(p,q)\,, \tag{III.18}$$

with the vertices

$$\frac{\delta^n\Gamma}{\delta\phi(p_1)\cdots\phi(p_n)} = \Gamma^{(n)}(p_1,...,p_n)\,, \qquad \text{with} \qquad \langle\varphi(p_1)\cdots\varphi(p_n)\rangle_{\rm 1PI} = \Gamma^{(n)}(p_1,...,p_n)\,. \tag{III.19}$$

The proof of the latter identity of the nth φ-derivatives with the 1PI n-point correlation functions we leave to the reader. Instead let us now come back to our simple example for spontaneous symmetry breaking. Let us assume for the moment that the full effective action resembles the classical action in (III.2). Then the ϕ^4-potential in (III.3) is the full quantum effective potential of the theory for $\rho \geq \rho_0$ (why is this not possible for smaller ρ?). The full propagator of the theory is now given by

$$\langle\varphi(p)\varphi(-p)\rangle_c = \frac{1}{\Gamma^{(2)}[\phi_{\rm EoM}]}(p,-p) = \frac{1}{p^2}\left(\delta^{ab}-\delta^{aN}\delta^{bN}\right) + \frac{1}{p^2+8\rho_0\lambda}\delta^{ab}\,, \tag{III.20}$$

which describes the massless propagation of the $N-1$ Goldstone modes, and that of one massive one, the radial field σ, with mass $m_\sigma^2 = 8\rho_0\lambda$. This links the curvature of the effective potential to the masses of the propagating modes in the theory. Note however, that this is a Euclidean concept and finally we are interested in the pole masses of the physical excitations. They are defined via the respective (inverse) screening lengths in the spatial and temporal directions. The latter are defined by

$$\lim_{\|\vec x-\vec y\|\to\infty}\langle\phi(x)\phi(y)\rangle \sim e^{-\|\vec x-\vec y\|/\xi_{\rm spat}}\,,\qquad \text{and} \qquad \lim_{|x_0-y_0|\to\infty}\langle\phi(x)\phi(y)\rangle \sim e^{-|x_0-y_0|/\xi_{\rm temp}}\,. \tag{III.21}$$

The screening lengths $\xi_{\rm spat/temp}$ are inversely related to the pole mass $m_{\rm pol} = 1/\xi_{\rm temp}$ and screening mass $m_{\rm screen} = 1/\xi_{\rm spat}$ respectively. In the present example with the classical dispersion p^2 these masses are identical and also agree with the curvature masses $m_{\rm curv}$ derived from the effective potential. This is easily seen from (III.20). The screening lengths and masses are derived from the Fourier transform of the propagator in momentum space and we have e.g. for the radial mode φ^N at $\vec p = 0$

$$\lim_{|x_0-y_0|\to\infty}\int\frac{dp_0}{(2\pi)}\langle\varphi^N(p_0,0)\varphi^N(-p_0,0)\rangle_c e^{ip_0\,(x_0-y_0)} \sim e^{-|x_0-y_0|8\rho_0\lambda}\,, \tag{III.22}$$

and hence $m_{\rm pol} = 1/\xi_{\rm temp} = m_{\rm curv}$. Here $\vec p = 0$ has only be chosen for convenience. A similar computation can be made for the spatial screening length which agrees with the temporal one. In summary this leaves us with the definition of the pole mass as the smallest value for

$$\Gamma^{(2)}(p_0 = m_{\rm pol}, \vec p = 0) = 0\,, \tag{III.23}$$

related to the pole (or cut) that is closest to the Euclidean frequency axis. A similar definition holds for the screening mass.

In principle this allows for the extraction of the pole and screening masses from the Euclidean propagators. In practice this quickly runs in an accuracy problem if the propagator is only known numerically. Moreover, this problem is tightly related to reconstruction problems of analyticity properties from numerical data which is an ill-posed problem without any further knowledge.

As a last remark we add that the above identity between screening lengths, and pole, screening and curvature masses fails in the full quantum theory:

- the coincidence of curvature and screening/pole masses hinges on the classical dispersion proportional to p^2, any non-trivial momentum dependence of the propagator leads to a violation.

- The coincidence of screening and pole mass hinges on the dispersion only being a function of p^2. While this is true in the vacuum (at vanishing temperature $T = 0$ and density/chemical potential $n/\mu = 0$), finite temperature and density singles out a rest frame and the dispersion depends on $\vec p^2$ and p_0^2 separately.

Having said this, in the following we shall first use simple approximations to the full low energy effective action of QCD for extracting the physics of chiral symmetry breaking and confinement, as well as the mechanisms behind these phenomena.

C. Little reminder on the Higgs mechanism

Now we are in the position to discuss the Higgs mechanism in the Standard Model. Again we refer to the literature for the details. The Higgs mechanisms serves as an example, at which we can discuss similarities and differences for strong chiral symmetry breaking. Moreover, it is the combination of both mechanisms of mass generation that leads to the observed world. The action of the Standard Model is given by

$$S_{\rm SM}[\Phi] = \frac{1}{4}\int_x F^a_{\mu\nu}F^a_{\mu\nu} + \frac{1}{4}\int_x W^a_{\mu\nu}W^a_{\mu\nu} + \frac{1}{4}\int_x B_{\mu\nu}B_{\mu\nu} + (D\phi)^\dagger D\phi + V_H(\phi) + \int_x \bar\psi\cdot\left(i\not{D} + i\,m_\psi(\phi) + i\mu\gamma_0\right)\cdot\psi\,, \tag{III.24}$$

where we have introduced the electroweak gauge bosons W, B and the Higgs, a complex scalar $SU(2)$-doublet ϕ,

$$\phi = \begin{pmatrix} \phi_1 \\ \phi_2 \end{pmatrix} , \tag{III.25}$$

with complex components ϕ_1, ϕ_2. The Higgs potential V_H is a ϕ^4-potential as (III.3) with

$$V_H(\phi) = -\frac{1}{2}\mu_\phi^2 \phi^\dagger \phi + \frac{\lambda_\phi}{8}(\phi^\dagger \phi)^2 \, . \tag{III.26}$$

with non-trivial vacuum manifold

$$\rho_0 = \frac{\mu_\phi^2}{\lambda_\phi} \qquad \text{with} \qquad \rho = \frac{1}{2}\phi^\dagger \phi \, . \tag{III.27}$$

In the spirit of the discussion at the end of chapter Section III A we should interpret V_H as an approximation of the full effective potential of the theory. The Higgs field couples to the electroweak gauge group with the covariant derivative

$$D_\mu \phi = (\partial_\mu - i g_W W_\mu - i g_H B_\mu)\, \phi \, , \tag{III.28}$$

The mass term in (III.24) is linear in the Higgs field and vanishes for $\phi = 0$. The left-handed fermions ψ_L in the Standard Model, leptons and quarks, couple to the weak isospin (fundamental representation) with weak isospin $\pm - 1/2$, while the right-handed fermions ψ_R do not couple (trivial representation) with weak isospin 0, that is for example

$$W_\mu \psi_R = 0 \, . \tag{III.29}$$

The related covariant derivative of the fermions reads

$$D_\mu \psi = (\partial_\mu - i g A_\mu - i g_W W_\mu - i g_H B_\mu)\, \psi \, . \tag{III.30}$$

The mass term $m(\phi)$ is linear in the Higgs field ϕ and hence constitues a Yukawa interaction. It relates to the Cabibbo-Kobayashi-Maskawa-Matrix (CKM) , and is not discussed in further details here. What is important in the present context, is, that a non-vanishing expectation value of the Higgs field, $\langle \phi \rangle = (0, \rho_0/\sqrt{2})$ provides mass terms for the weak gauge fields, the W, Z as well as for the (left-handed) quarks an leptons:

As in our $O(N)$-example in the previous section we expect spontaneous symmetry breaking in the scalar Higgs sector. The current masses of the leptons and quarks are then generated by the disappearance of the mass term for $\phi_0 \neq 0$. Since the structure of the full term is quite convoluted, we illustrate this at a simple example with one Dirac fermion ψ and a real scalar field σ. Then the Yukawa term reads in a mean field approximation

$$h \bar\psi \sigma \psi \xrightarrow{\text{mean field}} h\sigma_0 \, \bar\psi \psi \, , \tag{III.31}$$

with mass $m = h\sigma_0$ which is proportional to the vacuum expectation value of the scalar field (vacuum expectation value of the Higgs) and the Yukawa coupling h.

For the masses of the gauge field we cut a long story short and simply note that in a mean field analysis as that done above for the fermion

$$(W_\mu \phi)^\dagger (W_\mu \phi) \xrightarrow{\text{mean field}} (W_\mu \phi_0)^\dagger (W_\mu \phi_0) \, , \tag{III.32}$$

leads to mass terms for the gauge fields. Since the vacuum field ϕ_0 has vanishing upper component ϕ_1 it is a combination of the generator $t^3 = \sigma_3/2$ of the weak $SU(2)$ and the generator $\mathbb{1}$ of the hypercharge $U(1)$ which remains massless: the photon. This also determines the subgroup which leaves the vacuum invariant. The superficial analysis here also reveals that the quotient involves three generators and hence we have three Goldstone bosons. In summary we hence start with three gauge bosons with two physical polarisations each together with three Goldstone bosons, which adds up to nine field degrees of freedom (dof). A convenient reparameterisation (including an appropriate gauge fixing, e.g. the unitary gauge) of the Standard Model leads us to three massive vector bosons with three polarisations each, that is again nine dofs.

D. Low energy effective theories of QCD

The Higgs mechanism in the electroweak sector of the Standard Model leads to (current) quark masses for the up and down quark of a couple of MeVs, $(m_{u/d})_{\rm cur} \approx$ 2-5 MeV, see Table I. However, the masses of the nucleons, the protons and neutrons, is about 1 GeV (proton (uud) ≈ 938 MeV , neutron (udd) ≈ 940 MeV), that is two orders of magnitude bigger. In other words, the three constituent quarks in the nucleons must have an effective mass of about $(m_{u/d})_{\rm con} \approx$ 300-400 MeV, the constituent quark masses. We already infer from this that there should be a further mechanism to generate this mass scale.

In low energy QCD with its mass scale $\Lambda_{\rm QCD} \approx 200 - 300\,{\rm MeV}$, the electroweak sector of the Standard Model decouples as do the heavier quarks. We are left with two light (up and down) and one heavy quark (charm), Table I. Within fully quantitative computations of the QCD dynamics at low energies the strange quark with its current mass of about 1.2 GeV is also added. Still, its dynamics is very much suppressed at momentum scales of $\Lambda_{\rm QCD}$. For the present structural analysis we first resort to two flavour QCD ($N_f = 2$) with the Euclidean action

$$S_{\rm QCD}[\Phi] = \frac{1}{4}\int_x F^a_{\mu\nu}F^a_{\mu\nu} + \int_x \bar\psi \cdot (\not{D} + m_\psi - \mu\gamma_0)\cdot\psi\,, \tag{III.33}$$

where ψ is a Dirac spinor with two flavours and Φ is the two-flavour super field, see (I.35) and (I.36). The physics of the matter sector at low energies and temperatures, and not too large densities is well-described by quark-hadron models, the most prominent of which is the Nambu–Jona-Lasino model. From the perturbative point of view these models are seeded in the four-Fermi coupling already being generated from the propagators and couplings depicted in Figure 2 at tree level. The related one-loop diagram is depicted in Figure 6. It is built from one-gluon exchange tree level scatterings of quark–anti-quark pair into another one, which is highlighted in the red box in Figure 6. This t-channel process (in terms of the momentum routing the full one-loop diagram) has the structure

$$g^2\left(\bar\psi\gamma_\mu t^a\psi\right)(p)\left[\left(\delta_{\mu\nu} - (1-\xi)\frac{p_\mu p_\nu}{p^2}\right)\frac{1}{p^2}\right]\left(\bar\psi\gamma_\nu t^a\psi\right)(-p)\,, \tag{III.34}$$

with $t = p^2$. In (III.34) the t^a are generators of the color gauge group and the fermions are summed over the two flavours. The fermionic currents couple to each other via the exchange of a gluon with the classical gluon propagator in the square bracket, for the Feynman rules see Appendix A. In summary, (III.34) generates a four-Fermi interaction with a non-trivial momentum structure in the effective action of QCD.

The full momentum- and tensor structure is complicated even for the present simplified $N_f = 2$ case. As in the four-Fermi theory (Fermi theory) for weak interactions we resort to an approximation with point-like interactions (no momentum dependence). Then (III.34) can be rewritten in terms of an effective *local* (point-like) four-Fermi interaction. Such a rewriting in terms of local four-Fermi interactions holds for energies that are sufficiently low and do not resolve the large momentum structure of the scattering in (III.34). Moreover, the coupling is dimensionful and has the canonical momentum dimension -2 (related to the $1/p^2$ term in (III.34). In the Fermi theory of weak interactions this is the electroweak scale. In the present case it has to be related to the QCD mass gap proportional to $\Lambda_{\rm QCD}$.

We postpone the detailed analysis of this scale, and first concentrate on the tensor structure of (III.34). This is constrained by the symmetries of the theory, for a full discussion of the symmetry pattern we refer to the literature, e.g. [7, 8] and literature therein. Since the current masses of the light quarks are nearly vanishing we first work in the chiral limit. Then, any interaction that is generated by the dynamics of QCD carries chiral symmetry: the related four-Fermi interaction is chirally invariant, that is the invariance under the chiral transformations

$$\psi \to e^{i\frac{1\pm\gamma_5}{2}\alpha}\psi \quad\to\quad \bar\psi \to \bar\psi e^{i\frac{1\mp\gamma_5}{2}\alpha} \qquad \text{with} \qquad \gamma_5 = \gamma_0\gamma_1\gamma_2\gamma_3\,, \quad \text{and} \quad \{\gamma_5\,,\,\gamma_\mu\} = 0\,, \tag{III.35}$$

which holds separately for each vector current $\psi\gamma_\mu t^a\psi$. Furthermore, in the chiral limit QCD is invariant under flavour rotations $SU(N_f)$. For example, for $N_f = 2$ with up (u) and down (d) quarks and the flavour isospin group with $SU(2)$, the transformation reads

$$\psi = \begin{pmatrix} u \\ d \end{pmatrix} \to V\begin{pmatrix} u \\ d \end{pmatrix}\,, \qquad \text{with} \qquad V = e^{i\theta^a\tau^a} \in SU(2)\,, \tag{III.36}$$

with $a = 1, 2, 3$. For the 2+1 flavour case also considered here the respective symmetry is $SU(3)_F$. Chiral symmetry entails that the flavour rotations are a symmetry for the left- and right-handed quarks separately and the combined symmetry is $SU(2)_L \times SU(2)_R$ with symmetry transformations $V_{L/R} = e^{i\frac{1\pm\gamma_5}{2}\theta^a t^a}$. Including also the chiral $U(1)$

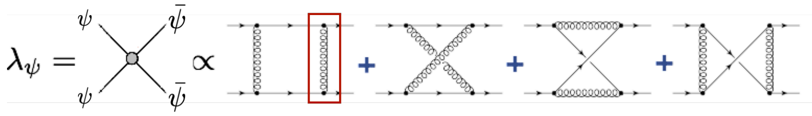

FIG. 6: One loop diagrams for the four-Fermi coupling λ_ψ in QCD.

rotations leads us to the full symmetry group

$$G_{\rm sym} = SU(N_c)\times SU(N_f)_V \times SU(N_f)_A \times U(1)_V \times U(1)_A\,, \tag{III.37}$$

where we have also taken into account the gauge group $SU(N_c)$. If we approximate (III.34) by a point-like four-Fermi interaction, one has to expand the tensor $\gamma_\mu \otimes \gamma_\nu$ multiplied by gauge group and flavour tensors. Then, the most general symmetric Ansatz is a combination of the tensor structures

$$\begin{aligned}(V-A) &= (\bar\psi\gamma^\mu\psi)^2 + (\bar\psi\gamma^\mu\gamma^5\psi)^2\\ (V+A) &= (\bar\psi\gamma^\mu\psi)^2 - (\bar\psi\gamma^\mu\gamma^5\psi)^2\\ (S-P) &= (\bar\psi^f\psi^g)^2 - (\bar\psi^f\gamma^5\psi^g)^2\\ (V-A)^{\rm adj} &= (\bar\psi\gamma^\mu t^a\psi)^2 + (\bar\psi\gamma^\mu\gamma^5 t^a\psi)^2\,,\end{aligned} \tag{III.38}$$

where f, g are flavour indices and $(\bar\psi^f\psi^g)^2 \equiv \bar\psi^f\psi^g\bar\psi^g\psi^f$. While each separate term in the tensors in (III.38) is invariant under gauge transformation, and under the flavour vector transformations, axial rotations in $SU(N_f)_A\times U(1)_A$ rotate the terms on the right hand side in (III.38) into each other. For a related full analysis we refer to the literature. However, below we shall exemplify these computations at the relevant example of the scalar–pseudo-scalar channel

The chiral invariants (III.38) can be rewritten using the Fierz transformations which relates different four-Fermi terms on the basis of the Grassmann natures of the fermions. These transformations are explained and detailed in the literature, see e.g. [7, 8]. Here we just concentrate on the scalar–pseudo-scalar channels in physical two-flavour QCD with $N_c = 3$ and $N_f = 2$. These channels are related to the scalar σ-meson and the pseudo-scalar pions $\vec\pi$. The $(S-P)$-channel is given by

$$(S-P) = \frac{1}{2}\left[(\bar\psi\psi)^2 + (\bar\psi\vec\tau\psi)^2 - (\bar\psi\gamma^5\psi)^2 - (\bar\psi\gamma^5\vec\tau\psi)^2\right]\,, \tag{III.39}$$

where $\vec\tau = (\sigma_1, \sigma_2, \sigma_3)$ with Pauli matrices

$$\sigma_1 = \begin{pmatrix} 0 & 1\\ 1 & 0\end{pmatrix}\,,\qquad \sigma_2 = \begin{pmatrix} 0 & -i\\ i & 0\end{pmatrix}\,,\qquad \sigma_3 = \begin{pmatrix} 1 & 0\\ 0 & -1\end{pmatrix}\,, \tag{III.40}$$

The representation (III.39) simplifies the identification of the scalar mode $\bar\psi\psi$ related to the scalar σ-meson, and the pseudo-scalar modes $\mathrm{i}\bar\psi\gamma_5\vec\tau\psi$ related to the pseudo-scalar (axial-scalar) pions $\vec\pi$.

We shall use the representation (III.39) in the following investigations of the chiral properties of low energy QCD. Hence we discuss its symmetry properties in more detail, and show explicitly its invariance under $G_{\rm sym}$. To begin with, the invariance of $(S-P)$ under gauge and flavour $U_V(1)$ transformation is apparent. The flavour $SU(2)_V$ transformations $\psi\to e^{i\theta^a\tau^a}\psi$ trivially leaves $\bar\psi\psi$ and $\bar\psi\gamma_5\psi$ invariant. For the vector and pseudo-vector bilinears we concentrate on infinitesimal transformations $e^{i\theta^a\tau^a} = 1 + i\theta^a\tau^a + O(\theta^2)$. Then the second term in (III.39) transforms as

$$(\bar\psi\vec\tau\psi)^2 \;\longrightarrow\; (\bar\psi\vec\tau\psi)^2 + 2i\,\theta^a(\bar\psi\vec\tau\psi)(\bar\psi[\vec\tau\,,\,\tau^a]\psi) = (\bar\psi\vec\tau\psi)^2 - 2\,\theta^a\epsilon^{bac}(\bar\psi\tau^b\psi)(\bar\psi\tau^c\psi) = (\bar\psi\vec\tau\psi)^2\,. \tag{III.41}$$

The invariance of the last term in (III.39) under $SU(2)_V$ transformations follows analogously. Finally, axial transformations related the first two terms to the last two terms. We exemplify this property with the axial $U_A(1)$ rotations $\psi\to e^{i\gamma_5\alpha}\psi$, where we consider infinitesimal transformations with $e^{i\gamma_5\alpha} = \mathbb{1} + i\gamma_5\alpha + O(\alpha^2)$. Concentrating on the scalar and pseudo-scalar terms we have

$$(\bar\psi\psi)^2 - (\bar\psi\gamma^5\psi)^2 \;\longrightarrow\; (\bar\psi\psi)^2 - (\bar\psi\gamma^5\psi)^2 + 4i\,\alpha\Big[(\bar\psi\psi)(\bar\psi\gamma_5\psi) - (\bar\psi\gamma^5\psi)(\bar\psi\psi)\Big] = (\bar\psi\psi)^2 - (\bar\psi\gamma^5\psi)^2\,, \tag{III.42}$$

The invariance for the full expression in (III.39) follows analogously. It is left to study $SU(2)_A$ transformations. Now we show that (III.39) also carries the $SU(2)_A$-invariance. To that end we consider infinitesimal $SU(2)_A$ transformations

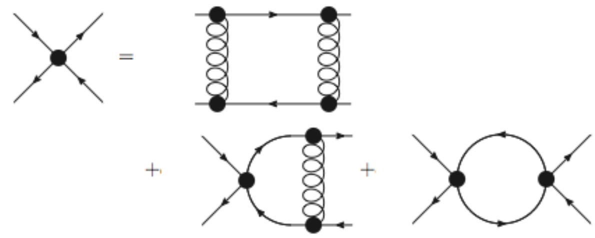

FIG. 7: One loop diagrams for the four-Fermi coupling λ_ψ from the action (III.50).

$e^{i\gamma_5\theta^a\tau^a} = 1 + i\gamma_5\theta^a\tau^a + O(\theta^2)$ of the combination $(\bar\psi\psi)^2 - (\bar\psi\gamma^5\vec\tau\psi)^2$, and use the Lie algebra identity

$$\tau^a\tau^b = \delta^{ab} + i\epsilon^{abc}\tau^c\,, \qquad \to \qquad \{\tau^a\,,\,\tau^b\} = 2\delta^{ab}\,. \tag{III.43}$$

Then we are led to

$$(\bar\psi\psi)^2 - (\bar\psi\gamma^5\vec\tau\psi)^2 \;\longrightarrow\; (\bar\psi\psi)^2 - (\bar\psi\gamma^5\vec\tau\psi)^2 + 2i\,\theta^a\Big[(\bar\psi\psi)(\bar\psi\gamma_5\tau^a\psi) - (\bar\psi\gamma^5\tau^b\psi)\left(\bar\psi\{\tau^a\,,\,\tau^b\}\psi\right)\Big] = (\bar\psi\psi)^2 - (\bar\psi\gamma^5\psi)^2\,. \tag{III.44}$$

The invariance of the combination $(\bar\psi\gamma_5\psi)^2 - (\bar\psi\vec\tau\psi)^2$ is shown along the same lines. Consequently (III.39) is invariant under $SU(2)_A$ transformation and hence under the full symmetry group $G_{\rm sym}$.

In QCD, we have experimental evidence for the breaking of the axial $U_A(1)$-symmetry, i.e. the pseudo-scalar η'-meson (in $N_f = 2$ the η) is anomalously heavy. This mass-difference can be nicely explained by the anomalous breaking of axial $U_A(1)$ symmetry. Consequently, giving up axial $U_A(1)$-symmetry we have to consider more four-Fermi interactions as in (III.38) (altogether 10 invariants for $N_f = 2$), in particular

$$\frac{1}{2}\left[(\bar\psi\psi)^2 - (\bar\psi\vec\tau\psi)^2 + (\bar\psi\gamma^5\psi)^2 - (\bar\psi\gamma^5\vec\tau\psi)^2\right]\,. \tag{III.45}$$

It is the relative minus signs in the scalar and pseudo-scalar terms in comparison to (III.39) that leads to the breaking of $U_A(1)$-symmetry. This is easily seen by re-doing the infinitesimal analysis (III.42) in (III.45). If also follows easily that the other symmetries still hold, in particular the $SU(2)_V \times SU_A(2)_A$ invariance follows as (III.45) contains the same $SU(2)_V \times SU_A(2)_A$-invariant combinations of four-quark terms as (III.39). Hence we conclude that the combination (III.45) only breaks $U_A(1)$-symmetry, and adding up the two channels (III.39) and (III.45) leads to the $U_A(1)$-breaking combination

$$\frac{1}{2}\left[(\bar\psi\psi)^2 - (\bar\psi\gamma^5\vec\tau\psi)^2\right]\,. \tag{III.46}$$

Equation (III.46) is invariant under the remaining symmetries $SU(N_c)\times SU(N_f)_V\times SU(N_f)_A\times U(1)_V$. This concludes our brief discussion of the global symmetries of QCD in the chiral limit.

In summary the following picture emerges: assume we perform a chain of scattering experiments of QCD/Standard Model starting at the electroweak scale ≈ 90 Gev towards the strong QCD scale $\Lambda_{\rm QCD}$. At each scale we can describe the quantum equations of motion and scattering experiments by a suitably chosen effective action $\Gamma[\phi]$. On the level of the path integral for QCD, (I.34), this is described by the Wilsonian idea of integrating out momentum modes above some momentum scale μ,

$$Z_\mu[J] = \int [{\rm d}\Phi]_{p^2\geq\mu^2}\, e^{-S_{\rm QCD}[\Phi]+\int_x J\cdot\Phi} \qquad \Rightarrow \qquad \text{Effective Action } \Gamma_\mu[\Phi]\,, \tag{III.47}$$

where the path integral measure only contains an integration over fields Φ_μ that are non-vanishing for $p^2 \geq \mu^2$: $\Phi_\mu(p^2 < \mu^2) \equiv 0$. After Legendre transformation this leads us to an effective action $\Gamma_\mu[\Phi]$ that only contains the quantum effects of scales larger than the running (RG) scale μ and serves as a classical action for the quantum effects with momentum scales $p^2 < \mu^2$. This effective action also carries the symmetries of the fundamental QCD action, as long as these symmetries are not (anomalously broken by quantum effects.

We know already from the perturbative renormalisation programme that this amounts to adjusting the (running) coupling in the (classical) action with the sliding (experimental) momentum scale. In such a Wilsonian setting this is very apparent. The running of the coupling comes from the loop diagrams that are evaluated at the momentum scale

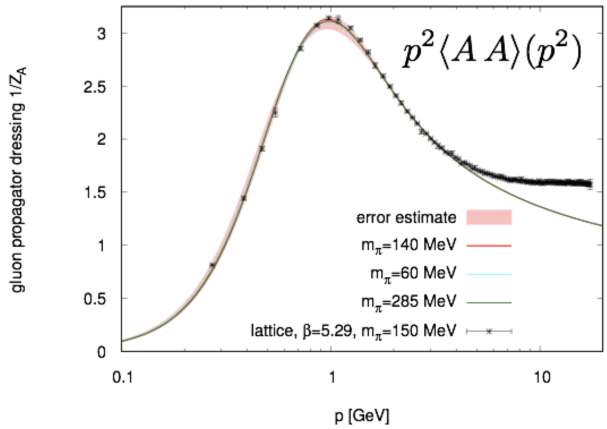

FIG. 8: Gluon propagator for $N_f = 2$ from the lattice and from non-perturbative diagrammatic methods, taken from [9].

μ. On top of this momentum adjustment of the fundamental parameters of the theory one also creates additional terms in the -effective- action. The one of importance for us is the four-Fermi terms argued for above. It is created at one-loop with the box diagrams depicted in depicted in Figure 6. This leads us finally to the following four-Fermi interaction in the effective action,

$$\Gamma_{4-\mathrm{fermi}}[\phi]|_{1-\mathrm{loop}} = -\frac{\lambda_\psi}{4}\int \left[(\bar\psi\psi)^2 - (\bar\psi\gamma^5\vec\tau\psi)^2\right] + \cdots \qquad \text{with} \qquad \lambda_\psi \propto \alpha_s^2\,, \tag{III.48}$$

where it is understood that the coupling λ_ψ carries the running momentum or RG scale μ introduced above. Together with the kinetic term of the quarks this is the classical action of the Nambu–Jona-Lasinio type model. Equation (III.48) holds for massless quarks and two flavours, $N_f = 2$. The two terms in (III.48) carry the same quantum number as the scalar and axial-scalar excitations in low energy QCD, the sigma-meson σ and pion $\vec\pi$ respectively. The one loop diagrams generating the four-Fermi coupling λ_ψ are depicted in Figure 6. In line with the picture outlined above the four-Fermi coupling λ_ψ at a given momentum scale $p = \mu$ should be computed with the loop momenta q in the box diagrams in Figure 6 being bigger than μ. Than the related diagram is peaked at this scale and we conclude by dimensional analysis that

$$\lambda_\psi(\mu) \simeq \alpha_s^2(\mu)\frac{1}{\mu^2}\,. \tag{III.49}$$

Note that this coupling feeds back into the loop expansion of other correlations functions such as the quark propagator and quark-gluon vertices. However, in comparison to other (one-loop) diagrams it is suppressed by additional orders of the strong coupling α_s. In turn, in the low momentum regime where α_s grows strong it gives potentially relevant contributions. Indeed, taking as a starting point for a loop analysis the sum of the QCD action (III.33) and the four-Fermi term (III.48)

$$\Gamma[\phi] \simeq S_{\mathrm{QCD}}[\phi] + \Gamma_{4-\mathrm{fermi}}[\phi]\,, \tag{III.50}$$

we get also self-interaction terms of the four-Fermi coupling proportional to λ_ψ^2 as well as terms proportional to $\alpha_s\lambda_\psi$. This is depicted in Figure 7.

The glue sector of QCD is expected to have a mass gap already present in the purely gluonic theory, related to the confinement property of Yang-Mills theory. Then this has to manifest itself in a decoupling of the gluonic contribution to the four-Fermi coupling in Figure 7. In the Landau gauge this mechanism is easily visible due to the mass gap in the gluon propagators, see Figure 8 for lattice results and results from non-perturbative diagrammatic methods.

Note that the gluon propagator is gauge dependent, and the careful statement is that the Landau gauge facilitates the access to the related physics. One should not confuse this with a massive gluon, as the gluon is no physical particle and shows positivity violation. Moreover, the gluonic sector is certainly relevant for the confining physics and hence the decoupling discussed above only takes place in the matter sector for the specific question under investigation, the mechanism of strong chiral symmetry breaking.

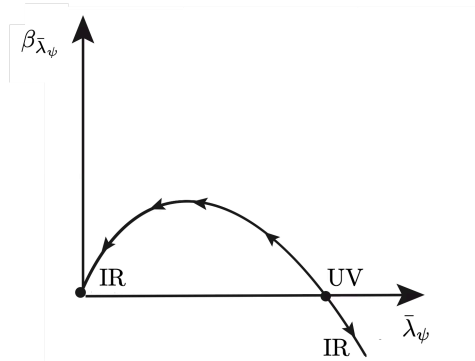

FIG. 9: Sketch of the β-function of the dimensionless four-quark coupling $\bar\lambda_\psi$ in NJL-type models.

E. Strong chiral symmetry breaking and quark-hadron effective theories

Assuming for the moment the gluonic decoupling we are left with a purely fermionic theory. The four-Fermi term (III.48) is the interaction part of the Nambu–Jona-Lasino model, one of the best-studied model for low energy QCD, see e.g. [7, 8, 10]. It is non-renormalisable as can be seen from the momentum dimension of the four-Fermi coupling which is -2. As shown above, in QCD it is generated by fluctuations with $\lambda_\psi(p) \propto \alpha_s(p)$ and tends to zero in the UV, that is for large momenta $p \to \infty$. Its momentum dependence is best extracted from the dimensionless coupling

$$\bar\lambda_\psi = \lambda_\psi(\mu)\mu^2\,, \tag{III.51}$$

where we have introduced the renormalisation group scale μ, here being identical with the momentum scale of the scattering process described, $\mu^2 = p^2$. The β-function of the dimensionless four-Fermi coupling in (III.51) is given by

$$\beta_{\bar\lambda_\psi} = \mu\partial_\mu \bar\lambda_\psi = 2\bar\lambda_\psi - A\,\bar\lambda_\psi^2 \qquad \text{with} \qquad A > 0\,, \tag{III.52}$$

and is depicted in Figure 9. The prefactor A depends on the RG-scale μ as well as other parameters of the theory such as the masses. The full RG equation for the four-quark coupling in QCD is depicted in Figure 11 and its analysis will be done in Section III F. Here we concentrate on the underlying mechanism of chiral symmetry breaking. The first term on the right hand side of (III.52) encodes the trivial dimensional running of $\bar\lambda_\psi$. The second term on the right hand side originates in the last diagram in Figure 7, the pure four-Fermi term. In the absense of other mass scales this loop has to be proportional to μ^2 leading to a factor two in the β-function in comparison to the loop itself. The key feature relevant for the description of chiral symmetry breaking is the sign of the diagram. It is negative, $-A\bar\lambda^2$, with a positive constant A leading to (III.52).

From the perspective of a one-loop investigation based on the classical fermionic action in (III.50) the coupling in the loop term on the right hand side of (III.52) is the classical one in this action. As we have done for the β-function of the strong coupling, e.g. (II.17), we can elevate this coupling to the full running coupling in terms of a one-loop RG-improvement. This accounts for a one-loop resummation of diagrams. In the present context the physics behind such an improvement is very apparent: As already indicated, the NJL-type action was derived within a successive integrating out of momentum modes, and constitutes an effective action for the UV physics with $p^2 \geq \mu^2$. Accordingly, its couplings depend on this RG-scale. In summary we end up with (III.52) with μ-dependen couplings on the right hand side. Note that this is only a one-loop RG improvement as we have discarded the μ-dependence of the couplings in the diagram when taking the μ-derivative. The related terms are proportional to $-A/2\,\bar\lambda_\psi\,\mu\partial_\mu\bar\lambda_\psi$ and can be shuffled to the left hand side. This accounts for a further resummation leading to (III.52) with a global factor $1/(1 + A/2\,\bar\lambda)$ on the right hand side. In the following qualitative analysis it is dropped and we strictly resort to the one-loop improvement.

The β-function of (III.52) is depicted in Figure 9. It divides the positive $\bar\lambda_\psi$-axis into two physically distinct regimes,

$$I_1 = [0, \bar\lambda_{\rm UV}) \qquad \text{and} \qquad I_2 = (\bar\lambda_{\rm UV}, \infty) \qquad \text{with} \qquad \beta_{\bar\lambda_\psi}(\bar\lambda_{\rm UV}) = 0 \qquad \text{with} \qquad \bar\lambda_{\rm UV} = \frac{2}{A}\,. \tag{III.53}$$

The zeroes of the β-function are fixed points of the renormalisation group flows, and $\bar\lambda_{\rm UV} \neq 0$ is a non-trivial fixed point FP of the β-function while $\bar\lambda_{\text{Gauß}} = 0$ is the trivial Gaußian fixed point (related to the free Gaußian theory). Now we initiate the RG-flow at an initial ultraviolet scale μ_{in} with some value of the dimensionless four-quark coupling

$$\bar\lambda_\psi(\mu_{\,\text{in}}) = \bar\lambda_{\psi,\,\text{in}}\,. \tag{III.54}$$

If $\bar\lambda_{\psi,\,\text{in}} < \bar\lambda_{\text{UV}}$ and we lower the running momentum scale, the RG-flow lowers the four-Fermi coupling towards 0. Accordingly $\bar\lambda_\psi(\mu\to 0)=0$. Since the regime of small couplings is governed by the linear term $2\bar\lambda_\psi$ in the β-function in (III.52) this entails $\lambda_\psi(\mu\to 0)=\lambda_0$. Here λ_0 is some finite value which is adjusted by the input $\bar\lambda_{\psi,\text{in}}$ at the initial scale μ_{in}.

In turn, if $\bar\lambda_{\psi,\,\text{in}} > \bar\lambda_{\text{UV}}$, the RG-flow toward smaller μ drives $\bar\lambda_\psi$ towards ∞. Then the linear term can be neglected as it is sub-leading and the RG-flow reads

$$\mu\partial_\mu\bar\lambda_\psi = -A\,\bar\lambda_\psi^2\,, \qquad \longrightarrow \qquad \bar\lambda_\psi(\mu) = \frac{\bar\lambda(\mu_0)}{1+\bar\lambda_\psi(\mu_0)A\,\log\mu/\mu_0}\,, \tag{III.55}$$

where μ_0 is some reference scale at which the approximation in the RG-flow in (III.55) is already valid. We conclude from (III.55) diverges at

$$\mu = \mu_0\exp\left\{-\frac{1}{A\,\bar\lambda(\mu_0)}\right\}\,, \tag{III.56}$$

which signals a resonance in the four-quark scalar-pseudo–scalar channel with the quantum numbers of the σ- mode and the pion.

At this scale chiral symmetry breaking occurs. To make this more apparent we resort to a further rewriting of our low energy effective theory in terms of the scalar, σ, and pseudo-scalar, $\vec\pi$, degrees of freedom. This is suggestive already for the reason that the divergence in (III.55) entails that these resonance are relevant degrees of freedom for lower momentum scales. For the rewriting of the theory we use the Hubbard-Stratonovich transformation, see e.g. [7, 8, 10]. With this transformation we a four-Fermi interaction using a scalar auxiliary field. Concentrating on the scalar part of the four-Fermi interaction in (III.48) we write at some momentum scale μ,

$$-\frac{\lambda_\psi}{4}(\bar\psi\psi)^2 = \left[\frac{h}{2}(\bar\psi\psi)\sigma + \frac{m_\varphi^2}{2}\sigma^2\right]_{\text{EoM}(\sigma)}\,, \qquad \text{with} \qquad \lambda_\psi = \frac{h^2}{m_\varphi^2}\,. \tag{III.57}$$

Accordingly we can extend the effective action $\Gamma[\phi]$ given in (III.50) by the right hand side of (III.57) while dropping the four-Fermi term. For the sake of simplicity we concentrate on the σ-meson first and reduce the four-Fermi term to its scalar part. Then

$$\Gamma[\phi]\to\Gamma[\phi,\sigma] = \Gamma[\phi]|_{\lambda_\psi\to 0} + \left[\frac{h}{2}(\bar\psi\psi)\sigma + \frac{m^2}{2}\sigma^2\right]_{h^2/m^2=\lambda_\psi}\,, \tag{III.58}$$

This new effective action agrees with the original one on the equation of motion of σ and hence carries the same physics. As a side remark, note that the 1PI correlation functions of quarks and gluon derived from $\Gamma[\phi,\sigma]$ at fixed σ do not agree with the quark and gluon correlation functions derived from $\Gamma[\phi]=\Gamma[\phi,\sigma_{\text{EoM}}(\phi)]$, the implicit dependences also contribute.

A similar derivation can be done for the pion part of the four-Fermi interaction, and hence the whole four-Fermi interaction can be bosonised. The mesonic equations of motion can be summarised in

$$\sigma_{\text{EoM}} = \frac{h}{2m_\varphi^2}\,\bar\psi\psi\,, \qquad\qquad \vec\pi_{\text{EoM}} = \frac{h}{2m_\varphi^2}\,\bar\psi\, i\gamma_5\vec\tau\psi\,. \tag{III.59}$$

On the level of the generating functional of QCD, (III.57) and its extension to pions can be implemented by a Gaußian path integral with

$$\exp\left\{\frac{\lambda_\psi}{4}\int\left[(\bar\psi\psi)^2-(\bar\psi\gamma^5\vec\tau\psi)^2\right]\right\} = \int \mathrm{d}\sigma\mathrm{d}\vec\pi\,\exp\left\{-\int_x\left(\frac{1}{2}m^2(\sigma^2+\vec\pi^2)+\frac{h}{2}\bar\psi\left[\sigma+i\gamma_5\vec\tau\vec\pi\right]\psi\right)\right\}_{h^2/m^2=\lambda_\psi}\,. \tag{III.60}$$

We also remark that as shift in the σ-field,

$$\sigma \to -\frac{2}{h} m_\psi + \sigma\,, \tag{III.61}$$

eliminates the quark mass term at the expense of the linear term in σ that can be interpreted as a source term. Inserting this identity in the path integral for the low energy dofs including the currents for the fundamental fields, the quarks and gluons (and ghosts) as well as current for the mesonic dofs we have the full generating functional in this setting. Performing the Legendre transformation we are immediately led to (III.58). Kinetic terms as well as a potential for σ are generated by further quantum effects. In summary this leads us finally to a low energy effective theory with a classical action $S_{\text{eff}} = \Gamma_{\text{UV}}$, where Γ_{UV} is the full quantum effective action including quantum fluctuations above a given cutoff scale Λ. This also entails that S_{eff} carries a Λ-dependence. S_{eff} is given by

$$S_{\text{eff}}[\psi,\bar\psi,\phi] \propto \int_x \bar\psi\cdot(\not{D}+m_\psi)\cdot\psi + \int_x \left[(\partial_\mu\sigma)^2+(\partial_\mu\vec\pi)^2\right] + \int_x \frac{h}{2}\bar\psi\left[\sigma+i\gamma_5\vec\tau\vec\pi\right]\psi + \int_x V_{\text{UV}}(\rho) \tag{III.62}$$

with $\phi = \ (\sigma,\vec\pi)$ and

$$V_{\text{UV}}(\rho) = m_\varphi^2\rho + \frac{\lambda}{2}\rho^2\,, \qquad \text{with} \qquad \rho = \frac{1}{2}\left(\sigma^2+\vec\pi^2\right)\,. \tag{III.63}$$

As indicated above, the quark mass term can be eliminated at the expense of a linear term in σ by the shift of σ in (III.61). On the level of the quadratic quark-meson interaction (III.60) this triggers a linear term $c_\sigma\sigma$ and the full potential reads

$$V_{\text{UV}}(\rho) = m_\varphi^2\rho + \frac{\lambda_\varphi}{2}\rho^2 - c_\sigma\,\sigma\,, \qquad \text{with} \qquad c_\sigma = \frac{2}{h}m_\varphi^2 m_\psi\,. \tag{III.64}$$

This concludes the derivation of the low energy effective theory with the action (III.62) from QCD by *integrating-out* QCD quantum fluctuations above the validity scale of the low energy effective theory. From the gluonic decoupling scale $\Lambda_{\text{dec}} \lesssim 1$ GeV one concludes that (III.62) should be seen as a classical action for quantum fluctuations with momenta $p^2 \lesssim 1$ GeV, see Figure 8. A more detailed analysis reveals that the initial scale for low energy effective theories has to be taken far lower for quantitative computations. Nonetheless, for qualitative considerations it is sufficient, and, as a matter of fact, low energy effective theories even work well quantitatively at surprisingly large moment scale about 1 GeV.

In (III.62) we have introduced a self-interaction of the mesonic fields proportional to ρ^2 as well as an explicit breaking term linear in σ related to the quark mass term. The question arises, is this the most general ϕ^4-term one can generate from QCD? As mentioned before, the symmetries of this low energy effective field theory (EFT) are determined by those of the action of QCD. In the chiral limit the full symmetry group is (III.37). The axial $U_A(1)$ symmetry is anomalously broken, hence our restriction to the $U_A(1)$-breaking combination (III.46). In its bosonised quark-meson mode version the symmetry transformations with G_{sym} also involve transformations of the mesonic fields. Their transformation properties can be most easily accessed in the matrix notation for the field. To that end we introduce

$$\hat\phi = \mathbb{1}\,\sigma + i\gamma_5\vec\tau\vec\pi \qquad \text{with} \qquad \hat\phi_{\text{EoM}} = \frac{h}{2m_\varphi^2}\left(\mathbb{1}\,\bar\psi\psi - \gamma_5\vec\tau\,\bar\psi\gamma_5\vec\tau\psi\right)\,, \tag{III.65}$$

where we have used (III.59) in the second equation. Now we can read-off the symmetry transformations under $V\in SU(N_c)\times SU(N_f)_V\times SU(N_f)_A\times U(1)_V$ from (III.65) by evoking the symmetry transformations of the quarks. One easily sees that axial $U(1)_A$-rotations do not close on σ and $\vec\pi$. For example, σ_{EoM} transforms into $\bar\psi\gamma_5\psi$. Furthermore, ϕ is invariant under vector $U_V(1)$ transformations. Similarly, σ is invariant under transformations with $e^{i\theta^a\tau^a}\in SU(2)_V$, while π is rotated, $\vec\pi\to V\vec\pi$ with $V=e^{\theta^a t^a}\in O(3)$ with $(t^a)^{bc}=\epsilon^{abc}$. This follows from

$$\bar\psi\gamma_5\vec\tau\psi \;\longrightarrow\; \bar\psi\gamma_5\vec\tau\psi + i\theta^a\bar\psi\gamma_5[\vec\tau\,,\,\tau^a]\psi = \bar\psi\gamma_5\vec\tau\psi - \theta^a\epsilon^{bac}\bar\psi\gamma_5\tau^c\psi\,. \tag{III.66}$$

Finally, transformations with $e^{i\gamma_5\theta^a\tau^a}\in SU(2)_A$ rotate $(\sigma,\vec\pi)$ into each other. This is read-off from the infinitesimal transformations of $\hat\phi_{\text{EoM}}$ leading to

$$\sigma\to\sigma+2\theta^a\pi^a\,, \qquad\qquad \pi^b\to\pi^b-\theta^b\sigma\,. \tag{III.67}$$

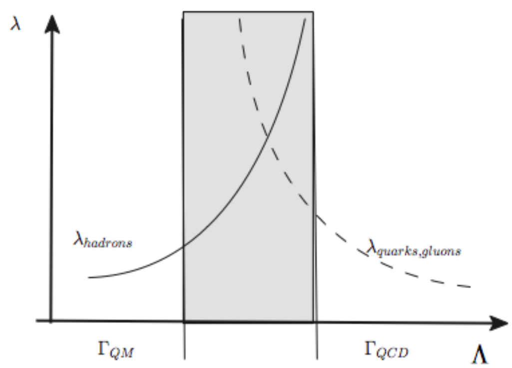

FIG. 10: Scale dependence of the effective four-Fermi coupling. The shaded area is the regime where the effective field theory is triggered.

Combining all the manifestations of the symmetry group we are led to an $O(4)$ invariance of our low energy effective field theory, sloppily written as

$$\psi \to V\psi \quad \text{with} \quad V \in G_{\text{sym}}/U_A(1)\,, \qquad \phi \to e^{\theta^a t^a}\phi\,, \qquad \text{with} \quad \phi = \begin{pmatrix} \vec{\pi} \\ \sigma \end{pmatrix} \quad \text{and} \quad e^{\theta^a t^a} \in O(4)\,. \tag{III.68}$$

In conclusion chiral symmetry breaking is in one-to-one correspondence to the breaking of the $O(4)$-symmetry. Moreover, the formulation with effective mesonic σ and pion degrees of freedom now allows us to discuss strong chiral symmetry breaking in complete analogy to the Higgs mechanism that served as an introductory example. Let us first consider the fully symmetric case with $c_\sigma = 0$. The mesonic sector of (III.62) simply is an $O(4)$-model, and the QCD four-Fermi coupling are related to the Yukawa coupling and the mesonic mass parameters via the relation (III.57) in the Hubbard-Stratonovich transformation. Accordingly, a diverging λ_ψ implies a vanishing m_φ if the Yukawa coupling is fixed. Hence, at the singularity of λ_ψ the mesonic mass parameter m_φ^2 changes sign. For $m_\varphi^2 < 0$ we are in the phase of -spontaneously- broken $O(4)$-symmetry. We choose the σ direction as our radial mode, and its expectation value is given by

$$\sigma_0 = \sqrt{\frac{-m_\varphi^2}{\lambda_\varphi}}\,, \tag{III.69}$$

in the chiral limit. This leads to an effective quark mass term with

$$m_\psi = \frac{h}{2}\sigma_0 = \frac{h}{2}\sqrt{\frac{-m_\varphi^2}{\lambda_\varphi}}\,, \tag{III.70}$$

which in QCD is of the order of 300 MeV.

In summary we have derivated low energy EFTs in QCD by successively integrating out momentum shells of quantum fluctuations in QCD. The first class of low energy EFTS we encountered are the *Nambu-Jona–Lasigno type four-quark models* (in short in a slight abuse of notation NJL-model), baptised after a seminal work of Nambu and Jona-Lasigno from 1961 introducing a four-Fermi model for Nucleons. NJL-type models are not renormalisable and requires a ultraviolet cutoff scale Λ_{UV} that cannot be removed.

In a second step we have bosonised the resonant scalar–pseudo-scalar channels of the four-quark interaction leading us to a Yukawa-type model, the *Quark-Meson Model* (QM-model). This model is renormalisable and its UV cutoff Λ_{UV} seemingly can be removed to infinity. However, we emphasise that the two models are equivalent on the level of the respective path integrals via the Hubbard-Stratonovich transformation. In other words, if one considers all quantum fluctuations in both models the physics results are the same, as must be the necessity of a ultraviolet cutoff scale Λ_{UV}. In the QM model this necessity is encoded in a UV-instability of the model. In other words, its renormalisability is of no help if it comes to the existence of the model at large scales.

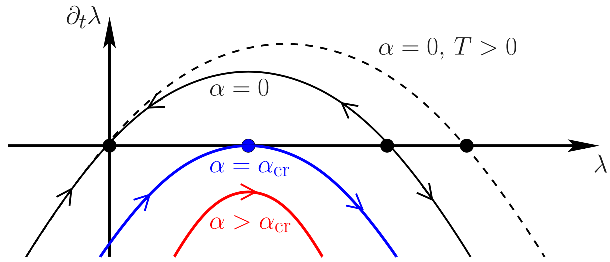

FIG. 11: Flow $\partial_t\bar\lambda_q$ of the dimensionless four-quark coupling $\bar\lambda_\psi = \lambda_\psi k^2$ in the scalar-pseudoscalar channel as a function of the four-quark coupling for different values of the strong couplings α_s. If the strong coupling is large enough, $\alpha_s > \alpha_{s,\rm cr}$ with the critical coupling $\alpha_{s,\rm cr}$, the flow is negative for all $\bar\lambda_q$. Then, chiral symmetry breaking happens for all initial values of $\bar\lambda_\psi$, for more details see the discussion below(III.71).

F. Chiral symmetry breaking in QCD

In the last Chapters we have derived low energy effective theories of QCD that capture chiral symmetry breaking in terms of the respective initial condition for the four-quark coupling at the UV-scale $\Lambda \propto 1\,\text{GeV}$ of these models. It is left to analyse how QCD triggers the respective symmetry-breaking four-quark couplings. For this analysis we extend the renormalisation group analysis of the four-quark coupling on the basis of (III.52) to that in full QCD. The respective RG-equation can be derived from the diagrammatic form of the four-quark coupling, its sketch has been provided in 7. In contradistinction to (III.52) the full β-function has two further terms, one is proportional to α_s^2 with $\alpha_s = g_s^2/(4\pi)$. It is given by $-C\,\alpha^2$ with a positive prefactor C and comprises the contributions of the quark-gluon box diagrams in (III.52), see also 6. These diagrams generate the four-quark coupling at large momentum scales in the first place. A further contribution comes from the mixed diagram in 7 with one gluon exchange and one four-quark coupling. Accordingly it is proportional to $\alpha_s\lambda_\psi$, and is given by -$B\,\alpha_s\bar\lambda_\psi$ with a positive prefactor B . In summary this leaves us with the full RG-equation for the dimensionless four-quark interaction $\bar\lambda_\psi$ in the scalar–pseudoscalar channel, schematically given by

$$\beta_{\bar\lambda_\psi} = 2\bar\lambda_\psi - A\,\bar\lambda_\psi^2 - B\bar\lambda_\psi\alpha_s - C\,\alpha_s^2 + \text{tadpole-terms}\,, \tag{III.71}$$

and the positive constants A, B, C depend on other parameters of the theory, and in particular on the mass scales. It is depicted in Figure 11. In (III.71), $2\bar\lambda_\psi$ is the canonical scaling term and the other terms are quantum corrections computed from the respective diagrams in the flow. For $\alpha_s = 0$, the β-function in(III.71) reduces to that of the four-quark coupling in an NJL-type model, (III.52). Then, for large enough initial coupling $\bar\lambda_\psi(\mu = \Lambda) > 2/A(\Lambda)$ at the UV cutoff scale Λ, the β-function $\partial_t\bar\lambda_\psi$ is negative and the coupling grows towards the infrared. It finally diverges at a pole that signals chiral symmetry breaking. In turn, for $\bar\lambda_\psi(\mu = \Lambda) < 2/A(\Lambda)$ the coupling weakens towards the infrared and runs into the Gaußian fixed point without chiral symmetry breaking.

When switching on the strong coupling, the β-function of the four-quark coupling in(III.71) is deformed: Firstly, the canonical running gets an anomalous part with $2\bar\lambda_\psi \to (2 - B\,\alpha_s)\bar\lambda_\psi$. More importantly the whole β-function is shifted down globally by $-C\,\alpha_s^2$, see Figure 11. This term originates from quark-gluon box diagrams and is negative. For large enough α_s the β-function $\beta_{\bar\lambda_\psi}$ is negative for all $\bar\lambda_\psi$,

$$\partial_t\bar\lambda_\psi < 0 \quad \forall\bar\lambda \quad \text{if} \quad \alpha_s > \alpha_{s,\rm cr}\,, \qquad \text{with} \qquad \alpha_{s,\rm cr} = \frac{2}{B + 2\sqrt{A\,C}}\,, \tag{III.72}$$

with the critical coupling $\alpha_{s,\rm cr}$, see Figure 11. Accordingly, if the growth of the strong coupling towards the infrared is unlimited, chiral symmetry breaking in QCD is always present, and is basically the converse of asymptotic freedom. More precisely it is the one-gluon exchange coupling in the quark-gluon box diagrams that has to satisfy(III.72) in the infrared. In this context it is important to mention that it is the gapping of the gluon depicted in Figure 8 related to confinement that stops the growth of the exchange couplings in the infrared and even leads to their decay for small momenta. In short, the glue dynamics decouples below momenta of one GeV, leaving us with the quark-hadron dynamics.

Moreover, the simple relation between the size of the strong coupling and chiral symmetry breaking also provides a simple explanation for the restoration at finite temperature, which we already add here as a sneak preview: the strong coupling melts down and finally we have $\alpha_s < \alpha_{s,\rm cr}$ for all frequencies and momenta, and spontaneous chiral symmetry breaking cannot happen any more.

In summary, the analyses in the last Chapters have revealed, how dynamical chiral symmetry breaking occurs in QCD and the glue dynamic decouples in the infrared, and the dynamics of low energy QCD is well-described with the low energy effective theories introduced before. Despite being low energy EFTs, these models have a complicated dynamics reflecting the strongly-correlated nature of low energy QCD. Hence, typically one resorts to approximations within these models. In the reminder of this chapter we shall discuss different approximations to the Quark-Meson model ranging from a mean-field treatment to a full non-perturbative renormalisation group study.

G. Low energy quantum fluctuations

In the last chapter we have derived the action of the QM-model by integrating out quantum fluctuations above a momentum scale $\Lambda \approx 1$ GeV. We have argued that below this scale the gluonic degrees of freedom become less important and decouple from the theory below the mass gap of QCD. Practically, this can be seen from the results for gluonic correlation functions such as the gluon propagator displayed in Figure 8. This entails that the action (III.62) serves as a classical action for the quantum fluctuations with momenta $p^2 \leq \Lambda^2$. More explicitly we use the definition (III.47) with $\mu = \Lambda$ and arrive at the path integral

$$Z \approx \int [d\phi\, d\psi d\bar\psi]_{p^2\leq\Lambda^2} e^{-S_{\text{eff},\Lambda}[\psi_<,\bar\psi_<,\phi_<]} \qquad \text{with} \qquad Z_\Lambda \simeq e^{-S_{\text{eff},\Lambda}}\,, \tag{III.73}$$

where we have dropped the source terms. The fields $\psi_<, \bar\psi_<, \phi_<$ only carry low momentum modes with momenta $p^2 < \Lambda^2$. Then the full quark field $\psi = \psi_< + \psi_>$ is a sum of $\psi_< = \psi_{p^2\geq\mu^2}$ and $\psi_> = \psi_{p^2\geq\mu^2}$. Note also that the path integral of the large momentum modes in (III.47) is performed in the presence of fields that also carry low momentum contributions,

$$Z_\Lambda[\psi_<,\bar\psi_<,\phi_<] = \int [\mathrm{d}\Phi]_{p^2\geq\mu^2}\, e^{-S[\phi,\Phi]}\,. \tag{III.74}$$

where S is the QCD action with a bosonised scalar–pseudo-scalar channel. Equation (III.73) is approximate as we do not integrate out the low momentum gluons. Therefore low energy quantum effects with momentum scales $p^2 \leq \Lambda$ are encoded in loop diagrams with the classical action $S_{\text{eff},\Lambda} \simeq \Gamma_\Lambda$ defined in (III.62). Here, Γ_Λ is the effective action that originates in the integrating-out of QCD fluctuations with momenta $p^2 \geq \Lambda^2$. Henceforth we drop the supscripts $_{<,>}$ for the sake of readability.

As we have seen at the end of the last chapter, the coupling parameters in the mesonic potential play a crucial rôle for chiral symmetry breaking. Here we compute the one-loop correction to the 'classical' potential V in (III.64) as well as studying its the renormalisation group or flow equation.

1. *Quark quantum fluctuations*

First we note that the quark path integral in (III.73) with the action $S_{\text{eff},\Lambda}$ in (III.62) is Gaußian, and hence the one-loop computation is exact. This leads to the following representation of (III.73),

$$Z \approx \int\int [d\phi]_{p^2\leq\Lambda^2} e^{-S_{\phi,\text{eff},\Lambda}[\phi]}\,, \tag{III.75}$$

with

$$S_{\phi,\text{eff},\Lambda}[\phi] = \int_x \left[(\partial_\mu\sigma)^2 + (\partial_\mu\vec\pi)^2\right] + \int_x V_{\text{UV}}(\rho) - \ln\left[\frac{1}{\mathcal{N}}\int [d\psi d\bar\psi]_{p^2\leq\Lambda^2} e^{-\int_x \bar\psi\cdot\left(\not{D} + m_\psi\right)\cdot\psi + \int_x \frac{h}{2}\bar\psi[\sigma + i\gamma_5\vec\tau\vec\pi]\psi}\right]\,, \tag{III.76}$$

where $1/\mathcal{N}$ is an appropriate, field-independent normalisation specified later. The quark path integral can be rewritten as follows,

$$\frac{1}{\mathcal{N}}\int [d\psi d\bar\psi]_{p^2\leq\Lambda^2}\, e^{-\int_x \bar\psi\cdot\left(\not{D} + \frac{h}{2}[\sigma + i\gamma_5\vec\tau\vec\pi]\right)\cdot\psi} = \frac{1}{\mathcal{N}} \det{}_\Lambda \left(\not{D} + \frac{h}{2}\left[\sigma + i\gamma_5\vec\tau\vec\pi\right]\right)\,, \tag{III.77}$$

where $\det_\Lambda$ is the determinant from momentum modes with $p^2 \leq \Lambda^2$. Expanded in powers of the field, the logarithm of (III.77) adds to the kinetic term in (III.76) as well as to the potential V. It also leads to terms with higher order derivatives or derivative couplings such as $Z(\rho)(\partial_\mu\phi)^2$, $(\phi\Delta\phi)^2$. As we work at low energies we drop these terms in the spirit of an expansion in p^2/m^2_{gap} where m^2_{gap} is the lowest mass scale in QCD. Evidently the pion plays a special role as is has a very small mass in comparison to the QCD mass scale Λ_{QCD} The mass scales m_{had} of all other hadronic low energy degrees of freedom in QCD satisfy $m_{\text{had}} \gtrsim \Lambda_{\text{QCD}}$. Accordingly the pion carries the quantum fluctuations in QCD for scales below Λ_{QCD}. These scale considerations are also behind the impressively successful framework of chiral perturbation theory. In summary at leading order the low energy effective action $S_{\phi,\text{eff}}$ only changes to $V_{\text{UV}} \to V_{\phi,\text{eff}}$,

$$V_{\phi,\text{eff}}(\rho) = V_{\text{UV}}(\rho) + \Delta V_q(\rho)\,, \tag{III.78}$$

with

$$\Delta V_q(\rho) = -\text{Tr}_\Lambda \ln\left(\not{D} + \frac{h}{2}\left[\sigma + i\gamma_5\vec{\tau}\vec{\pi}\right]\right) + \ln\mathcal{N}\,, \qquad\qquad V_{\text{UV}}(\rho) = m^2_\varphi \rho + \frac{\lambda_\varphi}{2}\rho^2\,. \tag{III.79}$$

In (III.79) we have used that for a given operator $\mathcal{O}$ we have $\ln\det_\Lambda \mathcal{O} = \text{Tr}_\Lambda \ln\mathcal{O}$, where the trace sums over momenta with $p^2 \leq \Lambda^2$, as well as Dirac and internal indices, and the 'classical' potential V defined in (III.63). For the present considerations and scales the gluonic fluctuations and background are irrelevant. Thus we have dropped the gluonic fluctuations and we also put the gauge field to zero, $A_\mu = 0$. At finite temperature and density we also will consider constant temporal backgrounds $A_0 \neq 0$ which is related to so-called *statistical confinement*. Finally we introduce a convenient choice for the normalisation $\ln\mathcal{N}$: the quark determinant at vanishing background,

$$\ln\mathcal{N} \simeq \frac{1}{2}\text{Tr}_\Lambda \ln\left(-\not{\partial}^2\right)\,, \tag{III.80}$$

where we have rewritten the determinant in terms of the positive semi-definite Laplace operator $-\not{\partial}^2 = -\partial_\mu^2$. Due to the symmetry analysis performed above the fermionic determinant can only depend on the $O(4)$-invariant combination $\rho = 1/2(\sigma^2 + \vec{\pi}^2)$, and we can simplify the computation by using $\vec{\pi} \equiv 0$. In momentum space we have

$$\begin{aligned} V_{\phi,\text{eff}}(\sigma^2/2) &= V_{\text{UV}}(\sigma^2/2) - N_f N_c \int \frac{d\Omega_4}{(2\pi)^4}\int_0^\Lambda dp\, p^3\, \text{tr}_{\text{Dirac}} \ln\frac{i\not{p} + \frac{h}{2}\sigma}{i\not{p}} \\ &= V_{\text{UV}}(\sigma^2/2) - \frac{6}{\pi^2}\int_0^\Lambda dp\, p^3 \ln\frac{p^2 + \frac{h^2}{4}\sigma^2}{p^2}\,, \end{aligned} \tag{III.81}$$

where $\int d\Omega_4 = 2\pi^2$ is the four-dimensional angular integration. The prefactor $N_f N_c = 6$ in the middle part in (III.81) results from the trace over flavour and colour space. The Dirac trace gives a factor 4, while the momentum symmetrisation with $p \to -p$ provides a factor $1/2$. The denominators in (III.81) take care of the normalisation (III.80). Note also that up to these prefactors (III.81) is nothing but the Coleman-Weinberg potential of a φ^4-theory with interaction $\lambda/4!\,\varphi^2$ where we substitute $\lambda\,\varphi^2 \to h^2\,\rho$. We have an important relative minus sign due to the fermion loop and a symmetry factor $4N_f N_c = 24$ due to the number of degrees of freedom. We simply could take over this well-known result, for a detailed discussion see e.g. Chapter 11.2 in the QFT I+II lecture notes from 2022/23 .

For its importance we recall the computation here, and also discuss some particularities due to the embedding in QCD in the present low energy EFT context. The momentum integral in (III.81) is easily performed. We also restore the full mesonic field content, $\sigma^2/2 \to \rho$, and arrive at

$$V_{\phi,\text{eff}}(\rho) = V_{\text{UV}}(\rho) - \frac{3}{8\pi^2}\left[2\Lambda^2 h^2\rho + h^4\rho^2\left[\ln\frac{h^2\rho}{2\Lambda^2} - \ln\left(1 + \frac{h^2\rho}{2\Lambda^2}\right)\right] + 4\Lambda^4 \ln\left(1 + \frac{h^2\rho}{2\Lambda^2}\right)\right]\,. \tag{III.82}$$

As mentioned above, up to the symmetry factor -24 this is precisely the result of the Coleman-Weinberg computation performed originally in the context of the Higgs mechanism. We note that (III.82) seemingly depends on the momentum cutoff scale Λ. However, the potential $V_{\text{UV}}(\rho)$ is the result of integrating-out quantum fluctuations up to the momentum scale Λ. Hence, it also carries a Λ-dependence. Now we use, that the full generating functional Z of QCD in (III.73) is Λ-independent: we only introduced Λ as an intermediate scale, splitting the path integral over momentum modes into a UV-part with $p^2 > \Lambda^2$ and an IR-part with $p^2 < \Lambda^2$. We conclude

$$\Lambda\frac{\partial Z}{\partial\Lambda} = 0\,. \tag{III.83}$$

Equation (III.83) is the (momentum cutoff) RG-equation for the generating functional of QCD. In the present context it is only approximately valid as we did not include the quantum fluctuations of gluons below the cutoff scale Λ. Accordingly, (III.83) only holds in our present EFT setting if the cutoff scale Λ is small enough. This will be apparent in the final, renormalised result, and we shall resume the discussion of the sufficient smallness of the cutoff scale there.

We start the analysis by first performing the integration over the quark fluctuations. This is a path integral with a bilinear action and can be readily performed. It leaves us with a purely mesonic low energy effective theory, and $V_{\phi,\text{eff}}(\rho)$ is the full *effective* potential computed from the fermionic quantum fluctuations, but also has the interpretation of a *classical* potential of the mesonic low energy effective theory. Using (III.83) for the full effective potential (III.81) or (III.82), $\Lambda\partial_\Lambda V_{\text{eff}} = 0$, leads us to scaling relations for the couplings in the potential V. As Λ only appears in the integration limit in (III.81), the integrand simply is the Λ-derivative and we obtain

$$\begin{aligned}\Lambda\partial_\Lambda V_{\text{UV}} =& \frac{6}{\pi^2}\Lambda^4 \ln\left(1+\frac{h^2\rho}{2\Lambda^2}\right)\\ =& \frac{3}{\pi^2}\left(\Lambda^2 h^2\rho - \frac{h^4}{4}\rho^2\right) + O(\rho^3/\Lambda^2)\,,\end{aligned} \tag{III.84}$$

and

$$\Lambda\partial_\Lambda V_{\text{UV}} = \Lambda\frac{\partial m_\varphi^2}{\partial\Lambda}\rho + \frac{1}{2}\Lambda\frac{\partial\lambda_\varphi}{\partial\Lambda}\rho^2\,. \tag{III.85}$$

The RG equation (III.85) signifies that the present quark-meson model is indeed renormalisable: the divergences can be absorbed in the couplings of the classical action. For the sake of completeness we remark that two further logarithmic singularities occur in a full analysis: the wave function renormalisations of quarks and mesons which also can be absorbed by wave functions in the classical action with e.g. $\partial_\mu\phi^2 \to Z_{\phi,\Lambda}\partial_\mu\phi^2$. The scale derivatives of m_φ^2 and λ_φ define the β-functions of meson mass and self-coupling respectively,

$$\beta_{m_\varphi^2} = \Lambda\frac{\partial(m_\varphi^2/\Lambda^2)}{\partial\Lambda}\,, \qquad\qquad \beta_{\lambda_\varphi} = \Lambda\frac{\partial\lambda_\varphi}{\partial\Lambda}\,, \tag{III.86}$$

in analogy to the β-function of the strong coupling in (I.38) and the four-Fermi coupling in (III.52) discussed before. Now we use $\Lambda\partial_\Lambda\Lambda^2 = 2\Lambda^2$ and $\Lambda\partial_\Lambda \ln\Lambda^2/\Lambda_{\text{QCD}}^2 = 2$ for integrating the RG-equation (III.84). For the logarithmic term we have to introduce a reference scale which we choose to be the dynamical scale of QCD, Λ_{QCD}^2. Practically this scale is identified with the UV cutoff scale of the low energy EFT which is proportional to Λ_{QCD}^2, and is typically of the order of 1 GeV. In summary this leads us to

$$m_\varphi^2 = m_{\varphi,\text{r}}^2 + \frac{3}{2\pi^2}\Lambda^2 h^2\,, \qquad\qquad \lambda_\varphi = \lambda_{\varphi,\text{r}} - \frac{3}{4\pi^2}h^4\ln\frac{\Lambda^2}{\Lambda_{\text{QCD}}^2}\,, \tag{III.87}$$

with the renormalised couplings $m_{\varphi,\text{r}}^2, \lambda_{\varphi,\text{r}}$. In the present approximation without the mesonic quantum fluctuations they directly carry the physics. The Λ-independent constant part in the subtraction is chosen such that the ρ^2-term in the effective potential has the coupling $\lambda_{\varphi,\text{r}}$. It is evident from (III.87) that a variation of the reference scale in the logarithmic term can be absorbed in an according variation of $\lambda_{\varphi,\text{r}}$,

$$\Lambda_{\text{QCD}}\frac{\partial\lambda_\varphi}{\partial\Lambda_{\text{QCD}}} = 0 \qquad \longrightarrow \qquad \Lambda_{\text{QCD}}\frac{\partial\lambda_{\varphi,\text{r}}}{\partial\Lambda_{\text{QCD}}} = \beta_{\lambda_\varphi}\,, \tag{III.88}$$

where we have assumed the absense of other scales. This relation is again governed by the β-function β_{λ_φ}, and reflects the invariance observables do not depend on this choice. Inserting these results back into (III.82) leads us to the final, Λ-independent effective potential

$$V_{\phi,\text{eff}}(\rho) = m_{\varphi,\text{r}}^2\rho + \frac{\lambda_{\varphi,\text{r}}}{2}\rho^2 - \frac{3}{8\pi^2}h^4\rho^2\left[\ln\frac{h^2\rho}{2\Lambda_{\text{QCD}}^2} - \frac{1}{2}\right]\,. \tag{III.89}$$

As already discussed in the beginning of the derivation, (III.89) is the Coleman-Weinberg result in disguise. Multiplying with the symmetry factor $-4N_fN_c = -24$ gives precisely the same logarithmic term in the ρ^2 contribution. The missing constant term simply originates in the different renormalisation procedure: with the present one all corrections to the relevant couplings including the constant parts are absorbed, that is $m_\varphi^2 \to m_{\varphi,\text{r}}^2$ and $\lambda_\varphi \to \lambda_{\varphi,\text{r}}$.

As these couplings have to be fixed by appropriate infrared observables this is a convenient choice. In summary we have the following practical and consistent RG procedure:

(0) Regularisation: Sharp momentum cutoff with $p^2 \leq \Lambda^2$ in all loops.

(1) Renormalisation: Remove all divergent terms in the loop contributions. For the logarithmic term substitute $\ln \Lambda^2 \to \ln \Lambda^2_{\mathrm{QCD}}$.

(2) Renormalisation scheme: we demand $\partial_\rho V_{\phi,\mathrm{eff}} = \partial_\rho V_{\phi,\mathrm{UV}} + O(\rho^2) + \ln\, \rho$–terms. This is arranged by the $-1/2$ in the bracket in (III.89). It enforces that the ρ-dependent pion mass function $m_\pi(\rho) = \partial_\rho V_{\phi,\mathrm{eff}}(\rho)$ simply is $m^2_{\phi,\mathrm{r}}$ in the symmetric regime, that is for vanishing ρ. Moreover, the linear term in ρ of m^2_π is given by the UV coupling $\lambda_{\phi,\mathrm{r}}$. This cannot be expressed within a Taylor expansion at $\rho = 0$ due to the logarithmic term.

(3) Physics: The relevant parameters $h, m_{\varphi,\mathrm{r}}, \lambda_{\varphi,\mathrm{r}}$ and the explicit symmetry breaking scale c are fixed by the pion decay constant f_π, the physical pion and σ pole masses, $m_{\pi,\mathrm{pol}}, m_{\sigma,\mathrm{pol}}$ and the constituent quark mass $m_{q,\mathrm{const}}$.

Depending on the values of $m^2_{\varphi,\mathrm{r}}, \lambda_{\varphi,\mathrm{r}}$ the effective potential in (III.89) has non-trivial minima or describes the symmetric phase. The effect of the fermionic quantum fluctuations is most easily accessed via the scale-running of the parameters in the 'classical' potential $V(\rho)$. Concentrating on the scale-dependence of the mass parameter m^2_φ in (III.87) we conclude that lowering the cutoff scale Λ lowers the effective mass m^2_φ. This entails that the fermionic quantum fluctuation<s indeed lower the mass parameter. Put differently, the quark fluctuations trigger chiral symmetry breaking.

Moreover, deep in the symmetric phase, that is for large Λ, the mesonic quantum fluctuations are suppressed in comparison to the quark fluctuations. In the vicinity of the symmetry breaking scale Λ_χ the mesonic fluctuations are getting massless, $m_\varphi \to 0$ and the mesonic fluctuations kick in. In turn, the effective quark mass grows in the chirally broken regime with $m_\psi = h/2\sigma_0$, and eventually the quark fluctuations are switched off for Λ below the constituent quark mass. ...

2. *Mesonic quantum fluctuations*

The remaining mesonic fluctuations can be treated at one loop similarly to the fermionic computation done above. The result is a Coleman-Weinberg type potential without the relative minus sign. Accordingly, the mesonic fluctuations work against chiral symmetry breaking. Due to the different scales and coupling sizes this is a marginal effect even in the chiral limit. In the physical scale with explicit chiral symmetry breaking and a pion mass of about 140 MeV the mesonic quantum fluctuations also decouple for scales Λ below the pion mass.

It is left to integrate-out the quantum fluctuations of the mesonic degrees of freedom in (III.75). Again concentrating on the low energy effective potential in the spirit of the lowest order of a derivative expansion we have

$$V_{\mathrm{eff}}(\rho) = V_{\phi,\mathrm{eff}}(\rho) + \Delta V_\phi(\rho) + c_\sigma\, \sigma \qquad \text{with} \qquad \Delta V_\phi(\rho) = \frac{1}{2}\mathrm{Tr}_\Lambda \ln\left[-\partial_\mu^2 + m^2_\phi(\rho)\right] , \tag{III.90}$$

where ΔV_ϕ is the one loop approximation to the mesonic path integral (III.75) with the 'classical' potential $V_{\phi,\mathrm{eff}}(\rho)$, and Tr_Λ sums over all momenta $p^2 \leq \Lambda^2$. In (III.90) we have re-introduced the linear term in σ that triggers the explicit symmetry breaking. In the present case ΔV_ϕ boils down to

$$\Delta V_\phi(\rho) = \frac{1}{4\pi^2}\int_0^\Lambda dp\, p^3 \left[3 \ln\left(p^2 + m^2_\pi(\rho)\right) + \ln\left(p^2 + m^2_\sigma(\rho)\right)\right] . \tag{III.91}$$

For (III.91) we have used that we can evaluate the expressions for vanishing $\vec\pi = 0$ as done in the quark case. Then the mass matrix is diagonal, see (III.10), and the meson loop splits into a sum of the pion and σ loops. The two diagonal mass functions read for a given potential V

$$m^2_\pi(\rho) = \partial_\rho V(\rho)\,, \qquad\qquad m^2_\sigma(\rho) = \left(\partial_\rho + 2\rho\partial^2_\rho\right)V(\rho)\,. \tag{III.92}$$

Accordingly, the factor three in front of the first term on the right hand side in (III.91) accounts for the $N_f^2 - 1 = 3$

pions. In the present case we have $V_{\phi,\text{eff}}(\rho)$ and we get

$$m_\pi^2(\rho) = m_{\varphi,\text{r}}^2 + \left(\lambda_{\varphi,\text{r}} - \frac{3}{4\pi^2}\, h^4 \ln \frac{h^2\rho}{2\Lambda_{\text{QCD}}^2}\right)\rho\,,$$

$$m_\sigma^2(\rho) = m_{\varphi,\text{r}}^2 + 3\left(\lambda_{\varphi,\text{r}} - \frac{1}{2\pi^2} - \frac{3}{4\pi^2}\, h^4 \ln \frac{h^2\rho}{2\Lambda_{\text{QCD}}^2}\right)\rho \tag{III.93}$$

The integration in (III.92) is the same as in the quark case and we arrive at

$$\Delta V_\phi(\rho) = \frac{3}{16\pi^2}\left\{\Lambda^2 m_\pi^2 + m_\pi^4\left[\ln\frac{m_\pi^2}{\Lambda^2} - \ln\left(1+\frac{m_\pi^2}{\Lambda^2}\right)\right] + \Lambda^4 \ln\left(1+\frac{m_\pi^2}{\Lambda^2}\right)\right]$$
$$+\frac{1}{16\pi^2}\left[\Lambda^2 m_\sigma^2 + m_\sigma^4\left[\ln\frac{m_\sigma^2}{\Lambda^2} - \ln\left(1+\frac{m_\sigma^2}{\Lambda^2}\right)\right] + \Lambda^4 \ln\left(1+\frac{m_\sigma^2}{\Lambda^2}\right)\right\}\,, \tag{III.94}$$

where m_π^2, m_σ^2 are the ρ-dependent masses defined in (III.92). Seemingly (III.94) introduces divergent terms that are neither proportional to ρ^0, ρ, ρ^2 due to ΔV_q in (III.92). However, (III.94) goes beyond one-loop (ΔV_q is already one-loop) and these terms are to be expected and can be removed within a consistent renormalisation procedure. Here, our simple renormalisation procedure discussed below (III.89) pays off. Then after renormalisation (III.94) turns into

$$\Delta V_\phi(\rho) = \frac{3}{16\pi^2} m_\pi^4\left[\ln\frac{m_\pi^2}{\Lambda_{\text{QCD}}^2} - \frac{1}{2}\right] + \frac{1}{16\pi^2} m_\sigma^4\left[\ln\frac{m_\sigma^2}{\Lambda_{\text{QCD}}^2} - \frac{1}{2}\right]\,, \tag{III.95}$$

where $m_\pi(\rho), m_\sigma(\rho)$ are derived from (III.92). In (III.95) we have applied to renormalisation scheme summarised in the points (1)-(4) below (III.89). The factor $-1/2$ in the brackets arrange for

$$m_{\text{eff},\pi}^2(\rho) = \partial_\rho V_{\text{eff}}(\rho) = m_{\varphi,\text{r}}^2 + \lambda_{\varphi,\text{r}}\rho - \frac{3}{8\pi^2}\rho \ln\frac{h^2\rho}{2\Lambda_{\text{QCD}}^2} + \frac{3}{8\pi^2} m_\pi^2 (\partial_\rho m_\pi^2) \ln\frac{m_\pi^2}{\Lambda_{\text{QCD}}^2}\,. \tag{III.96}$$

From (III.95) we can proceed in several ways:

(0) We drop ΔV_ϕ completely. As in (2) the missing quantum fluctuations are partially absorbed in the couplings $m_\varphi, \lambda_\varphi$. This approximation is also called 'extended mean field' in the literature. It is very close to the mean field approximation with $V_{\text{eff}}(\rho) = V(\rho)$, where we also drop ΔV_q.

(1) As ΔV_q already is a one loop expression we drop it in the computation of (III.95). This leads us to a consistent one-loop computation. This amounts to dropping some quantum contributions in comparison to (1). However, as in (1) we have to fix the parameters $h, m_\varphi, \lambda_\varphi$ in the effective potential with the low energy observables. This implicitly absorbes (part of the) dropped contributions in these couplings. Differences between (1) and (2) only occur due to missing contributions in (2) in the couplings $\lambda_{\varphi,n}$ of the ρ^n-terms in V_{eff} with $n \geq 3$.

(2) For the evaluation of (III.90) with $V + \Delta V_q$ in (III.89) and ΔV_ϕ in (III.95) we have to take into account that already the effective potential $V + \Delta V_q$ may not be convex. In non-convex regimes its second derivatives are not positive definite: $m_\pi < 0$ for $\rho < \rho_\pi$, where ρ_π is the solution of the reduced EoM: $V_{\text{cl}}'(\rho_\pi) + \Delta V_q'(\rho_\pi) = 0$. The σ mass also gets negative for even smaller ρ.

A simple resolution of this artefact of the approximation is to continue the result from larger $\rho \geq \rho_\pi$. The more consistent way is to resolve the related renormalisation group (RG) equation for the effective potential. The RG approach is able to deal consistently with the regimes with negative curvature which are indeed flattened out by quantum fluctuations. This effect cannot be seen in perturbation theory.

In any case the result of this computation is an effective potential $V_{\text{eff}}(\rho)$ which depends on the couplings $h, m_\varphi, \lambda_\varphi$. We either compute these couplings from QCD or we fix them with low energy observables such as the meson mass, the pion decay constant and the constituent quark mass. Here we use the latter way which is described in details below.

(3) We solve the full renormalisation group equation, (III.83), for the effective potential, that governs its scale-dependence, see (III.97) below. Integrating the RG equation provides an iterative and fully consistent inclusion

of the fluctuation effects. The RG is described in the chapter Section III G 3 below, where it is also detailed how it boils down to the procedures (0)-(2) described above.

In the following we will consider all of these approximations, in particular at finite temperature and density. This allows us to evaluate the importance of the quantum (and later thermal) fluctuations as well as the stability of the results.

3. RG equation for the effective potential*

The present considerations are but one step away from a consistent treatment of the low energy effective theory with functional renormalisation group methods. For that purpose let us reconsider the RG equation for the ultraviolet potential V_{UV} derived from (III.83). Below (III.83) we have discussed the renormalisation group scaling that originates in the quark quantum fluctuations. In the general case the RG-scaling of the potential comes from both quark and meson fluctuations. This leads us to

$$\Lambda\partial_\Lambda V_{\mathrm{UV}} = -\Lambda\partial_\Lambda \left(\Delta V_q + \Delta V_\phi\right) . \tag{III.97}$$

Equation (III.97) entails how the UV effective potential V_{UV} at a large cutoff scale Λ changes with lowering or increasing the cutoff scale. In the discussion so far we have concentrated on the UV relevant terms that scale with positive powers of the cutoff Λ. Then we ensured the cutoff independence of the full effective potential $V_{\mathrm{eff}} = V_{\mathrm{UV}} + \Delta V_q + \Delta V_\phi$ by an appropriate renormalisation procedure. The low energy quark and meson fluctuation are encoded in the terms $\Delta V_q + \Delta V_\phi$. Such a treatment assumes an asymptotically large cutoff scale.

Here we take a different point of view: iteratively lowering to cutoff scale Λ from large values (w.r.t. the non-perturbative infrared pyhsics) leads to shifting more and more infrared fluctuations from $\Delta V_q + \Delta V_\phi$ to V_{UV}. Indeed, at $\Lambda = 0$ we have

$$V_{\mathrm{eff}} = V_{\Lambda=0}\,, \qquad \text{with} \qquad V_\Lambda = V_{\mathrm{UV},\Lambda}\,, \tag{III.98}$$

the former 'UV' effective potential is the full quantum effective potential. Evidently, if the cutoff scale is not asymptotically large, also the UV-irrelevant terms cannot be neglected in (III.97). Note also that its right hand side has to be seen as a function of V_Λ, the one-loop computations done before indeed used V_Λ a a classical potential. Hence, it is only left to bring (III.97) in a form that only depends on V_Λ on both sides.

To that end we consider an infinitesimal RG step with $\Lambda^2 \to \Lambda^2(1-\epsilon)$. This is governed by the path integral

$$Z \approx \int_{\Lambda^2(1-\epsilon)}^{\Lambda^2} [d\phi\, d\psi d\bar\psi] e^{-S_{\mathrm{eff},\Lambda}[\psi,\bar\psi,\phi]} \qquad \text{with} \qquad e^{-S_{\mathrm{eff},\Lambda}} \simeq Z_\Lambda\,. \tag{III.99}$$

Now we exploit that each loop in a loop expansion of (III.99) is proportional to ϵ as it only takes into account momenta with $\Lambda^2(1-\epsilon) \leq p^2 \leq \Lambda^2$. Hence, for $\epsilon \to 0$ the one-loop contribution is leading, and the ϵ-derivative can be converted in the Λ-derivative of the momentum integration boundary of the one-loop expressions for ΔV_q and ΔV_ϕ, (III.79) and (III.90) respectively. This leads us to

$$\Lambda\partial_\Lambda V_\Lambda = -\frac{1}{4\pi^2}\Lambda^4 \left[3\ln\left(1+\frac{m_\pi^2(\rho)}{\Lambda^2}\right) + \ln\left(1+\frac{m_\sigma^2(\rho)}{\Lambda^2}\right)\right] + \frac{6}{\pi^2}\Lambda^4 \ln\left(1+\frac{h^2}{2}\frac{\rho}{\Lambda^2}\right)\,, \tag{III.100}$$

where

$$m^2_{\pi/\sigma}(\rho) = \Gamma^{(2)}_{\Lambda,\pi\pi/\sigma\sigma}(\rho,p=0) = V^{(2)}_{\Lambda,\pi\pi/\sigma\sigma}(\rho)\,, \qquad \frac{h^2}{2}\rho = \Gamma^{(2)}_{\Lambda,\psi\bar\psi}(\rho,p=0)\,, \qquad \text{with} \qquad \Gamma^{(2)}_\Lambda = \Gamma_{\mathrm{UV},\Lambda}\,, \tag{III.101}$$

are the second derivatives of the scale-dependent 'UV' effective action Γ_Λ. We emphasise that the implicit Λ-dependence in $\Gamma^{(2)}$ is not hit by the ϵ-derivative.

The approximations (0)-(2) now follow from respective approximations of (III.100): For (0) we drop the meson fluctuations, for (1) we do not feed back the RG-running of V_{UV} on the right hand side of (III.100), for (2) we integrate out the quarks first. This is done with introducing separate cutoffs for quarks, Λ_q and mesons, Λ_ϕ and take the limit $\Lambda_q/\Lambda_\phi \to 0$.

Equation (III.100) is the Wegner-Houghton equation [11] for the effective potential of the current Quark-Meson Model. For the sake of completeness we also quote the full Wegner-Houghton equation for the effective action: as the derivation of (III.100) simply follows from the RG-invariance of the generating functional Z, it also applies to the full effective action. Hence we conclude

$$\Lambda\partial_\Lambda \Gamma_\Lambda[\psi,\bar\psi,\phi] = -\frac{1}{2}\mathrm{Tr}_{p^2=\Lambda^2} \ln \frac{\Gamma^{(2)}_{\phi\phi}}{\Lambda^2} + \mathrm{Tr}_{p^2=\Lambda^2} \ln \frac{\Gamma^{(2)}_{\psi\bar\psi}}{\Lambda^2}\,, \tag{III.102}$$

where the trace $\mathrm{Tr}_{p^2=\Lambda^2} = \mathrm{Tr}\,\delta(\sqrt{p^2}-\Lambda)$ only sums over the momentum shell with $p^2=\Lambda^2$. Equation (VII.34) is, together with the Callan-Symanzik equation [12, 13], the first of many functional renormalisation group equations for the effective action. These continuum RG equations are based on continuum version [14, 15] of the Kadanoff block spinning procedure on the lattice, [16], for the first seminal work on the RG see [17, 18]. In particular the pioneering work [17] already emphasises and details the full power of the renormalisation group, and is still very much under-appreciated by the community.

4. *EFT couplings and QCD*

It is left to fix the couplings parameters in our low energy effective theory with the classical action S_{eff} defined (III.62). After integrating out the quarks and mesons we are led to the full low energy effective action Γ_{lowE} with

$$\Gamma_{\mathrm{lowE}}[\psi,\bar\psi,\phi] = \int_x \bar\psi\cdot(\not{D}+m_\psi)\cdot\psi + \int_x \left[(\partial_\mu\sigma)^2 + \partial_\mu\vec\pi)^2\right] + \int_x \frac{h}{2}\bar\psi\left[\sigma + i\gamma_5\vec\tau\vec\pi\right]\psi + \int_x V_{\mathrm{eff}}(\rho)\,, \tag{III.103}$$

with the effective potential $V_{\mathrm{eff}} = V_{\phi,\mathrm{eff}} + \Delta V_\phi + c\sigma$ defined in (III.90) with $V_{\phi,\mathrm{eff}} = V_{\mathrm{UV}} + \Delta V_q$. In the best approximation discussed here, $V_{\phi,\mathrm{eff}}$ is given by (III.89) and ΔV_ϕ by (III.95). We have the fermion mass m_ψ or mesonic shift parameter c, the Yukawa coupling h, the mesonic mass parameter m_ϕ^2 and the mesonic self-coupling λ_ϕ. The fermion mass can be traded for the shift parameter c as argued before. The value of the latter determines the expectation value of the σ-field which is, in the present approximation, simply is the pion decay constant,

$$\sigma_0 = \langle\sigma\rangle = f_\pi\,, \qquad\qquad f_\pi \approx 93\,\mathrm{MeV}\,. \tag{III.104}$$

The latter value related to the physical f_π's $(f_\pi^\pm, f_\pi^0)$ measured in the experiment. Consequently c could be dropped, we simply evaluate the theory on this expectation value. Accordingly, h is determined by the constituent quark mass,

$$m_{\psi,\mathrm{con}} = \frac{1}{2}h\langle\sigma\rangle = \frac{1}{2}h\, f_\pi \qquad \longrightarrow \qquad h\approx 6.45 \quad \text{with} \quad m_{\psi,\mathrm{con}} \approx 300\,\mathrm{MeV}\,. \tag{III.105}$$

Note that the constituent quark masses of the quarks depend on the model and approximation used, typical values for up and down quark constituent masses are $m_{\psi,\mathrm{con}} \approx 350$ MeV in full QCD. A reduced value in (III.105) for two flavour QCD is common place in the $N_f=2$ quark-meson model. The related observable is the chiral condensate,

$$\langle\bar\psi(x)\psi(x)\rangle = -\int \frac{d^4p}{(2\pi)^4}\mathrm{tr}\,\langle\psi(p)\bar\psi(-p)\rangle\,, \tag{III.106}$$

where the trace sums over Dirac and flavour indices.

Finally we have to fix λ_ϕ and m_ϕ with the Yukawa coupling and σ-expectation value σ_0 deduced above, see also Table II. Note also, that a potential further input is the value of the pion decay constant in the chiral limit,

$$f_{\pi,\chi} = f_\pi(m_\pi = 0) \approx 88\,\mathrm{MeV}\,, \tag{III.107}$$

which can be determined with chiral perturbation theory, functional continuum methods or from chiral extrapolations of lattice results at different finite pion masses. This leaves us with a triple of 'observables' $(m_\pi, m_\sigma, f_{\pi,\chi})$, see Table II, and a triple of EFT couplings $(m_\phi, \lambda_\phi, c_\sigma)$. Note that the inclusion of $f_{\pi,\chi}$ as an 'observable' relates to the correct chiral dynamics reflected in the curvature and four-meson interaction in the chiral limit. The pion and sigma masses are related to those found in the Particle Data Booklet (2016), [19] of the Particle Data Group (PDG). Here, the pion mass is taken between that of the charged pions $\pi^\pm$ with $m_{\pi^\pm} \approx 139.57$ MeV and the neutral pion π^0 with $m_{\pi^0} \approx 134.98$ MeV, and the mass of the sigma meson is taken to be that of the $f_0(500)$, see [20], that is $m_\sigma \approx 450\,\mathrm{MeV}$, despite the f_0 certainly not being a simple $q\bar q$ state. The unclear nature of the value of m_σ is one of the biggest uncertainties for low energy EFTs. Typically, its values range from 400–550 MeV, see PDG, [19].

Seemingly, this leaves us with as many unknowns as physics input. However, c can be determined from the pion

Observables	Value [MeV]	EFT couplings	Value
f_π	93	$\sigma_0 = f_\pi$	93 MeV
m_{con}	300	$h = \dfrac{2m_{\text{con}}}{f_\pi}$	6.45
m_π	138	m_ϕ	$m_\phi(m_\pi, m_\sigma)$
m_σ	450	λ_ϕ	$\lambda_\phi(m_\pi, m_\sigma)$
$f_{\pi,\chi}$	88	$c_\sigma = f_\pi m_\pi^2$	$1.77 * 10^6 \text{MeV}^3$

TABLE II: Low energy observables and related EFT couplings as used for the $N_f = 2$ computations. While the σ-expectation value σ_0 and the Yukawa coupling are directly related to pion decay constant and constituent quark masses in the present approximations, the other EFT couplings depend on the approximations (0)–(3) described below (III.96).

mass and the pion decay constant with $m_\pi^2 = \partial_\rho V_{\text{eff}}(\rho_0)$ and $\rho_0 = \sigma_0^2/2 = f_\pi^2/2$. This follows from the EoM for σ,

$$\partial_\sigma V_{\text{eff}}(\rho_0) = \sigma_0 m_\pi^2 = c_\sigma \qquad \longrightarrow \qquad c_\sigma = f_\pi m_\pi^2 \approx 1.77 * 10^6 \,\text{MeV}^3 \,. \tag{III.108}$$

We conclude that in the current approximation to the UV effective action, the pion decay constant in the chiral limit, $f_{\pi,\chi}$, is a prediction.

Here we present a crude (mean-field) estimate of its value based on the assumption of being close to the chiral limit. It is based on the expansion of the full effective potential about the unperturbed minimum in the broken phase,

$$V_{\text{eff}} = \sum_{n=2}^{\infty} \frac{\lambda_n}{n!} \left(\rho - \kappa\right)^n + c_\sigma \sigma \,, \qquad \text{with} \qquad \kappa = \frac{f_{\pi,\chi}^2}{2} \,, \quad \lambda_2 = \lambda_{\phi,\text{eff}} \,. \tag{III.109}$$

Close to the chiral limit the difference $(f_\pi - f_{\pi,\chi})/f_\pi \ll 1$ is small. In the vicinity of the unperturbed minimum κ the full effective potential can be written as

$$V_{\text{eff}} = \frac{\lambda_{\phi,\text{eff}}}{2} \left(\rho - \kappa\right)^2 + c_\sigma \sigma + O\left(\left(\rho - \kappa\right)^2\right) \,. \tag{III.110}$$

Dropping the higher terms leads us to

$$m_\pi^2 = \lambda_{\phi,\text{eff}} \frac{f_\pi^2 - f_{\pi,\chi}^2}{2} \,, \qquad\qquad m_\sigma^2 = \lambda_{\phi,\text{eff}} \frac{3 f_\pi^2 - f_{\pi,\chi}^2}{2} \,. \tag{III.111}$$

In this leading order, the mesonic self-coupling drops out of the ratio of m_π^2/m_σ^2 which can be used for determining the pion decay constant in the chiral limit. We get

$$f_{\pi,\chi} = f_\pi \sqrt{\frac{1 - 3\frac{m_\pi^2}{m_\sigma^2}}{1 - \frac{m_\pi^2}{m_\sigma^2}}} \approx 83 \,\text{MeV} \,, \qquad \text{and} \qquad \lambda_{\phi,\text{eff}} = \frac{m_\sigma^2 - m_\pi^2}{f_\pi^2} \approx 21.2 \,. \tag{III.112}$$

This is a very good agreement with the theoretical prediction of $f_{\pi,\chi} \approx 88\,\text{MeV}$, in particular given the crude nature of the present estimate, which can be improved if going beyond the current mean field level.

The above analysis elucidates that the current EFT provides a prediction for either $f_{\pi,\chi}$ or m_σ, and the question arises which of them should be taken as a physics input: we first note that $f_{\pi,\chi} \approx 88\,\text{MeV}$ is under far better theoretical control than the mass of the σ-meson. Apart from the difficulties of identifying directly the σ-mesons in the EFT's at hand with a resonance in the particle spectrum, it has a large width. Hence it cannot be assumed that the curvature mass $m_{\sigma,\text{curv}}$ we use here is in good agreement with the pole mass $m_{\sigma,\text{pol}}$, see the discussion at the end of chapter Section III B. This is in stark contradistinction to the pion masses where the (non-trivial) identification $m_{\pi,\text{curv}} \approx m_{\pi,\text{pol}}$ holds true on the percent level. This suggests to adjust m_σ such that $f_{\pi,\chi} \approx 88$ MeV. In the mean field discussion done here this leads to $m_\sigma^2 \approx 600 - 650\,\text{MeV}$. Note that with a future better determination of the curvature mass $m_{\sigma,\text{curv}}$ a semi-quantitative EFT might require higher oder mesonic UV-couplings such as $\lambda_{3,\text{UV}} \neq 0$ in (III.110). This is related to the fact that the physical UV cutoff $\Lambda_{\text{UV}} \approx 1$ GeV, at which the low energy EFT is initiated, is less than one order of magnitude larger than the physical scales.

This discussion completes our EFT picture of chiral symmetry breaking in QCD. In essence it also extends to the $N_f = 2 + 1$ flavour case and beyond, then, however, a consistent determination of the low energy couplings including the correct chiral dynamics, e.g. $f_{\pi,\chi}$ is far more intricate.

IV. PARTON DENSITIES

At the end of Section II B the discussion of different energy regimes for R experimentally makes sense — at an e^+e^- collider we can tune the energy of the initial state. At hadron colliders the situation is very different. The energy distribution of incoming quarks as parts of the colliding protons has to be taken into account. We first assume that quarks move collinearly with the surrounding proton such that at the LHC incoming partons have zero p_T. Under that condition we can define a probability distribution $f_i(x)$ for finding a parton i with a given fraction $x = 0 \cdots 1$ of the proton's longitudinal momentum, the so-called parton density function (pdf). In this section we will see how it is related to the splitting kernels describing the collinear and soft divergences of QCD parton splitting.

A pdf is not an observable, only a distribution in the mathematical sense: it has to produce reasonable results when we integrate it together with a test function. Different parton densities have very different behavior — for the valence quarks (uud) they peak somewhere around $x \lesssim 1/3$, while the gluon pdf is small at $x \sim 1$ and grows very rapidly towards small x. For some typical part of the relevant parameter space ($x = 10^{-3} \cdots 10^{-1}$) the gluon density roughly scales like $f_g(x) \propto x^{-2}$. Towards smaller x values it becomes even steeper. This steep gluon distribution was initially not expected and means that for small enough x LHC processes will dominantly be gluon fusion processes.

While we cannot actually compute parton distribution functions $f_i(x)$ as a function of the momentum fraction x there are a few predictions we can make based on symmetries and properties of the hadrons, leading to to sum rules:

1. The parton distributions inside an antiproton are linked to those inside a proton through the CP symmetry, which is an exact symmetry of QCD. Therefore, we know that

$$f_q^{\bar{p}}(x) = f_{\bar{q}}(x) \qquad\qquad f_{\bar{q}}^{\bar{p}}(x) = f_q(x) \qquad\qquad f_g^{\bar{p}}(x) = f_g(x) \tag{IV.1}$$

for all values of x.

2. If the proton consists of three valence quarks uud, plus quantum fluctuations from the vacuum which can either involve gluons or quark–antiquark pairs, the contribution from the sea quarks has to be symmetric in quarks and antiquarks. The expectation values for the signed numbers of up and down quarks inside a proton have to fulfill

$$\langle N_u \rangle = \int_0^1 dx \; (f_u(x) - f_{\bar{u}}(x)) = 2 \qquad\qquad \langle N_d \rangle = \int_0^1 dx \; (f_d(x) - f_{\bar{d}}(x)) = 1 \; . \tag{IV.2}$$

3. The total momentum of the proton has to consist of sum of all parton momenta. We can write this as the expectation value of $\sum x_i$

$$\left\langle \sum x_i \right\rangle = \int_0^1 dx \; x \; \left(\sum_q f_q(x) + \sum_{\bar{q}} f_{\bar{q}}(x) + f_g(x) \right) = 1 \tag{IV.3}$$

What makes this prediction interesting is that we can compute the same sum only taking into account the measured quark and antiquark parton densities. We find

$$\int_0^1 dx \; x \; \left(\sum_q f_q(x) + \sum_{\bar{q}} f_{\bar{q}}(x) \right) \approx \frac{1}{2} \; . \tag{IV.4}$$

Half of the proton momentum is then carried by gluons.

Given the correct definition and normalization of the pdf we can now compute the hadronic cross section from its partonic counterpart,

$$\boxed{\sigma_\text{tot} = \int_0^1 dx_1 \int_0^1 dx_2 \; \sum_{ij} f_i(x_1) \, f_j(x_2) \; \hat{\sigma}_{ij}(x_1 x_2 S)} \; , \tag{IV.5}$$

where i,j are the incoming partons with the momentum factions $x_{i,j}$. The partonic energy of the scattering process is $s = x_1 x_2 S$ with the LHC proton energy of $\sqrt{S} = 13.6$ TeV. The partonic cross section $\hat{\sigma}$ includes all the necessary θ

and δ functions for energy–momentum conservation. When we express a general n–particle cross section $\hat{\sigma}$ including the phase space integration, the x_i integrations and the phase space integrations can of course be interchanged, but Jacobians will make life hard.

A. DGLAP equation

We know that collinear parton splitting affects the incoming partons at hadron colliders. For example in $pp \to Z$ production incoming partons inside the protons transform into each other until they enter the Z production process as quarks. According to Eq.(II.62), the factorized phase space and splittings depend on the energy fraction z and the so-called virtuality t. The same has to be true for the parton densities, $f(x_n, -t_n)$. The additional parameter t is new compared to the purely probabilistic picture in Eq.(IV.5).

More quantitatively, we start with a quark inside the proton with an energy fraction x_0, as it enters the hadronic phase space integral. As this quark is confined inside the proton, it can only have small transverse momentum, which means its four-momentum squared t_0 is negative and its absolute value $|t_0|$ is small. For the incoming partons which if on–shell have $p^2 = 0$ it gives the distance to the mass shell. Let us simplify our kinematic argument by assuming that there exists only one splitting, namely successive gluon radiation off an incoming quark, where the outgoing gluons are not relevant

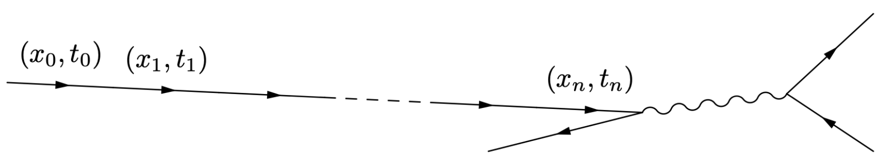

In that case each collinear gluon radiation will decrease the quark energy and increase its virtuality through recoil,

$$x_{j+1} < x_j \qquad \text{and} \qquad |t_{j+1}| = -t_{j+1} > -t_j = |t_j| \ . \tag{IV.6}$$

We know what the successive splitting means in terms of splitting probabilities and can describe how the parton density $f(x, -t)$ evolves in the $(x - t)$ plane as depicted in Figure 12. The starting point (x_0, t_0) is, probabilistically, given by the energy and kinds of parton and hadron. We then interpret each branching as a step downward in $x_j \to x_{j+1}$ and assign to a increased virtuality $|t_{j+1}|$ after the branching. The actual splitting path in the $(x - t)$ plane is made of discrete points. The probability of a splitting to occur is given by Eq.(II.62),

$$\frac{\alpha_s}{2\pi} \, \hat{P}(z) \, \frac{dt}{t} \, dz \equiv \frac{\alpha_s}{2\pi} \, \hat{P}_{q \leftarrow q}(z) \, \frac{dt}{t} \, dz \ . \tag{IV.7}$$

At the end of the path we will probe the evolved parton density at (x_n, t_n), entering the hard scattering process and its energy–momentum conservation.

To convert a partonic into a hadronic cross section, we probe the probability or the parton density $f(x, -t)$ over an infinitesimal square,

$$[x_j, x_j + \delta x] \qquad \text{and} \qquad [|t_j|, |t_j| + \delta t] \ . \tag{IV.8}$$

Using our (x, t) plane we can compute the flows into this square and out of this square, which together define the net shift in f in the sense of a differential equation,

$$\delta f_{\text{in}} - \delta f_{\text{out}} = \delta f(x, -t) \ . \tag{IV.9}$$

We compute the incoming and outgoing flows from the history of the (x, t) evolution. At this stage our picture becomes a little subtle; the way we define the path between two splittings in Figure 12 it can enter and leave the square either vertically or horizontally. Because we want to arrive at a differential equation in t we choose the vertical drop, such that the area the incoming and outgoing flows see is given by δt. If we define a splitting as a vertical drop in x at the target value t_{j+1}, an incoming path hitting the square can come from any x-value above the square. Using this convention and following the fat solid lines in Figure 12 the vertical flow into (and out of) the square (x, t) square

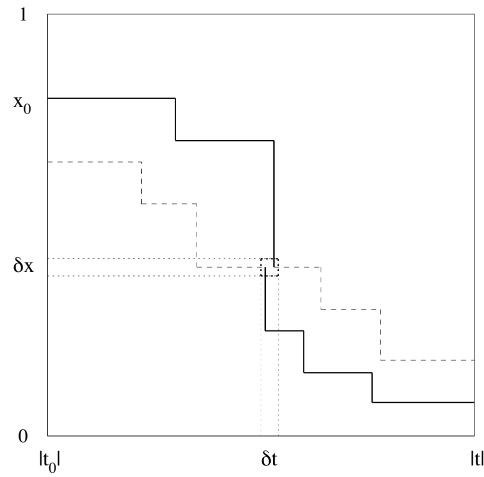

FIG. 12: Path of an incoming parton in the $(x-t)$ plane. Because we define t as a negative number its axis is labelled $|t|$.

is proportional to δt as the size of the covered interval

$$\begin{aligned}\delta f_{\rm in}(-t) &= \delta t \left(\frac{\alpha_s \hat{P}}{2\pi t} \otimes f \right)(x,-t) \\ &= \frac{\delta t}{t} \int_x^1 \frac{dz}{z} \, \frac{\alpha_s}{2\pi} \, \hat{P}(z) f\left(\frac{x}{z},-t\right) \\ &\equiv \frac{\delta t}{t} \int_0^1 \frac{dz}{z} \, \frac{\alpha_s}{2\pi} \, \hat{P}(z) f\left(\frac{x}{z},-t\right) \qquad \text{assuming } f(x',-t)=0 \text{ for } x'>1 \; . \end{aligned} \tag{IV.10}$$

We use the definition of a convolution

$$(f\otimes g)(x) = \int_0^1 dx_1 dx_2 f(x_1) g(x_2) \, \delta(x-x_1x_2) = \int_0^1 \frac{dx_1}{x_1} f(x_1) g\left(\frac{x}{x_1}\right) = \int_0^1 \frac{dx_2}{x_2} f\left(\frac{x}{x_2}\right) g(x_2) \; . \tag{IV.11}$$

The outgoing flow we define as leaving the infinitesimal square vertically. Following the fat solid line in Figure 12 it is also proportional to δt

$$\delta f_{\rm out}(-t) = \delta t \int_0^1 dy \frac{\alpha_s \hat{P}(y)}{2\pi t} \, f(x,-t) = \frac{\delta t}{t} f(x,-t) \int_0^1 dy \, \frac{\alpha_s}{2\pi} \, \hat{P}(y) \; . \tag{IV.12}$$

The y-integration is not a convolution, because we know the starting condition and integrate over all final configurations. Combining Eq.(IV.10) and Eq.(IV.12) we can compute the change in the quark pdf as

$$\begin{aligned}\delta f(x,-t) &= \frac{\delta t}{t} \left[\int_0^1 \frac{dz}{z} \, \frac{\alpha_s}{2\pi} \, \hat{P}(z) \, f\left(\frac{x}{z},-t\right) - \int_0^1 dy \, \frac{\alpha_s}{2\pi} \, \hat{P}(y) \, f(x,-t) \right] \\ &= \frac{\delta t}{t} \int_0^1 \frac{dz}{z} \, \frac{\alpha_s}{2\pi} \left[\hat{P}(z) - \delta(1-z) \int_0^1 dy \hat{P}(y) \right] \, f\left(\frac{x}{z},-t\right) \\ &\equiv \frac{\delta t}{t} \int_x^1 \frac{dz}{z} \, \frac{\alpha_s}{2\pi} \, \hat{P}(z)_+ \, f\left(\frac{x}{z},-t\right) \\ \Leftrightarrow \qquad \frac{\delta f(x,-t)}{\delta(-t)} &= \frac{1}{(-t)} \int_x^1 \frac{dz}{z} \, \frac{\alpha_s}{2\pi} \, \hat{P}(z)_+ \, f\left(\frac{x}{z},-t\right) \end{aligned} \tag{IV.13}$$

Strictly speaking, we require α_s to only depend on t and introduce the so-defined plus subtraction

$$F(z)_+ \equiv F(z) - \delta(1-z) \int_0^1 dy \, F(y) \qquad \text{or} \qquad \int_0^1 dz \, \frac{f(z)}{(1-z)_+} = \int_0^1 dz \, \left(\frac{f(z)}{1-z} - \frac{f(1)}{1-z} \right) \; . \tag{IV.14}$$

For the second definition we choose $F(z) = 1/(1-z)$, multiply it with an arbitrary test function $f(z)$ and integrate over z.

The plus–subtracted integral is by definition finite in the limit $z \to 1$, where some of the splitting kernels diverge. At this stage the plus prescription is simply a convenient way of writing a complicated combination of splitting kernels, but we will see that it also has a physics meaning. We can check that the plus prescription indeed acts as a regularization. Obviously, the integral over $f(z)/(1-z)$ is divergent at the boundary $z \to 1$, which we know we can cure using dimensional regularization. For $f(z) = 1$ we illustrates the relation between the two regularization techniques,

$$\int_0^1 dz \, \frac{1}{(1-z)^{1-\epsilon}} = \int_0^1 dz \, \frac{1}{z^{1-\epsilon}} = \left. \frac{z^\epsilon}{\epsilon} \right|_0^1 = \frac{1}{\epsilon} \qquad \text{with } \epsilon > 0 \; , \tag{IV.15}$$

corresponding to $4+2\epsilon$ dimensions. This change in sign avoids the analytic continuation of the usual value $n = 4-2\epsilon$ to $\epsilon < 0$. We can relate the dimensionally regularized integral to the plus subtraction as

$$\begin{aligned}
\int_0^1 dz \, \frac{f(z)}{(1-z)^{1-\epsilon}} &= \int_0^1 dz \, \frac{f(z)-f(1)}{(1-z)^{1-\epsilon}} + f(1) \int_0^1 dz \, \frac{1}{(1-z)^{1-\epsilon}} \\
&= \int_0^1 dz \, \frac{f(z)-f(1)}{1-z} \left(1 + \mathcal{O}(\epsilon)\right) + \frac{f(1)}{\epsilon} \\
&= \int_0^1 dz \, \frac{f(z)}{(1-z)_+} \left(1 + \mathcal{O}(\epsilon)\right) + \frac{f(1)}{\epsilon} \qquad \text{by definition} \\
\Leftrightarrow \qquad \int_0^1 dz \, \frac{f(z)}{(1-z)^{1-\epsilon}} - \frac{f(1)}{\epsilon} &= \int_0^1 dz \, \frac{f(z)}{(1-z)_+} \left(1 + \mathcal{O}(\epsilon)\right) \; .
\end{aligned} \tag{IV.16}$$

The dimensionally regularized integral minus the pole, *i.e.* the finite part of the dimensionally regularized integral, is the same as the plus–subtracted integral modulo terms of the order ϵ. The third line in Eq.(IV.16) shows that the difference between a dimensionally regularized splitting kernel and a plus–subtracted splitting kernel manifests itself as terms proportional to $\delta(1-z)$. Physically, they represent contributions to a soft–radiation phase space integral.

Finally, we turn to our splitting kernel $\hat{P}_{q \leftarrow q}$ in Eq.(II.59). If the plus prescription regularizes the pole at $z \to 1$, what is the effect of the numerator of the regularized quark splitting kernel? The finite difference between the two subtracted kernels is

$$\begin{aligned}
\left(\frac{1+z^2}{1-z} \right)_+ - (1+z^2) \left(\frac{1}{1-z} \right)_+ &= \frac{1+z^2}{1-z} - \delta(1-z) \int_0^1 dy \, \frac{1+y^2}{1-y} - \frac{1+z^2}{1-z} + \delta(1-z) \int_0^1 dy \, \frac{1+z^2}{1-y} \\
&= -\delta(1-z) \int_0^1 dy \, \left(\frac{1+y^2}{1-y} - \frac{2}{1-y} \right) \\
&= \delta(1-z) \int_0^1 dy \, \frac{y^2-1}{y-1} = \delta(1-z) \int_0^1 dy \, (y+1) = \frac{3}{2} \delta(1-z) \; .
\end{aligned} \tag{IV.17}$$

This means we can write the quark splitting kernel in two equivalent ways

$$P_{q \leftarrow q}(z) \equiv C_F \left(\frac{1+z^2}{1-z} \right)_+ = C_F \left[\frac{1+z^2}{(1-z)_+} + \frac{3}{2} \delta(1-z) \right] \; . \tag{IV.18}$$

Going back to our differential equation, the infinitesimal Eq.(IV.13) is the Dokshitzer–Gribov–Lipatov–Altarelli–Parisi or DGLAP equation. It describes the virtuality or scale dependence of the quark parton density. Quarks do not only appear in $q \to q$ splitting, but also in gluon splitting. Therefore, we generalize Eq.(IV.13) to include quarks and gluons. This generalization implies a sum over all allowed splittings and the plus–subtracted splitting kernels.

For the quark density on the left hand side it is

$$\boxed{\frac{df_q(x,-t)}{d\log(-t)} = -t\,\frac{df_q(x,-t)}{d(-t)} = \sum_{j=q,g}\int_x^1 \frac{dz}{z}\,\frac{\alpha_s}{2\pi}\,P_{q\leftarrow j}(z)\,f_j\left(\frac{x}{z},-t\right)} \qquad \text{with} \quad P_{q\leftarrow j}(z) \equiv \hat{P}_{q\leftarrow j}(z)_+ \,. \tag{IV.19}$$

Going back to Eq.(IV.13) the relevant splittings in that form give us

$$\begin{aligned}\delta f_q(x,-t) = \frac{\delta t}{t}\,\Bigg[&\int_0^1 \frac{dz}{z}\,\frac{\alpha_s}{2\pi}\,\hat{P}_{q\leftarrow q}(z)\,f_q\left(\frac{x}{z},-t\right) + \int_0^1 \frac{dz}{z}\,\frac{\alpha_s}{2\pi}\,\hat{P}_{q\leftarrow g}(z)\,f_g\left(\frac{x}{z},-t\right) \\ &- \int_0^1 dy\,\frac{\alpha_s}{2\pi}\,\hat{P}_{q\leftarrow q}(y)\,f_q(x,-t)\Bigg] \,.\end{aligned} \tag{IV.20}$$

Of the three terms on the right hand side the first and the third together define the plus–subtracted splitting kernel $P_{q\leftarrow q}(z)$, just following the argument above. The second term is a convolution proportional to the gluon pdf. Quarks can be produced in gluon splitting but cannot vanish into it. Therefore, the second term in Eq.(IV.20) includes $P_{q\leftarrow g}$, without a plus–regulator

$$P_{q\leftarrow g}(z) \equiv \hat{P}_{q\leftarrow g}(z) = T_R\left[z^2+(1-z)^2\right] \,. \tag{IV.21}$$

In the functional form of this kernel we are indeed missing the soft-radiation divergence for $z\to 1$ from $P_{q\leftarrow q}(z)$.

The second QCD parton density we have to study is the gluon density. The incoming contribution to the infinitesimal square is given by the sum of four splitting scenarios each leading to a gluon with virtuality $-t_{j+1}$

$$\begin{aligned}\delta f_{\text{in}}(-t) &= \frac{\delta t}{t}\int_0^1 \frac{dz}{z}\,\frac{\alpha_s}{2\pi}\,\left[\hat{P}_{g\leftarrow g}(z)\left(f_g\left(\frac{x}{z},-t\right)+f_g\left(\frac{x}{1-z},-t\right)\right)+\hat{P}_{g\leftarrow q}(z)\left(f_q\left(\frac{x}{z},-t\right)+f_{\bar{q}}\left(\frac{x}{z},-t\right)\right)\right] \\ &= \frac{\delta t}{t}\int_0^1 \frac{dz}{z}\,\frac{\alpha_s}{2\pi}\,\left[2\hat{P}_{g\leftarrow g}(z)f_g\left(\frac{x}{z},-t\right)+\hat{P}_{g\leftarrow q}(z)\left(f_q\left(\frac{x}{z},-t\right)+f_{\bar{q}}\left(\frac{x}{z},-t\right)\right)\right] \,,\end{aligned} \tag{IV.22}$$

using $P_{g\leftarrow\bar{q}} = P_{g\leftarrow q}$ in the first line and $P_{g\leftarrow g}(1-z) = P_{g\leftarrow g}(z)$ in the second. To leave the volume element in (x,t)-space a gluon can either split into two gluons or radiate one of n_f light-quark flavors. Combining the incoming and outgoing flows we find

$$\begin{aligned}\delta f_g(x,-t) =&\frac{\delta t}{t}\int_0^1 \frac{dz}{z}\,\frac{\alpha_s}{2\pi}\,\left[2\hat{P}_{g\leftarrow g}(z)f_g\left(\frac{x}{z},-t\right)+\hat{P}_{g\leftarrow q}(z)\left(f_q\left(\frac{x}{z},-t\right)+f_{\bar{q}}\left(\frac{x}{z},-t\right)\right)\right] \\ &-\frac{\delta t}{t}\int_0^1 dy\,\frac{\alpha_s}{2\pi}\,\left[\hat{P}_{g\leftarrow g}(y)+n_f\hat{P}_{q\leftarrow g}(y)\right]f_g(x,-t)\end{aligned} \tag{IV.23}$$

Unlike in the quark case these terms do not immediately correspond to regularizing the diagonal splitting kernel using the plus prescription.

First, the contribution to δf_{in} proportional to f_q or $f_{\bar{q}}$ which is not matched by the outgoing flow. From the quark case we already know how to deal with it. The corresponding splitting kernel does not need any regularization, so we define

$$P_{g\leftarrow q}(z) \equiv \hat{P}_{g\leftarrow q}(z) = C_F\,\frac{1+(1-z)^2}{z} \,. \tag{IV.24}$$

We see that the structure of the DGLAP equation implies that the two off-diagonal splitting kernels do not include any plus prescription $\hat{P}_{i\leftarrow j} = P_{i\leftarrow j}$. We could have expected these kernels are finite in the soft limit, $z\to 1$.

Next, we can compute the y-integral describing the gluon splitting into a quark pair directly,

$$\begin{aligned}-\int_0^1 dy\,\frac{\alpha_s}{2\pi}\,n_f\,\hat{P}_{q\leftarrow g}(y) &= -\frac{\alpha_s}{2\pi}\,n_f\,T_R\int_0^1 dy\,\left[1-2y+2y^2\right] \qquad \text{using Eq.(IV.21)} \\ &= -\frac{\alpha_s}{2\pi}\,n_f\,T_R\left[y-y^2+\frac{2y^3}{3}\right]_0^1 \\ &= -\frac{2}{3}\,\frac{\alpha_s}{2\pi}\,n_f\,T_R \,.\end{aligned} \tag{IV.25}$$

Finally, the two terms proportional to the pure gluon splitting $P_{g\leftarrow g}$ in Eq.(IV.23) require some work. The y-integral from the outgoing flow has to consist of a finite term and a term we can use to define the plus prescription for $\hat{P}_{g\leftarrow g}$. The integral gives

$$\begin{aligned}
-\int_0^1 dy\, \frac{\alpha_s}{2\pi}\, \hat{P}_{g\leftarrow g}(y) &= -\frac{\alpha_s}{2\pi}\, C_A \int_0^1 dy\, \left[\frac{y}{1-y} + \frac{1-y}{y} + y(1-y)\right] \qquad \text{using Eq.(II.55)} \\
&= -\frac{\alpha_s}{2\pi}\, C_A \int_0^1 dy\, \left[\frac{2y}{1-y} + y(1-y)\right] \\
&= -\frac{\alpha_s}{2\pi}\, C_A \int_0^1 dy\, \left[\frac{2(y-1)}{1-y} + y(1-y)\right] - \frac{\alpha_s}{2\pi}\, C_A \int_0^1 dy\, \frac{2}{1-y} \\
&= -\frac{\alpha_s}{2\pi}\, C_A \int_0^1 dy\, \left[-2+y-y^2\right] - \frac{\alpha_s}{2\pi}\, 2C_A \int_0^1 dz\, \frac{1}{1-z} \\
&= -\frac{\alpha_s}{2\pi}\, C_A \left[-2+\frac{1}{2}-\frac{1}{3}\right] - \frac{\alpha_s}{2\pi}\, 2C_A \int_0^1 dz\, \frac{1}{1-z} \\
&= \frac{\alpha_s}{2\pi}\, \frac{11}{6}\, C_A \; - \frac{\alpha_s}{2\pi}\, 2C_A \int_0^1 dz\, \frac{1}{1-z}\; .
\end{aligned} \tag{IV.26}$$

The second term in this result is what we need to replace the first term in the splitting kernel of Eq.(II.55) proportional to $1/(1-z)$ by $1/(1-z)_+$. We can see this using $f(z)=z$ and correspondingly $f(1)=1$ in Eq.(IV.14). The two finite terms in Eq.(IV.25) and Eq.(IV.26) are included in the definition of $\hat{P}_{g\leftarrow g}$ ad hoc. Because the regularized splitting kernel appears in a convolution, the two finite terms require an explicit factor $\delta(1-z)$. Collecting all of them we arrive at

$$P_{g\leftarrow g}(z) = 2C_A \left(\frac{z}{(1-z)_+} + \frac{1-z}{z} + z(1-z)\right) + \frac{11}{6}\, C_A\, \delta(1-z) - \frac{2}{3}\, n_f\, T_R\, \delta(1-z)\; . \tag{IV.27}$$

This result concludes our computation of all four regularized splitting functions which appear in the DGLAP equation Eq.(IV.19).

Before discussing and solving the DGLAP equation, let us briefly recapitulate: for the full quark and gluon particle content of QCD we have derived the DGLAP equation which describes a factorization scale dependence of the quark and gluon parton densities. The universality of the splitting kernels is obvious from the way we derive them — no information on the n-particle process ever enters the derivation.

The DGLAP equation is formulated in terms of four splitting kernels of gluons and quarks which are linked to the splitting probabilities, but which for the DGLAP equation have to be regularized. With the help of a plus–subtraction all kernels $P_{i\leftarrow j}(z)$ become finite, including in the soft limit $z\to 1$. However, splitting kernels are only regularized when needed, so the finite off-diagonal quark–gluon and gluon–quark splittings are unchanged. This means the plus prescription really acts as an infrared renormalization, moving universal infrared divergences into the definition of the parton densities. The original collinear divergence has vanished as well.

The only approximation we make in the computation of the splitting kernels is that in the y-integrals the running coupling α_s does not depend on the momentum fraction. In its standard form and in terms of the factorization scale $\mu_F^2 \equiv -t$ the <u>DGLAP equation</u> reads

$$\boxed{\frac{df_i(x,\mu_F)}{d\log\mu_F^2} = \sum_j \int_x^1 \frac{dz}{z}\, \frac{\alpha_s}{2\pi}\, P_{i\leftarrow j}(z)\, f_j\left(\frac{x}{z},\mu_F\right) = \frac{\alpha_s}{2\pi} \sum_j \left(P_{i\leftarrow j}\otimes f_j\right)(x,\mu_F)}\; . \tag{IV.28}$$

B. Solving the DGLAP equation

Solving the integro-differential DGLAP equation Eq.(IV.28) for the parton densities is clearly beyond the scope of this writeup. Nevertheless, we will sketch how we would approach this. This will give us some information on the structure of its solutions which we need to understand the physics of the DGLAP equation.

One simplification we can make is to postulate eigenvalues in parton space and solve the equation for them. This gets rid of the sum over partons on the right hand side. One such parton density is the <u>non–singlet parton density</u>, defined as the difference of two parton densities

$$f_q^{\text{NS}} = (f_q - f_{\bar{q}}) \; . \tag{IV.29}$$

Since gluons cannot distinguish between quarks and antiquarks, the gluon contribution to their evolution cancels, at least in the massless limit, at arbitrary loop order. The corresponding DGLAP equation with leading order splitting kernels is

$$\frac{df_q^{\text{NS}}(x,\mu_F)}{d\log\mu_F^2} = \int_x^1 \frac{dz}{z}\,\frac{\alpha_s}{2\pi}\,P_{q\leftarrow q}(z)\;f_q^{\text{NS}}\left(\frac{x}{z},\mu_F\right) \; . \tag{IV.30}$$

To solve it we need a transformation which simplifies a convolution, leading us to the Mellin transform. Starting from a function $f(x)$ of a real variable x we define the Mellin transform into moment space m

$$\mathcal{M}[f](m) \equiv \int_0^1 dx\, x^{m-1} f(x) \qquad\qquad f(x) = \frac{1}{2\pi i}\int_{c-i\infty}^{c+i\infty} dm\;\frac{\mathcal{M}[f](m)}{x^m} \; , \tag{IV.31}$$

where for the back transformation we choose an arbitrary appropriate constant $c > 0$, such that the integration contour for the inverse transformation lies to the right of all singularities of the analytic continuation of $\mathcal{M}[f](m)$. The important property for us is that the Mellin transform of a convolution is the product of the two Mellin transforms, which gives us the transformed DGLAP equation

$$\begin{aligned} \frac{d\mathcal{M}[f_q^{\text{NS}}](m,\mu_F)}{d\log\mu_F^2} &= \frac{\alpha_s}{2\pi}\,\mathcal{M}\left[\int_0^1 \frac{dz}{z} P_{q\leftarrow q}\left(\frac{x}{z}\right) f_q^{\text{NS}}(z)\right](m) \\ &= \frac{\alpha_s}{2\pi}\,\mathcal{M}[P_{q\leftarrow q}\otimes f_q^{\text{NS}}](m) \\ &= \frac{\alpha_s}{2\pi}\,\mathcal{M}[P_{q\leftarrow q}](m) \quad \mathcal{M}[f_q^{\text{NS}}](m,\mu_F) \; , \end{aligned} \tag{IV.32}$$

with the simple solution

$$\begin{aligned} \mathcal{M}[f_q^{\text{NS}}](m,\mu_F) &= \mathcal{M}[f_q^{\text{NS}}](m,\mu_{F,0})\;\exp\left(\frac{\alpha_s}{2\pi}\,\mathcal{M}[P_{q\leftarrow q}](m)\log\frac{\mu_F^2}{\mu_{F,0}^2}\right) \\ &= \mathcal{M}[f_q^{\text{NS}}](m,\mu_{F,0})\;\left(\frac{\mu_F^2}{\mu_{F,0}^2}\right)^{\frac{\alpha_s}{2\pi}\mathcal{M}[P_{q\leftarrow q}](m)} \\ &\equiv \mathcal{M}[f_q^{\text{NS}}](m,\mu_{F,0})\;\left(\frac{\mu_F^2}{\mu_{F,0}^2}\right)^{\frac{\alpha_s}{2\pi}\gamma(m)} \; , \end{aligned} \tag{IV.33}$$

defining $\gamma(m) = \mathcal{M}[P](m)$.

This solution still includes μ_F and α_s as two free parameters. To simplify this form we can include $\alpha_s(\mu_R^2)$ in the running of the DGLAP equation and identify the renormalization scale μ_R of the strong coupling with the factorization scale

$$\mu_F \equiv \mu_R \equiv \mu \; . \tag{IV.34}$$

Physically, this identification is clearly correct for all one-scale problems where we have no freedom to choose either of the two scales. In the DGLAP equation it allows us to replace $\log\mu^2$ by α_s as

$$\frac{d}{d\log\mu^2} = \frac{d\log\alpha_s}{d\log\mu^2}\,\frac{d}{d\log\alpha_s} = \frac{1}{\alpha_s}\,\frac{d\alpha_s}{d\log\mu^2}\,\frac{d}{d\log\alpha_s} = -\alpha_s b_0\,\frac{d}{d\log\alpha_s} \; . \tag{IV.35}$$

The additional factor of α_s will cancel the factor α_s on the right hand side of the DGLAP equation Eq.(IV.32)

$$\begin{aligned}
\frac{d\mathcal{M}[f_q^{\rm NS}](m,\mu)}{d\log\alpha_s} &= -\frac{1}{2\pi b_0}\gamma(m)\;\mathcal{M}[f_q^{\rm NS}](m,\mu)\\
\mathcal{M}[f_q^{\rm NS}](m,\mu) &= \mathcal{M}[f_q^{\rm NS}](m,\mu_0)\;\exp\left(-\frac{1}{2\pi b_0}\;\gamma(m)\log\frac{\alpha_s(\mu^2)}{\alpha_s(\mu_0^2)}\right)\\
&= \mathcal{M}[f_q^{\rm NS}](m,\mu_{F,0})\;\left(\frac{\alpha_s(\mu_0^2)}{\alpha_s(\mu^2)}\right)^{\frac{\gamma(m)}{2\pi b_0}}\quad .
\end{aligned} \tag{IV.36}$$

Among other things, in this derivation we neglect that some splitting functions have singularities and therefore the Mellin transform is not obviously well defined. Our convolution is not really a convolution either, because we cut it off at Q_0^2 etc; but the final structure in Eq.(IV.36) really holds.

Instead of the non-singlet parton densities we find the same kind of solution in pure Yang–Mills theory, *i.e.* in QCD without quarks. Looking at the different color factors in QCD this limit can also be derived as the leading terms in N_c. In that case there also exists only one splitting kernel defining an anomalous dimension γ. We find in complete analogy to Eq.(IV.36)

$$\mathcal{M}[f_g](m,\mu) = \mathcal{M}[f_g](m,\mu_0)\;\left(\frac{\alpha_s(\mu_0^2)}{\alpha_s(\mu^2)}\right)^{\frac{\gamma(m)}{2\pi b_0}}\quad . \tag{IV.37}$$

The solutions to the DGLAP equation are not completely determined, because it an integration constant in terms of μ_0. The DGLAP equation does not determine parton densities, it only describes their evolution from one scale μ_F to another, just like a renormalization group equation for the strong coupling.

Remembering how we arrive at the DGLAP equation we notice an analogy to the case of ultraviolet divergences and the running coupling. We start from universal infrared divergences. We describe them in terms of splitting functions which we regularize using the plus prescription. The DGLAP equation plays the role of a renormalization group equation for example for the running coupling. It links parton densities evaluated at different scales μ_F. In analogy to the scaling logarithms considered in Section II A 3 we should test if we can point to a type of logarithm the DGLAP equation resums by reorganizing our perturbative series of parton splitting.

C. Resumming collinear logarithms

In our discussion of the DGLAP equation and its solution we for instance encounter the splitting probability in the exponent. To make sense of such a structure we remind ourselves that such ratios of α_s values to some power can appear as a result of a resummed series. Such a series would need to include powers of $(\mathcal{M}[\hat{P}])^n$ summed over n which corresponds to a sum over splittings with a varying number of partons in the final state. Parton densities cannot be formulated in terms of a fixed final state because they include effects from any number of collinear partons summed over the number of such partons. For the processes we can evaluate using parton densities fulfilling the DGLAP equation this means that they always have the form

$$\boxed{pp \to \mu^+\mu^- + X} \qquad\qquad \text{where } X \text{ includes any number of collinear jets.} \tag{IV.38}$$

The same argument leads us towards the logarithms the running parton densities re-sum. To identify them we build a physical model based on collinear splitting, but without using the DGLAP equation. We then solve it to see the resulting structure of the solutions and compare it to the structure of the DGLAP solutions in Eq.(IV.37).

We start from the basic equation defining the physical picture of parton splitting in Eq.(II.54). Only taking into account gluons in pure Yang–Mills theory the starting point of our discussion was a factorization, schematically written as

$$\sigma_{n+1} = \int dz\frac{dt}{t}\;\frac{\alpha_s}{2\pi}\;\hat{P}_{g\leftarrow g}(z)\sigma_n\;. \tag{IV.39}$$

For a moment, we forget about the parton densities and assume that they are part of the hadronic cross section σ_n.

To treat initial state splittings, we need a definition of the virtuality t. If we remember that $t = p_b^2 < 0$ we can follow Eq.(II.61) and introduce a positive transverse momentum variable $\vec{p}_T^{\,2}$ in the usual Sudakov decomposition, such that

$$-t = -\frac{p_T^2}{1-z} = \frac{\vec{p}_T^2}{1-z} > 0 \qquad\qquad \Rightarrow \qquad \frac{dt}{t} = \frac{dp_T^2}{p_T^2} = \frac{d\vec{p}_T^2}{\vec{p}_T^2} \; . \tag{IV.40}$$

From the definition of p_T in Eq.(II.44) we see that $\vec{p}_T^2$ is really the transverse three-momentum of of the parton pair after splitting. The factorized form in Eq.(IV.39) becomes a convolution in the collinear limit,

$$\sigma_{n+1}(x,\mu_F) = \int_{x_0}^1 \frac{dx_n}{x_n}\, P_{g\leftarrow g}\left(\frac{x}{x_n}\right) \sigma_n(x_n,\mu_0) \int_{\mu_0^2}^{\mu_F^2} \frac{d\vec{p}_{T,n}^2}{\vec{p}_{T,n}^2} \frac{\alpha_s(\mu_R^2)}{2\pi} \; . \tag{IV.41}$$

Because the splitting kernel is infrared divergent we cut off the convolution integral at x_0. Similarly, the transverse momentum integral is bounded by an infrared cutoff μ_0 and the physical external scale μ_F. This is the range in which an additional collinear radiation is included in σ_{n+1}.

For splitting the two integrals in Eq.(IV.41) it is crucial that μ_0 is the only scale the matrix element σ_n depends on. The other integration variable, the transverse momentum, does not feature in σ_n because collinear factorization is defined in the limit $\vec{p}_T^2 \to 0$. All through the argument of this subsection we should keep in mind that we are looking for assumptions which allow us to solve Eq.(IV.41) and compare the result to the solution of the DGLAP equation. To develop this physics picture of the DGLAP equation we make three assumptions:

1. If μ_F is the global upper boundary of the transverse momentum integration for collinear splitting, we can apply the recursion formula in Eq.(IV.41) iteratively

$$\begin{aligned} \sigma_{n+1}(x,\mu_F) \sim & \int_{x_0}^1 \frac{dx_n}{x_n}\, P_{g\leftarrow g}\left(\frac{x}{x_n}\right) \cdots \int_{x_0}^1 \frac{dx_1}{x_1}\, P_{g\leftarrow g}\left(\frac{x_2}{x_1}\right) \sigma_1(x_1,\mu_0) \\ & \times \int_{\mu_0}^{\mu_F} \frac{d\vec{p}_{T,n}^2}{\vec{p}_{T,n}^2} \frac{\alpha_s(\mu_R^2)}{2\pi} \cdots \int_{\mu_0} \frac{d\vec{p}_{T,1}^2}{\vec{p}_{T,1}^2} \frac{\alpha_s(\mu_R^2)}{2\pi} \; . \end{aligned} \tag{IV.42}$$

2. We identify the scale of the strong coupling α_s with the transverse momentum scale of the splitting,

$$\mu_R^2 = \vec{p}_T^2 \; . \tag{IV.43}$$

   This way we can fully integrate $\alpha_s/(2\pi)$ and link the final result to the global boundary μ_F.

3. Finally, we assume strongly ordered splittings in the transverse momentum. If the ordering of the splitting is fixed externally by the chain of momentum fractions x_j, this means

$$\mu_0^2 < \vec{p}_{T,1}^2 < \vec{p}_{T,2}^2 < \cdots < \mu_F^2 \tag{IV.44}$$

   We will study motivations for this *ad hoc* assumptions in Section V B.

Under these three assumptions the transverse momentum integrals in Eq.(IV.42) become

$$\begin{aligned} & \int_{\mu_0}^{\mu_F} \frac{d\vec{p}_{T,n}^2}{\vec{p}_{T,n}^2} \frac{\alpha_s(\vec{p}_{T,n}^2)}{2\pi} \cdots \int_{\mu_0}^{p_{T,3}} \frac{d\vec{p}_{T,2}^2}{\vec{p}_{T,2}^2} \frac{\alpha_s(\vec{p}_{T,2}^2)}{2\pi} \int_{\mu_0}^{p_{T,2}} \frac{d\vec{p}_{T,1}^2}{\vec{p}_{T,1}^2} \frac{\alpha_s(\vec{p}_{T,1}^2)}{2\pi} \\ =& \int_{\mu_0}^{\mu_F} \frac{d\vec{p}_{T,n}^2}{\vec{p}_{T,n}^2} \frac{1}{2\pi b_0 \log \dfrac{\vec{p}_{T,n}^2}{\Lambda_{\text{QCD}}^2}} \cdots \int_{\mu_0}^{p_{T,3}} \frac{d\vec{p}_{T,2}^2}{\vec{p}_{T,2}^2} \frac{1}{2\pi b_0 \log \dfrac{\vec{p}_{T,2}^2}{\Lambda_{\text{QCD}}^2}} \int_{\mu_0}^{p_{T,2}} \frac{d\vec{p}_{T,1}^2}{\vec{p}_{T,1}^2} \frac{1}{2\pi b_0 \log \dfrac{\vec{p}_{T,1}^2}{\Lambda_{\text{QCD}}^2}} \\ =& \frac{1}{(2\pi b_0)^n} \int_{\mu_0}^{\mu_F} \frac{d\vec{p}_{T,n}^2}{\vec{p}_{T,n}^2} \frac{1}{\log \dfrac{\vec{p}_{T,n}^2}{\Lambda_{\text{QCD}}^2}} \cdots \int_{\mu_0}^{p_{T,3}} \frac{d\vec{p}_{T,2}^2}{\vec{p}_{T,2}^2} \frac{1}{\log \dfrac{\vec{p}_{T,2}^2}{\Lambda_{\text{QCD}}^2}} \int_{\mu_0}^{p_{T,2}} \frac{d\vec{p}_{T,1}^2}{\vec{p}_{T,1}^2} \frac{1}{\log \dfrac{\vec{p}_{T,1}^2}{\Lambda_{\text{QCD}}^2}} \; . \end{aligned} \tag{IV.45}$$

We can solve the individual integrals by switching variables, for example in the last integral

$$\int_{\mu_0}^{p_{T,2}} \frac{d\vec{p}_{T,1}^{\,2}}{\vec{p}_{T,1}^{\,2}} \frac{1}{\log \dfrac{\vec{p}_{T,1}^{\,2}}{\Lambda_{\text{QCD}}^2}} = \int_{\log\log \mu_0^2/\Lambda^2}^{\log\log p_{T,2}^2/\Lambda^2} d\log\log \frac{\vec{p}_{T,1}^{\,2}}{\Lambda_{\text{QCD}}^2} \qquad \text{with} \qquad \frac{d(ax)}{(ax)\log x} = d\log\log x$$
$$= \log \frac{\log \vec{p}_{T,2}^{\,2}/\Lambda_{\text{QCD}}^2}{\log \mu_0^2/\Lambda_{\text{QCD}}^2} \; . \tag{IV.46}$$

This gives us for the chain of transverse momentum integrals, shifted to get rid of the lower boundaries,

$$\begin{aligned}
&\int^{p_{T,n}\equiv\mu_F} d\log \frac{\log \vec{p}_{T,n}^{\,2}/\Lambda_{\text{QCD}}^2}{\log \mu_0^2/\Lambda_{\text{QCD}}^2} \cdots \int^{p_{T,2}\equiv p_{T,3}} d\log \frac{\log \vec{p}_{T,2}^{\,2}/\Lambda_{\text{QCD}}^2}{\log \mu_0^2/\Lambda_{\text{QCD}}^2} \int^{p_{T,1}\equiv p_{T,2}} d\log \frac{\log \vec{p}_{T,1}^{\,2}/\Lambda_{\text{QCD}}^2}{\log \mu_0^2/\Lambda_{\text{QCD}}^2} \\
&= \int^{p_{T,n}\equiv\mu_F} d\log \frac{\log \vec{p}_{T,n}^{\,2}/\Lambda_{\text{QCD}}^2}{\log \mu_0^2/\Lambda_{\text{QCD}}^2} \cdots \int^{p_{T,2}\equiv p_{T,3}} d\log \frac{\log \vec{p}_{T,2}^{\,2}/\Lambda_{\text{QCD}}^2}{\log \mu_0^2/\Lambda_{\text{QCD}}^2} \left(\log \frac{\log \vec{p}_{T,2}^{\,2}/\Lambda_{\text{QCD}}^2}{\log \mu_0^2/\Lambda_{\text{QCD}}^2} \right) \\
&= \int^{p_{T,n}\equiv\mu_F} d\log \frac{\log \vec{p}_{T,n}^{\,2}/\Lambda_{\text{QCD}}^2}{\log \mu_0^2/\Lambda_{\text{QCD}}^2} \cdots \frac{1}{2} \left(\log \frac{\log \vec{p}_{T,3}^{\,2}/\Lambda_{\text{QCD}}^2}{\log \mu_0^2/\Lambda_{\text{QCD}}^2} \right)^2 \\
&= \int^{p_{T,n}\equiv\mu_F} d\log \frac{\log \vec{p}_{T,n}^{\,2}/\Lambda_{\text{QCD}}^2}{\log \mu_0^2/\Lambda_{\text{QCD}}^2} \left(\frac{1}{2} \cdots \frac{1}{n-1} \right) \left(\log \frac{\log \vec{p}_{T,n}^{\,2}/\Lambda_{\text{QCD}}^2}{\log \mu_0^2/\Lambda_{\text{QCD}}^2} \right)^{n-1} \\
&= \frac{1}{n!} \left(\log \frac{\log \mu_F^2/\Lambda_{\text{QCD}}^2}{\log \mu_0^2/\Lambda_{\text{QCD}}^2} \right)^n = \frac{1}{n!} \left(\log \frac{\alpha_s(\mu_0^2)}{\alpha_s(\mu_F^2)} \right)^n \; .
\end{aligned} \tag{IV.47}$$

This is the final result for the chain of transverse momentum integrals in Eq.(IV.42). After integrating over the transverse momenta, the strong coupling is evaluated at $\mu_R \equiv \mu_F$. This leaves us with the convolution integrals from Eq.(IV.41),

$$\sigma_{n+1}(x,\mu) \sim \frac{1}{n!} \left(\frac{1}{2\pi b_0} \log \frac{\alpha_s(\mu_0^2)}{\alpha_s(\mu^2)} \right)^n \int_{x_0}^1 \frac{dx_n}{x_n} P_{g\leftarrow g}\left(\frac{x}{x_n}\right) \cdots \int_{x_0}^1 \frac{dx_1}{x_1} P_{g\leftarrow g}\left(\frac{x_2}{x_1}\right) \sigma_1(x_1,\mu_0) \; . \tag{IV.48}$$

As before, we Mellin-transform the equation into moment space

$$\begin{aligned}
\mathcal{M}[\sigma_{n+1}](m,\mu) &\sim \frac{1}{n!} \left(\frac{1}{2\pi b_0} \log \frac{\alpha_s(\mu_0^2)}{\alpha_s(\mu^2)} \right)^n \mathcal{M}\left[\int_{x_0}^1 \frac{dx_n}{x_n} P_{g\leftarrow g}\left(\frac{x}{x_n}\right) \cdots \int_{x_0}^1 \frac{dx_1}{x_1} P_{g\leftarrow g}\left(\frac{x_2}{x_1}\right) \sigma_1(x_1,\mu_0) \right](m) \\
&= \frac{1}{n!} \left(\frac{1}{2\pi b_0} \log \frac{\alpha_s(\mu_0^2)}{\alpha_s(\mu^2)} \right)^n \gamma(m)^n \, \mathcal{M}[\sigma_1](m,\mu_0) \qquad\qquad \text{using } \gamma(m) \equiv \mathcal{M}[P](m) \\
&= \frac{1}{n!} \left(\frac{1}{2\pi b_0} \log \frac{\alpha_s(\mu_0^2)}{\alpha_s(\mu^2)} \, \gamma(m) \right)^n \mathcal{M}[\sigma_1](m,\mu_0) \; .
\end{aligned} \tag{IV.49}$$

Finally, we sum the production cross sections for up to n collinear jets,

$$\begin{aligned}
\sum_{n=0}^\infty \mathcal{M}[\sigma_{n+1}](m,\mu) &= \mathcal{M}[\sigma_1](m,\mu_0) \sum_n \frac{1}{n!} \left(\frac{1}{2\pi b_0} \log \frac{\alpha_s(\mu_0^2)}{\alpha_s(\mu^2)} \, \gamma(m) \right)^n \\
&= \mathcal{M}[\sigma_1](m,\mu_0) \, \exp\left(\frac{\gamma(m)}{2\pi b_0} \log \frac{\alpha_s(\mu_0^2)}{\alpha_s(\mu^2)} \right) \\
&= \mathcal{M}[\sigma_1](m,\mu_0) \left(\frac{\alpha_s(\mu_0^2)}{\alpha_s(\mu^2)} \right)^{\frac{\gamma(m)}{2\pi b_0}} \; .
\end{aligned} \tag{IV.50}$$

This is the same structure as the DGLAP equation's solution in Eq.(IV.37). It means that we can understand the physics of the DGLAP equation using our model calculation of a successive gluon emission, including the generically variable number of collinear jets in the form of $pp \to \mu^+\mu^- + X$, as shown in Eq.(IV.38). On the left hand side of Eq.(IV.50) we have the sum over any number of additional collinear partons; on the right hand side we see fixed order

Drell–Yan production without any additional partons, but with an exponentiated correction factor. Comparing this to the running parton densities we can draw the analogy that any process computed with a scale dependent parton density where the scale dependence is governed by the DGLAP equation includes any number of collinear partons.

We can also identify the logarithms which are resummed by scale dependent parton densities. Going back to Eq.(II.41) reminds us that we start from the divergent collinear logarithms $\log p_T^{\max}/p_T^{\min}$ arising from the collinear phase space integration. In our model for successive splitting we replace the upper boundary by μ_F. The collinear logarithm of successive initial–state parton splitting diverges for $\mu_0 \to 0$, but it gets absorbed into the parton densities and determines the structure of the DGLAP equation and its solutions. The upper boundary μ_F tells us to what extent we assume incoming quarks and gluons to be a coupled system of splitting partons and what the maximum momentum scale of these splittings is. Transverse momenta $p_T > \mu_F$ generated by hard parton splitting are not covered by the DGLAP equation and hence not a feature of the incoming partons anymore. They belong to the hard process and have to be consistently simulated. While this scale can be chosen freely we have to make sure that it does not become too large, because at some point the collinear approximation $C \simeq$ constant in Eq.(II.41) ceases to hold.

V. JET RADIATION

Jet vetos play a crucial role at the LHC, for instance when looking for Higgs production in weak boson fusion. If we add a virtual gluon exchange between the two quark lines in the leading order diagram, we find a vanishing color factor

$$\mathrm{tr}T^a \; \mathrm{tr}T^b \; \delta^{ab} = 0 \; . \tag{V.1}$$

We also know that virtual gluon exchange and real gluon emission are very closely related. Radiating a gluon off any of the quarks in the weak boson fusion process will lead to a double infrared divergence, one because the gluon can be radiated at small angles and one because the gluon can be radiated with vanishing energy. The divergence at small angles is removed by redefining the quark densities in the proton. The soft, non–collinear divergence has to cancel between real gluon emission and virtual gluon exchange. However, if virtual gluon exchange does not appear, non–collinear soft gluon radiation cannot appear either. This means that additional QCD jet activity as part of the weak boson fusion process is limited to collinear radiation, *i.e.* radiation along the beam line or at least in the same direction as the far forward tagging jets. Gluon radiation into the central detector is suppressed by the color structure of the weak boson fusion process.

While it is not immediately clear how to quantify such a statement it is a very useful feature, for example looking at the top pair backgrounds. The $WWb\bar{b}$ final state as a background to $qqH, H \to WW$ searches includes two bottom jets which can mimic the signal's tagging jets. At the end, it turns out that it is much more likely that we will produce another jet through QCD jet radiation, *i.e.* $pp \to t\bar{t}$+jet, so only one of the two bottom jets from the top decays needs to be forward. One way to isolate the Higgs signal is to look at additional central jets. This strategy is referred to as central jet veto. Note that it has nothing to do with rapidity gaps at HERA or pomeron exchange, it is a QCD feature completely accounted for by standard perturbative QCD.

	renormalization scale μ_R	factorization scale μ_F
source	ultraviolet divergence	collinear (infrared) divergence
poles cancelled	counter terms (renormalization)	parton densities (mass factorization)
summation	resum self energy bubbles	resum parton splittings
parameter	running coupling $\alpha_s(\mu_R^2)$	running parton density $f_j(x, \mu_F)$
evolution	RGE for α_s	DGLAP equation
large scales	decrease of σ_{tot}	increase of σ_{tot} for gluons/sea quarks
theory background	renormalizability proven for gauge theories	factorization proven all orders for DIS proven order-by-order DY...

TABLE III: Comparison of renormalization and factorization scales appearing in LHC cross sections.

A. Jet ratios

If we assign a probability pattern to the radiation of jets from the core process we can compute the survival probability P_{pass} of such a jet veto. As an example we assume NNLO or two-loop precision for the Higgs production rate

$$\sigma = \sigma_0 + \alpha_s \sigma_1 + \alpha_s^2 \sigma_2 \; , \tag{V.2}$$

where we omit the over–all factor α_s^2 in σ_0. Consequently, we define the cross section passing the jet veto

$$\sigma^{(\text{pass})} = P_{\text{pass}} \, \sigma = \sum_j \alpha_s^j \sigma_j^{(\text{pass})} \; . \tag{V.3}$$

Because the leading order prediction only includes a Higgs in the final state we know that $\sigma_0^{(\text{pass})} = \sigma_0$. Solving this definition for the veto survival probability we can compute

$$P_{\text{pass}} = \frac{\sigma^{(\text{pass})}}{\sigma} = \frac{\sigma_0 + \alpha_s \sigma_1^{(\text{pass})} + \alpha_s^2 \sigma_2^{(\text{pass})}}{\sigma_0 + \alpha_s \sigma_1 + \alpha_s^2 \sigma_2} \; . \tag{V.4}$$

One ansatz for the distribution of any number of radiated jets is motivated by soft photon emission off a hard electron. From quantum field theory we know that it gives us a Poisson distribution in the numbers of jet in the soft limit. In that case, the probability of observing exactly n jets given an expected $\bar{n}$ jets is

$$f(n;\bar{n}) = \frac{\bar{n}^n e^{-\bar{n}}}{n!} \qquad \Rightarrow \qquad \boxed{P_{\text{pass}} \equiv f(0;\bar{n}) = e^{-\bar{n}}} \; . \tag{V.5}$$

Note that this probability links rates for exactly n jets, no at least n jets, *i.e.* it described the exclusive number of jets. The Poisson distribution defines the so-called exponentiation model when we fix the expectation value in terms of the inclusive cross sections producing at least zero or at least one jet,

$$\bar{n} = \frac{\sigma_1(p_T^{\text{min}})}{\sigma_0} \qquad \Rightarrow \qquad P_{\text{pass}} = e^{-\sigma_1/\sigma_0} \; . \tag{V.6}$$

Using this expectation value $\bar{n}$ in Eq.(V.5) returns a veto survival probability of around 88% for the weak boson fusion signal and as 24% for the $t\bar{t}$ background.

An alternative model starts from a constant probability of radiating a jet, which in terms of the inclusive cross sections σ_n, *i.e.* the production rate for the radiation of at least n jets, reads

$$\frac{\sigma_{n+1}(p_T^{\text{min}})}{\sigma_n(p_T^{\text{min}})} = R^{(\text{incl})}_{(n+1)/n}(p_T^{\text{min}}) = \text{const} \; . \tag{V.7}$$

The expectation value for the number of jets, weighted with the respective cross sections, is then

$$\begin{aligned} \bar{n} &= \frac{1}{\sigma_0} \sum_{j=1} j(\sigma_j - \sigma_{j+1}) = \frac{1}{\sigma_0} \left(\sum_{j=1} j\sigma_j - \sum_{j=2} (j-1)\sigma_j \right) = \frac{1}{\sigma_0} \left[\sigma_1 + \sum_{j=2} \sigma_j \right] \\ &= \frac{\sigma_1}{\sigma_0} \sum_{j=0} (R^{(\text{incl})}_{(n+1)/n})^j = \frac{R^{(\text{incl})}_{(n+1)/n}}{1 - R^{(\text{incl})}_{(n+1)/n}} \; , \end{aligned} \tag{V.8}$$

Radiating jets with such a constant probability has been observed at many experiments, including most recently the LHC, and is in the context of W+jets referred to as staircase scaling. Both, Poisson and staircase scaling can be derived from generating functionals. The former appears for large splitting probabilities and large scale ratios, while the latter is generated for democratic scales and smaller splitting probabilities. We can summarize the main properties of the n-jet rates in terms of the upper incomplete gamma function $\Gamma(n, \bar{n})$:

	staircase scaling	Poisson scaling
$\sigma_n^{(\text{excl})}$	$\sigma_0^{(\text{excl})}\, e^{-bn}$	$\sigma_0\, \dfrac{e^{-\bar{n}}\bar{n}^n}{n!}$
$R_{(n+1)/n} = \dfrac{\sigma_{n+1}^{(\text{excl})}}{\sigma_n^{(\text{excl})}}$	e^{-b}	$\dfrac{\bar{n}}{n+1}$
$R_{(n+1)/n}^{(\text{incl})} = \dfrac{\sigma_{n+1}}{\sigma_n}$	e^{-b}	$\left(\dfrac{(n+1)\, e^{-\bar{n}}\, \bar{n}^{-(n+1)}}{\Gamma(n+1) - n\Gamma(n,\bar{n})} + 1 \right)^{-1}$
$\langle n \rangle$	$\dfrac{1}{2}\dfrac{1}{\cosh b - 1}$	$\bar{n}$
P_{pass}	$1 - e^{-b}$	$e^{-\bar{n}}$

B. Ordered emission

An interesting theory aspect is the postulated ordering of the splittings in Eq.(IV.44). Our argument follows from the leading collinear approximation introduced in Section II B 1, so the strong p_T-ordering can in practice mean angular ordering or rapidity ordering, just applying a linear transformation.

For example the emission of a gluon off a hard quark line is governed by distinctive soft and collinear phase space regimes. When we exponentiate this gluon radiation we need to require multiple emission to be ordered by some parameter. In that case we can neglect interference terms when squaring the multiple-emission matrix element. These interference diagrams are called non–planar diagrams. The question is if we can justify to neglect them from first principles field theory and QCD. There are three reasons to do this.

First, an arguments for a strongly ordered gluon emission comes from the divergence structure of soft and collinear gluon emission. Two successively radiated gluons look like

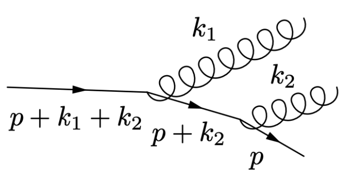

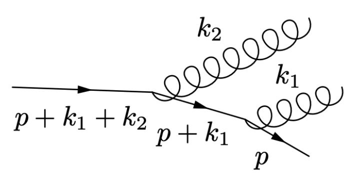

Single gluon radiation with momentum k off a hard quark with momentum p is described by the combination of a propatator and the polarization sum $(\epsilon p)(pk)$. For successive radiation the two Feynman diagrams give us the combined kinetic terms

$$
\begin{aligned}
&\frac{(\epsilon_1 p)}{(p+k_1+k_2)^2 - m^2}\,\frac{(\epsilon_2 p)}{(p+k_2)^2 - m^2} + \frac{(\epsilon_2 p)}{(p+k_1+k_2)^2 - m^2}\,\frac{(\epsilon_1 p)}{(p+k_1)^2 - m^2} \\
&\quad = \frac{(\epsilon_1 p)}{2(pk_1) + 2(pk_2) + (k_1+k_2)^2}\,\frac{(\epsilon_2 p)}{2(pk_2)} + \frac{(\epsilon_2 p)}{2(pk_1) + 2(pk_2) + (k_1+k_2)^2}\,\frac{(\epsilon_1 p)}{2(pk_1)} \qquad k_1^2 = 0 = k_2^2 \\
&\quad \simeq \frac{(\epsilon_1 p)}{2\max_j (pk_j)}\,\frac{(\epsilon_2 p)}{2(pk_2)} + \frac{(\epsilon_2 p)}{2\max_j (pk_j)}\,\frac{(\epsilon_1 p)}{2(pk_1)} \qquad (pk_j) \gg (k_1 k_2) \text{ strongly ordered} \\
&\quad \simeq \begin{cases} \dfrac{(\epsilon_1 p)(\epsilon_2 p)}{2\max_j (pk_j)}\ \dfrac{1}{2(pk_2)} & (pk_2) \ll (pk_1) \quad k_2 \text{ softer} \\[3ex] \dfrac{(\epsilon_1 p)(\epsilon_2 p)}{2\max_j (pk_j)}\ \dfrac{1}{2(pk_1)} & (pk_1) \ll (pk_2) \quad k_1 \text{ softer}\ . \end{cases}
\end{aligned} \tag{V.9}
$$

Once one of the gluons is significantly softer, the Feynman diagram with the later soft emission dominates. After squaring the amplitude there will be no phase space regime where interference terms between the two diagrams are numerically relevant. The coherent sum over gluon radiation channels reduces to a incoherent sum, ordered by the softness of the gluon. Note that this argument is based on an ordering of the (pk_j). A small value of (pk_j) can as well point to a collinear divergence; every step of our argument still applies.

Second, we can derive ordered soft-gluon emission from the phase space integration in the eikonal approximation. There, gluon radiation is governed by the so-called radiation dipoles. For successive gluon radiation off a quark leg the question we are interested in is where the soft gluon k is radiated, for example in relation to the hard quark p_1 and the harder gluon p_2. The kinematics of this process is the same as the simpler soft gluon radiation off a quark–antiquark pair produced in an electroweak process. A well–defined process with all momenta defined as outgoing is

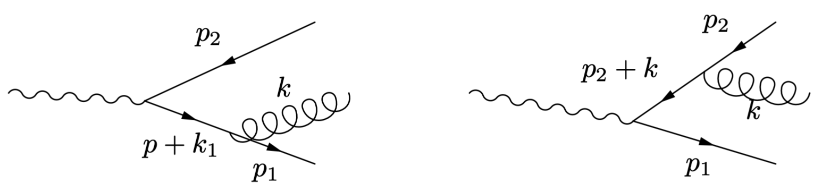

We start by symmetrizing the leading soft radiation dipole for zero masses with respect to the two hard momenta in a particular way,

$$\begin{aligned}
\frac{(p_1p_2)}{(p_1k)(p_2k)} &= \frac{1}{k_0^2}\frac{1-\cos\theta_{12}}{(1-\cos\theta_{1k})(1-\cos\theta_{2k})} \qquad \text{in terms of opening angles } \theta \\
&= \frac{1}{2k_0^2}\left(\frac{1-\cos\theta_{12}}{(1-\cos\theta_{1k})(1-\cos\theta_{2k})}+\frac{1}{1-\cos\theta_{1k}}-\frac{1}{1-\cos\theta_{2k}}\right)+(1\leftrightarrow 2) \\
&\equiv \frac{W_{12}^{[1]}+W_{12}^{[2]}}{k_0^2} \; .
\end{aligned} \tag{V.10}$$

The last term is an implicit definition of the two terms $W_{12}^{[1]}$. The pre-factor $1/k_0^2$ is given by the leading soft divergence. In each of the two terms we need to integrate over the gluon's phase space, including the azimuthal angle ϕ_{1k}.

To compute the actual integral we express the three parton vectors in polar coordinates where the initial parton p_1 propagates into the x direction, the interference partner p_2 in the $(x-y)$ plane, and the soft gluon in the full three-dimensional space described by polar coordinates,

$$\begin{aligned}
\hat{p}_1 &= (1,0,0) && \text{hard parton} \\
\hat{p}_2 &= (\cos\theta_{12},\sin\theta_{12},0) && \text{interference partner} \\
\hat{k} &= (\cos\theta_{1k},\sin\theta_{1k}\cos\phi_{1k},\sin\theta_{1k}\sin\phi_{1k}) && \text{soft gluon} \\
\Rightarrow \qquad \cos\theta_{2k} &\equiv (\hat{p}_2\hat{k}) = \cos\theta_{12}\cos\theta_{1k}+\sin\theta_{12}\sin\theta_{1k}\cos\phi_{1k} \; .
\end{aligned} \tag{V.11}$$

From the scalar product between these four-vectors we see that of the terms appearing in Eq.(V.10) only the opening angle θ_{2k} includes ϕ_{1k}, which for the azimuthal angle integration means

$$\begin{aligned}
\int_0^{2\pi} d\phi_{1k}\, W_{12}^{[1]} &= \frac{1}{2}\int_0^{2\pi} d\phi_{1k}\,\left(\frac{1-\cos\theta_{12}}{(1-\cos\theta_{1k})(1-\cos\theta_{2k})}+\frac{1}{1-\cos\theta_{1k}}-\frac{1}{1-\cos\theta_{2k}}\right) . \\
&= \frac{1}{2}\,\frac{1}{1-\cos\theta_{1k}}\int_0^{2\pi} d\phi_{1k}\,\left(\frac{1-\cos\theta_{12}}{1-\cos\theta_{2k}}+1-\frac{1-\cos\theta_{1k}}{1-\cos\theta_{2k}}\right) \\
&= \frac{1}{2}\,\frac{1}{1-\cos\theta_{1k}}\left(2\pi+(\cos\theta_{1k}-\cos\theta_{12})\int_0^{2\pi} d\phi_{1k}\,\frac{1}{1-\cos\theta_{2k}}\right) \; .
\end{aligned} \tag{V.12}$$

We can solve the azimuthal angle integral in this expression for $W_{12}^{[i]}$,

$$
\begin{aligned}
\int_0^{2\pi} d\phi_{1k} \frac{1}{1-\cos\theta_{2k}} &= \int_0^{2\pi} d\phi_{1k} \frac{1}{1-\cos\theta_{12}\cos\theta_{1k} - \sin\theta_{12}\sin\theta_{1k}\cos\phi_{1k}} \\
&\equiv \int_0^{2\pi} d\phi_{1k} \frac{1}{a - b\cos\phi_{1k}} \\
&= \oint_{\text{unit circle}} dz \, \frac{1}{iz} \frac{1}{a - b\dfrac{z+1/z}{2}} \qquad \text{with} \quad z = e^{i\phi_{1k}}, \; \cos\phi_{1k} = \frac{z+1/z}{2} \\
&= \frac{2}{i} \oint dz \, \frac{1}{2az - b - bz^2} \\
&= \frac{2i}{b} \oint \frac{dz}{(z-z_-)(z-z_+)} \qquad \text{with} \quad z_\pm = \frac{a}{b} \pm \sqrt{\frac{a^2}{b^2} - 1} \, .
\end{aligned} \tag{V.13}
$$

This integral is related to the sum of all residues of poles inside the closed integration contour. Of the two poles z_- is the one which typically lies within the unit circle, so we find

$$
\int_0^{2\pi} d\phi_{1k} \frac{1}{1-\cos\theta_{2k}} = \frac{2i}{b} \, 2\pi i \frac{1}{z_- - z_+} = \frac{2\pi}{\sqrt{a^2 - b^2}} \tag{V.14}
$$

We can use the above definitions of a and b to compute

$$
\begin{aligned}
a^2 - b^2 &= (1 - \cos\theta_{12}\cos\theta_{1k})^2 - \sin\theta_{12}^2 \sin\theta_{1k}^2 \\
&= 1 - 2\cos\theta_{12}\cos\theta_{1k} + \cos^2\theta_{12}\cos^2\theta_{1k} - (1 - \cos^2\theta_{1k} - \cos^2\theta_{12} + \cos^2\theta_{12}\cos^2\theta_{1k}) \\
&= (\cos\theta_{1k} + \cos\theta_{12})^2 \, ,
\end{aligned} \tag{V.15}
$$

and find for the azimuthal angle integral

$$
\int_0^{2\pi} d\phi_{1k} \frac{1}{1-\cos\theta_{2k}} = \frac{2\pi}{\sqrt{(\cos\theta_{1k} - \cos\theta_{12})^2}} = \frac{2\pi}{|\cos\theta_{1k} - \cos\theta_{12}|} \, . \tag{V.16}
$$

The entire integral in Eq.(V.12) then becomes

$$
\begin{aligned}
\int_0^{2\pi} d\phi_{1k} \, W_{12}^{[1]} &= \frac{1}{2} \, \frac{1}{1-\cos\theta_{1k}} \left(2\pi + (\cos\theta_{1k} - \cos\theta_{12}) \, \frac{2\pi}{|\cos\theta_{1k} - \cos\theta_{12}|} \right) \\
&= \frac{\pi}{1-\cos\theta_{1k}} \left(1 + \text{sign}(\cos\theta_{1k} - \cos\theta_{12}\right) \\
&= \begin{cases} \dfrac{2\pi}{1-\cos\theta_{1k}} & \text{if} \quad \theta_{1k} < \theta_{12} \\ 0 & \text{else} \, . \end{cases}
\end{aligned} \tag{V.17}
$$

The soft gluon is only radiated at angles between zero and the opening angle of the initial parton p_1 and its hard interference partner or spectator p_2. The same integral over $W_{12}^{[2]}$ gives the same result, with switched roles of p_1 and p_2. The soft gluon is always radiated within a cone centered around one of the hard partons and with a radius given by the distance between the two hard partons. Again, the coherent sum of diagrams reduces to an incoherent sum. This derivation angular ordering is exact in the soft limit.

The third argument for ordered emission comes from color factors. Crossed successive splittings or interference terms between different orderings are color suppressed. For example in the squared diagram for three jet production in e^+e^- collisions the additional gluon contributes a color factor

$$
\text{tr}(T^a T^a) = \frac{N_c^2 - 1}{2} = N_c C_F \tag{V.18}
$$

When we consider the successive radiation of two gluons the ordering matters. As long as the gluon legs do not cross each other we find the color factor

$$\begin{aligned}
\mathrm{tr}(T^aT^aT^bT^b) &= (T^aT^a)_{il}(T^bT^b)_{li} \\
&= \frac{1}{4}\left(\delta_{il}\delta_{jj} - \frac{\delta_{ij}\delta_{jl}}{N_c}\right)\left(\delta_{il}\delta_{jj} - \frac{\delta_{ij}\delta_{jl}}{N_c}\right) \qquad \text{using} \quad T^a_{ij}T^a_{kl} = \frac{1}{2}\left(\delta_{il}\delta_{jk} - \frac{\delta_{ij}\delta_{kl}}{N_c}\right) \\
&= \frac{1}{4}\left(\delta_{il}N_c - \frac{\delta_{il}}{N_c}\right)\left(\delta_{il}N_c - \frac{\delta_{il}}{N_c}\right) \\
&= N_c\,\left(\frac{N_c^2-1}{2N_c}\right)^2 = N_c C_F^2 = \frac{16}{3}
\end{aligned} \tag{V.19}$$

Similarly, we can compute the color factor when the two gluon lines cross. We find

$$\mathrm{tr}(T^aT^bT^aT^b) = -\frac{N_c^2-1}{4N_c} = -\frac{C_F}{2} = -\frac{2}{3}\;. \tag{V.20}$$

Numerically, this color factor is suppressed compared to 16/3. This kind of behavior is usually quoted in powers of N_c where we assume N_c to be large. In those terms non–planar diagrams are suppressed by a factor $1/N_c^2$ compared to the planar diagrams.

We can also try the argument for a purely gluonic theory. The color factor for single gluon emission after squaring is

$$f^{abc}f^{abc} = N_c\delta^{aa} = N_c(N_c^2-1) \sim N_c^3\;, \tag{V.21}$$

using the large-N_c limit in the last step. For planar double gluon emission with the exchanged gluon indices b and f we find

$$f^{abd}f^{abe}f^{dfg}f^{efg} = N_c\delta^{de}\;N_c\delta^{de} = N_c^3\;. \tag{V.22}$$

Splitting one radiated gluon into two gives

$$f^{abc}\;f^{cef}f^{def}\;f^{abd} = N_c\delta^{cd}\;N_c\delta^{cd} = N_c^3\;. \tag{V.23}$$

This means that planar emission and successive splittings cannot be separated based on the color factor. We can use the color factor argument only for abelian splittings to justify ordered gluon emission.

VI. LATTICE QCD AND CONFINEMENT IN A NUTSHELL

In this chapter we pick up the analysis of the strongly correlated infrared regime in QCD. In Section III we have evaluated the dynamics of strong chiral symmetry breaking with the help of diagrammatic QCD approaches and in particular low energy effective theories. Now we discuss the second challenging phenomenon in QCD, the confinement of quarks. To that end we introduce a fully non-perturbative approach for solving QCD numerically, lattice QCD. One of the chief advantages of lattice QCD is the property, that it allows for a numerical full solution of QCD (and other statistical and quantum field theories) in terms of the full generating functional or rather its correlation functions. For that purpose the infinite-dimensional statistical integral is approximated by a finite dimensional one on a space-time or spatial lattice. This allows us to study confinement analytically, see Section VI D. While this analytical solution holds true only on the lattice, it provides a very valuable insight into confinement.

We shall use the scalar ϕ^4 theory with a real scalar field $\phi(t,\vec{x})$ as a simple example theory for introducing the lattice formulation. We consider a three-dimensional spatial cube $\mathcal{B}$ with length L in all directions. This cube has the volume $\mathcal{V} = L^3$, and we now approximate the box with a regular rectangular grid of points with a (lattice) distance $a = L/N$ and a (large) natural number N. Then, the field takes real values on the grid points, and the infinite-dimensional path integral turns into a high- but finite-dimensional integral with N^3 computations. Evidently, in the limit $N\to\infty$ the full path integral is recovered if the limit exists. Moreover, for small enough N, the finite-dimensional integral maybe solved numerically with Monte-Carlo methods, typically applied to high-dimensional integration problems.

This set-up leaves us with the exiting possibility to simply solve interacting quantum field theories numerically within $N\to\infty$ of the corresponding lattice field theory. An obvious and intriguing advantage of such a formulation is, that it can be formulated for generic coupling strength and does not rely on a small coupling or other constraints, that typically come with systematic expansion schemes. Put differently, lattice field theories are the method of choice for strongly correlated systems, if the $N \to \infty$ can be taken.

This leaves us with the following general tasks, which we have to solve for QCD:

Task (i) Recast QCD in terms of lattice QCD, while trying to preserve as much of its symmetries. Evidently, for the example above with a regular rectangular lattice spatial rotation invariance is broken, and is only recovered in the limit $N \to \infty$. This statement extends to full space-time symmetries, a fact that e.g. complicates the construction of supersymmetric lattice theories. A further important symmetry that requires attention is the chiral symmetry. This symmetry plays a very important rôle in QCD and beyond, and will be discussed thoroughly, when discussing lattice fermions. Finally, the lattice formulations of gauge theories has great advantages over corresponding (diagrammatic) formulations in the vacuum: lattice gauge theories are explicitly gauge invariant while most continuum approaches are based on gauge fixed formulations.

Task (ii) Control of the limit $N \to \infty$. Here we have to distinguish the thermodynamic limit, $\mathcal{V} \to \infty$ and the continuum limit, $a \to 0$. While these limits both require $N \to \infty$, they are different. In any case they are signalled by the respective scaling behaviour (with either a or $\mathcal{V}$), and its evaluation is one of the largest systematic error sources in lattice QCD.

Task (iii) Complex action as occurs in QCD at finite density and in the context of its Lee-Yang zeros, require the computation of high dimensional integrals with complex (or at least non-positive) measure factors. The respective numerics may be *NP-hard*.

We close this introduction with the cautionary remark that a full introduction in lattice QCD can only be provided within fully dedicated lecture courses on lattice field theories, see Lattice field theories and Advanced lattice field theories, also containing links to lattice codes. Accordingly, the purpose of the present Chapter is that of offering a non-technical introduction of the main concepts of lattice QCD and offering a glimpse at confinement.

A. Scalar quantum field theory on the Lattice

Our starting point is the Euclidean generating functional for a real scalar field $\phi \in \mathbb{R}$. While $\phi \in \mathbb{R}$ described a neutral spin 0 field, a complex scalar field $\phi \in \mathbb{C}$ describes a charged spin 0 field. For the latter field we have the Euclidean path integral

$$Z[J] = \frac{1}{\mathcal{N}} \int \mathcal{D}\phi \, \exp\left\{ -S[\phi] + \int_x J(x)\phi(x) \right\} , \tag{VI.1a}$$

with the path integral measure

$$\mathcal{D}\phi(x) = \prod_x d\phi_x \,, \tag{VI.1b}$$

where $\phi(x)$ is the integration measure of the complex variable $\phi_x = \phi(x)$. The classical action in (VI.1a) is given by

$$S[\phi] = \int d^d x \left[\phi^\dagger(x) \, (-\Delta) \, \phi(x) + V(\phi^\dagger \phi) \right] , \quad \text{with} \quad \Delta = \partial_\mu^2 \,. \tag{VI.1c}$$

The potential in (VI.1c) is a ϕ^4-potential with

$$V(\rho) = m_\phi^2 \, \rho + \frac{\lambda_\phi}{2} \rho^2 \qquad \text{where} \qquad \phi = \frac{1}{\sqrt{2}} \, (\phi_1 + \mathrm{i}\phi_2) \ , \quad \text{and} \quad \rho = \phi^\dagger \phi = \frac{1}{2} (\phi_1^2 + \phi_2^2) \,. \tag{VI.1d}$$

The scalar theory shows a sufficiently rich phase structure and strongly correlated regimes to be of interest in its own, one example being the fluctuation induced Coleman-Weinberg phase transition. As already mentioned above, we shall use it here for introducing both conceptual particularities on the lattice as well as numerical techniques.

1. *Lattice action of scalar field theories*

Now we put the scalar theory defined in (VI.1) on a space-time grid, a depiction of such a lattice in $d = 1 + 1$ dimensions with the *lattice sites* $(n_0 \, a, n_1 \, a) \in \mathbb{Z}^2$ is found in Figure 13. While we still note the x-axis with n_0, it is

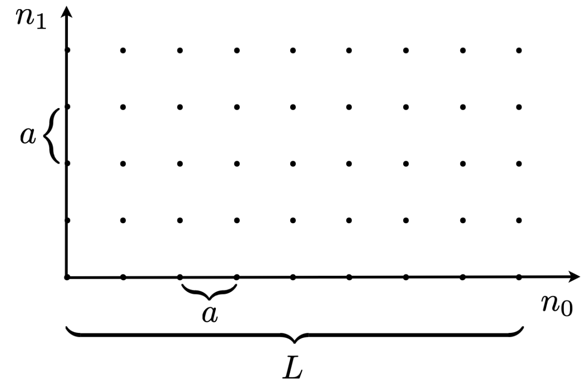

FIG. 13: Depiction of a finite 2-dimensional lattice with a lattice size L and a lattice distance a. The space-time vector takes values $x = n_0\hat{e}_0 + n_1\hat{e}_1$, and $L/a = 8$.

simply another Euclidean direction.

This lattice is defined by the box $\mathcal{B}_{a,L}$ with periodic boundary conditions.

$$\mathcal{B}_{a,L} = \Big\{ x = a\,n\,, \quad \text{with} \quad n = n_\mu\,\hat{e}_\mu\,, \quad \mu = 1,...,d \quad \text{with} \quad n_\mu \in \mathbb{Z} \quad \text{and} \quad |n_\mu| \leq L/a = N \Big\}\,. \tag{VI.2}$$

with the Cartesian orthonormal basis

$$(\hat{e}_\mu)_\nu = \delta_{\mu\nu}\,, \qquad \text{with} \qquad \hat{e}_\mu\hat{e}_\nu = \delta_{\mu\nu}\,. \tag{VI.3}$$

At the time being we consider a hyper cubic lattice, lattices with different spatial and temporal extend are used for finite temperature applications, $L = L_i = L_j \neq L_0$ with $i, j = 1, ..., d-1$. This typically also leads to a different number of points in spatial and temporal directions, with $N_\tau = L_0/a \neq N = N_i = L_i/a$. Note that it is indeed N_τ, N which defines the lattice scales together with the dimensionless parameters of the action. This will be discussed later.

The periodic boundary conditions are either implemented directly on the box by identifying opposite faces or simply considering only fields ϕ with

$$\phi(x + L\hat{\mu}) = \phi(x)\,, \qquad \text{for} \qquad \mu = 0, 1, ..., d-1\,, \qquad \text{and} \qquad \hat{\mu} = \hat{e}_\mu\,, \tag{VI.4}$$

that live on the *lattice sites* $x = n_\mu a$. With the lattice fields in (VI.4), we have to define the lattice version of the classical action (VI.1c), as well as the lattice analogue of the path integral measure $\mathcal{D}\phi$ in (VI.1a), already indicated in (VI.1b) To begin with, the space-time integration in the action turns into finite sums,

$$\int_{\mathcal{B}_L} d^d x \to a^d \sum_{x\in\mathcal{B}_{a,L}}\,, \tag{VI.5}$$

where $\mathcal{B}_L = \mathcal{B}_{0,L} = L^d$, and the sum sums over the $(L/a)^d = N^d$ lattice points, or, more generally, $N_\tau \times N^{d-1}$ lattice points. Quantum field theories on such a lattice are both, ultraviolet finite and infrared finite. The latter property is evident as the theory is defined on a finite volume, and the maximal correlation length on such a lattice is given by the *lattice extend* L. In turn, ultraviolet divergences occur for infinitely small distances, and the minimal distance on the lattice is the *lattice distance* a. Therefore we do not expect any divergences to occur for finite a and L, both are controlled on a finite lattice. However, this also entails that in particular the ultraviolet divergences resurface in the limit $a \to 0$, which has to be carefully studied, invoking renormalisation group techniques. This will be discussed later.

As already indicated above, it is convenient to express everything in dimensionless quantities in units of the lattice distance. For example, the field can now be written in terms of the dimensionless field $\hat{\phi}$ with

$$\phi(na) = a^{1-\frac{d}{2}}\,\hat{\phi}_n\,, \qquad \rho(n\,a) = a^{2-d}\hat{\rho}_n\,, \tag{VI.6a}$$

where the prefactor $a^{1-d/2}$ takes care of the canonical dimension of the scalar field ϕ. In particular, in $d = 4$ we have $\phi = 1/a\,\hat{\phi}$. Moreover, the dimensionless field $\hat{\phi}_n$ can only depend on n and not on the lattice distance a. Similarly we can write the mass m and the coupling λ in (VI.1d) in terms of a scaling prefactor in terms of the lattice distance and the dimensionless lattice mass and coupling,

$$m_\phi = \frac{1}{a}\hat{m}_\phi\,, \qquad\qquad \lambda_\phi = a^{d-4}\hat{\lambda}_\phi\,, \tag{VI.6b}$$

reflecting the standard canonical momentum dimensions of couplings and fields in QFT. For example, the momentum dimension of the coupling is $4-d\geq 0$ for $d\leq 4$. This indicates that ϕ^4-theories are renormalisable for dimensions $d\leq 4$. The upper limit, $d=4$ is the critical dimension, and there ϕ^4-theory faces the triviality problem: for all we know it has no UV closure.

With the dimensionless fields, couplings and masses the potential term (VI.1d) is readily cast into its lattice form,

$$\int_{\mathcal{B}_L} V(\rho) = a^d \sum_{|n_\mu|\leq N}\left[a^{-d}\,\hat{m}_\phi^2\hat{\rho}_n + a^{-d}\,\frac{\hat{\lambda}_\phi}{2}\,\hat{\rho}_n^2\right] = \sum_{|n_\mu|\leq N}\left[\hat{m}_\phi^2\,\hat{\rho}_n + \frac{\hat{\lambda}_\phi}{2}\,\hat{\rho}_n^2\right]. \tag{VI.7}$$

Note, that the lattice distance a has disappeared from (VI.7), and the continuum limit $a\to 0$ has to be taken as the respective limit of the dimensionless mass and coupling $\hat{m}_\phi$ and $\hat{\lambda}_\phi$. This already indicates the property of lattice field theories, that the continuum limit is achieved within a scaling limit of the dimensionless parameters of the theory. Moreover, the exponential of the potential term factorises in a product of exponentials of the potential $\hat{V}(\hat{\rho}(n)) = \hat{m}_\phi^2\hat{\rho}(n) + \hat{\lambda}_\phi/2\hat{\rho}^2(n)$ on the single lattice points,

$$\exp\left\{-\sum_{|n_\mu|\leq N}\left[\hat{m}_\phi^2\hat{\rho}(n) + \frac{\hat{\lambda}_\phi}{2}\hat{\rho}^2(n)\right]\right\} = \prod_{|n_\mu|\leq N} e^{-\left[\hat{m}_\phi^2\hat{\rho}(n)+\frac{\hat{\lambda}_\phi}{2}\hat{\rho}^2(n)\right]} = \prod_{|n_\mu|\leq N} e^{-\hat{V}(\hat{\rho}(n))}\,. \tag{VI.8}$$

Clearly this factorisation takes place for all potentials V without derivative terms. This factorisation mirrors that in the path integral measure see **??**. On the lattice and in terms of the dimensionless field $\hat{\phi}_n$, the path integral measure (VI.1b) turns into

$$\int\mathcal{D}\phi \to \prod_{|n_\mu|\leq N}\int_{\mathbb{C}} d\hat{\phi}(n) \simeq \prod_{|n_\mu|\leq N}\int_{\mathbb{R}} d\hat{\phi}_1(n)\int_{\mathbb{R}} d\hat{\phi}_2(n)\,, \tag{VI.9}$$

with integrations over the amplitude of the real and imaginary part of the dimensionless scalar field, $\hat{\phi}_1$ and $\hat{\phi}_2$ respectively. This leads to an interesting intermediate result,

$$\int\mathcal{D}\phi\, e^{-\int_x V(x)} \to \prod_{|n_\mu|\leq N}\int_{\mathbb{C}} d\hat{\phi}(n)\, e^{-\hat{V}(\hat{\rho}(n))}\,, \tag{VI.10}$$

in the absence of the kinetic term the path integral factorises in a product of single site models that can be solved independently. We also remark that the above integral is manifestly finite as already argued above. The full lattice theory tends towards (VI.10) in the *strong coupling limit*, $\hat{\lambda}\to\infty$. Seemingly this entails that QFTs with strong *physical* coupling can be solved trivially on the lattice. However, an inspection of (VI.6b) leads to the conclusion that a strong but finite coupling λ requires $\hat{\lambda}\to 0$ for $d<4$ according to the canonical dimensional running. In the presence of quantum effects this canonical running is augmented by an anomalous part as computed in Section II A. This analysis is deferred to Section VI E 2, for the time being we just keep in mind that the continuum limit obviously requires a scaling limit of the dimensionless lattice parameters.

It is left to put forward the lattice version of the kinetic term, $-\int_x \phi^\dagger\Delta\phi$. This is done with a discretised version of the Laplace operator Δ in (VI.1c). To begin with, we define the left, right and symmetric lattice derivatives,

$$\partial_\mu^L\phi(x) = \frac{\phi(x)-\phi(x-\hat{\mu}a)}{a}\,,\qquad \partial_\mu^R\phi(x) = \frac{\phi(x+\hat{\mu}a)-\phi(x)}{a}\,,\qquad \partial_\mu^S\phi(x) = \frac{\phi(x+\hat{\mu}a)-\phi(x-\hat{\mu}a)}{2a}\,, \tag{VI.11a}$$

whose continuum limits with $a\to 0$ define the standard left, right and symmetric derivatives. In terms of the dimensionless lattice fields these derivatives turn into

$$\partial_\mu^{L,R,S}\phi(x) = a^{-\frac{d}{2}}\hat{\partial}^{L,R,S}\hat{\phi}_n\,, \tag{VI.11b}$$

with the difference operators

$$\hat\partial^L_\mu \hat\phi_n = \hat\phi_n - \hat\phi_{n-\hat\mu}\,, \qquad \hat\partial^R_\mu \hat\phi_n = \hat\phi_{n+\hat\mu} - \hat\phi_n\,, \qquad \hat\partial^S_\mu \hat\phi_n = \frac{1}{2}\left(\hat\phi_{n+\hat\mu} - \hat\phi_{n-\hat\mu}\right)\,. \tag{VI.11c}$$

While all the finite difference operators in (VI.11) have the same continuum limit, the convergence of the path integral for the different choices may be quantitatively or even qualitatively different. For example, the symmetric operator $\hat\partial^S$ does not single out a direction, which may lead to a quicker convergence. In this context we also remark that the difference operators in (VI.11) have a matrix form with $\hat\partial_{nm}\hat\phi_m = \hat\partial\hat\phi_n$ with

$$(\partial^L_\mu)_{nm} = \delta_{n,m} - \delta_{n-\hat\mu,m}\,, \qquad (\partial^R_\mu)_{nm} = \delta_{n+\hat\mu,m} - \delta_{n,m}\,, \qquad (\partial^S_\mu)_{nm} = \frac{1}{2}\left(\delta_{n+\hat\mu,m} - \delta_{n-\hat\mu,m}\right)\,. \tag{VI.12}$$

With the matrix representation (VI.12) it follows straightforwardly, that the symmetric difference operator $\mathrm{i}(\partial^S_\mu)_{nm}$ is a hermitian matrix, while the two other difference operators are not. We close this discussion of lattice derivative operators with the remark that (VI.11c) are by no means the only possible choices: Clearly, $\partial^{L,R}$ are the only next neighbour definitions and $\hat\partial^S$ already connects next-to-next lattice sites. If we allow for a large and larger amount of lattice sites to be involved, this leads to a large number of possible lattice derivatives. Typically, for standard applications in scalar theories one sticks to the 'canonical' choices, but we shall pick up this discussion again in Section VI B 1 on lattice fermions.

Finally, with the difference operators (VI.11c) we can define lattice Laplacians. As for the derivatives, also the Laplacian is not unique. Here we take the symmetric choice,

$$\hat\Delta = \hat\partial^L_\mu \hat\partial^R_\mu = \hat\partial^R_\mu \hat\partial^L_\mu\,, \qquad \text{with} \qquad \hat\Delta_{nm} = \sum_{\mu>0}\left[\delta_{n+\hat\mu,m} + \delta_{n-\hat\mu,m} - 2\,\delta_{n,m}\right]\,. \tag{VI.13}$$

Evidently, this matrix is hermitian, while the choices $(\hat\partial^{L,R}_\mu)^2$ are not. With the lattice Laplacian (VI.13) we arrive at the lattice version of the kinetic term,

$$\int_x \phi^\dagger\left(-\Delta + m^2\right)\phi \to \sum_{n,m} \hat\phi^\dagger_n K_{nm}\,\hat\phi_m\,, \tag{VI.14}$$

where we included the mass term from the potential and the restriction $|n_\mu|, |m_\mu| \leq N$ is implied in the sum. The hermitian kinetic operator K_{nm} in (VI.14) reads

$$K_{nm} = -\sum_{\mu>0}\left[\delta_{n+\hat\mu,m} + \delta_{n-\hat\mu,m} - 2\,\delta_{\hat n,\hat m}\right] + \hat m^2\,\delta_{nm} = -\sum_{\mu>0}\left[\delta_{n+\hat\mu,m} + \delta_{n-\hat\mu,m}\right] + (\hat m^2 + 2d)\,\delta_{nm}\,. \tag{VI.15}$$

This leads us to our final expression for the lattice path integral of a complex scalar field in a finite volume $\mathcal{V} = L^d$ with the lattice distance a,

$$Z[\hat J] = \frac{1}{\mathcal{N}}\int \prod_n d\hat\phi_n\,\exp - S[\hat\phi] + 2\sum_n \hat J_n \hat\phi_n\,, \tag{VI.16}$$

with $2\hat J_n\hat\phi_n = \hat J_{1,n}\hat\phi_{1,n} + \hat J_{2,n}\hat\phi_{2,n}$, the normalisation $\mathcal{N}$ and the lattice action

$$S[\hat\phi] = -\sum_{n,m}\hat\phi^\dagger_n K_{nm}\hat\phi_m + \frac{\hat\lambda}{2}\sum_n \hat\rho_n^2\,, \qquad \text{with} \qquad \hat\rho_n = \hat\phi^\dagger_n\hat\phi_n\,. \tag{VI.17}$$

We have already considered this theory in the absence of a kinetic term, see (VI.10). Now we discuss the opposite limit, we drop the interaction term (but keep the mass term). This leads us to the (Gaußian) free theory, which can be integrated analytically. We get from (VI.16) for the generating functional of the free theory, $Z_0[J]$,

$$Z_0[J] \simeq \frac{1}{\det K_{nm}} e^{\frac{1}{2}\sum_{n,m}\hat J_n K^{-1}_{nm}\hat J_m}\,. \tag{VI.18}$$

where both the Gaußian integral over the real and imaginary part of the field lead to a factor $1/\sqrt{\det K}$. With derivatives w.r.t. the current we generate the correlation functions of this theory with

$$\frac{\partial^m Z_0[J]}{\partial \hat{J}_{n_1}\cdots \hat{J}_{n_m}} = \langle \hat{\phi}_{n_1}\cdots \hat{\phi}_{n_m}\rangle \,. \tag{VI.19}$$

These correlation functions are either vanishing ($m=2i+1$) or are sums of products of the two-point function. The latter is given by

$$\frac{1}{Z_0[J]}\frac{\partial^m Z_0[J]}{\partial \hat{J}_n \partial \hat{J}_m} = \langle \hat{\phi}_n \hat{\phi}_m\rangle = K^{-1}_{nm}\,, \tag{VI.20}$$

the standard result in QM and QFT: the second derivative of (the logarithm of) the generating functional is the propagator. In the current free theory it is the classical propagator $1/K$.

It is very instructive to transform fields and correlation functions to their momentum representation with a Fourier transformation, i.e. the dispersion $K(p)$ and the propagator $1/K(p)$. In momentum space we will see the ultraviolet finiteness explicitly. In order to facilitate the access we use a lattice of infinite extent, $L\to\infty$, related to the *thermodynamic* limit of the theory. Not that this limit is different from the continuum limit, $a\to 0$ (augmented with an appropriate rescaling of the couplings), and they should not be confused.

In any case the Fourier transform on a lattice with infinite extent is defined by

$$\hat{\phi}(\hat{p}) = \sum_{n\in\mathbb{Z}^d} \hat{\phi}_n\, e^{-\mathrm{i}\hat{p}_\mu n_\mu}\,, \qquad\qquad \hat{\phi}_n = \int_{-\pi}^{\pi}\frac{d^d\hat{p}}{(2\pi)^d}\,\hat{\phi}(\hat{p})\, e^{\mathrm{i}\hat{p}_\mu n_\mu}\,, \tag{VI.21}$$

with the dimensionless momentum $\hat{p} = a\,p$ for the 'standard' momentum p, defined similarly to $x = a\,n$. The integration over the dimensionless momentum is restricted to the Brillouin zone

$$\mathcal{B}_{\hat{p}} = [-\pi,\pi]^d\,, \tag{VI.22}$$

originally introduced in condensed matter physics, see also Wigner-Seitz cells. A shift of the momentum $\hat{p}_\mu$ by $2\pi m_\mu$ with $m_\mu\in\mathbb{Z}$ leads to

$$e^{\mathrm{i}(\hat{p}_\mu + 2\pi\, m_\mu)n_\mu} = e^{\mathrm{i}\hat{p}_\mu n_\mu}\,, \tag{VI.23}$$

as $e^{\mathrm{i}\hat{m}_\mu n_\mu} = 1$. Accordingly, physical momenta are restricted by $-\pi/a \leq p_\mu \leq \pi/a$, and while we will not do lattice perturbation theory in this lecture course, all momentum loops in a loop expansion or any other diagrammatic expansions are manifestly ultraviolet finite. Note also that this convenient property comes at the price of violating Euclidean symmetry, instead the full Euclidean group O(d) in d dimensions the lattice only admits rotations by $n\pi$ with $n\in\mathbb{Z}$.

We now perform a Fourier transform of the kinetic operator K_{nm} in (VI.15) to $K(\hat{p},\hat{q})$,

$$K_{nm} = \int_{-\pi}^{\pi}\frac{d^d\hat{p}}{(2\pi)^d}K(\hat{p})e^{\mathrm{i}\hat{p}(n-m)}\,, \qquad \text{with} \qquad K(\hat{p}) = 4\sum_{\mu=0}^{d-1}\sin^2\left(\frac{\hat{p}_\mu}{2}\right) + \hat{m}^2\,, \tag{VI.24}$$

where we have used

$$\delta_{nm} = \int_{-\pi}^{\pi}\frac{d^d\hat{p}}{(2\pi)^d}e^{\mathrm{i}\hat{p}(n-m)}\,. \tag{VI.25}$$

Note that the classical dispersion is obtained for $\hat{p}\to 0$, where $K(\hat{p})\to \hat{p}^2+\hat{m}^2$. The physical dispersion is given by $1/a^2 K(\hat{p}) \to p^2 + m^2$. This entails that in the continuum limit only the neighbourhood of the zeros of $\sin^2(\hat{p}_\mu/2)$ survives, all other momenta are suppressed by $1/a^2$. This is clearly seen by re-instating all dimensions to the action. Then we have for the kinetic term on the lattice,

$$\int_{-\pi}^{\pi}\frac{d^d\hat{p}}{(2\pi)^d}\hat{\phi}^\dagger(-\hat{p})\,K(\hat{p})\,\phi(\hat{p}) = \int_{-\frac{\pi}{a}}^{\frac{\pi}{a}}\frac{d^dp}{(2\pi)^d}\phi^\dagger(-p)\,\frac{1}{a^2}K(pa)\,\phi(p)\,. \tag{VI.26}$$

For momenta $\hat{p}=pa$ with finite values of $K(pa)$, the expression in (VI.26) diverges for $a\to 0$, as does the full action. Accordingly, configurations $\phi(p)$ with support for these momenta are suppressed in the continuum limit. In turn, configurations with support in momentum regimes $\hat{p} = pa \propto a$ with $K(pa) \propto a^2$ survive. In the present case there is only one such zero at $\hat{p} = 0$. Note that seemingly another definition for the dispersion with $\sin^2(\hat{p}_\mu)$ would work as well, but with this definition there are also zeros of the dispersion at the corners of the Brillouin zone, leading to additional fields in the continuum limit (doublers). This will be important in the case of fermions. In summary this entails that discretisation details matters.

B. Fermions on the Lattice

In the last chapter we have discussed the lattice formulation of scalar field theories. As in standard quantum field theory this includes the showcase example, the ϕ^4-theory, and also covers many interesting phenomena. However, all matter fields in the Standard Model except the Higgs are fermionic, as are also the fundamental fields in many interesting condensed matter and statistical systems. In this Chapter we discuss the lattice formulation of fermionic theories. We shall see that the numerical implementation of these theories is not as straightforward as that of scalar theories or that of gauge theories treated in the next Chapter. In relativistic theories, the respective problems are related to the spin 1/2 nature of fermions which neither allows for a straightforward implementation of the importance sampling due to the Grassmannian nature of the fermionic fields (and the linear dispersion), nor does it admit the straightforward implementation of one Weyl fermion on the lattice due to the linear Dirac dispersion: the fermionic *doubling problem* covered by the *Nielsen-Ninomiya theorem.* We note in passing that, while these properties obstruct the numerical simulation of fermionic theories, they also carry some very interesting (and cool) mathematics and physics.

We initiate this discussion with a short summary on the properties of fermionic continuum path integrals. In Euclidean space-time the fermionic path integral of the free Dirac action in analogy of (VI.1),

$$Z[\eta,\bar\eta] = \frac{1}{\mathcal{N}} \int \mathcal{D}\bar\psi\, \mathcal{D}\psi\, e^{-S_\psi[\psi,\bar\psi]+\int_x \left(\bar\eta\,\psi - \bar\psi\,\eta\right)}\,. \tag{VI.27}$$

with the free Euclidean Dirac action

$$S_\psi\left[\psi,\bar\psi\right] = \int_x \bar\psi\left(\partial\!\!\!/ + m_\psi\right)\psi\,, \qquad \text{where} \qquad \partial\!\!\!/ = \gamma_\mu \partial_\mu\,, \tag{VI.28}$$

Grassmann fields $\psi, \bar\psi$ with $\psi^2 = \bar\psi^2 = 0$, and the Euclidean version of the Clifford algebra

$$\{\gamma_\mu\,,\,\gamma_\nu\} = 2\delta_{\mu\nu}\,, \qquad \text{and} \qquad \{\gamma_\mu\,,\,\gamma_5\} = 0 \quad \text{with} \quad \gamma_5 = \mathrm{i}\gamma_0\gamma_1\gamma_2\gamma_3\,, \tag{VI.29}$$

with the 4×4 dimensional Dirac matrices in $d = 4$, and the hermitian $\gamma_5 = \gamma_5^\dagger$. In general dimensions, the Clifford algebra is $2^{\frac{d}{2}} \times 2^{\frac{d}{2}}$ in even dimensions $d = 2l$ with $l \in \mathbb{N}$, and $2^{\frac{d-1}{2}} \times 2^{\frac{d-1}{2}}$ in odd dimensions $d = 2l-1$. While the Euclidean anti-fermion $\bar\psi$ is independent from the fermion ψ as there is no Euclidean Dirac conjugation, one still writes $\bar\psi = \psi^\dagger\gamma_0$.

In any case we can expand the fermionic fields in a convenient set of basis functions, for example the eigenfunctions of $\partial\!\!\!/$ with

$$\psi(x) = \sum_n a_n \varphi_n(x)\,, \qquad \bar\psi(x) = \sum_n \bar b_n \varphi_n^\dagger(x)\,, \qquad \text{with} \qquad \mathrm{i}\partial\!\!\!/\varphi_n = \lambda_n\varphi_n\,, \tag{VI.30}$$

with the Grassmann expansion coefficients $a_n a_m = -a_m a_n$, $\bar b_n \bar b_m = -\bar b_m \bar b_n$ and $a_n \bar b_m = -\bar b_m a_n$. Within the basis (VI.30) the Dirac action (VI.28) has the simple form

$$S_\psi\left[\psi,\bar\psi\right] = \sum_n \lambda_n \bar b_n a_n\,. \tag{VI.31}$$

and the Grassmann measure in (VI.27) reads,

$$\int \mathcal{D}\bar\psi\,\mathcal{D}\psi \simeq \prod_n \int d\bar b_n\, da_n\,. \tag{VI.32}$$

Using the above relations in the path integral, it yields

$$\int \mathcal{D}\bar{\psi}\,\mathcal{D}\psi\, e^{-S_\psi[\psi,\bar{\psi}]} \simeq \int \left[\prod_n d\bar{b}_n\, da_n\right] e^{-\sum_n \lambda_n \bar{b}_n a_n} = \prod_n \left[\int d\bar{b}_n\, da_n\, \lambda_n a_n \bar{b}_n\right] = \prod_n \lambda_n = \det\left(\partial\!\!\!/ + m\right)\,, \tag{VI.33}$$

where we have used the rules for Grassmann integrations,

$$\int da\, a^n = \delta_{1n}\,. \tag{VI.34}$$

1. *Lattice action of fermionic field theories*

We now formulate the lattice version of the path integral (VI.27) in analogy of the scalar theory: To begin with, we define our dimensionless lattice fields and parameters as in (VI.6). The dimensionless fermionic fields read,

$$(\,\psi(x), \bar{\psi}(x)\,) \to \frac{1}{a^{\frac{d-1}{2}}}\left(\hat{\psi}_n, \hat{\bar{\psi}}_n\right)\,, \tag{VI.35a}$$

and the lattice derivative and mass,

$$\partial_\mu \psi(x) \to \frac{1}{a^{\frac{d+1}{2}}} \hat{\partial}_\mu \hat{\psi}_n\,, \qquad\qquad m_\psi \to \frac{1}{a}\hat{m}_\psi\,, \tag{VI.35b}$$

where we have chosen the symmetric lattice derivative, $\hat{\partial}_\mu = \hat{\partial}^S_\mu$, see (VI.11c), with

$$\hat{\partial}_\mu \hat{\psi}(n) = \frac{1}{2}\left(\hat{\psi}_{n+\hat{\mu}} - \hat{\psi}_{n-\hat{\mu}}\right)\,. \tag{VI.36}$$

With the definitions (VI.35) the lattice version of the Dirac action is given by,

$$S_\psi\left[\hat{\psi}, \hat{\bar{\psi}}\right] = \sum_{\substack{n,m\\ \alpha,\beta}} \hat{\bar{\psi}}_{\alpha,n} K_{\alpha\beta,nm} \hat{\psi}_{\beta,m} \tag{VI.37a}$$

with the space-time points n, m and the Dirac indices α, β. The kinetic operator or matrix K reads,

$$K_{\alpha\beta,nm} = \sum_\mu (\gamma_\mu)_{\alpha\beta} \frac{\delta_{m,n+\hat{\mu}} - \delta_{m,n-\hat{\mu}}}{2} + \hat{m}_\psi \delta_{mn}\delta_{\alpha\beta}\,. \tag{VI.37b}$$

The generating functional (VI.27) turns into,

$$Z[\eta,\bar{\eta}] \simeq \int \prod_{n,\alpha} d\hat{\psi}_{\alpha,n} \prod_{m,\beta} d\hat{\bar{\psi}}_{\beta,m}\, e^{-S_\psi\left[\hat{\psi},\hat{\bar{\psi}}\right] + \sum_{n,\alpha}\left(\bar{\eta}_{\alpha,n}\hat{\psi}_{\alpha,n} - \hat{\bar{\psi}}_{\alpha,n}\eta_{\alpha,n}\right)}\,. \tag{VI.38}$$

The Grassmann integrals in (VI.38) are easily performed as in (VI.33), and yield,

$$Z[\eta,\bar{\eta}] \simeq \det K \exp\left\{-\sum_{\substack{n,m\\ \alpha,\beta}} \bar{\eta}_{\alpha,n} K^{-1}_{\alpha\beta,nm} \eta_{\beta,m}\right\}\,, \tag{VI.39}$$

with the fermionic two-point function

$$\langle \hat{\psi}_\alpha \hat{\bar{\psi}}_\beta \rangle = K^{-1}_{\alpha\beta,nm}\,. \tag{VI.40}$$

Equation (VI.39) and (VI.40) are lookalikes of (VI.18) and (VI.20) respectively. Seemingly the only difference is the different power of the determinant. However, another surprise is buried in the kinetic operator. This is more clearly

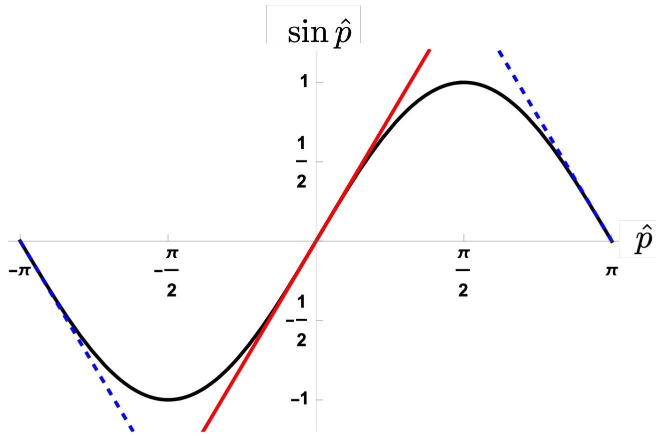

FIG. 14: Fermionic lattice dispersion in one dimension.

seen in momentum space. There we have

$$K_{\alpha\beta,nm} = \int_{-\pi}^{\pi} \frac{d^4\hat{p}}{(2\pi)^4} \tilde{K}_{\alpha\beta}(\hat{p}) e^{i\hat{p}(n-m)} \tag{VI.41}$$

with

$$\tilde{K}_{\alpha\beta}(\hat{p}) = i\,(\gamma_\mu)_{\alpha\beta} \sin\hat{p}_\mu + \hat{m}_\psi\,. \tag{VI.42}$$

Now we proceed with the same argument as around (VI.26): only the zeros of the dispersion (VI.42) survive in the continuum limit, as

$$\int_{-\pi}^{\pi} \frac{d^d\hat{p}}{(2\pi)^d} \hat{\bar{\psi}}_\alpha(-\hat{p}) K(\hat{p}) \psi_\beta(\hat{p}) = \int_{-\frac{\pi}{a}}^{\frac{\pi}{a}} \frac{d^d p}{(2\pi)^d} \bar{\psi}_\alpha(-p) \frac{1}{a} K(pa) \psi(p)\,. \tag{VI.43}$$

Accordingly, only configurations with support for momenta $\hat{p}$ with $K(pa) \propto a$ lead to a finite action. Let us first look at an oversimplified example, the dispersion in $1+0$ dimensions,

$$\tilde{K}(\hat{p}) \sim \sin\hat{p}\,, \tag{VI.44}$$

also depicted in Figure 14. Naturally, the dispersion (VI.44) vanishes at the middle of the Brillouin zone at $p = 0$ and shows a linear dispersion with a positive slope, $1/a\tilde{K}(\hat{p} \to 0) \to 1/a\hat{p} = p$, depicted by the *straight red* tangent line in Figure 14. On the boundary points of the Brillouin zone, the dispersion also vanishes with $1/a\tilde{K}(\hat{p}) \to -p$ depicted by the *dashed blue* tangent line in Figure 14. This leaves us with *two* fermions in the continuum limit, one with dispersion p and one with the dispersion $-p$. Note that the latter fermion is distributed at the two boundary points of the lattice $\hat{p} = \pi$ (positive dispersion) and $\hat{p} = -\pi$ (negative dispersion). In summary our attempt of putting one fermion on the lattice ended in having two of them in the continuum limit. This is a baby version of the *fermion doubling problem*.

Let us now try to get rid of the doubler in (VI.44), Figure 14. Note first that the problem can be avoided by using left or right derivatives instead of the symmetric one (show it). However, these derivatives are not anti-hermitian, which leaves us with complex eigenvalues for the Dirac operator that only turn real in the continuum limit. This is a hefty price to pay. Another possibility consists out of adding higher derivatives terms such as $K(\hat{p}) \to \sin\hat{p} + r/2\sin^2\hat{p}/2$, where the second term is nothing but the lattice Laplacean (VI.13) in momentum space, (VI.24). Evidently for $\hat{p} \propto a$ this term vanishes linear with the lattice distance in the physical dispersion $1/aK(\hat{p})$, while it leads to a $1/a$ divergence at $\hat{p} \to \pi, -\pi$. Accordingly, the doubler disappears in the continuum limit.

After this little excursion we come back to the fermionic lattice field theory. As in our baby example we collect all the zeros of the dispersion. For example, in two dimensions we have the four zeros

$$(0,0)\,, \quad \{(0,\pm\pi)\}\,, \quad \{(\pm\pi,0)\}\,, \quad \{(\pm\pi,\pm\pi)\}\}\,. \tag{VI.45}$$

More generally we have 2^d zeros in d dimensions: at all points where all p_μ take values $(0, \pm\pi)$,

$$\hat{p}_\mu \in \{0\,,\, \pm\pi\} \qquad \forall \mu = 1, ..., d\,. \tag{VI.46}$$

At these points the continuum limit of the propagator is given by

$$\lim_{a\to 0}\frac{1}{a^3}\int_{-\pi}^{\pi}\frac{d^4\hat{p}}{(2\pi)^4}\frac{e^{i\hat{p}(n-m)}}{\tilde{K}(\hat{p})} = -\lim_{a\to 0}\int_{-\pi/a}^{\pi/a}\frac{d^4p}{(2\pi)^4}\frac{e^{ip(x-y)}}{i\gamma_\mu\frac{1}{a}\sin ap_\mu + m} = -\sum_j\int_{\varepsilon_1}\frac{d^4p}{(2\pi)^4}\frac{e^{ip(x-y)}}{(-1)^{j+1}i\gamma_\mu p_\mu + m} + \mathcal{O}(a)\,. \tag{VI.47}$$

Note that the sign of the γ- matrices can be flipped by a $\hat{p}$-dependent similarly transformation $S(\hat{p})$,

$$S(\hat{p})\gamma_\mu S^{-1}(\hat{p}) = (-1)^{j+1}\gamma_\mu\,. \tag{VI.48}$$

In summary we have produced 16 fermions on the lattice. This is the (in)famous doubling problem on the lattice. We note in passing, that the rather heuristic statement above can be cast in a mathematical form by considering the fermions in momentum space, $\hat{\psi}(\hat{p})$. As in position space, fermions are periodic in momentum space,

$$\hat{\psi}(\hat{p} + \hat{\mu}) = \hat{\psi}(\hat{p} + 2\pi\hat{\mu})\,, \tag{VI.49}$$

which singles out the Brillouin zone in the first place. Therefore, fermions can be seen as maps from the d-dimensional (momentum) torus into the field space, e.g. $\mathbb{T}^4 \to \mathbb{C}^4$ for a four-dimensional single Dirac fermion. In general even dimensions, the latter has $2^{d/2}$ (complex) components as the Clifford algebra is $2^{d/2}$-dimensional. Then, left- and right-handed eigenspaces can be defined by momentum dependent projections, and the winding numbers of these projections is related to the total chirality of the theory, see e.g. [21] and references therein.

For the purposes of the present lecture course it is sufficient to briefly discuss possible resolutions and concentrate on the simple practical ones, the topic is picked up later, when discussing the continuum limit in more detail, including an renormalisation group (Kadanoff block-spinning) analysis on the lattice.

2. Wilson fermions

We have already indicated above in the discussion of our baby example, that the introduction of higher derivative terms in the kinetic term gives us the possibility to suppress the doublers in the continuum limit. This is done by augmenting them with masses proportional to $1/a$,

$$K^{(W)}_{\alpha\beta,nm} = K_{\alpha\beta,nm} + \frac{r}{2}\sum_{\substack{n,m\\ \alpha,\beta}}\hat{\bar{\psi}}_{\alpha,n}\hat{\Delta}_{n,m}\hat{\psi}_{\beta,m}\,. \tag{VI.50}$$

with $K_{\alpha\beta,nm}$ in (VI.37b) and the dimensionless Wilson parameter r and the lattice Laplacian (VI.13). In Momentum space this kinetic term reads

$$K^{(W)}_{\hat{p}} = i\gamma_\mu\sin\hat{p}_\mu + \hat{m}_\psi + 2r\sum_{\mu=0}^{d-1}\sin^2\left(\frac{\hat{p}_\mu}{2}\right)\,, \tag{VI.51}$$

with the lattice Laplacian in momentum space in (VI.24). The Wilson term vanishes for the fermion at $\hat{p} \to 0$, while it diverges at all the doubler points defined by (VI.46),

$$d\frac{r}{2a} \geq \frac{2r}{a}\sum_{\mu=0}^{d-1}\sin^2\left(\frac{\hat{p}_\mu}{2}\right) \geq \frac{r}{2a}\,, \qquad \text{for} \qquad \hat{p} \neq 0 \quad \text{and} \quad \hat{p}_\mu \in \{0\,,\, \pm\pi\}\,. \tag{VI.52}$$

Evidently, (VI.51) breaks chiral symmetry as it includes the momentum dependent Wilson mass term proportional to the identity in Dirac space. Only in the continuum limit chiral symmetry is restored (in the absence of explicit fermion masses, $m_\psi = 0$). While this is a heavy price to pay for theories with chiral symmetry or that 'close' to chiral symmetry such as present for the light current quark masses of the up and down quark in QCD, it is a simple deformation which is amiable to numerical implementation in simulations.

3. Staggered fermions

Another possibility is the exploitation of the doublers as physical mode. For example, as we have indicated above, putting one (massless) Weyl fermion on the lattice leads us to 2^d Weyl fermions in the continuum limit with different chirality. Now, we even can assign different mass gaps to the fermions which allows us to define them as different flavours of the original fermion.

Staggered fermions exploit this possibility. Before we come to some technical details, we would like to give the flavour of the argument (pun intended). The most efficient way of their implementation is a simple counting and distribution of fermionic degrees of freedom. In the following, we restrict ourselves to even dimensions, specifically $d = 2$ and $d = 4$. In even dimensions d, a Dirac fermion has $2^{d/2}$ complex components, that can be distributed over 2^d zeros of the dispersion at the positions (VI.46). This leads us to minimally $2^{d/2}$ different Dirac fermions in this formulation, called different *tastes*. For example, in QCD in $d = 4$ dimensions we then would have 4 tastes. It is tempting to identify them with the *flavours* in QCD, so a minimal version of lattice QCD would have four flavours, up, down, strange charm. However, the latter have significantly different masses, and the chiral structure of the theory crucially depends on the mass ordering, typically indicated 2+1+1 in order to single out the two light quarks, u, d with current masses $m_{u,d} \sim 2 - 5\,\mathrm{MeV}$, the heavier strange quark with a current quark mass of $m_s \sim 10^2\,\mathrm{MeV}$ and the charm quark with a current quark mass of $m_c \sim 10^3\,\mathrm{MeV}$.

However, the fact, that in our QCD example we have four tastes with identical masses, leads us to

$$\exp\left\{\mathrm{tr}_{\mathrm{lattice}} \log K\right\} = \det_{\mathrm{lattice}} K \to \left(\det_{\mathrm{cont}} [\not{p} + m_\psi]\right)^4 = \exp\left\{4\mathrm{tr}_{\mathrm{cont}} \log\left(\not{p} + m_\psi\right)\right\} . \tag{VI.53}$$

Equation (VI.53) suggests to e.g. simply take the square root of (VI.53), if considering two-flavour QCD in the isopsin-symmetric limit $m_u = m_d$. The latter is typically chosen in many applications as both, the current quark masses m_u, m_d and the mass difference $m_u - m_d$ is rather small in comparison to the mass arising from spontaneous strong chiral symmetry breaking $\sim 300 - 400\,\mathrm{MeV}$.

Evidently, for one Dirac fermion one has to consider the fourth root of (VI.53). Effectively, this is done on the level of the exponent on the left hand side of (VI.53)

$$\mathrm{tr}_{\mathrm{lattice}} \log K \to \frac{1}{N} \mathrm{tr}_{\mathrm{lattice}} \log K \to \mathrm{tr}_{\mathrm{cont}} \log\left[\not{p} + m_\psi\right] , \tag{VI.54}$$

with $N = 16$ in the case of a four-dimensional Dirac fermion. Such a rooting is commonplace, but has its problems. While (VI.54) provides the core of the argument, the remaining Dirac fermion is de-localised on the lattice, its component being distributed at the points (VI.46).

How one can construct such a fermion technically, is discussed now at the example of a single Dirac fermion in $d = 4$. We recall its action (VI.37),

$$S_\psi\left[\hat{\psi}, \hat{\bar{\psi}}\right] = -\sum_{n,m} \hat{\bar{\psi}}_n \left[\sum_{\mu=1}^{4} \gamma_\mu \frac{\delta_{m,n+\hat{\mu}} - \delta_{m,n-\hat{\mu}}}{2} + \hat{m}_\psi \delta_{mn}\right] \hat{\psi}_m , \tag{VI.55}$$

and we make a site-dependent transformation of the fermions in Dirac space such that the Dirac structure 'disappears', and the component fermions $\psi_{\alpha,m}$ run the show. This is done with the *staggered transformations*

$$\hat{\psi}_n = \gamma_1^{n_1} \gamma_2^{n_2} \gamma_3^{n_3} \gamma_0^{n_0}\, \hat{\psi}' , \qquad \text{and} \qquad \hat{\bar{\psi}}_n = \hat{\bar{\psi}}'_n\, \gamma_0^{n_0} \gamma_3^{n_3} \gamma_2^{n_2} \gamma_1^{n_1} . \tag{VI.56}$$

The staggered transformation rotates the fermions from one lattice site to the next such that the Dirac structure of the next neighbour hopping terms is absorbed into the fields. Moreover, for the site terms we have $\hat{\bar{\psi}}_n \hat{\psi}_n = \hat{\bar{\psi}}'_n \hat{\psi}'_n$ owing to $\gamma_\mu^2 = \mathbb{1}$.

Now we consider exemplary one hopping term in the $\mu = 3$ direction. There we have

$$\hat{\bar{\psi}}_n \gamma_3 \hat{\psi}_{n\pm\hat{3}} = \hat{\bar{\psi}}'_n\, \gamma_0^{n_0} \gamma_3^{n_3} \gamma_2^{n_2} \gamma_1^{n_1}\, \gamma_3\, \gamma_1^{n_1} \gamma_2^{n_2} \gamma_3^{n_3 \pm 1} \gamma_0^{n_0}\, \hat{\psi}'_{n\pm\hat{3}} = (-1)^{n_1+n_2} \hat{\bar{\psi}}'_n \hat{\psi}'_{n\pm\hat{3}} . \tag{VI.57}$$

Here, the factor $(-1)^{n_1+n_2}$ counts, how many times we have to have to anti-commute γ_1 and γ_2 with the explicit γ_3 in the middle. Again using $\gamma_\mu^2 = \mathbb{1}$ we arrive at (VI.57), and similarly for the other hopping terms.

Inserting all these transformations into (VI.55), we are led to,

$$S_\psi[\psi,\bar\psi] = \sum_{n,\mu}\left[\frac{1}{2}\,\eta_{n,\mu}\,\hat{\bar\psi}{}'_n\left(\hat\psi'_{n+\hat\mu} - \psi'_{\hat n-\hat\mu}\right) + \hat m_\psi\,\hat{\bar\psi}{}'_n\hat\psi'_n\right], \tag{VI.58}$$

with

$$\eta_{n,1} = 1\,, \qquad \eta_{n,2} = (-1)^{n_1}\,, \qquad \eta_{n,3} = (-1)^{n_1+n_2}\,, \qquad \eta_{n,0} = (-1)^{n_1+n_2+n_3}\,. \tag{VI.59}$$

Importantly, (VI.58) is diagonal in Dirac space in the rotated Dirac fields $\psi_{\alpha,n}$, and all components have the same action. Accordingly, the rooting (VI.54) simply amounts to dropping the Dirac sum in (VI.58), only considering one component, $\hat\chi_n = \hat\psi_{\alpha,n}$. We arrive at the final result,

$$S_\chi[\chi,\bar\chi] = \sum_{n,\mu}\left[\frac{1}{2}\,\eta_{n,\mu}\,\hat{\bar\chi}_n\left(\hat\chi_{n+\hat\mu} - \chi_{\hat n-\hat\mu}\right) + \hat m_\psi\,\hat{\bar\chi}_n\hat\chi_n\right], \tag{VI.60}$$

With this procedure we have reduced the number of 16 Dirac fermions to 4 Dirac fermions (tastes). In the current lecture course we will rarely use staggered fermions, and if, we will use the rooting prescription indicated above. Hence, for more details as well as a detailed discussion of chiral symmetry and *taste violation*, we refer to the literature, in particular to [22], chapter 4 and [23], chapter 10.1.

4. *Chiral symmetry on the lattice & the fate of the axial anomaly∗*

However, for its importance as well as its illustrative nature we briefly discuss the fate of (naive) chiral symmetry on the lattice. We emphasise that the derivation below is sketchy and the single step, while straightforward, are a bit tedious. This topic will be picked up later within a more elaborated point of view also involving renormalisation group (RG) arguments.

To begin with, let us assume that we have coupled an external gauge field to the fermion, this will be detailed in the next chapter. Then, the Dirac action reads

$$S_\psi\left[\hat\psi,\hat{\bar\psi}\right] = -\sum_{n,m}\left[\hat{\bar\psi}_n\mathcal{D}_{n,m} + \hat m_\psi\delta_{mn}\right]\hat\psi_m\,, \tag{VI.61}$$

with the naive interacting lattice Dirac operator $\mathcal{D}_{n,m}$ that is proportional to γ_μ and hence it anti-commutes with γ_5 defined in (VI.29),

$$\{\mathcal{D},\gamma_5\} = 0\,, \tag{VI.62}$$

It is precisely the property (VI.62), that the Dirac operator of Wilson fermions violates, and indeed one can show, that one either has doublers or one looses (VI.62).

In **??** we keep the mass but consider the limit $\hat m_\psi \to 0$. Now we apply local chiral transformations

$$\hat\psi_n \to e^{\mathrm{i}\alpha(n)\gamma_5}\hat\psi_n\,, \qquad \hat{\bar\psi}_n \to \hat{\bar\psi}_n\,e^{\mathrm{i}\alpha(n)\gamma_5}\,. \tag{VI.63}$$

to the action (VI.61). Using (VI.61) as the action in the fermionic path integral, the theory is still Gaußian (free). Expanding the transformed path integral in powers of α, we are led to the standard (partial) axial current conservation,

$$\hat\partial_\mu\langle j_{5,\mu}\rangle = 2\hat m_\psi\langle\hat{\bar\psi}_n\gamma_5\hat\psi_n\rangle\,, \qquad \text{with} \qquad j_{5,\mu} = \hat{\bar\psi}_n\gamma_5\hat\psi_n\,, \tag{VI.64}$$

where the derivative is the symmetric lattice derivative. Now we sum over the lattice, and the left hand side vanishes as it is a total derivative. There are no boundary terms due to the periodic boundary conditions. This leads us instantly to

$$\hat m_\psi\sum\langle\hat{\bar\psi}_n\gamma_5\hat\psi_n\rangle = -\hat m_\psi\mathrm{Tr}\gamma_5\langle\hat\psi_n\hat{\bar\psi}_m\rangle = 0\,. \tag{VI.65}$$

The expectation value under the trace is nothing but the propagator

$$\langle\hat{\psi}_n\hat{\bar{\psi}}_m\rangle = \left[\frac{1}{\mathcal{D}+\hat{m}_\psi}\right]_{nm}\,. \tag{VI.66}$$

with the anti-hermitian operator $\mathcal{D}$ with the spectrum

$$\mathcal{D}\hat{\varphi}_j = \mathrm{i}\lambda_j\varphi_j\,,\qquad \text{with}\qquad j\in\mathbb{N}\,, \tag{VI.67}$$

For every $\lambda_j \neq 0$, $\gamma_5\varphi_j$ also is an Eigenfunction to the Eigenvalue $-\mathrm{i}\lambda_j$. Since $\lambda_j \neq 0$, we have

$$\sum_n \varphi_j(n)\gamma_5\varphi_j(n) = 0\,. \tag{VI.68}$$

This leads us to

$$-\hat{m}_\psi \mathrm{Tr}\gamma_5\langle\hat{\psi}_n\hat{\bar{\psi}}_m\rangle = n_+ - n_- = 0\,, \tag{VI.69}$$

where n_+ and n_- is the number Eigenfunctions $\varphi^{(0)}$ of vanishing Eigenvalues with positive and negative chirality respectively.

$$\gamma_5\varphi^{(0)} = \pm\varphi^{(0)}\,,\qquad \text{as}\qquad \varphi^{(0)}_{j_1}\left\{\gamma_5\,,\,\mathcal{D}\right\}\varphi^{(0)}_{j_2} = 0\,. \tag{VI.70}$$

In conclusion, the total chirality of the fermionic lattice theory is vanishing. Again this reflects the Nielsen-Ninomiya theorem on the lattice. In this formulation is also hints at some serious physics problems, as the (non-vanishing) axial anomaly carries important physics.

C. Gauge Fields on the Lattice

With lattice formulations of scalar fields and fermions as introduced in Section VI A and Section VI B respectively, we close our discussion of lattice formulations of field theories with that of gauge theories. Before introducing lattice gauge theories, we recapitulate the basiscs of gauge theories in the continuum, see Section I. For the better comparability with lattice gauge theory textbooks we shall use a slightly different notation here than in Section I. We start with an Abelian gauge theory with a Dirac fermion,

$$S_\psi\left[\psi,\bar{\psi},A_\mu\right] = \int_x \bar{\psi}\left(\not{D}+m_\psi\right)\psi\,,\qquad\text{where}\qquad \not{D} = \gamma_\mu D_\mu\,,\qquad D_\mu = \partial_\mu + \mathrm{i}eA_\mu\,. \tag{VI.71}$$

with the Abelian gauge field $A_\mu \in \mathbb{R}$, that is in the algebra of the gauge group U(1). Note that the definition of the covariant derivative differs from that in with $D_\mu = \partial_\mu - \mathrm{i}eA_\mu$ by a relative minus sign. The action (VI.71) is invariant under gauge transformations $\Omega(x) = \exp \mathrm{i}\omega(x) \in$U(1) of the Dirac fermion and the gauge field,

$$\psi(x)\to\Omega(x)\psi(x)\,,\qquad \bar{\psi}(x)\to\bar{\psi}(x)\Omega^\dagger(x)\,,\qquad A_\mu \to -\frac{\mathrm{i}}{e}\Omega\left(D_\mu\Omega^\dagger\right) = A_\mu - \partial_\mu\omega\,. \tag{VI.72}$$

The transformation of the gauge field implies that the covariant derivative transforms as a tensor under gauge transformations

$$D_\mu \to \Omega\, D_\mu\,\Omega^\dagger\,, \tag{VI.73}$$

where we use the notation $\Omega \in$U(1) for gauge transformations, instead of U as in (I.5). The pure gauge field part of the gauge field is given by the standard U(1) action with

$$S_A[A_\mu] = \frac{1}{4}\int_x F^2_{\mu\nu}\,,\qquad\text{with}\qquad F_{\mu\nu} = -\frac{\mathrm{i}}{e}\left[D_\mu\,,\,D_\nu\right] = \partial_\mu A_\nu - \partial_\nu A_\mu\,. \tag{VI.74}$$

The relative minus sign in comparison to (I.7) originates in the definition of the covariant derivative.

This set-up is easily generalised to non-Abelian gauge theories, where we restrict ourselves to SU(N$_c$) theories coupled to fermions ψ^A in the fundamental representation with $A = 1,...,$N$_c$, where N$_c$ is generically called the number of colors, referring to QCD. We have

$$S_\psi\left[\psi,\bar\psi,A_\mu\right]=\int_x \bar\psi^A\left(\not{D}+m_\psi\right)^{AB}\psi^B\,,\qquad\text{where}\qquad D_\mu^{AB}=\partial_\mu\delta^{AB}+\mathrm{i}gA_\mu^c(t^c)^{AB}\,,\tag{VI.75}$$

with $a=1,...,\mathrm{N}^2-1$, and $A_\mu^a(x)\in\mathbb{R}$. The action (VI.75) is invariant under gauge transformations $\Omega(x)=\exp\mathrm{i}\omega(x)\in\mathrm{SU(N}_c)$ with the Lie algebra valued exponent $\omega(x)=\omega^a(x)t^a\in\mathrm{su(N}_c)$ of the Dirac fermion and the gauge field, similarly to (VI.76),

$$\psi(x)\to\Omega(x)\psi(x)\,,\qquad\bar\psi(x)\to\bar\psi(x)\Omega^\dagger(x)\,,\qquad A_\mu\to-\frac{\mathrm{i}}{g}\Omega\left(D_\mu\Omega^\dagger\right)\,,\tag{VI.76}$$

the difference being the non-commutativity of the gauge field. The transformation of the gauge field implies that the covariant derivative transforms as a tensor under gauge transformations

$$D_\mu\to\Omega D_\mu\Omega^\dagger\,,\tag{VI.77}$$

with $D_\mu\Omega^\dagger\psi=(D_\mu\Omega^\dagger)\psi+\Omega^\dagger(D_\mu\psi)$. The pure gauge field action (Yang-Mills action) is given by

$$S_A[A_\mu]=\frac12\int_x\mathrm{tr_f}F_{\mu\nu}^2=\frac14\int_x(F_{\mu\nu}^a)^2\,,\tag{VI.78}$$

with the field strength $F_{\mu\nu}=F_{\mu\nu}^at^a$ with

$$F_{\mu\nu}=-\frac{\mathrm{i}}{g}\left[D_\mu\,,\,D_\nu\right]\,,\qquad\text{and}\qquad F_{\mu\nu}^a=\partial_\mu A_\nu^a-\partial_\nu A_\mu^a-g\,f^{abc}A_\mu^bA_\mu^c\,,\tag{VI.79}$$

As already mentioned above, QCD has the gauge group SU(3) (three colours), and the fermions are the quarks (u,d,s,c,b,t) or a subset thereof. It is also very common to do simulations in SU(2) theories as these theories share many communalities but SU(2) is far simpler to simulate, in particular at finite densities. There, however, it is also differs significantly from QCD with three colours. Moreover, the SU(2) case is also the weak sector of the Standard Model (SM), and with the hyper charge U(1) it adds up to the electroweak sector of the SM.

In the latter case we also have to consider a scalar field, the Higgs field, that carries a representation of the electroweak gauge group. Hence, more generally, we consider the kinetic term of a complex scalar field also carrying the fundamental representation of a non-Abelian gauge group,

$$S_\phi[\phi,A_\mu]=\int_x(\phi^\dagger)^A(D_\mu^2)^{AB}\phi^B\,,\qquad\text{with}\qquad\phi=\frac{1}{\sqrt2}(\phi_1+\mathrm{i}\phi_2)\,.\tag{VI.80}$$

The gauge transformation of the scalar field is given by

$$\phi(x)\to\Omega(x)\phi\,,\qquad\phi^\dagger(x)\to\phi^\dagger\Omega^\dagger(x)\tag{VI.81}$$

and the gauge invariance of the action (VI.80) follows readily.

With the matter actions (VI.71), (VI.75), (VI.80) and the pure gauge theory actions (VI.74) and (VI.78) we have all ingredients of the Standard Model, except the chiral structure of the electroweak interaction.

1. Lattice action of gauge field theories

We start our discussion of the action of lattice gauge theories by first working out the lattice analogue of (VI.81). The arguments work the same way for the fermionic action.

As in the continuum we introduce the gauge transformation for the complex matter field $\hat\phi_n$, living on the sites,

$$\hat\phi_n\to\Omega(n)\hat\phi_n,\qquad\hat\phi_n^\dagger\to\hat\phi_n^\dagger\Omega^\dagger(n)\,,\tag{VI.82}$$

where $\Omega(n)\in\mathrm{SU(N}_c)$ or $\Omega(n)\in\mathrm{U}(1)$. The lattice action of the free (complex) scalar theory is given in (VI.14) with the dispersion K_{nm} defined in (VI.15), which we recall here for the sake of convenience.

$$K_{nm} = -\sum_{\mu>0} [\delta_{n+\hat\mu,m} + \delta_{n-\hat\mu,m}] + (\hat m_\phi^2 + 2d)\,\delta_{nm}\,. \tag{VI.83}$$

The terms in $\phi^\dagger K_{nm}\phi$ living on a site (part of K_{nm} proportional to δ_{nm}) are invariant under (VI.82), and we have to ensure gauge invariance for e.g.

$$\hat\phi_n^\dagger \hat\phi_{n+\hat\mu}\,. \tag{VI.84}$$

This entails that we have to *transport* the group element $\Omega^\dagger(n+\hat\mu)$ from the lattice point $n+\hat\mu$ to n. To that end we define the *link variable* $U_\mu(n)\in$SU(N$_c$) with

$$U_\mu(n) \to \Omega(n) U_\mu(n) \Omega^\dagger(n+\hat\mu)\,, \tag{VI.85}$$

and the parametrisation $U_\mu(n) = e^{i\hat\theta_\mu(n)}$ with the Lie algebra field $\theta_\mu(n) \in$ su(N$_c$). The link variable is nothing but a parallel transporter along the link between the sites n and $n+\hat\mu$. It 'lives' on the link between n and $n+\hat\mu$. Accordingly, the term $\hat\phi_n^\dagger U_\mu(n)\hat\phi_{n+\mu}$ is gauge invariant: The link variable $U_\mu(n)$ parallel transports (infinitesimally) the gauge transformation from the lattice site $n+\hat\mu$ to the lattice site n. There it is annihilated. Explicitly, this upgrade of (VI.84) transforms with

$$\hat\phi_n^\dagger\, U_\mu(n)\, \hat\phi_{n+\mu} \to \hat\phi_n^\dagger\, \Omega^\dagger(n)\Omega(n)\, U_\mu(n)\, \Omega^\dagger(n+\hat\mu)\Omega(n+\hat\mu)\, \hat\phi_n\,. \tag{VI.86}$$

Trivially, this also holds for $\phi_n^\dagger U_\mu^\dagger(n-\hat\mu)\phi_{n-\mu}$. Then the free action (VI.14) turns into,

$$S[\hat\phi,U] = -\sum_{\substack{n\\ \mu>0}} \left(\hat\phi_n^\dagger U_n^\dagger(n-\hat\mu)\hat\phi_{n-\hat\mu} + \hat\phi_n^\dagger U_\mu\,(n)\,\hat\phi_{n+\hat\mu}\right) + \sum_n \hat\phi_n^\dagger\hat\phi_n\left(2d+\hat m_\phi^2\right)\,, \tag{VI.87}$$

which reduces to (VI.14) for $U_\mu = \mathbb{1}$.

We proceed by showing that the continuum limit of the gauge invariant lattice action is the continuum action (VI.80). To that end we write

$$U_\mu(n) = e^{ig_0 a A_\mu(an)} = \mathbb{1} + ig_0 a A_\mu(an) - \frac{1}{2}\left(ig_0 a A_\mu(an)\right)^2 + O(a^3)\,, \tag{VI.88}$$

which defines a gauge field A_μ on the lattice. In the following we only need (VI.88) up to the quadratic term in the lattice distance a as displayed in (VI.88). This already entails that (VI.88) is not the unique definition of the gauge field. Moreover, we shall see that order a^2 terms in the exponent of U_μ vanish in the continuum limit. Accordingly, the gauge field is only defined up to terms $O(a)$, and these terms disappear in the continuum limit.

Now we expand (VI.87) in powers of the lattice spacing a, using (VI.88) as well as (VI.6). For the sake of simplicity we restrict ourselves to $d=4$. First, using the expansion in (VI.88) we get,

$$S[\hat\phi,U] \overset{a\to 0}{\to} -\sum_{n,m}\hat\phi_n^\dagger K_{nm}\hat\phi - \sum_{\substack{n\\ \mu>0}}\hat\phi_n^\dagger\left[-iag_0 A_\mu(na-\hat\mu a)\hat\phi_{n-\hat\mu} + iag_0 A_\mu(na)\hat\phi_{n+\hat\mu}\right] - \sum_n \hat\phi_n^\dagger\left(iag_0 A_\mu\right)^2\hat\phi_n\,, \tag{VI.89}$$

where we only keep the terms up to order a^2. Now we use (VI.6) to map our dimensionless scalar lattice fields to the dimensionful ones, $\hat\phi_n = a\,\phi(na)$. Moreover, we use

$$\phi(na\pm a\hat\mu) = \phi(na) \pm a\partial_\mu\phi(na) + O(a^2)\,, \qquad A_\mu(na\pm\hat\mu a) = A_\mu(na) + a\partial_\mu A_\mu(na) + O(a^2)\,, \tag{VI.90}$$

where no sum is implied. Collecting all the terms on the right hand side of (VI.89), we arrive at

$$-a^4\left\{\sum_{n,m}\phi^\dagger(na)\frac{K_{nm}}{a^2}\phi(ma) + ig_0\sum_{\substack{n\\ \mu>0}}\phi^\dagger(na)\left[\partial_\mu A_\mu(na) + A_\mu(na)\partial_\mu\right]\phi(na) + \sum_n\hat\phi_n^\dagger\left(ig_0A_\mu\right)^2\hat\phi_n + O(a)\right\}\,. \tag{VI.91}$$

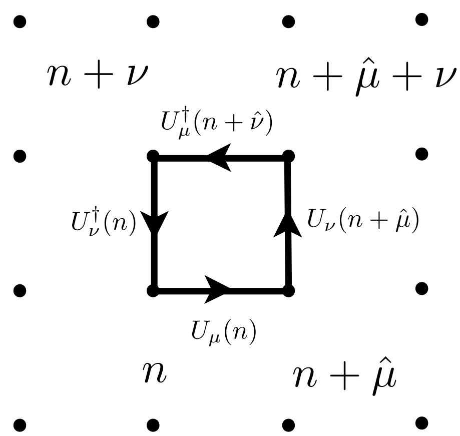

FIG. 15: Plaquette variable $U_{\mu\nu}(n)$.

We use that in the continuum limit we have $a^4\sum_n \to \int_{\mathbb{R}^4}$ and arrive at

$$S[\hat{\phi}, U] \to \int d^4x \phi^\dagger(x) \left[D_\mu^2 + m_\phi^2\right] \phi(x) + O(a)\,. \tag{VI.92}$$

In summary, we have obtained the desired result, our gauge invariant lattice action (VI.87) reduces to the gauge invariant continuum action (VI.80) for $a \to 0$.

Now we proceed with defining a lattice analogue of the pure gauge action (VI.74) or (VI.78). The building block of the pure gauge action is the field strength tensor $F_{\mu\nu}$, which in the continuum is the curvature tensor $1/(ig)\,[D_\mu\,,\,D_\nu]$, see (VI.79). The covariant derivative D_μ induces an infinitesimal parallel transport in the direction $\hat{\mu}$, and hence the commutator is first transporting in the ν-, then in the μ-direction, and then back in the inverse path. On the lattice, this operation is implemented by the Plaquette variable,

$$U_{\mu v}(n) = U_\mu(n) U_\nu(n+\hat{\mu}) \hat{U}^\dagger_\mu(n+\hat{\nu}) U^\dagger_\nu(n)\,. \tag{VI.93}$$

As the link variable, the Plaquette variable lives in the gauge group. In analogy to the algebra-valued gauge field defined in the exponent of the link variable in (VI.88), we can define an algebra-valued field strength in the exponent of the Plaquette,

$$U_{\mu\nu}(n) = e^{ig_0 a^2 \mathcal{F}_{\mu\nu}(n)} \tag{VI.94}$$

with lattice field strength tensor $\mathcal{F}_{\mu\nu}$. In QED we derive from (VI.93),

$$\mathcal{F}_{\mu\nu}(n) = \frac{1}{a}\left[\underbrace{\left(A_\nu(n+\hat{\mu}) - A_\nu(n)\right)}_{\hat{\partial}^R_\mu A_\nu} - \underbrace{\left(A_\mu(n+\hat{\nu}) - A_\mu(n)\right)}_{\hat{\partial}^R_\nu A_\mu}\right]\,, \tag{VI.95}$$

where the left and right derivatives in (VI.95) ensure the anti-symmetry of the expression. In non-Abelian gauge theories such as QCD we use the Baker-Campbell-Hausdorff formula for the expansion,

$$e^A e^B = e^{A+B+\frac{1}{2}[A\,,\,B]+\cdots}\,. \tag{VI.96}$$

With (VI.96) we arrive at,

$$\mathcal{F}_{\mu\nu}(n) = \frac{1}{a}\left[\hat{\partial}^R_\mu A_\nu - \hat{\partial}^R_\nu A_\mu + ig_0 a\,[A_\mu\,,\,A_\nu](n) + \mathcal{O}(a)\right]\,. \tag{VI.97}$$

Both, (VI.95) and (VI.97) imply that the Plaquette variable can be expanded in powers of the field strength in the continuum limit, each power going with higher orders of the lattice distance,

$$U_{\mu\nu}(n) \overset{a\to 0}{\to} 1 + ig_0 a\mathcal{F}_{\mu\nu}(n) - \frac{g_0^2a^2}{2}\mathcal{F}^2_{\mu\nu}(n) + \mathcal{O}(a^3)\,. \tag{VI.98}$$

Summed over μ,ν, the $F^2_{\mu\nu}$-term in (VI.98) is the Yang-Mills action in the continuum, up to prefactors. In turn, the unity and linear term have to be cancelled. Evidently, the linear term is removed by adding the adjoint of the Plaquette to (VI.98),

$$U_{\mu\nu}(n) + U^\dagger_{\mu\nu}(n) = 2 - g_0^2a^2\mathcal{F}^2_{\mu\nu}(n) + \mathcal{F}\left(a^3\right)\,. \tag{VI.99}$$

Then, the constant term simply can be subtracted and we arrive at a lattice analogue of the pure Yang-Mills action in the continuum,

$$S_W\left[U_\mu\right] = \beta\sum_{\substack{n\\ \mu<\nu}}\left(1 - \frac{1}{2\mathrm{N}_c}\mathrm{tr_f}\left(U_{\mu\nu}(n) + U^\dagger_{\mu\nu}(n)\right)\right)\,,\qquad \text{with}\qquad \beta = \frac{2\mathrm{N}_c}{g_0^2}\,. \tag{VI.100}$$

Here, β takes the rôle of an expansion parameter getting small for large lattice coupling g_0, and we shall later derive analytic results in such a *strong coupling expansion* about $\beta = 0$, that is $g_0^2 \to \infty$. Here we simply check the naïve continuum limit of (VI.100), to wit,

$$S_W\left[U_\mu\right] \overset{a\to 0}{\longrightarrow} S_A\left[A\right] = \frac{1}{2}\int d^4x\,\mathrm{tr_f}F^2_{\mu\nu}\,, \tag{VI.101}$$

where we have used,

$$\sum_{\mu<\nu}\left(1 - \frac{1}{2N_c}\mathrm{tr}\,\left(U_{\mu\nu} + U^\dagger_{\mu\nu}\right)\right) = \sum_{\mu<\nu}\frac{g_0^2a^2}{2N_c}\mathrm{tr}\,\mathcal{F}^2_{\mu\nu} + O\left(a^3\right) = \frac{g_0a^2}{4N_c}\mathrm{tr}\,\mathcal{F}_{\mu\nu} + \mathcal{O}\left(a^3\right)\,. \tag{VI.102}$$

This finally leads us to a well-defined generating functional for compact Yang-Mills theory and U(1)-theory on the lattice,

$$Z \simeq \int \mathcal{D}U e^{-S_W[U_\mu]}\,, \tag{VI.103}$$

with the Wilson action S_W in (VI.100). The path integral measure in (VI.103) is the *finite* product of *finite* Haar measures of the link variables,

$$DU = \prod_{\substack{l\\ \uparrow\\ \text{links}}} \underset{\substack{\uparrow\\ \text{Haar measure}}}{dU_l}\,. \tag{VI.104}$$

The Haar measure is the measure on the gauge group, that is invariant under a gauge rotation with a group element,

$$\int dU^V = \int dVUV^\dagger = \int dU = 1\,. \tag{VI.105a}$$

$$\int dUU^{ab} = 0\,,\qquad \int dUU^{ab}U^{cd} = 0\,,\qquad \int dU\,\underbrace{U^{ab}\left(U^\dagger\right)^{bd}}_{\delta_{ad}} = \delta_{ad}\,, \tag{VI.105b}$$

For the gauge group of QCD, SU(3), we also have more specifically,

$$\int dU U^{ab} \left(U^\dagger\right)^{cd} = \frac{1}{3}\delta_{ad}\delta_{bc}\,, \qquad\qquad \int dU U^{a_1 b_1} U^{a_2 b_2} U^{a_3 b_3} = \frac{1}{3!}\varepsilon_{a_1 a_2 a_3}\varepsilon_{b_1 b_2 b_3}\,. \tag{VI.106}$$

where the 1/3 reflects the number of colours, $1/N_c$. The relations in (VI.106) are confirmed straightforwardly by summing over the indices. For example, summing over b with $b = c$ in the first relation in (VI.106) and using (VI.105a) leads to δ^{ad} on both sides.

Finally, from the path integral we can derive correlation functions such as,

$$\left\langle U^{a_1 b_1}_{\mu_1}(n_1)\cdots U^{a_m b_m}_{\mu_m}(n_m)\right\rangle = \frac{1}{Z}\int DU\, U^{a_1 b_1}_{\mu_1}(n_1)\cdots U^{a_m b_m}_{\mu_m}(n_m)\, e^{-S_w[U_\mu]} \tag{VI.107}$$

that can be computed either by numerical sampling or, for small lattices or, within appropriate expansion schemes, analytically.

The generating functional (VI.103) is the lattice analogue of the generating functional of Yang-Mills theory or pure $U(1)$ theory in the continuum **??** in **??**, with

$$Z[J] \simeq \int \mathcal{D}A_\mu\, e^{-S_A[A]+\int_x J_\mu A_\mu}\,. \tag{VI.108}$$

In (VI.108) we have dropped a potential gauge fixing and Faddeev-Popov ghost action that typically have to be implemented in the continuum. Another difference is apparent from the comparison of (VI.103) with (VI.108): the latter is built on an integration over the gauge field A_μ living in the algebra of the gauge group while the former is built on an integration over the link variable living in the gauge group. Locally, the respective quantum theories are the same, they may differ globally. Indeed, in two-dimensional gauge theories the two quantisations are known to differ.

D. The Wilson Loop & the Static Quark Potential

With the Wilson action for Abelian and non-Abelian gauge theories we introduce the strong coupling expansion at the example of the expectation value of the *Wegner-Wilson* Loop, called the *Wilson* loop in the literature. In QCD or rather pure Yang-Mills theory, this observable serves as an order parameter, and below we discuss its physics interpretation and its computation in the limit $\beta \to 0$.

1. *Wilson loop in QED & QCD*

To that end we first consider an electron-positron pair or quark-anti-quark pair, which is created at some initial time, pulled apart, kept at some distance L and then annihilated, see Figure 16 for a depiction of the respective worldline or path $\mathcal{C}$. Here we use the electron-positron $(e^+ - e^-)$ pair as an example with particles that can be observed as asymptotic states. In turn, the process of interest with the quark-anti-quark $(q - \bar{q})$ pair does not relate to asymptotic states as quarks are not. It is precisely this property we want to test here.

The physical process can be related to the path integral with the current J_μ of the world line $\mathcal{C}$ of the e^+e^- pair to the photon in the source term $\exp \int_x J_\mu A_\mu$ of the (continuum) path integral (VI.108). The precise definition in terms of states will be described below. In any case, the exponent reads

$$\int d^4x J_\mu A_\mu = ie\int_{t_0}^{t_1} dt\left(A_0(t,\vec{x}) - A_0(t,\vec{y})\right) + ie\int_{\vec{x}}^{\vec{y}} d\vec{z}\left(\vec{A}(t_1,\vec{z}) - \vec{A}(t_0,\vec{z})\right), \tag{VI.109}$$

where the difference in the two terms takes into account the parallel horizontal and vertical path segments, see also the charge flow in Figure 16. The worldline current deduced from (VI.109) is given by

$$J_\mu(x) = ie\int_{\mathcal{C}} dz_\mu\, \delta^{(4)}(z-x)\,, \tag{VI.110}$$

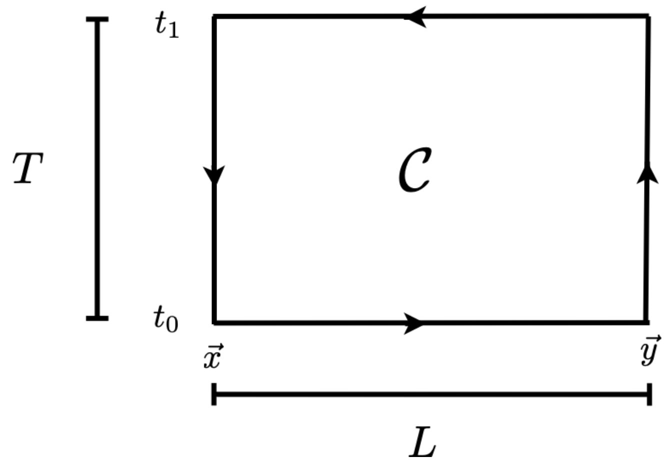

FIG. 16: Wordline or path $\mathcal{C}$ of a static $e^+ - e^-$ or $q - \bar{q}$ pair created at the time t_0 and pulled apart the distance $L = \|\vec{x} - \vec{y}\|$ and kept at this distance for the time $T = t_1 - t_0$. At the time t_1 it is annihilated. The arrows indicate the electric or colour charge flow.

and the full source term is given by the *Wilson loop* $W_{\mathcal{C}}$,

$$W_{\mathcal{C}} := e^{\int d^4x J_\mu A_\mu} = e^{ie \int_{\mathcal{C}} dz_\mu \,, A_\mu(z)} \,. \tag{VI.111}$$

The expectation of the Wilson loop $W_{\mathcal{C}}$ is proportional to the exponential of the free energy $F_{e^+e^-}$ of the $e^+ - e^-$ pair,

$$\langle W_{\mathcal{C}} \rangle \sim e^{-F_{e^+e^-}(\mathcal{C})} \,, \tag{VI.112}$$

and we are interested in its behaviour for large distances L and long times T. As we are working in a Euclidean set-up, the distinction between L and T is an artificial one (for vanishing temperature) and the behaviour in T is the same as that in L.

For (VI.112) being a physical observable, the Wilson loop operator (VI.111) has to be gauge invariant. To that end we consider the Wilson loop with the gauge-transformed gauge field $A^\Omega_\mu = A_\mu - \partial_\mu \omega$ in (VI.72),

$$W_{\mathcal{C}}(A^\Omega) = e^{ie \int_{\mathcal{C}} dz_\mu A^\Omega_\mu(z)} = e^{ie \int_{\mathcal{C}} dz_\mu \left(A_\mu - \frac{1}{e}\partial_\mu \omega\right)} = e^{ie \int_{\mathcal{C}} dz_\mu A_\mu} \,. \tag{VI.113}$$

With the same line of arguments one readily proves that an *open* Wilson *line* with a generic path $\mathcal{C}_{x,y}$

$$W_{\mathcal{C}_{x,y}}(A) = e^{ie \int_{\mathcal{C}_{x,y}} dz_\mu A_\mu(z)} \tag{VI.114}$$

transforms similarly to a U(1) link variable on the lattice. Indeed $W_{\mathcal{C}_{x,y}}$ is a parallel transport from y to x. As such, its infinitesimal form for $y = x + \epsilon\hat{\mu}$ with $\epsilon \to 0$ is the continuum version of the the U(1)-link variable (with $a \to \epsilon$). Under a gauge transformation $\Omega(x)$ the Wilson line (VI.114) transforms covariantly,

$$W_{\mathcal{C}_{x,y}}(A) = \Omega(x) W_{\mathcal{C}_{x,y}}(A) \Omega^\dagger(y) \,, \tag{VI.115}$$

see (VI.85) for comparison. With these definitions we can conclude our derivation of the state or matrix element for the process Figure 16. To that end we consider the matrix element of the propagation of an electron (field) from a position y to the position x. It is given by

$$\langle \bar{\psi}(x) W_{\mathcal{C}_{x,y}}(A) \psi(y) \rangle \,, \tag{VI.116}$$

where the Wilson line is required for gauge invariance, it parallel transports the gauge group element from y to x. For static quarks the phase carries the full dynamics and for closed worldlines $\mathcal{C}$ we are led to the Wilson loop (VI.111) in the $U(1)$ theory.

This derivation is now repeated for a non-Abelian gauge group. However, instead of starting with the worldline we

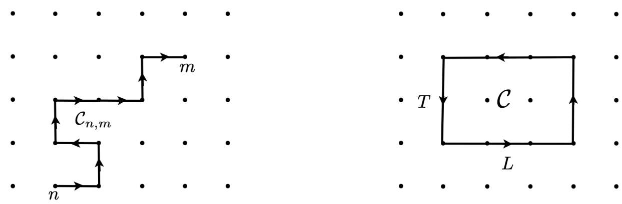

FIG. 17: Wordline or closed paths $\mathcal{C}$ and open paths $\mathcal{C}_{n,m}$ on the lattice

rather use the analogue of the matrix element (VI.116). The non-Abelian Wilson line has to parallel transport the gauge transformation Ω from y to x which leads us to a product of infinitesimal Wilson lines along the path $\mathcal{C}_{x,y}$. This is nothing but a path-ordered exponential similarly to the time-ordered time evolution operator known from the derivation of the path integral. We define

$$U_{\mathcal{C}_{x,y}} = \mathcal{P}\, e^{ig\int_{\mathcal{C}_{x,y}} dz_\mu A_\mu(z)}\,, \tag{VI.117}$$

with the path ordering operator $\mathcal{P}$. For a consecutive order of paths with $\mathcal{C}_{x,y}$ being composed out of the path from y to z, $\mathcal{C}_{z,y}$ and then from z to x, $\mathcal{C}_{x,z}$,

$$\mathcal{P}\, e^{ig\int_{\mathcal{C}_{x,y}} dz_\mu A_\mu(z)} = \mathcal{P}\, e^{ig\int_{\mathcal{C}_{x,z}} dz_\mu A_\mu(z)}\; \mathcal{P}\, e^{ig\int_{\mathcal{C}_{z,y}} dz_\mu A_\mu(z)}\,. \tag{VI.118}$$

We remark that the definition of the Wilson line (VI.118) in terms of the gauge field A_μ makes very explicit its rôle as a parallel transporter. In particular the covariant derivative is given as the parallel transport of the partial derivative,

$$U^\dagger_{\mathcal{C}_{y,x}} \partial^x_\mu U_{\mathcal{C}_{y,x}} = \partial_\mu + igA_\mu\,. \tag{VI.119}$$

This property can be used to write the Dirac equation in terms of the phase factor $U_{\mathcal{C}_{x,y}}$ and the free Dirac operator. The same follows for the respective solution $\psi = U_{\mathcal{C}_{x,y}}\psi_{\text{free}}$ of the full Dirac equation.

The closed Wilson loop with a closed Worldline $\mathcal{C}$ is given by the trace of the Wilson loop operator $U_{\mathcal{C}}$,

$$W_{\mathcal{C}} = \frac{1}{\mathrm{N}_c}\mathrm{Tr}\, U_{\mathcal{C}}\,, \tag{VI.120}$$

the traced Wilson loop in a non-Abelian gauge theory. In summary we conclude that the expectation value of a static $q\bar{q}$-pair is proportional to that of the traced Wilson loop with

$$W[L,T] = \langle W_{\mathcal{C}}\rangle = \frac{1}{Z}\int dA W_{\mathcal{C}}(A) e^{-S_A[A]} \tag{VI.121}$$

and a similar expression holds for QED. There, we can resort to perturbation theory, and recover the Coulomb potential. This exemplary computation is done in Appendix D, and leads to (D.5),

$$V_{e^+e^-}(L) = -\frac{e^2}{4\pi}\frac{1}{L}\,, \tag{VI.122}$$

as expected. The derivation in Appendix D also entails, that the contributions come via the resummation of multi-photon exchange diagrams presented in Figure 35 in Appendix D. The Coulomb potential (VI.122) serves as our references result for the computation of the potential of static quarks in the strong coupling expansion in Section VI D 2.

The whole derivation and the final expression (VI.121) is easily translated to the lattice,

$$W\,[L,T] = \frac{1}{Z}\int \mathcal{D}U\, W_{\mathcal{C}}[U]\, e^{-S_w[U]} \tag{VI.123}$$

with the lattice path $\mathcal{C}$ depicted in Figure 17 and the general Wilson line

$$W_{\mathcal{C}}[U] = \mathrm{tr}_{\mathrm{f}}\, U_{\mathcal{C}} \qquad \text{with} \qquad U_{\mathcal{C}_{n,m}} = \prod_{l\in\mathcal{C}_{n,m}} U_l\,, \tag{VI.124}$$

for a path $\mathcal{C}_{n,m}$ also depicted in Figure 17. As already discussed above, up to a multiplicative constant, this expectation value is related to the free energy of a quark–anti-quark state at a distance L, hold there for a time T. This leads us to

$$\lim_{T\to\infty} W[L,T] = F(L)\, e^{-E(L)T}\,, \tag{VI.125}$$

where, $F(L)$ is the overlap with the ground state.

2. Static quark potential in the strong coupling expansion

In non-Abelian gauge theories the perturbative computation done in Appendix D for QED within the Gaußian approximation does not work, as we deal with a strongly-correlated system. If performed it yields a Coloumb potential as in (VI.122). The full computation can only be done numerically, and with the current computer resources it is easily done on a laptop for physical lattice sizes. This is beyond the scope of the present lecture course.

As a first step towards the full simulation we perform an analytic computation in the strong coupling expansion with $g_0 \to \infty$, to wit,

$$\beta = \frac{2N_c}{g_0^2} \to 0\,. \tag{VI.126}$$

Now we use that the Wilson action (VI.100) has a field independent summand which cancels out in the numerator and in the denominator in (VI.103). Then the expectation value (VI.123) turns into

$$W\,[L,T] = \frac{\int \mathcal{D}U\, W_c[U]\, e^{\beta \sum_P S_P}}{\int \mathcal{D}U\, e^{\beta \sum_P S_P}} = \langle W_c[U]\rangle \tag{VI.127}$$

with the Plaquette action

$$S_P = \frac{1}{2N_c} \mathrm{tr}\left(U_P + U_P^\dagger\right) \qquad \text{with} \qquad U_P = U_{\mu\nu}\,, \tag{VI.128}$$

and $\sum_P$ in (VI.127) summing over all plaquettes on the lattice. Now we expand the exponential measure factor $\exp \beta \sum_P S_P$ in powers of the (inverse) coupling β,

$$e^{\beta \sum_P S_P} = \prod_P e^{\beta\, S_P} = \prod_P \sum_n \frac{\beta^n}{n!}\Big(S_P\Big)^n\,. \tag{VI.129}$$

Now we use the integration rules of the Haar measure in (VI.105) in the denominator of (VI.127) as well as the expansion (VI.129). This leads us to

$$\int \mathcal{D}U e^{\beta \sum_p S_p} = \int \mathcal{D}U + \mathcal{O}(\beta) = 1 + \mathcal{O}(\beta)\,. \tag{VI.130}$$

Hence, the normalisation is nothing but the product of the Haar measure of the link variables, which we have normalised to unity. In the numerator, the respective term of $O(\beta^0)$ vanished as the integration for the link variables U_l with $l \in \mathcal{C}$ vanish: There we have $\int dU_l\, U_l = 0$, see (VI.105).

Accordingly we need at least one $U_l^\dagger$ for a finite result. This can only be achieved by inserting an $\beta U_p^\dagger$ from the expansion of $e^{\beta \sum_p S_p}$ done in (VI.129), see the left figure in Figure 18.

However, while this matches the link variable $U_{l_m}^\dagger$, it also creates three 'free' links from $U_p^\dagger$ which have to be matched. This is achieved by augmenting also these lines with the respective $\beta\, U_p^\dagger$'s, yet again generating further 'free' links. The generating of further free links stops for plaquette variables with links being on the contour $\mathcal{C}$. In

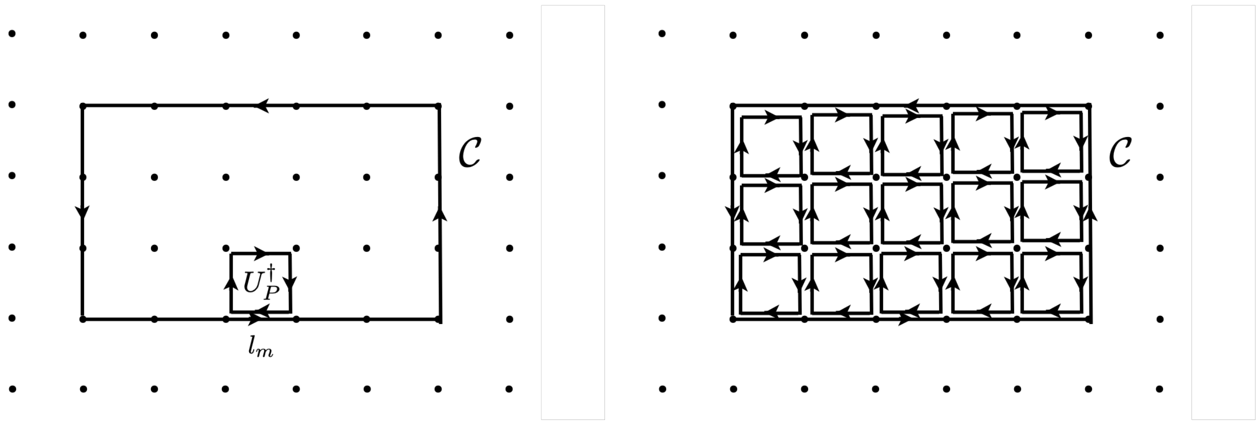

FIG. 18: Wilson loop with one adjunct plaquette (left). Wilson loop with plaquettes filling the interior (right).

conclusion, the smallest number of Plaquettes with all links matched is given by the right figure in Figure 18. There, the Wilson loop is paired with

$$\overbrace{T/a}^{\hat{T}}\,\overbrace{L/a}^{\hat{L}} = \frac{A}{a^2} = \hat{A}\,, \tag{VI.131}$$

plaquettes, each of which carries a factor β. We emphasise that the indices on $\mathcal{C}_\mathcal{A}$ are summed over due to the trace in the Wilson loop. The expression in (VI.131) is nothing but the dimensionless area, counting the number of plaquettes inside the path $\mathcal{C}$. This leads us to

$$W[T,L] = \prod_{l\in A_\mathcal{C}} \int dU_l U_l^{a_l b_l} \left(U_l^\dagger\right)^{c_l d_l} \left(\frac{\beta}{2N_c}\right)^{\hat{A}} + \mathcal{O}(\beta^{\hat{A}+1})\,, \tag{VI.132}$$

where $A_\mathcal{C}$ is the area bounded by $\mathcal{C}$. This area contains (including the boundary) $2\hat{A}+\hat{L}+\hat{T}$ links (for each plaquette 2 independent links: $2\hat{A}$, and the remaining half boundary: $\hat{L}+\hat{T}$). At each link we integrate over $UU^\dagger$ with (VI.106). Moreover, at each lattice site all group indices of parallel links and adjoint links are the same and summed over,

$$\delta^{a_1a_2}\delta^{a_2a_3}\delta^{a_3a_4}\delta^{a_4a_1} = N_c\,. \tag{VI.133}$$

As there are $(\hat{L}+1)(\hat{T}+1)$ lattice sites within the loop including the boundary, we are led to,

$$\left(\frac{1}{N_c}\right)^{2\hat{A}+\hat{L}+\hat{T}} N_c^{\overbrace{(\hat{L}+1)(\hat{T}+1)}^{\#\text{ lattice sites}}} = N_c \left(\frac{1}{N_c}\right)^{\hat{A}}\,. \tag{VI.134}$$

Putting everything together, we arrive at the final result,

$$W[T,L] = N_c \left(\frac{\beta}{2N_c^2}\right)^{\hat{A}} + \mathcal{O}\left(\beta^{\hat{A}+1}\right)\,, \tag{VI.135}$$

which entails an area law for the Wilson loop. This is the desired result as it entails an growth of the free energy with the area $A_\mathcal{C}$ surrounded by the Wilson loop. Evidently, if only the distance L is varied, this entails a linearly rising potential, the two proportionalities go hand in hand. The logarithm of (VI.135) is the static $q\bar{q}$-potential,

$$\hat{V}(L) = -\lim_{\hat{T}\to\infty} \frac{1}{\hat{T}} \ln\left\langle W_\mathcal{C}[U]\right\rangle = \hat{\sigma}\,(g_0)\,\hat{L} \qquad \text{with} \qquad \hat{\sigma} = -\ln\frac{\beta}{2N_c^2}\,, \tag{VI.136}$$

with the string tension $\hat{\sigma}$, measured in lattice units. In summary, lattice Yang-Mills theory shows confinement in the strong coupling limit (VI.126). However, we will see shortly that this exciting result does not survive the continuum limit:

To begin with, we have not used in the derivation above that the gauge group is *non*-Abelian. Indeed, it can be straightforwardly carried out in the U(1) case as well without any qualitative changes. In conclusion, also *compact* U(1) theory has a linearly rising static U(1)-potential in the strong coupling limit. Accordingly, compact U(1) has a confining phase on the lattice, while it has a Coulomb potential in the continuum (quantised over the algebra). Note however, that also the lattice version has a Coulomb phase with a $1/r$-potential, and it is this phase which encompasses the continuum limit.

This already casts some doubt on the survival of the SU(N_c) result (VI.135) and (VI.136) in the continuum. These doubts are solidified if discussing the bare lattice coupling g_0. In terms of momentum scales, $g_0(a)$ is the coupling of 'classical' Yang-Mills theory, defined at the 'microscopic' scale a, that is related to the momentum scale π/a. In the continuum limit the lattice distance a is approaching zero, and we are probing the coupling $g(a)$ at successively larger momentum scales. Luckily, the running coupling in Yang-Mills theory enjoys asymptotic freedom with the continuum β-function being

$$\beta_g = -\frac{1}{16\pi^2}\frac{11}{3}N_c g_0^3\,. \tag{VI.137}$$

Indeed, this well-known universal result carries over into the present lattice set-up. In any case the sign of the β-function is negative and we have

$$g_0(a) \stackrel{\text{cont. limit}}{\longrightarrow} 0\,. \tag{VI.138}$$

Accordingly, the continuum limit is safely governed by (lattice) perturbation theory in the *bare* lattice coupling $g_0(a)$. As it is the only coupling or free parameter in Yang-Mills theory, tuning the continuum limit simply amounts to

$$\beta = \frac{2N_c}{g_0^2} \to \infty\,, \tag{VI.139}$$

the opposite limit of (VI.126), which confirms our suspicion.

E. The continuum limit and the renormalisation group

In this Chapter we discuss the continuum limit of lattice field theories. This limit is obtained by keeping the physical scales fixed, while taking the lattice distance to zero, $a \to 0$. In the following we concentrate on the system with one fundamental scale. This physical scale is well represented by the correlation length ξ on the lattice that can be extracted from the fundamental two point correlation functions of the theory. For the present introduction we simply consider a real scalar field theory with

$$\lim_{r\to\infty}\langle\phi(\vec x)\phi(\vec y)\rangle_c \propto e^{-r/\xi}\,, \qquad \text{where} \qquad r = \|\vec x - \vec y\|\,, \tag{VI.140}$$

where $x_0 = y_0$. The spatial correlation length is nothing but the inverse (screening) mass gap of the theory. Again we consider a simple example, the classical propagator of the three-dimensional scalar field theory with

$$\langle\phi(p)\phi(-p)\rangle_{c,\text{cl}} = \frac{1}{p^2+m_\phi^2}\,, \qquad \longrightarrow \qquad \langle\phi(p_0=0,\vec x)\phi(p_0=0,\vec y)\rangle_{c,\text{cl}} = \int\frac{d^3p}{(2\pi)^4}\frac{e^{i\vec p(\vec x-\vec y)}}{\vec p^2+m_\phi^2} = \frac{1}{8\pi}\frac{1}{r}e^{-m_\phi r}\,. \tag{VI.141}$$

This leads us to $\xi = 1/m_\phi$. In the above case the temporal screening length is the same as the spatial one. This is readily shown by repeating the same computation as in (VI.141) with the rôles of x_0, y_0 and $\vec x, \vec y$ switched. This equivalence is a consequence of Euclidean $O(4)$ symmetry and also holds true for theories with Lorentzian signatures.

More generally, the correlation length is nothing but the distance of the nearest singularity in the complex momentum plane of the correlation function at hand and defines the mass gap of the modes contributing to the correlation function. We note in passing that the statement above holds true for fields that are directly related to asymptotic states and the situation in gauge theories is far more complicated. However, in the present context this is not relevant.

Evidently this mass gap in general depends on the chosen correlation function as not all of them may overlap with the lowest lying states in the theory. The mass gap of the theory is then given by the smallest mass gap carried by the correlation functions. Again, a simple example is provided by a free scalar theory with two fields, ϕ_1 and ϕ_2 with masses $m_{\phi_1} < m_{\phi_2}$. Clearly, the propagators of the two fields have different correlation lengths $\xi_1 > \xi_2$ and the mass gap of the theory is given by m_{ϕ_1}.

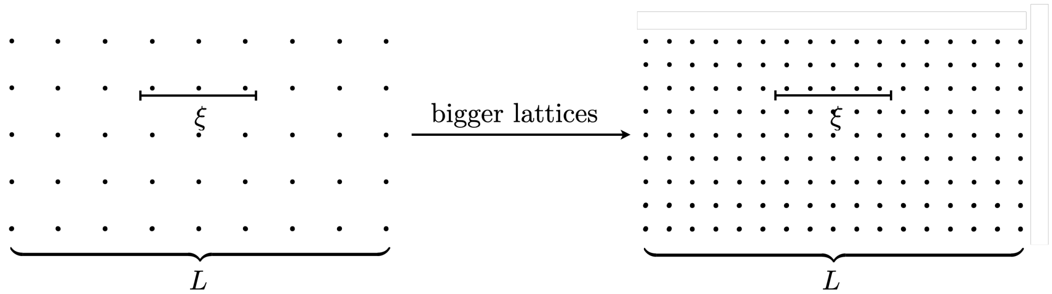

FIG. 19: Going from a lattice theory with correlation length ξ, defined on a lattice with lattice spacing a and length L to a theory on a finer lattice with the same correlation length and length, but half the lattice spacing, $a \to a/2$.

1. *Block-spinning transformations and the RG*

So far we have defined lattice field theories by simply introducing an infinite volume lattice with a lattice spacing a as well as defining a discrete version of the classical action, that approaches the continuum action for $a \to 0$ up to $\mathcal{O}(a)$-terms. More precisely, the continuum limit is achieved by taking $a \to 0$, while keeping the physical correlation length ξ fixed.

Let us now go to the more realistic situation in numerical applications: a lattice with a finite extent L in all d directions. Then we deal with a hyper-cubic lattice with $(\hat{L}+1)^d$ lattice sites ($\hat{L}^d$ independent ones). A step towards the continuum limit in a two-dimensional theory at fixed L is depicted in Figure 19 with $a \to a/2$. This implies $\hat{L} \to 2\hat{L}$ and hence this procedure increases the number of lattice sites by 2^d.

Typically one does not have the luxury of achieving the continuum limit by simply increasing the number of lattice sites. Instead, one is using the maximal lattice one (or rather the computing resources) numerically can cope with and decreases the lattice spacing, see Figure 20. Then, $\hat{L}$ is kept fixed as is ξ. Instead the dimensionless lattice parameters are changed, most clearly this happens for the mass $\hat{m}_\phi = m_\phi a$: at fixed m_ϕ we have $\hat{m}_\phi \to 2\hat{m}_\phi$. Iterating this procedure i times leads to a lattice spacing $2^i\, a$ and a lattice extent of $L/2^i$. Evidently, this implies that the correlation length eventually will exceed the lattice extent, $2^i\, \xi/L > 1$, and the finite volume effects will dominate the physics. Already the cartoon situation in Figure 20 makes this abundantly clear.

In summary this asks for a careful, mathematically sound description of such a rescaling of lattice field theories, which should also allow us to facilitate and optimise numerical computations. This is done with the renormalisation group (Stueckelberg, Petermann (1953)), that has been introduced for describing the change of a given theory under general rescalings (and reparametrisations). The discrete version of renormalisation group transformations for lattice theories is the block-spinning transformation (Kadanoff (1966)). At its heart it is Wilson's (1971) renormalisation group, that underlies most modern applications of the renormalisation group.

Such a block-spinning transformation is introduced as a transformation from a finer lattice with lattice distance a to the coarser lattice with lattice distance $2a$. For this transformation we average (*coarse grain*) the field values

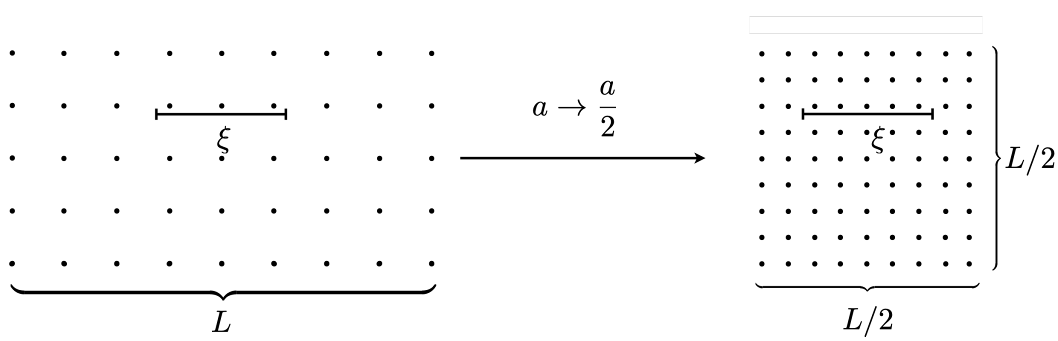

FIG. 20: Mapping the lattice theory with correlation length ξ, defined on a lattice with lattice spacing a and length L to a theory on a finer lattice with the same correlation length, but half the lattice spacing and length: $a \to a/2$ and $L \to L/2$.

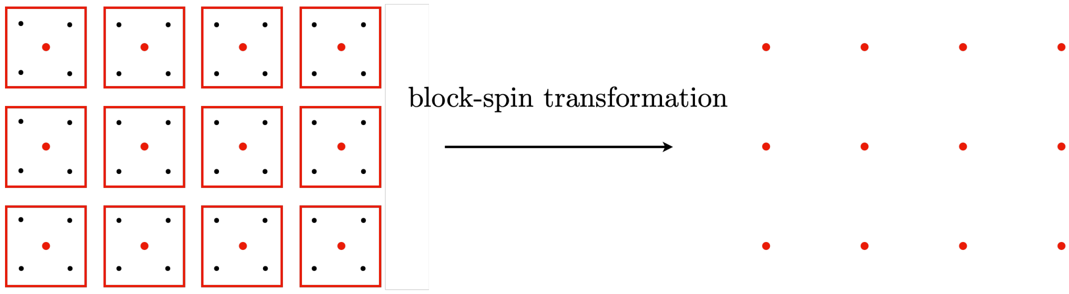

FIG. 21: *Block-Spinning* on the lattice: we average (*coarse graining*) the field on the finer lattice (black dots) with lattice distance a on fundamental squares or plaquettes. This defines a field on a lattice with lattice distance $2a$ (red dots).

over square blocks of neighbouring lattice sites, see fig. 21. This procedure is called coarse graining and is the *first block-spinning step*. Applied to the finer lattice in Figure 19 with lattice distance $a/2$, it brings us back to the original lattice with lattice distance a. Applied to the finer lattice in Figure 20, is gives us back the original lattice with half the lattice extent.

Note that this step implies a loss of resolution at fixed correlation length ξ. This is reflected in momentum space by the fact, that the Brillouin zone reduces from $p_\mu \in [-\pi/a\,,\,\pi/a]$ to $p_\mu \in [-\pi/(2a)\,,\,\pi/(2a)]$. This entails that the quantum fluctuations of the momentum shell

$$|p_\mu| \in [-\pi/(2a)\,,\,\pi/(2a)]\,, \tag{VI.142}$$

are averaged over (integrated out). Put differently, this is an information loss, evident in Figure 21, and is mirrored in $\hat\xi = \xi/a$, which transforms $\hat\xi \to 1/2\,\hat\xi$.

However, in a *second block spinning step* we can recover the original situation on the right hand side of fig. 21. To that end we rescale ξ by a factor 2 with $\xi \to 2\,\xi$. The latter implies that all the dimensionfull parameters in the lattice theory have to be rescaled accordingly, i.e. $m_\phi \to 1/2\,m_\phi$ leading to $\hat m_\phi \to 1/2\,\hat m_\phi$. Moreover, this implies that L is kept fixed. Then the final lattice field theory has the same correlation length as before as before the two block-spinning steps, and we have,

$$\hat\xi \quad \stackrel{\text{step 1}}{\longrightarrow} \quad \frac{\hat\xi}{2} \quad \stackrel{\text{step 2}}{\longrightarrow} \quad \hat\xi\,, \qquad \text{and} \qquad \hat m_\phi \quad \stackrel{\text{step 1}}{\longrightarrow} \quad 2\hat m_\phi \quad \stackrel{\text{step 2}}{\longrightarrow} \quad \hat m_\phi\,, \qquad \hat\lambda \stackrel{\text{step 1\&2}}{\longrightarrow} \hat\lambda\,. \tag{VI.143}$$

We emphasise again that on a finite lattice, the combination of the two steps is no identity transformation, as

$$\hat L \stackrel{\text{step 1\&2}}{\longrightarrow} \frac{\hat L}{2}\,. \tag{VI.144}$$

The above example is the simple case of more coarse grainings and rescalings. For example, in a Ising spin system, the blocking on fundamental plaquettes is not well-defined as the spins can average to zero, while the spin operators on the coarse grained lattice only take values ± 1. Generally, we introduce a blocking

$$\phi'_{n'} = f_{n'}(\phi_n)\,, \tag{VI.145}$$

with a potentially non-linear blocking function $f_{n'}(\phi_n)$. In the example above the n' are the vectors of the center of fundamental plaquettes and $f_{n'}$ simply sums the field over the sites of the plaquette. The coarse grained field ϕ' lives on the coarse-grained lattice. For a given lattice action $S[\phi_n]$ the block-spinning amounts to

$$e^{-S'[\phi'_{n'}]} = \int \prod_n d\phi_n\, \delta[\phi'_{n'} - f_{n'}(\phi_n)]\, e^{-S[\phi_n]}\,, \tag{VI.146}$$

which also defines a lattice action on $S'[\phi'_{n'}]$ the coarse-grained lattice. Note that the generating functional Z is unchanged as the Dirac δ-function is removed by the integral over all field values on the sites on the coarse-grained lattice,

$$\int d\phi'_{n'}\, \delta[\phi'_{n'} - f_{n'}(\phi_n)] = 1\,, \tag{VI.147}$$

and hence we conclude

$$Z' = \int \prod_n d\phi'_{n'}\, e^{-S'[\phi'_{n'}]} = \int \prod_n d\phi'_{n'} \int \prod_n d\phi_n\, \delta[\phi'_{n'} - f_{n'}(\phi_n)]\, e^{-S[\phi_n]} = \int \prod_n d\phi_n\, e^{-S[\phi_n]} = Z\,. \tag{VI.148}$$

Again this emphasises the point that the coarse-grained system has the same expectation values for correlations $\phi'_{n'}$, that can also be simulated on the original lattice, but does not resolve smaller distances than $2a$.

In summary, our analysis entails that a lattice action at a given lattice distance a, or rather a/ξ, comprises already quantum effects of momenta $p_\mu > \pi/a$, as these momenta can be integrated out shell-wise, see (VI.142), starting at an infinitely fine lattice. Coarser lattices are approached by successive block-spinning or coarse graining within block-spinning RG-steps. The opposite procedure is, strictly speaking only possible on a lattice with infinite extent, therefore called an inverse RG step. Both, RG and inverse RG are used for optimising lattice simulations as well as conceptual investigations.

2. *The Continuum Limit of Lattice Yang-Mills*

With the understanding gained in Section VI E 1 we now come back to the continuum limit of Lattice Yang-Mills theories, already sketchily discussed at the end of Section VI D 2. In the continuum limit of a lattice theory we keep the physical correlation length

$$\xi = 1/m_{\text{gap}}\,, \tag{VI.149}$$

fixed, where m_{gap} is the mass gap of the theory; in a scalar theory the mass gap is simply the pole mass of the scalar field, $m_{\text{gap}} = m_{\phi,\text{pole}}$. Note that the latter is not the mass parameter in the action, but rather defined as the singularity (at $p_0^2 = -m^2_{\phi,\text{pole}}$) of the propagator. In Yang-Mills theory the situation is more complicated as the classical action features no mass scale (the theory has conformal symmetry on the classical level). The quantised theory has a mass gap given by the mass of the lowest lying glueball state.

In any case, (VI.149) implies, that the dimensionless mass gap tends to zero on the lattice,

$$\hat m_{\text{gap}} = m_{\text{gap}}\, a \to 0\,, \tag{VI.150}$$

and hence the correlation length $\hat\xi = 1/\hat m$ diverges, This is the signature of a 2nd order phase transition. At this point the system has infinite many points inside a physical distance measured in units of the correlation length. As discussed above, in lattice YM we only have the *bare* strong coupling g_0 on the lattice for tuning this limit,

$$\hat\xi\,(g_0) \underset{g_0\to g_*}{\to} \infty\,, \tag{VI.151}$$

where g^* is the fixed point value of the *bare* lattice coupling g_0.

It is left to extract the dependence of $g_0(a)$ on the lattice spacing a in the continuum limit. To that end we discuss the g_0 and a dependence of a general observable $\mathcal{O}$ in the continuum limit. Its relation to the dimensionless lattice observable $\hat{\mathcal{O}}$ is given by

$$\mathcal{O}\,(g_0, a) = \left(\frac{1}{a}\right)^{d_{\mathcal{O}}} \hat{\mathcal{O}}\,(g_0) \tag{VI.152}$$

where $d_{\mathcal{O}}$ is the momentum dimension of the observable $\mathcal{O}$. In the continuum limit we have,

$$\mathcal{O}\,(g_0 \to g_*, a \to 0) = \mathcal{O}_{\text{phys}} \tag{VI.153}$$

Thus, if we know the functional dependence of $\mathcal{O}$ on g_0, we know $g_0(a)$ with $\mathcal{O}\,(g_0, a) = \mathcal{O}_{\text{phys}}$. The above argument seemingly implies that $g_0(a)$ depends on the choice of $\mathcal{O}$. However, the coupling $g_0(a)$ is two-loop *universal*, to that order it does not depend on the observable or the renormalisation procedure. In the continuum limit with $a \to 0$ we shall see, that also the coupling $g_0 \to 0$ and hence the continuum limit is governed by the universal running of the

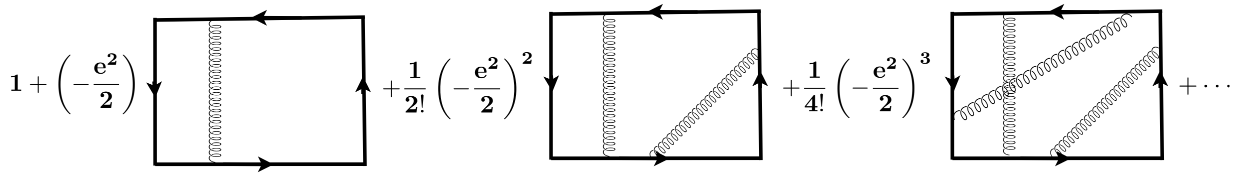

FIG. 22: Diagrams contributing to the effective potential $V(L)$ up to order g_0^4.

coupling.

Let us now take as $\mathcal{O}$ the $q\bar{q}$-potential V defined in the previous section:

$$V\left(L, g_0, a\right) = \frac{1}{a}\hat{V}\left(\hat{L}, g_0\right) \tag{VI.154}$$

Now, keeping $V\left(L, g_0, a\right)$ fixed at its physics value $V_{\rm phys}$ while $a \to 0$ implies

$$\left(a\frac{\partial}{\partial a} - \beta\left(g_0\right)\frac{\partial}{\partial g_0}\right) V\left(L, g_0, a\right) = 0 \tag{VI.155}$$

with the lattice β-function,

$$\beta\left(g_0\right) = -a\frac{\partial g_0}{\partial a}\,. \tag{VI.156}$$

The standard continuum formulation with a cutoff or RG scale Λ is obtained with $\Lambda \sim 1/a$ and hence $\Lambda\partial_\Lambda = -a\partial_a$. We now consider the RG-equation up to the forth order in the *bare* lattice coupling g_0^4. The respective diagrams are depicted in Figure 22 and the potential is computed as

$$V(L) = -\frac{g_0^2(a)}{4\pi L}C_2(f)\left[1 + g_0^2(a)\frac{11N_c}{24\pi^2}\ln\hat{L} + \text{const}\right]\,. \tag{VI.157}$$

If we insert (VI.157) in (VI.156) we get

$$\beta\left(g_0\right) = -\frac{g_0^3}{16\pi^2}\frac{11}{3}N_c = \beta_0 g_0^3\,, \tag{VI.158}$$

the well-known continuum result (I.38) in Sections I B 2 and II A 2. Since $\beta(g_0) < 0$ is smaller (asymptotic freedom), the coupling is driven to zero in the limit $a \to 0$.

$$a = \frac{1}{\Lambda_L}e^{\frac{1}{2\beta_0 g_0^2}} \tag{VI.159}$$

This concludes the discussion of the scaling of lattice Yang-Mills theory in the limit $a \to 0$. Let us now rewrite the RG-equation (VI.155) in terms of physical scales, substituting a with the distance scale L in the heavy quark potential (not to be confused with the extend of the lattice, which is assumed to be infinite here). With (VI.157) this leads us to

$$\left(L\frac{\partial}{\partial L} + \beta\left(g_0\right)\frac{\partial}{\partial g_0}\right) V(L, g_0, a) = -V(L, g_0, a)\,, \tag{VI.160}$$

where the right hand side of (VI.160) originates in the $1/L$ factor in (VI.157), and constitutes an inhomogeneous term in the RG equation. It simply entails the dimension-scaling of the potential, and hence can be undone if we rescale the potential V with L in order to make it dimensionless. The homogeneous form of the RG has the advantage that we can directly read of the running coupling from it, as discussed below. We define the dimensionless potential $\bar{V}$ with

$$\bar{V}(\hat{L}, g_0) = LV(\hat{L}, g_0)\,, \qquad \text{with} \qquad \hat{L} = \frac{L}{a}\,. \tag{VI.161}$$

In (VI.161) we have used that the dimensionless potential can only depend on dimensionless variables, and hence it only can depend on the ratio of the two length scales L and a. Put differently, the distance scale in the potential has to be measured in units of the lattice distance, the only scale in the system.

Inserting $V = 1/L\bar{V}$ into (VI.160) gives us the desired homogeneous RG equation,

$$\left(L\frac{\partial}{\partial L} + \beta\left(g_0\right)\frac{\partial}{\partial g_0}\right)\bar{V}(\hat{L}, g_0) = 0\,. \tag{VI.162}$$

Equation (VI.162) entails that a change in the physical distance L can be absorbed in a corresponding change of the bare coupling g_0. It is nothing but the lattice version of the renormalisation group equation for the running coupling of QCD discussed in Sections I B 2 and II A 2. Now we perform yet another change of variables, and change from the bare coupling $g_0(a)$ to the running coupling $g(L)$ in analogy to our discussion in QCD, where we went from the renormalised coupling $\alpha_{s,\mathrm{ren}}(\mu)$ to the running coupling $\alpha_s(p)$. In the present analysis, the rôle of the momentum p is taken by π/L. In this spirit we write

$$\bar{V} = \bar{V}(L, g(L))\,, \qquad \text{with} \qquad L\frac{\partial}{\partial L}g(L) = -\beta(\bar{g}(L))\,, \tag{VI.163}$$

in a slight abuse of notation. We emphasise that (VI.163) is not simply obtained by substituting the bare coupling in (VI.161) by the running coupling. It implies a reshuffling of explicit L and implicit L-dependences as can be seen from the RG equation for the running coupling. The solution of the RG equation of the coupling has been already discussed in Sections I B 2 and II A 2, see (I.39). In the present case we obtain

$$g^2(L) = \frac{g_0^2}{1+\beta_0 g_0^2 \ln L^2/a^2}\,, \qquad \text{with} \qquad g_0 = g(a)\,. \tag{VI.164}$$

Using (VI.164) in $\bar{V}$ and V with (VI.157) and (VI.161) leads to,

$$V(L) = -C_F\frac{\alpha_S(L)}{L}\,, \qquad \text{with} \qquad \alpha_s(L) = \frac{\bar{g}^2(L)}{4\pi}\,. \tag{VI.165}$$

The prefactor in (VI.165) is the Casimir invariant $C_F = N_c^2 - 1/(2N_c)$, in QCD we have $C_F = 4/3$. Our result (VI.165) seemingly depends on a. However, with the relation (VI.166), the a-independence is apparent,

$$\alpha_s(L) = \frac{1}{4\pi}\frac{g_0^2}{1+\beta_0 g_0^2 \ln L^2\Lambda_L^2 e^{-1/\beta_0 \bar{a}_0^2}} = \frac{4\pi}{\beta_0}\frac{1}{\ln L^2\Lambda_L^2}\,. \tag{VI.166}$$

with $\beta_0 = 11/3N_c$, and the lattice version of Λ_{QCD},

$$\Lambda_L = \frac{1}{a}e^{\frac{1}{2\beta_0 g_0^2}}\,, \qquad \text{with} \qquad a\frac{d}{da}\Lambda_L = \left(a\frac{\partial}{\partial a} - \beta(g_0)\frac{\partial}{\partial g_0}\right)\left(\frac{1}{a}e^{\frac{1}{2\beta_0 g_0^2}}\right) = 0\,. \tag{VI.167}$$

Equation (VI.166) is the lattice version of (I.39). In the present one-loop treatment the coupling diverges at the infrared Landau pole $L = 1/\Lambda_L$. For a better accuracy we may invoke two-loop perturbation theory or even higher orders even though this quickly gets unsolvable on the lattice.

VII. PHASE STRUCTURE OF QCD

In its early stages the universe undergoes a thermal or rather non-equilibrium phase transition from the initial quark-gluon phase into the hadronic phase, it is in nowadays. The description of this chiefly important evolution requires the access to QCD at finite temperature and density and for a full description one also has to incorporate non-equilibrium effects. The QCD phase structure is also studied at heavy ion facilities such as the FAIR facility, RHIC, HIAF and others.

The study of non-equilibrium QCD is beyond the scope of the present lecture course. Here we only provide a brief overview on QCD at finite temperature and density and defer the participants to dedicated lectures for further insights. Moreover, instead of discussing first principle QCD at finite temperature and density, we shall use a combination of low energy effective theories or descriptions, we have set up in the course of this lecture course. As for non-equilibrium QCD, the resolution of the phase structure of QCD from first principles is a very intricate and not yet fully resolved task and goes beyond the scope of the current lecture course. More details can be found in Non-perturbative Aspects of Gauge Theories.

The access to the QCD phase structure requires to assess chiral symmetry breaking and confinement, as discussed in Section III and Section VI E 2, at finite temperature and density. In Section VII A we introduce quantum fields at finite temperature and evaluate the thermal chiral phase transition. In ?? we evaluate the confinement-deconfinement phase transition at finite temperature with a variant of the Wilson loop expectation value introduced in Section VI E 2. Finally, in Section VII C, we put the pieces together and study the phase structure of QCD at finite temperature and density.

A. Chiral phase transition

In Section III we have learned that chiral symmetry breaking is triggered by the quark fluctuations, while the mesonic low energy fluctuations work against symmetry breaking. The symmetry breaking scale Λ_χ is of the order of 300-400 MeV. This vacuum physics is used to fix the parameters of the low energy effective theory such as the mesonic mass function, the Yukawa coupling, and the expectation value of the radial mode, $\langle\sigma\rangle$. The related observables are the pion and sigma pole masses, the constituent quark mass as well as the pion decay constant.

In heavy ion collisions or the early universe the temperature is/has been high of the order of hundreds of MeV. In Kelvin this translates into $100\,\mathrm{MeV}\approx\, 1.16 * 10^{12}$ Kelvin. It is expected that a high temperatures the system undergoes a phase transition to the chirally symmetric phase. As a rough estimate the phase transition temperature T_c is expected to be of the order of the chiral symmetry breaking scale Λ_χ which itself has been argued to be of the order of $\Lambda_{\rm QCD}$, the only intrinsic scale in QCD.

1. *Mesons at finite temperature*

For a more quantitative investigation we need a thermal formulation of QCD or at least of the low energy effective theory we have derived in the previous chapter. Here we give a brief introduction to the -Euclidean- path integral at finite temperature, where we follow the introduction of the path integral in Chapter 9 & 10, QFT I+II lecture notes. We start with the partition function of a scalar theory at finite temperature

$$Z_T = \mathrm{Tr}\, e^{-\beta \hat H} = \sum_n e^{-\beta E_n} \quad \text{with} \quad \beta = \frac{1}{T} \quad \text{and} \quad \hat H |n\rangle = E_n |n\rangle \,, \tag{VII.1}$$

with the Hamiltonian operator of a scalar theory

$$\hat H[\hat\phi,\hat\pi] = \int d^3x \left[\frac{1}{2}\hat\pi^2 + \frac{1}{2}(\vec\nabla\phi)^2 + V(\hat\phi)\right] , \tag{VII.2}$$

with field operator $\hat\phi$ and field momentum operator $\hat\pi$. In (VII.1) we dropped the source term for the sake of brevity. Eq.(VII.1) is the standard statistical partition function at finite temperature well known from quantum mechanics. Now we rewrite this partition function in terms of a basis in field and canonical momentum space. First we note that the trace in (VII.1) can be rewritten in terms of field eigenstates with

$$\mathrm{Tr}\, e^{-\beta \hat H} = \int d\phi\, \langle\phi|\, e^{-\beta \hat H}\, |\phi\rangle \qquad \text{with} \qquad \hat\phi(\vec x)|\phi\rangle = \phi(\vec x)|\phi\rangle \,, \tag{VII.3}$$

with the eigenvalues $\phi(\vec x)$. Moreover, the statistical operator $e^{-\beta\hat H}$ can be interpreted as the evolution operator $U(0,i\beta)$ in an imaginary time from the initial state $|\phi(t_{\rm i})\rangle$ at $t_{\rm i}=0$ to the final state $|\phi(t_{\rm f})\rangle$ at $t_{\rm f}=i\beta$ with

$$U(0,i\beta) = e^{i\hat H(t_{\rm f}-t_{\rm i})} \qquad \text{and} \qquad |\phi(t_{\rm f})\rangle = |\phi(t_{\rm i})\rangle \,. \tag{VII.4}$$

The identification of initial and final state is the trace condition in (VII.3). Now we simply repeat all the steps for the derivation of the path integral of a scalar theory. Also adding a source term we arrive at

$$Z_T[J] = \int_{\phi(\beta,\vec x)=\phi(0,\vec x)} d\phi\, e^{-S_T[\phi]+\int_0^\beta d^4x\, J(t,\vec x)\phi(\vec x)} \,, \tag{VII.5}$$

with the periodic fields $\phi(t+\beta,\vec{x})=\phi(t,\vec{x})$ and the finite temperature action $S_T[\phi]$ with

$$S_T[\phi]=\int_0^\beta d^4x\left[\frac{1}{2}(\partial_\mu\phi)^2+V(\phi)\right]\,,\qquad \text{where}\qquad \int_0^\beta d^4x=\int_0^\beta dt\int d^3x\,. \tag{VII.6}$$

Accordingly, the path integral of a finite temperature field theory is related to a Euclidean path integral with a finite time extent in imaginary time $t\in[0\,,\,\beta]$. Note that this time does *not* describe the time evolution of the system but simply the statistical nature of the thermal partition function. The real time correlation function are obtained by a Wick rotation, for more details see finite temperature quantum field theory books such as Le Bellac or Kapusta. The correlation functions are periodic in imaginary time,

$$\langle\phi(x_1)\cdots\phi(t_i+\beta,\vec{x})\cdots\phi(x_n)\rangle=\langle\phi(x_1)\cdots\phi(t_i,\vec{x})\cdots\phi(x_n)\rangle\,. \tag{VII.7}$$

Finally we want to repeat the computation of the effective potential in the last chapter section III G at finite temperature. This is done in momentum frequency space and we would like to illustrate the differences at finite temperature at the important example of the propagator

$$G_\phi(x-y)=\langle\phi(x)\phi(y)\rangle-\langle\phi(x)\rangle\langle\phi(y)\rangle\,. \tag{VII.8}$$

The propagator in spatial momentum and frequency space is given by

$$G_\phi(\omega_n,\vec{p})=\int_0^\beta d^4x\,e^{i\,(\omega_n t+\vec{p}\vec{x})}\,G_\phi(t,\vec{x})\,,\qquad\text{where}\qquad \omega_n=2\pi Tn\,,\qquad\text{with}\quad n\in\mathbb{Z}\,. \tag{VII.9}$$

The discrete frequencies ω_n are called Matsubara frequencies and originate in the finite imaginary time extent. The frequency Fourier transformation back gives

$$G_\phi(t,\vec{p})=\sum_{n\in\mathbb{Z}}e^{-i\omega_n t}G_\phi(\omega_n,\vec{p})\,, \tag{VII.10}$$

which has the necessary periodicity in imaginary time, $G(t+\beta,\vec{p})=G(t,\vec{p})$, of a correlation function, see (VII.7). In frequency and spatial momentum space the classical propagator looks the same as in the vacuum. We have

$$G_\phi(\omega_n,\vec{p})=\frac{1}{\omega_n^2+\vec{p}^2+m^2}\qquad\text{with}\qquad m^2(\phi)=\partial_\phi^2V(\phi)\,. \tag{VII.11}$$

While the Fourier transformation w.r.t. spatial momentum is also the same as at $T=0$, that w.r.t. frequency changes. Here we discuss the Fourier transformation for $t=0$ for the mixed representation $G_\phi(t,\vec{p})$,

$$G_\phi(t=0,\vec{p})=T\sum_{n\in\mathbb{Z}}\frac{1}{\omega_n^2+\vec{p}^2+m^2}=\frac{1}{2\epsilon_p^\phi}\coth\beta\,\epsilon_p^\phi=\frac{1}{2\epsilon_p^\phi}\left[1+2\,n_B(\epsilon_p^\phi)\right]\,, \tag{VII.12}$$

with the dispersion ϵ_p^ϕ and the thermal distribution function $n_B(\omega)$ given by

$$\epsilon_p^\phi(m)=\sqrt{\vec{p}^2+m^2}\,,\qquad\qquad n_B(\omega)=\frac{1}{e^{\beta|\omega|}-1} \tag{VII.13}$$

The latter is the standard Bose-Einstein distribution and clearly shows the thermal nature of the Matsubara path integral.

As a warm-up of the computation for the effective potential in the quark-meson theory at finite temperature we compute that of the scalar theory used here as an example. Its thermal part is related to the thermal pressure of the theory with potential. To that end we remind ourselves that the scalar free energy density Ω_ϕ and the pressure of the theory are given by

$$Z_T[0]=e^{-\beta\mathcal{V}\,\Omega_\phi}\,,\qquad\qquad p_\phi=-\frac{\partial\mathcal{V}\Omega_\phi}{\partial\mathcal{V}}\quad\text{with}\quad\mathcal{V}=\int d^3x\,. \tag{VII.14}$$

The one-loop contribution to the free energy density and pressure are hence given by

$$\Omega_\phi \simeq \frac{1}{2\mathcal{V}} T \,\mathrm{Tr} \ln\left(-\partial_\mu^2 + m^2\right) = \frac{1}{2} T \sum_{n\in\mathbb{Z}} \int \frac{d^3p}{(2\pi)^3} \ln\left(\omega_n^2 + \vec{p}^2 + m^2\right) , \quad p_\phi \simeq -\frac{1}{2} T \sum_{n\in\mathbb{Z}} \int \frac{d^3p}{(2\pi)^3} \ln\left(\omega_n^2 + \vec{p}^2 + m^2\right) , \tag{VII.15}$$

where we dropped the normalisations in Ω_ϕ and p_ϕ. We also remind the reader that $m^2 = m^2(\phi)$ as introduced in (VII.11). Note also that the pressure is nothing but (minus) the effective potential at finite temperature. At vanishing temperature we encountered singularities in the computation of the effective potential proportional to Λ^4, λ^2 and $\ln \Lambda$ that had to be absorbed in the bare couplings. The highest singularity proportional to Λ^4 we disregarded as the absolute value of the potential energy which cannot be measured. The expressions in (VII.15) are also infinite, showing the standard divergence of zero point functions at vanishing temperature. Similarly, we could introduce a spatial momentum cutoff Λ with $p^2 \leq \Lambda^2$ and proceed as in the last chapter. In the following we shall not make this cutoff explicit for the following reason: it is one of the cornerstones, and can be proven in thermal field theory all singularities are temperature-independent. This statement can be understood heuristically as the ultraviolet singularities are short-distance singularities. At short-distance singularities the finite extent in time-direction cannot be accessed. For detailed discussions we refer to the literature, here this fact will simply come out.

For the computation we take the mass (squared) derivative of the pressure, $\partial_{m_\phi^2} p$. This removes the logarithm from the expression and leaves us with integrals and sums that can be computed by complex analysis. The mass-derivative of the pressure is related to the momentum integral of the propagator in the mixed representation $G(0,\vec{p})$ computed in (VII.12),

$$\partial_{m^2} p_\phi \simeq -\frac{1}{2} \int \frac{d^3p}{(2\pi)^3} G_\phi(0,\vec{p}) = -\frac{1}{4} \int \frac{d^3p}{(2\pi)^3} \frac{1}{\epsilon_p^\phi} \left[1 + 2\, n_B(\epsilon_p^\phi)\right] . \tag{VII.16}$$

Eq.(VII.16) entails that the mass-derivative of the pressure, and hence the pressure, only carries a temperature-independent singularity proportional to $1/\epsilon_p^\phi$. The term proportional to n_B vanishes in the zero temperature limit. Upon integration over m^2 the pressure is given by

$$p_\phi \simeq -\int \frac{d^3p}{(2\pi)^3} \left[\frac{1}{2}\epsilon_p^\phi + T \ln\left(1 - e^{-\beta\epsilon_p^\phi}\right)\right] . \tag{VII.17}$$

The singular, temperature-independent piece pressure in (VII.17) proportional to ϵ_p^ϕ is nothing but the effective potential at vanishing temperature which we have computed for a fermionic theory in the last chapter. Its renormalisation can be performed analogously. Here we are only interested in the thermal pressure, and we subtract the pressure at vanishing temperature,

$$\begin{aligned} p_{\phi,\mathrm{thermal}} =& \, p_\phi(T) - p_\phi(T=0) \\ =& - T \int \frac{d^3p}{(2\pi)^3} \ln\left(1 - e^{-\beta\epsilon_p^\phi}\right) = -\frac{T}{2\pi^2} \int_0^\infty dp\, p^2 \ln\left(1 - e^{-\beta\epsilon_p^\phi}\right) . \end{aligned} \tag{VII.18}$$

Eq.(VII.18) is manifestly finite as for large momenta $p^2 \gg m_\phi^2, T^2$ the exponential in the logarithm decays with $\exp(-p/T$, the typical thermal decay. It is also positive as the argument in the logarithm is always smaller than one and hence the logarithm is strictly negative. With the minus sign in front of the integral this leads to a positive expression, as expected for a thermal pressure. For a given temperature (VII.18) takes its maximal value for $m_\phi^2 = 0$ and decays monotonously with increasing m_ϕ^2 as the thermal part of the mass-derivative is negative, see (VII.16). For $m_\phi^2 \to \infty$ the thermal pressure vanishes. Accordingly the pressure is positive for all m_ϕ^2. For large masses $m_\phi \gg T$ the pressure decays exponentially with $\exp(-m_\phi/T)$ (up to polynomial prefactors). For vanishing masses the momentum integration can be performed easily and we arrive at

$$p_{\phi,\mathrm{thermal}}\big|_{m^2=0} = \frac{\pi^2 T^4}{90} . \tag{VII.19}$$

The explicit result for vanishing mass is the Stefan-Boltzmann pressure of a free gas. It is the tree-level thermal pressure. Note also that (VII.18) is the result for the thermal part of the (one-loop) effective potential of a bosonic theory, see (VII.18).

Now we have collected all results for discussing the mesonic fluctuations in our $N_f = 2$ low energy effective theory. The mesonic contribution to the pressure and hence to minus the free energy density/effective potential are simply given by summing up (VII.18) for the sigma and the three pions leading to

$$\Big[\Omega_{\phi,T}(\phi) - \Omega_{\phi,T=0}(\phi)\Big]_{\text{mes.flucs.}} \simeq \frac{T}{2\pi^2}\int_0^\infty dp\, p^2\, \ln\left(1 - e^{-\beta\epsilon_p^\phi(m_\sigma)}\right) + 3\frac{T}{2\pi^2}\int_0^\infty dp\, p^2\, \ln\left(1 - e^{-\beta\epsilon_p^\phi(m_\pi)}\right)\,, \tag{VII.20}$$

The concentration on the thermal part of the fluctuations allows us to simply add (VII.20) to the low energy effective action at valishing temperature regardless of how we have treated the mesonic fluctuations there. Note also in this contect that (VII.20) is finite as it should be: in thermal field theory all UV divergences can be treated already in the $T = 0$ case and the subtractions can be chosen to be temperature-independent.

In (VII.20) this comes about as it only summarises the thermal fluctuations and momentum fluctuations with $p \gg T$ are suppressed. Accordingly in the context of our low energy EFT setup (VII.20) is only valid for $T/\Lambda \ll 1$. For larger temperatures already the Matsubara sum that takes account of high frequencies is at odds with the fact that $p_0^2 + \vec p^2 \leq \Lambda^2$.

2. *Quarks at finite temperature*

In summary we are but one step away from our goal of accessing the thermal chiral phase transition in QCD in the quark-meson EFT. For that task we need to translate the results above to the -free- quark path integral. The computation of the last chapter in the vacuum carries over here, we only have to discuss the fermionic Matsubara frequencies. For that end we redo the derivation of the thermal path integral for fermions again by starting from partition function Z_T as defined in the scalar case in (VII.1). Everything goes as in the scalar case except one subtlety concerning the trace. More details can be found in Chapter 12, QFT I+II lecture notes. As in the case of the bosonic field we need coherent states that allow us to define $\hat\psi|\psi\rangle = \psi|\psi\rangle$. For the sake of the argument we restrict ourselves to one creation and annihilation operator $a, a^\dagger$ and Grassmann variable c. A coherent state is given by

$$|c\rangle = (1 - c\, a^\dagger)|0\rangle = e^{-c\, a^\dagger}|0\rangle \qquad \text{with} \qquad a|c\rangle = c\, a\, a^\dagger)|0\rangle = c|0\rangle = c(1 - c\, a^\dagger)|0\rangle = c|c\rangle\,, \tag{VII.21}$$

where the latter property proves the coherence property of the state. The dual state $\langle c| = |c\rangle^\dagger$ has the property

$$\langle c|a^\dagger = -\langle c|c^*\,. \tag{VII.22}$$

In consequence, instead of periodicity of the fields in time in the scalar case coming from the trace in (VII.1) we have anti-periodicity,

$$\psi(t+\beta, \vec x) = -\psi(t, \vec x)\,, \tag{VII.23}$$

that reflects the Grassmannian nature of the fermionic field. The fermionic path integral Z_q with the Dirac action at finite temperature then reads

$$Z_{q,T}[J] = \int_{\psi(\beta,\vec x) = -\psi(0,\vec x)} d\bar\psi\, d\psi\, e^{-S_{D,T}[\phi] + \int_0^\beta d^4x\, \bar J_\psi(t,\vec x)\psi(\vec x) - \bar\psi J_\psi}\,, \qquad S_{D,T}[\psi] = \int_0^\beta d^4x\, \bar\psi\cdot(\not{D} + m_\psi + i\,\gamma_0\mu)\cdot\psi\,. \tag{VII.24}$$

As in the scalar case we can reveal the thermal nature of correlation functions derived from the generating functional (VII.24) by looking at the Dirac propagator of the quarks in the mixed representation at vanishing time, $G_q(t, \vec p)$. To that end we first notice that the Fourier transformation of the anti-periodic fermionic fields is reflected in a shift of the Matsubara modes by πT. We have

$$\psi(x) = T\sum_{n\in\mathbb{Z}}\int \frac{d^3p}{(2\pi)^3} e^{-i(\omega_{n,f}t + \vec p\vec x)}\psi(p_0, \vec p)\,, \qquad \omega_{n,f} = 2\pi\left(n + \frac{1}{2}\right)\,, \tag{VII.25}$$

where the additional factor $e^{i\pi T\, t}$ leads to the minus sign in the periodicity relation (VII.23) with $e^{i\pi T\,(t+\beta)} = e^{i\pi}e^{i\pi T\, t} = -e^{i\pi T\, t}$. Now we perform the computation for the frequency sum of the quark propagator G_q with N_f

flavours and N_c colors,

$$\frac{1}{m_\psi}\frac{1}{4N_f N_c}\,\mathrm{tr}\,G_q(t=0,\vec{p}) = T\sum_{n\in\mathbb{Z}}\frac{1}{\omega_{n,f}^2+\vec{p}^2+m_\psi^2} = \frac{1}{2\epsilon_p^\psi}\tanh\beta\epsilon_p^\psi = \frac{1}{2\epsilon_p^\psi}\left[1+2n(\epsilon_p^\psi)\right]\,, \tag{VII.26}$$

where the trace tr in (VII.26) sums over flavour, color and Dirac space. The dispersion ϵ_p and the thermal distribution function $n(\omega)$ are given by

$$\epsilon_p^\psi(m_\psi) = \sqrt{\vec{p}^2+m_\psi^2}\,, \qquad\qquad n_F(\omega) = \frac{1}{e^{\beta\omega}+1}\,. \tag{VII.27}$$

The latter is the expected Fermi-Dirac distribution. The difference to the Bose-Einstein statistics in the scalar case originates in the anti-periodicity of the fermions related to their Grassmannian nature. The free energy and pressure can be derived analogously to the scalar case. The one-loop contribution to the quark free energy density Ω_q and the pressure are hence given by

$$\Omega_q \simeq -\frac{T}{2\mathcal{V}}\,\mathrm{Tr}\ln\left(-\partial_\mu^2+m^2\right) = -2N_cN_f\,T\sum_{n\in\mathbb{Z}}\int\frac{d^3p}{(2\pi)^3}\,\ln\left(\omega_{n,f}^2+\vec{p}^2+m^2\right)\,,$$

$$p_q \simeq 2N_cN_f\,T\sum_{n\in\mathbb{Z}}\int\frac{d^3p}{(2\pi)^3}\,\ln\left(\omega_{n,f}^2+\vec{p}^2+m^2\right) = 12\,T\sum_{n\in\mathbb{Z}}\int\frac{d^3p}{(2\pi)^3}\,\ln\left(\omega_{n,f}^2+\vec{p}^2+m^2\right)\,, \tag{VII.28}$$

where as in the scalar case we dropped the normalisations in Ω_q and p_q. For the pressure we have also inserted the $N_f=2, N_c=3$ case discussed here.

For a first simple computation we also use $\mu=0$, a vanishing quark chemical potential. The prefactor -2 in comparison to the prefactor $1/2$ in the scalar case comes from the relative minus sign and factor 2 of the fermionic loop, the symmetrisation of the frequency and spatial momentum trace and the Dirac trace: $-1*1/2*4=-2$ instead of $1/2$ in the scalar case. The factor N_cN_f counts the degrees of freedom. For the computation of the thermal pressure we proceed similar to the scalar case with a m_ψ^2-derivative which maps the pressure to (VII.26). We also remove the divergent vacuum contribution which is the effective potential at vanishing temperature, see (III.89). The grand potential and thermal quark pressure in the $N_f=2$ case is then given by

$$\Omega_{q,T}(\psi,\bar\psi,\phi)-\Omega_{q,T=0}(\psi,\bar\psi,\phi) = -\frac{12}{\pi^2}T\int_0^\infty dp\,p^2\,\ln\left(1+e^{-\beta\epsilon_p^\psi}\right) = -p_{q,\mathrm{thermal}}\,, \tag{VII.29}$$

where

$$m_\psi^2(\phi) = \frac{1}{2}h^2\rho\,. \tag{VII.30}$$

This has to be compared with (VII.20) for the mesons. Both expressions for the pressure are strictly positive which is due to

$$\mp\ln\left(1\mp e^{-\beta\epsilon_p^{\phi/\psi}}\right)\geq 0\,, \tag{VII.31}$$

with the minus signs in the bosonic case and the plus sign in the fermionic one. The global $\mp$ in (VII.31) reflects the relative sign of fermionic and bosonic loops while the $\mp$ reflects the Bose-Einstein vs Fermi-Dirac quantum statistics.

The sum of (VII.20) and (VII.38),

$$\Omega_T(\psi,\bar\psi,\phi)-\Omega_{T=0}(\psi,\bar\psi,\phi) = \Omega_{\phi,T}+\Omega_{q,T}-\Omega_{\phi,T=0}+\Omega_{q,T=0} \tag{VII.32}$$

encodes all thermal fluctuations on one loop. As in the vaccum case for $T=0$ we have several possibilities of how to integrate out the thermal fluctuations, e.g. either in parallel or successively. Even though being relevant for the quantitative results, it is irrelevant for the access of the mechnism of chiral symmetry restauration at large temperatures: At large temperatures the quark exhibits a Matsubara gapping as the lowest lying Matsubara mode is πT in comparison to the vanishing one in the mesonic case. For higher temperatures more and more of the infrared quark fluctuations are gapped. However, the quark fluctuations triggers strong chiral symmetry breaking in the first place. Consequently at large enough temperatures chiral symmmtry breaking is melted away.

3. RG for the effective potential at finite temperature*

For quantitative statements the RG equation as in chapter III G 3 or similar non-perturbative techniques such as Dyson-Schwinger equations or 2PI/nPI techniches (2-particle irreducible/n-particle irreducible) should be used. Here we just extend the Wegner-Houghton equation we have derived for the $T = 0$ case in chapter III G 3. There we have the frequency and spatial momentum integration with an $O(4)$-dimensional momentum cutoff with $p^2 \geq \Lambda^2$ in the integrals.

At finite temperature the four-momentum is given by $(2\pi T)^2 n^2 + \vec{p}^2$ and the related θ-function is $\theta(2\pi T)^2 n^2 + \vec{p}^2 - \Lambda^2)$. A four dimensional cutoff leads to discontinuous flows as it jumps if we sweep over one of the Matsubara modes. In (VII.34) we would have to substitute

$$\mathrm{Tr}\delta(\sqrt{p^2} - \Lambda) \to \mathrm{Tr}\delta(\sqrt{(2\pi T)^2 n^2 + \vec{p}^2} - \Lambda)\,, \tag{VII.33}$$

which makes the non-analyticity apparent. Even though the spatial momentum integration smoothens the non-analyticity, it is present and hampers in particular the simple computation of the thermodynamical properties such as the pressure, see [24]. This is not a conceptual problem as these jumps have to be absorbed in the Λ-dependence of the initial condition, it hampers explicit computations.

For that reason we choose a spatial momentum cutoff $\vec{p}^2 > \Lambda^2$, leading us to the functional Wegner-Houghton equation

$$\Lambda\partial_\Lambda \Gamma_\Lambda[\psi, \bar{\psi}, \phi] = -\frac{1}{2}\mathrm{Tr}_{\vec{p}^2=\Lambda^2} \ln \frac{\Gamma^{(2)}_{\phi\phi}}{\Lambda^2} + \mathrm{Tr}_{\vec{p}^2=\Lambda^2} \ln \frac{\Gamma^{(2)}_{\psi\bar{\psi}}}{\Lambda^2}\,, \tag{VII.34}$$

where the trace

$$\mathrm{Tr}_{\vec{p}^2=\Lambda^2} = T\sum_n \int \frac{d^3p}{(2\pi)^3}\delta(\sqrt{p^2} - \Lambda)\,, \tag{VII.35}$$

now only sums over the spatial momentum shell with $p^2 = \Lambda^2$, but over all Matsubara modes. In the line of the arguments in chapter III G 3 this cutoff is now applied to all fluctuations and not only to the thermal ones.

Practically our computations so far allow us to read off the flow equation for the effective potential. For the meson part we start with (VII.17) for a scalar mode, leading to

$$\Omega_{\phi,\Lambda} \simeq \frac{1}{2\pi^2}\int_\Lambda^{\Lambda_{\mathrm{UV}}} dp\, p^2 \left[\frac{1}{2}\epsilon_p^\phi + T\, \ln\left(1 - e^{-\beta\epsilon_p^\phi}\right)\right] + \Omega_{\phi,\Lambda_{\mathrm{UV}}}\,, \tag{VII.36}$$

including the vacuum part. Hence, we simply read-off (minus) the integrand as the Λ-derivative of Ω_ϕ. Applying this immediately to the mesonic part of our EFT we arrive at

$$\Lambda\partial_\Lambda\Omega_{\phi,\Lambda}(\phi) = -\frac{\Lambda^3}{2\pi^2}\left\{\frac{1}{2}\left[\epsilon_\Lambda^\phi(m_\sigma) + \frac{3}{2}\epsilon_\Lambda^\phi(m_\pi)\right] + T\left[\ln\left(1 - e^{-\beta\epsilon_\Lambda^\phi(m_\sigma)}\right) + \ln\left(1 - e^{-\beta\epsilon_\Lambda^\phi(m_\pi)}\right)\right]\right\}\,, \tag{VII.37}$$

where the spatial momentum arguments in the dispersions ϵ_p^ϕ are now taken at the cutoff scale, $p = \lambda$. The first two terms on the right hand side is the $T = 0$ flow as the second term vanishes for $T = 0$. It is different from its counter part in (III.100) as (VII.37) only involves a spatial momentum cutoff, reflected in the cubic power of Λ.

The derivation of the quark part of the flow proceeds similarly. We start with the expression for Ω_q or $-p_q$ after integration of the Matsubara frequency, (VII.38) and restore the $T = 0$ part,

$$\Omega_{q,\Lambda}(\psi, \bar{\psi}, \phi) = -\frac{12}{\pi^2}\int_\Lambda^{\Lambda_{\mathrm{UV}}} dp\, p^2 \left[\epsilon_p^\psi + T\, \ln\left(1 + e^{-\beta\epsilon_p^\psi}\right)\right] + \Omega_{q,\Lambda_{\mathrm{UV}}}(\psi, \bar{\psi}, \phi)\,, \tag{VII.38}$$

leading us to the flow

$$\Lambda\partial_\Lambda\Omega_{q,\Lambda}(\psi, \bar{\psi}, \phi) = \frac{12\Lambda^3}{\pi^2}\left[\epsilon_\Lambda^\psi + T\, \ln\left(1 + e^{-\beta\epsilon_\Lambda^\psi}\right)\right]\,. \tag{VII.39}$$

As in the mesonic part, the first term on the right hand side is the $T = 0$ part of the flow. It also does not match its counterpart in (III.100) due to the different cutoffs.

In summary we are led to the full flow

$$\Lambda\partial_\Lambda \Omega_\Lambda(\psi,\bar\psi,\phi) = -\frac{\Lambda^3}{2\pi^2}\Bigg\{\frac{1}{2}\left[\epsilon^\phi_\Lambda(m_\sigma)+\frac{3}{2}\epsilon^\phi_\Lambda(m_\pi)\right]-12\,\epsilon^\psi_\Lambda$$
$$+T\left[\ln\left(1-e^{-\beta\epsilon^\phi_\Lambda(m_\sigma)}\right)+\ln\left(1-e^{-\beta\epsilon^\phi_\Lambda(m_\pi)}\right)-24\,T\,\ln\left(1+e^{-\beta\epsilon^\psi_\Lambda}\right)\right]\Bigg\}, \tag{VII.40}$$

where the first line is the $T=0$ part of the flow, while the second line is the thermal part. Note that both parts are dependent on derivatives of Ω via the mass-functions and hence feed into each other. One cannot simply solve the $T=$-part first. For example, the thermal pressure is given by (minus) the Λ-integral of the second line on the solution of the full flow equation. If we take Λ-independent mass functions, the Λ-integral gives the one-loop expressions we have started with.

B. Confinement-deconfinement phase transition at finite temperature

The dynamics of confinement and the confinement-deconfinement phase transition is the second cornerstone of the low energy QCD phenomenology we have to unravel. Here we aim at a treatment of this phenomenon within the continuum formulation of QCD similar to that of the chiral phase structure in chapter VII A. We mainly concentrate on the effective potential of the order parameter, the Polyakov loop. This observable is derived directly from the Wilson loop discussed before.

1. *Polyakov loop*

We consider a rectangular Wilson loop, Figure 16, within the static situation also used in our discussion of confinement on the lattice in Section VI D 2. At finite temperature T the time is limited to $t\in[0,\beta]$ with $\beta=1/T$, see chapter VII A 1. Moreover, the gauge fields are periodic in time up to gauge transformations, i.e.

$$A_\mu(t+\beta,\vec x) = \frac{i}{g}T(t,\vec x)\left(D_\mu T^\dagger(t,\vec x)\right)\,, \tag{VII.41}$$

with $T(t,\vec x)\in SU(N)$ are the *transition functions*. It follows from (VII.76) that under gauge transformations they transform as

$$T^U(t,\vec x) = U(t+\beta,\vec x)\,T(t,\vec x)\,U^\dagger(t,\vec x)\,, \tag{VII.42}$$

they parallel transport gauge transformations from t to $t+\beta$. The transformation property (VII.76) ensures the periodicity of gauge invariant quantitites. It is indeed possible to restrict ourselves to strictly periodic fields, $t\equiv 1\!\!1$, even though this limits the possible gauge choice. For the time being we restrict ourselves to the periodic case and discuss the general case at the end. We want to construct the state, that desribes a static quark–anti-quark pair for all times. To that end we take a path that extends in time direction from $t=0$ to β. Then the spatial paths at fixed time $t=0$ and $t=\beta$ have to be identified up to the opposite orientation due to the periodicity on the lattice. Since the paths at t_0 and t_1 are identified up to the orientation, their combined phases would simply be unity for Abelian gauge theories and periodic gauge fields. In the non-Abelian case these contribution simply gives rise to an overall normalisation, see e.g. [25, 26] for respective lattice studies.

We conclude that the path $\mathcal{C}[L,\beta]$ splits into two loops winding around the time direction at the points $\vec x$ and $\vec y$ with $L=|\vec x-\vec y|$. The Wilson loop expectation value is then given by

$$\frac{1}{N_C^2}W[L,\beta] = \langle \mathcal{W}_{\mathcal{C}[L,\beta]}[A]\rangle \sim \langle L[A_0](\vec x)L^\dagger[A_0](\vec y)\rangle\,, \tag{VII.43}$$

where we have dropped the normalisation in the second identity, and $L[A_0]$ is the Polyakov loop variable with

$$L=\frac{1}{N_c}\mathrm{tr}_\mathrm{f}\,P(\beta,\vec x)\,,\qquad \text{with}\qquad P(t,\vec x)=\mathcal{P}e^{-i\,g\int_0^t A_0(\tau,\vec x)d\tau}\,. \tag{VII.44}$$

The normalisation of the Polyakov loop is such that it is unity for a vanishing gauge field, $L[0] = 1$. It lives in the fundamental representation as it is related to a creation operator of a quark. It is gauge invariant under periodic gauge transformations that keep the strict periodicity of the gauge field we have required. In general we have

$$L[A^U] = \frac{1}{N_c}\mathrm{tr}_\mathrm{f}\,\left[U^\dagger(\beta,\vec{x})U(0,\vec{x})\right]\,P(\beta,\vec{x})\,, \tag{VII.45}$$

where we have used the cyclicity of the trace. The combination $\left[U^\dagger(\beta,\vec{x})U(0,\vec{x})\right]$ is unity for periodic gauge transformations, which is the case we have restricted ourselves to when deriving (VII.43) from the gauge invariant Wilson loop. In the general case the two spatial parts of the path at $t = 0, \beta$ only cancel up to the transition functions. Working through the derivation we get

$$L = \frac{1}{N_c}\mathrm{tr}_\mathrm{f}\, T(0,\vec{x})P(\beta,\vec{x})\,, \tag{VII.46}$$

which is also gauge invariant under non-periodic gauge transformations. Here we only consider $T \equiv 1\!\!1$ but (VII.46) has to be used for example in the temporal axial gauge $A_0 \equiv 0$. Evidently, in this gauge (VII.44) simply is one. However, in order to achieve this gauge non-periodic gauge transformations (in time) have to be used. Then, the whole physics information of the Polyakov loop is stored in the transition function T instead of the gauge field. While this is not a convenient choice in continuum formulations it is a common choice on the lattice. There is is obtained by taking trivial temporal link variables $U_0 = 1\!\!1$ for all but the last link from $t = \beta - a$ to β.

We now come back to our main line of arguments, and restrict ourselves to the fully periodic case. The Wilson loop in (VII.43) is an order parameter for confinement: in the confining phase it tends towards zero for large distances, $L \to \infty$, due to the area law,

$$\lim_{L\to\infty} W[L,\beta] \simeq \lim_{L\to\infty} e^{-\sigma\beta L} = 0\,. \tag{VII.47}$$

In turn, in the deconfined regime of the theory the quark–anti-quark potential $V_{q\bar{q}}$ is Coulomb-like, $V_{q\bar{q}} \propto 1/|\vec{x}-\vec{y}|$ and the Wilson loop follows a perimeter law, leading to

$$\lim_{L\to\infty} W[L,\beta] > 0\,. \tag{VII.48}$$

In conclusion the Wilson loop expectation value or Polyakov loop two-point correlation function for $L \to \infty$ serves as an order parameter for confinement at finite temperature. Moreover, in this limit we can use the clustering decomposition property of a *local* quantum field theory,

$$\lim_{|\vec{x}-\vec{y}|\to\infty} \langle A(\vec{x})B(\vec{y})\rangle - \langle A(\vec{x})\rangle\,\langle B(\vec{y})\rangle = 0\,. \tag{VII.49}$$

for local operators A and B. Hence we conclude that

$$\lim_{L\to\infty} W[L,\beta] \sim \langle L[A_0](\vec{x})\rangle\,\langle L^\dagger[A_0](\vec{y})\rangle\,, \tag{VII.50}$$

it only depends on the temporal component of the gauge field. Again we have dropped the normalisation factor already discussed above (VII.43). It is irrelevant for the present line of arguments.

The Polyakov loop expectation value $\langle L[A_0]\rangle$ does not depend on the spacial variable due to translation invariance. Thus also the Polyakov loop expectation value itself serves as an order parameter for confinement,

$$\langle L[A_0]\rangle = \begin{cases} 0 & \text{confining phase} \\ \neq 0 & \text{deconfining phase} \end{cases} \tag{VII.51}$$

2. Center-Symmetry and the confinement-deconfinement phase transition

So far we have argued on a heuristic level which led us to (VII.51) as an order parameter, without even discussing the symmetry behind the pattern in (VII.51): we are searching for a symmetry that is preserved by the Yang-Mills action but does not keep $\langle L[A_0]\rangle$ invariant. This is the center symmetry of the gauge group. The center elements are those elements that commute with all other elements in the gauge group. In $SU(N)$ these are the Nth roots of unity in the groups. For the cases used here, the example group $SU(2)$ and the physical group $SU(3)$, the centers $\mathcal{Z}$ are

$$\mathcal{Z}_{SU(2)} = \{\mathbb{1}, -\mathbb{1}\} \simeq Z_2 \,, \qquad\qquad \mathcal{Z}_{SU(3)} = \{\mathbb{1}, \mathbb{1}\, e^{\frac{2}{3}\pi i}, \mathbb{1}\, e^{\frac{4}{3}\pi i}\} \simeq Z_3 \,. \tag{VII.52}$$

where the identities $\mathbb{1}$ in $SU(2)$ and $SU(3)$ are $\mathbb{1}_{2\times 2}$ and $\mathbb{1}_{3\times 3}$ respectively. The non-trivial center elements in (VII.52) are related to combinations of generators in the algebra. This relation is not unique as the eigenvalues of the combination of algebra elements is only determined up to $2\pi n$ with $n \in \mathbb{Z}$. For example, one representation is

$$SU(2): \quad -\mathbb{1} = e^{\pi i \sigma_3} \,, \qquad\qquad SU(3): \quad \mathbb{1}\, e^{\frac{2}{3}\pi i} = e^{2\pi i \frac{1}{\sqrt{3}} \lambda_8} \,, \qquad \mathbb{1}\, e^{\frac{4}{3}\pi i} = e^{2\pi i \frac{2}{\sqrt{3}} \lambda_8} \,. \tag{VII.53}$$

with the Pauli matrices in (III.40) and the Gell-Mann matrices

$$\lambda_1 = \begin{pmatrix} 0 & 1 & 0 \\ 1 & 0 & 0 \\ 0 & 0 & 0 \end{pmatrix} , \qquad \lambda_2 = \begin{pmatrix} 0 & -i & 0 \\ i & 0 & 0 \\ 0 & 0 & 0 \end{pmatrix} , \qquad \lambda_3 = \begin{pmatrix} 1 & 0 & 0 \\ 0 & -1 & 0 \\ 0 & 0 & 0 \end{pmatrix} , \qquad \lambda_4 = \begin{pmatrix} 0 & 0 & 1 \\ 0 & 0 & 0 \\ 1 & 0 & 0 \end{pmatrix} ,$$

$$\lambda_5 = \begin{pmatrix} 0 & 0 & -i \\ 0 & 0 & 0 \\ i & 0 & 0 \end{pmatrix} , \qquad \lambda_6 = \begin{pmatrix} 0 & 0 & 0 \\ 0 & 0 & 1 \\ 0 & 1 & 0 \end{pmatrix} , \qquad \lambda_7 = \begin{pmatrix} 0 & 0 & 0 \\ 0 & 0 & -i \\ 0 & i & 0 \end{pmatrix} , \qquad \lambda_8 = \frac{1}{\sqrt{3}} \begin{pmatrix} 1 & 0 & 0 \\ 0 & 1 & 0 \\ 0 & 0 & -2 \end{pmatrix} , \tag{VII.54}$$

in the fundamental representation of $SU(3)$. The generators of the $SU(3)$ algebra are $t^a_{\text{fund}} = \lambda^a/2$. In the adjoint repesentation the generators of the algebra are given by the structure constants, see **??**. The $SU(3)$ structure constants are given by

$$\begin{aligned} &SU(2): \quad f^{abc} = \epsilon^{abc} \,, \\ &SU(3): \quad f^{123} = 1 \,, \quad f^{147} = f^{246} = f^{257} = f^{345} = \frac{1}{2} \,, \quad f^{156} = f^{367} = \frac{1}{2} \,, \quad f^{458} = f^{678} = \frac{1}{2} \,. \end{aligned} \tag{VII.55}$$

Hence, in the adjoint representation these elements are all represented by id_{ad}, the unit element in the adjoint representation,

$$Z_{\text{ad}} = \mathbb{1}_{\text{ad}} \,, \qquad \text{for} \qquad Z \in \mathcal{Z} \,. \tag{VII.56}$$

In the adjoint representation every center element is mapped to the identity, $z = \mathbb{1}_{\text{ad}}, \forall z \in \mathcal{Z}$. Hence we have

$$\mathcal{Z}_{\text{ad}} = \{\mathbb{1}_{\text{ad}}\} \,. \tag{VII.57}$$

As the gauge fields and the ghosts live in the adjoint representation, the gauge-fixed Yang-Mills action is trivially invariant under center transformations. However, they cause a non-trivial $T \in \mathcal{Z}$. Accordingly, this leads us to

$$P(\beta, \vec{x}) \to z\, P(\beta, \vec{x}) \,, \qquad \text{with} \qquad z \in \mathcal{Z} \,, \tag{VII.58}$$

with $A_0 \to A_0^{U(z)}$. Here, the gauge transformation $U(z)$ triggers a center transformation of P (or rather the transition function). In the adjoint representation (VII.58) is an identity transformation. However, the Polyakov loop $L[A_0]$, as we have discussed it, is the trace of the Polyakov line $P(\beta, \vec{x})$ in the *fundamental* representation, see (VII.44). The underlying reason is its connection to the quark that carries the *fundamental* representation. Hence, with (VII.58) we arrive at

$$L[A_0] \to z\, L[A_0] \,, \qquad \text{with} \qquad z \in Z_n \,. \tag{VII.59}$$

Note that in (VII.59), the z's are now simple phase factors and not SU(N)-matrices, in a slight abuse of notation. We conclude that in the center-symmetric phase of the theory the Polyakov loop expectation value (VII.51) has to vanish while in the center-broken phase it is finite.

The center symmetry can be made even more explicit on the level of the gauge fields that live in the algebra of the gauge field. For this purpose we rewrite the Polyakov loop $P(\beta, \vec{x})$ in (VII.44) in terms of the exponential of an algebra field,

$$P(\beta, \vec{x}) = e^{-2\pi i\, \hat{\varphi}(\vec{x})} \,, \qquad\qquad \hat{\varphi}(\vec{x}) \xrightarrow{U} U^\dagger(0, \vec{x}) \hat{\varphi}(\vec{x}) U(0, \vec{x}) \,. \tag{VII.60}$$

The algebra field transforms as a tensor under periodic gauge transformations: in (VII.60) we have used $U(\beta,\vec{x}) = U(0,\vec{x})$. Moreover, in the absence of the path ordering the algebra field $2\pi\hat{\varphi}$ would just be identical to the exponent $i\,g\int_0^t A_0(\tau,\vec{x})d\tau$ in (VII.44). This holds true for gauge fields in the Cartan subalgebra. In the following we consider the approximation of constant (mean) gauge fields, which can always be rotated into the Cartan subalgebra with constant gauge transformations. This leads us to

$$\hat{\varphi} = \frac{\beta g}{2\pi} A_0\,, \qquad\qquad L(\hat{\varphi}) = L[A_0] = \frac{1}{N_c}\mathrm{tr}\, e^{-2\pi i\,\hat{\varphi}}\,. \tag{VII.61}$$

with $\hat{\varphi}$ in the Cartan subalgebra. For the two gauge groups considered, $SU(2)$ and $SU(3)$, we find

$$SU(2):\; \hat{\varphi} = \varphi_3 \frac{\sigma^3}{2}\,, \qquad\qquad SU(3):\; \hat{\varphi} = \left(\varphi_3\frac{\lambda^3}{2} + \varphi_8\frac{\lambda^8}{2}\right)\,, \tag{VII.62}$$

with $\lambda^{3,8}$ given in (VII.54). The eigenvalue equation of the field $\hat{\varphi}$ in the fundamental representation is given by

$$\hat{\varphi}^{\mathrm{f}}|\varphi_n^{\mathrm{f}}\rangle = \nu_n^{\mathrm{f}}|\varphi_n^{\mathrm{f}}\rangle\,, \qquad n \in 1,...,N_c\,, \tag{VII.63}$$

where the superscript ^{f} indicates the fundamental representation. The eigenvalues for $SU(2)$ and $SU(3)$ are given by

$$SU(2):\; \nu_n^{\mathrm{f}} \in \left\{\pm\frac{\varphi_3}{2}\right\}\,, \qquad\qquad SU(3):\; \nu_n^{\mathrm{f}} \in \left\{\pm\frac{\varphi_3 + \frac{1}{\sqrt{3}}\varphi_8}{2}\,,\, -\frac{1}{\sqrt{3}}\varphi_8\right\}\,. \tag{VII.64}$$

Using (VII.63) and (VII.64) in the Polyakov loop in $SU(2)$ we arrive at

$$L(\varphi) = \cos\pi\varphi\,, \tag{VII.65}$$

For $SU(3)$ we have

$$L(\varphi_3,\varphi_8) = \frac{1}{3}\left[e^{\frac{2\pi i\,\varphi_8}{\sqrt{3}}} + 2\cos(\pi\varphi_3)\,e^{-\frac{2\pi i\,\varphi_8}{\sqrt{3}}}\right]\,, \tag{VII.66}$$

As the Polyakov loop potential (for vanishing chemical potential) has minima at $\varphi_3 = 0$ we can work with the Polyakov loop variable at $\varphi_8 = 0$,

$$L(\varphi) = \frac{1}{3}\left(1 + 2\cos\pi\varphi\right)\,, \tag{VII.67}$$

with $L(\varphi) = L(\varphi_3 = \varphi, 0)$. Then, confinement is signaled by the (mean) gauge field configurations

$$\varphi = \frac{1}{2} \quad \text{for } SU(2)\,, \qquad \text{and} \qquad \varphi = \frac{2}{3} \quad \text{for } SU(3)\,. \tag{VII.68}$$

Having identified the symmetry we can envoke universality to predict the scaling of the order parameter in the vicinity of the phase transition:

For $SU(2)$ we are in the Ising universality class, the symmetry group being Z_2. If $SU(2)$-Yang-Mills exhibits a second order phase transition (and it does), it should have Ising scaling. This is indeed seen. For $SU(3)$ the symmetry group is Z_3 and we epxect a first order phase transition which is also seen. Our explicit computations later will not encorporate the full fluctuation analysis so detecting Ising scaling is out of reach here. However, we are able to see the seoncd and first order nature of the respective phase transitions. This closes our very rough symmetry discussion.

We also would like to add some more arguments for the intuitive understanding for the Polyakov loop expectation value. We have argued for the Wilson loop expectation value, that it is related to the expectation value of a static quark–anti-quark pair,

$$W[L,\beta] \simeq \langle \bar{q}(\vec{x})\,\mathcal{P}e^{-i\,g\int_{\mathcal{C}_{\vec{x},\vec{y}}} A_\mu dz_\mu} q(\vec{y})\rangle\,, \tag{VII.69}$$

where the path-ordered phase ensures gauge invariance. Using -naively- the clustering decomposition property (or short declustering) for $|\vec{x}-\vec{y}| \to \infty$, we can decompose the expectation value in (VII.69) in the product of the expectation value of a quark state and and anti-quark state. Naturally the latter have to vanish as the creation of a single quark or anti-quark requires an infinite energy. However, be aware of the fact that the quark and anti-quark states do not belong to the Hilbert space of QCD and hence we cannot apply declustering that easily.

Still, the Polyakov loop expectation value is related to the heuristic situation described above. To see this more clearly let us consider a static quark. This situation can be achieved by taking the infinite quark mass limit, $m_q \to \infty$. The Dirac equation

$$(\not{D} + m_\psi)\,\psi = 0\,, \tag{VII.70}$$

then reduces to a space-independent equation as the quark cannot move, $\vec{\partial}_x \psi = 0$. Hence, the Dirac equation (VII.70) reads in the static limit

$$(\gamma_0 D_0 + m_\psi)\,\psi = 0\,. \tag{VII.71}$$

A solution to this equation is given by

$$\psi(x) = P^\dagger(t,\vec{x})\psi_0(x)\,, \qquad \text{with} \qquad (\gamma_0\partial_0 + m_\psi)\,\psi_0 = 0\,. \tag{VII.72}$$

where ψ_0 solves the free Dirac equation, and $P(t,\vec{x})$ is the untraced Polyakov loop (VII.44). For proving (VII.72) we use that $(D_0 P^\dagger(t,\vec{x})) = 0$ following from (VII.44). Hence, in a -vague- sense we can identify the expectation value of the trace Polyakov loop L, (VII.44), with the interaction part of a static quark.

3. *Polyakov loop potential*

As in the case of chiral symmetry breaking we would like to compute the effective potential of the order parameter, $V_{\rm Pol}[L]$. This turns out to be a formidable task both on the lattice and in the continuum. Note however, that the computation of the expectation value itself is simple on the lattice.

In the continuum we compute the effective potential of QCD, that is the effective action $\Gamma[\Phi]$ for constant fields. Before we embark on the explicit computation we first have to deal with the issue of gauge invariance in the gauge-fixed approach we are working in. To that end we upgrade our covariant gauge fixing to the *background gauge*: To that end we split our gauge field in a background $\bar{A}$ and a fluctuation a, to wit

$$A_\mu = \bar{A}_\mu + a_\mu\,. \tag{VII.73}$$

While the background $\bar{A}$ is kept fixed, a carries all the quantum fluctuations. In the path integral the integration over A then turns into one over a. So far nothing has been changed. Now we modify our gauge fixing,

$$\partial_\mu A_\mu = 0 \to \bar{D}_\mu a = 0\,, \qquad \text{with} \qquad \bar{D}_\mu = D_\mu(\bar{A})\,. \tag{VII.74}$$

For $\bar{A} = 0$ we regain the orginial covariant gauge fixing. For the background gauge fixing the gauge fixed classical action with ghost term reads

$$S_A[\bar{A},a,c,\bar{c}] = S_{\rm A}[A] + \frac{1}{2\xi}\int_x (\bar{D}^{ab}_\mu a^b_\mu)^2 + \bar{c}^a \bar{D}^{ad}_\mu D^{db}_\mu c^b\,. \tag{VII.75}$$

At finite temperature T, the time integration in (VII.75) is limited to $t \in [0,\beta]$ with $\beta = 1/T$ as discussed in Section VII A 1. Moreover, the gauge fields are periodic in time up to gauge transformations, i.e.

$$A_\mu(t+\beta,\vec{x}) = \frac{i}{g}T(t,\vec{x})\left(D_\mu T^\dagger(t,\vec{x})\right)\,, \qquad c(t+\beta,\vec{x}) = T(t,\vec{x})\,c(t,\vec{x})\,T^\dagger(t,\vec{x})\,, \quad \bar{c}(t+\beta,\vec{x}) = T(t,\vec{x})\,\bar{c}(t,\vec{x})\,T^\dagger(t,\vec{x})\,, \tag{VII.76}$$

with $T(t,\vec{x}) \in SU(N)$ are the *transition functions*. It follows from (VII.76) they transform under gauge transformations as

$$T^U(t,\vec{x}) = U(t+\beta,\vec{x})\,T(t,\vec{x})\,U^\dagger(t,\vec{x})\,, \tag{VII.77}$$

they parallel transport gauge transformations from t to $t+\beta$. The transformation property (VII.76) ensures the periodicity of gauge invariant quantitites. It is indeed possible to restrict ourselves to strictly periodic fields, $t \equiv 1\!\!1$, even though this limits the possible gauge choice. For the time being we restrict ourselves to the periodic case and discuss the general case at the end. The state we want to construct is the one, where we desribe a static quark–anti-quark pair for all times. To that end we take a path that extends in time direction from $t = 0$ to β. Then the spatial paths at fixed time $t = 0$ and $t = \beta$ have to be identified (up to the orientation) due to the periodicity on the lattice, as well as the fact that we have restricted ourselves to periodic gauge fields.

In the presence of the background field and with the gauge fixing (VII.74) we have an additional -auxiliary- gauge symmetry: the gauge-fixed action is invariant under *background gauge transformations*

$$\bar{A}^U_\mu = \frac{i}{g} U\,(\bar{D}_\mu U^\dagger)\,, \qquad a^u = U\, a_\mu\, U^\dagger \quad \longrightarrow \quad A^U = \frac{i}{g} U\,(D_\mu U^\dagger)\,. \tag{VII.78}$$

Evidently this is true for the Yang-Mills action, it is left to show this for the gauge fixing and ghost term. The gauge fixing condition (VII.74) transforms as a tensor under (VII.78): $\bar{D}_\mu a \to U\, \bar{D}_\mu a\, U^\dagger$ and hence $\mathrm{tr}(\bar{D}_\mu a)^2$ is invariant under (VII.78). The Faddeev-Popov operator $\mathcal{M}$ in the background gauge is given by

$$\mathcal{M} = -\bar{D}_\mu D_\mu \to U\, \bar{D}_\mu D_\mu\, U^\dagger\,. \tag{VII.79}$$

It also transforms as a tensor and hence the ghost term is gauge invariant under (VII.78). However, the background gauge transformations are an auxiliary symmetry. The physical gauge transformations are those of the fluctuation field at fixed background $\bar{A}$, the *quantum gauge transformations*

$$\bar{A}^U_\mu = \bar{A}_\mu\,, \qquad a^u = U\,(D_\mu U^\dagger) \quad \longrightarrow \quad A^U = \frac{i}{g} U\,(D_\mu U^\dagger)\,. \tag{VII.80}$$

Again this can be understood by choosing the standard covariant gauge with a vanishing background. Then, (VII.80) is the only gauge transformation left, while (VII.78) leads to a non-vanishing background and hence changes the gauge fixing. The neat feature of the background field formalism is that it can be shown that both transformations are indeed related via *background independence* of the quantum equations of motion. Therefore background gauge invariance under the transformations (VII.78) carries physical gauge invariance, more details can be found in Appendix C

Still, the introduction of the background seems to complicate matters but it indeed facilitates computations and gives a more direct access to physics. Here we explore both properties. First we note that the introduction of $\bar{A}$ leads to an effective action that depends on two fields,

$$\Gamma[A] \to \Gamma[\bar{A}, a]\,. \tag{VII.81}$$

Switching of the mean value of the fluctuation field, $a = 0$ leads to a (background) gauge invariant action

$$\Gamma[A] = \Gamma[A, a = 0] \tag{VII.82}$$

As mentioned before, this is the physical gauge invariance. Moreover, one can show that the background correlation functions are directly related to S-matrix elements. In summary the effective action $\Gamma[A]$ defined in (VII.82) carries the information about the Polyakov loop potential.

Now we proceed with the explicit computation of the effective potential at one loop. For the Polyakov loop potential the only mean field of interest is the temporal component of the gauge field, and the other fields are put to zero. We will perform this computation first on the one-loop level with the classical ghost and gluon propagators. Finally we will introduce the fully non-perturbative propagators to this one-loop computation. This re-sums infinitely many diagrams and carries the essential non-perturbative computation. The explicit results are in semi-quantitative agreement with the full results obtained with functional renormalisation group methods and also show a good agreement with the lattice results.

In summary the Polyakov loop potential for constant temporal gauge fields is given by

$$V_{\text{Pol}}(A_0) = \frac{1}{2}\mathrm{Tr}\,\ln G_A^{-1}(A_0) - \mathrm{Tr}\, G_c^{-1}(A_0) - \mathcal{N}\,, \tag{VII.83}$$

where the color traces in (VII.83) are in the adjoint representation and CN is the normalisation of the potential which we leave open for now. For the one-loop computation we have $G^{-1} = S_A^{(2)}$ with S_A in (VII.75) and hence

$$G_A^{-1}(A_0) = -D_\rho^2\, \delta^{\mu\nu} + \left(1 - \frac{1}{\xi}\right) D_\mu D_\nu\,, \qquad\qquad G_c^{-1}(A_0) = -D_\rho^2\,. \tag{VII.84}$$

In (VII.84) we have used that the spin one terms proportional to $F_{\mu\nu}$ drop out for a constant A_0-background. In the re-summed non-perturbative approximation we use numerical results, e.g. the Yang-Mills analogue of Figure 8 at finite temperature.

As a preparation for the full computation we go through the perturbative computation. This already reveals the main mechanism we need for the access of the confinement-deconfinement phase transition. This computation has been done independently in [27] and [28] in 1980 (published 81). The potential is often called the Weiss potential.

For the explicit computation we restrict ourselves to $SU(2)$. The result does not depend on the gauge fixing parameter ξ and we choose $\xi = 1$, Feynman gauge, in order to facilitate the computation. Then the Lorentz part of the trace in the gauge field loop can be performed immediately, leading to a factor four for the four polarisations of a vector field. We have

$$V_{\text{Pol}}(A_0) \simeq 4 * \frac{1}{2}\text{Tr}\,\ln(-D_\rho^2) - 2 * \frac{1}{2}\text{Tr}\,\ln(-D_\rho^2) = 2\frac{1}{2}\text{Tr}\,\ln(-D_\rho^2)\,, \tag{VII.85}$$

where we have made explicit the multiplicities of gluon and ghost, and we dropped the normalisation. The gluon dominates and the final result is twice that of one polarisation, which accounts for the two physical polarisations of the gluon. This is an expected property as we compute a gauge invariant potential that should reflect the fact that we only have two physical polarisations, and the gauge fixing is only a means to finally compute gauge invariant quantities. Now we use that we can diagonalise the operator D_ρ^2 in the adjoint representation in the algebra. The color eigenfunctions and eigenvalues in the adjoint representation are given by

$$\hat\varphi^{\text{ad}} = \frac{g\beta}{2\pi} A_0^{\text{ad}}\,, \qquad\qquad \hat\varphi^{\text{ad}}\,|\varphi_n^{\text{ad}}\rangle = \nu_n^{\text{ad}}|\varphi_n^{\text{ad}}\rangle\,, \qquad n\in 1,...,N_c^2-1\,, \tag{VII.86}$$

and

$$SU(2):\; \nu_n^{\text{ad}} \in \{0\,,\,\pm\varphi\}\,, \qquad SU(3):\; \nu_n^{\text{ad}} \in \left\{0\,,\,0\,,\,\pm\varphi_3\,,\,\pm\frac{\varphi_3 \pm \sqrt{3}\varphi_8}{2}\right\}\,, \tag{VII.87}$$

in comparison to the eigenvalues (VII.64) in the fundamental representation. Note for example, that the eigenvalues of T^3_{ad} are ± 1, while they are $\pm 1/2$ in the fundamental representation. This relative factor $1/2$ reflects the sensitivity to center transformations in the fundamental representation and the insensitivity in the adjoint representation.

With these preparations we can compute the one-loop Polyakov loop potential analytically. Performing the trace in (VII.85) in terms of the eigenfunctions $|\varphi_n\rangle$ and momentum modes, we arrive at

$$V_{\text{Pol}}(A_0) \simeq 2\Big[V_{\text{mode}}(\varphi) + V_{\text{mode}}(-\varphi)\Big]\,, \tag{VII.88}$$

with V_{Pol} being $1/2\,\text{Tr}\ln(-D^2)$, where the gauge field is substitute by one eigenmode,

$$\begin{aligned} V_{\text{mode}}(\varphi) &= \frac{T}{2}\sum_{n\in\mathbb{Z}}\int\frac{d^3p}{(2\pi)^3}\left\{\ln\frac{(2\pi T)^2(n+\varphi)^2+\vec p^2}{(2\pi T)^2n^2+\vec p^2}\right\}\\ &= \frac{T}{4\pi^2}\sum_{n\in\mathbb{Z}}\int_0^\infty dp\,p^2\left\{\ln\frac{(2\pi T)^2(n+\varphi)^2+p^2}{(2\pi T)^2n^2+p^2}\right\}\,, \end{aligned} \tag{VII.89}$$

where the denominator in the logarithm in (VII.89) is a normalisation of the mode potential at vanishing φ: $V_{\text{mode}}(0) = 0$. The sum in (VII.89) can be performed analytically by taking first a derivative w.r.t. p^2 and then using contour integrals. It results in

$$V_{\text{mode}}(\varphi) = \frac{T}{4\pi^2}\int_0^\infty dp\,p^2\left\{\left[\sum_\pm \ln\sinh\frac{\beta p \pm 2\pi i\,\varphi}{2}\right] - 2\ln\sinh\frac{\beta p}{2}\right\}\,. \tag{VII.90}$$

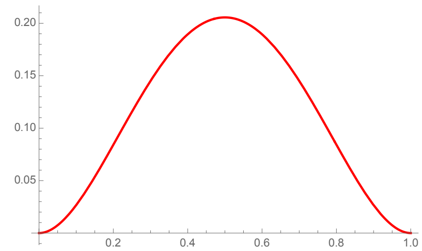

FIG. 23: One loop Polyakov loop potential for $SU(2)$.

Now we use that

$$\sum_\pm \ln\sinh\frac{\beta p \pm 2\pi i\,\varphi}{2} - 2\ln\sinh\frac{\beta p}{2} = \sum_\pm \ln(1-e^{-\beta p \pm 2\pi i\,\varphi}) - 2\ln(1-e^{-\beta p})$$

$$= \sum_\pm \sum_{n=1}^\infty \frac{1}{n}\, e^{-\beta p n}\left(e^{\pm 2\pi i\, n\varphi}-1\right)\,. \tag{VII.91}$$

In (VII.91) we have pulled out a factor $\ln\exp(\beta p \pm 2\pi i\varphi)/2 = (\beta p \pm 2\pi i\varphi)/2$ from the $\ln\sinh$-terms with φ, and $2\ln\exp\beta p/2 = \beta p$ from the $\ln\sinh$-term in the normalisation. These terms cancel each other and we are led to the right hand sid e of (VII.91). Then we have expanded the logarithms in a Taylor expansion in the exponentials. In summary this leads us to

$$V_{\rm mode}(\varphi) = \frac{T}{4\pi^2}\int_0^\infty dp\, p^2 \sum_\pm\sum_{n=1}^\infty \frac{1}{n}\, e^{-\beta p n}\left(e^{\pm 2\pi i\, n\varphi}-1\right)$$

$$= \frac{T^4}{\pi^2}\sum_{n=1}^\infty \frac{1}{n^4}\left(\cos 2\pi n\varphi - 1\right)\,. \tag{VII.92}$$

The sum in (VII.92) is gain easily performed with methods of complex analysis and we arrive at

$$\beta^4\, V_{\rm mode}(\varphi) = \frac{\pi^2}{48}\left[4\left(\tilde\varphi-\frac{1}{2}\right)^2-1\right]^2\,, \qquad \tilde\varphi = \varphi \bmod 1\,, \tag{VII.93}$$

where we have devided out the trivial dimensional thermal factor T^4. Inserting (VII.93) in (VII.88) for the Polyakov loop potential we are led to

$$\beta^4\, V_{\rm pol}(A_0) = \frac{\pi^2}{12}\left[4\left(\tilde\varphi-\frac{1}{2}\right)^2-1\right]^2\,, \tag{VII.94}$$

for $SU(2)$, while for $SU(3)$ the potential is given by

$$V_{\rm pol}(A_0) = \sum_{n=1}^{8} V_{\rm mode}(\nu_n)\,, \tag{VII.95}$$

with the eigenvalues ν_n in (VII.87). We have plotted the $SU(2)$ potential in Figure 23 as it has a very simple form which carries already the relevant information. The potential has minima at $\varphi = 0, 1$ and a maximum at $\varphi = 1/2$. For the minima the Polyakov loop variable $L[A_0]$ takes the value ± 1, the maximum is the center-symmetric value $L[A_0] = 0$. This structure is also present for all $SU(N)$-theories and originates in the -necessary- center symmetry of the potential. The center transformation in $SU(2)$ is given by

$$\varphi \to 1-\varphi\,, \tag{VII.96}$$

which maps $L[\varphi = 0] = 1 \to L[\varphi = 1] = -1$ and vice versa, this comes via the multiplication of the Polyakov line $P(\vec{x})$ with the center element $-\mathbb{1}$. We conclude that in perturbation theory the potential has its minimum at the maximally center-breaking values, the theory is in the center-broken phase. At large temperatures perturbation theory is valid and quantum fluctuations are small: the fluctuating gauge field is close to $A_0 = 0$. This leads to

$$\lim_{T\to\infty} L[\langle A_0\rangle] = 1\,. \tag{VII.97}$$

In turn, for small temperatures the potential should exhibit a minimum at $\varphi = 1/2$. Interestingly, this is achieved within the one loop computation if the gluon contributions are switched off, and the ghost contribution is left.

Finally we come back to the normalisation of $V_{\rm pol}(A_0)$ in (VII.83). We have normalised it such that $V_{\rm pol}(A_0) = 0$. However, if we choose the normalisation as

$$\mathcal{N} = \left[\frac{1}{2}\mathrm{Tr}\,\ln G_A^{-1}(0) - \mathrm{Tr}\,G_c^{-1}(0)\right]_{T=0}\,, \tag{VII.98}$$

the value of the effective potential simply is the thermal pressure of the theory. The difference between (VII.98) and that chosen in (VII.89) for the mode potential is given by

$$\Delta\mathcal{N} = 2(N_c^2-1)\left[\frac{T}{2}\sum_{n\in\mathbb{Z}}\int\frac{d^3p}{(2\pi)^3}\ln\left[(2\pi T)^2 n^2 + \vec{p}^2\right] - \int\frac{d^4p}{(2\pi)^4}\ln p^2\right] = -p_{A,\rm SB} \quad \text{with} \quad p_{A,\rm SB} = \frac{\pi^4 T^4}{45}(N_c^2-1)\,. \tag{VII.99}$$

(VII.99) is nothing but (minus) the Stefan-Boltzmann pressure of a $SU(N_c)$ gauge theory, see (VII.19) for the scalar case. It is the scalar pressure times the number of physical modes: two physical transversal polarisations times the number of color modes, (N_c^2-1), leading to $2(N_c^2-1)p_{\phi,\rm SB}$. This leads us to our final result

$$\beta^4\, V_{\rm pol}(A_0) = \frac{\pi^2}{12}\left[4\left(\tilde{\varphi}-\frac{1}{2}\right)^2 - 1\right]^2 - \frac{\pi^4}{45}(N_c^2-1)\,. \tag{VII.100}$$

We proceed with a non-perturbative computation of the Polyakov loop potential which still keeps the analogy to the one loop computation above. Even though this is an approximation, both the numerical result as well as the conceptual structure are also present in the full computation. We again start with (VII.83). Now, instead of using the classical inverse propagators we utilise the fully non-perturbative ones. These propagators can only be computed with numerical non-perturbative approaches, either gauge fixed lattice simulations or with functional methods such as the functional renormalisation group (FRG) already used in the low energy EFT for chiral symmetry breaking or Dyson-Schwinger equations (DSEs). Instead of using the available numerical data we add another approximation in order to keep our approach semi-analytic.

From Fig. 8 we know that the gluon propagator exhibits a mass gap for low momenta. In turn, for large momenta is runs logarithmically. This behaviour is also present at finite temperature, see Fig. 25. There we plot the momentum dependence of the dressing of the chromo-magnetic gluon propagator for different temperatures. Both, results from functional methods and from gauge-fixed lattice simulations are shown. The dressing is defined as

$$\frac{1}{Z_A^{\rm M}(\vec{p}^2)} = \frac{1}{2}\,\vec{p}^2\,\langle A_i(0,\vec{p})A_i(0,-\vec{p})\rangle\,, \tag{VII.101}$$

it is the dressing of the gluon propagator perpendicular ro the heat bath. In Fig. 24 we plot the temperature-dependent mass (screening mass) of chromo-electric gluon propagator, the gluon propagator parallel to the heat bath,

$$\frac{1}{Z_A^{\rm E}(\vec{p}^2)} = \vec{p}^2\,\langle A_0(0,\vec{p})A_0(0,-\vec{p})\rangle\,. \tag{VII.102}$$

Note that the simple relations (VII.101), (VII.102) are only valid for $p_0 = 0$. For $p_0 \neq 0$ one has to use the thermal projection operators, see e.g. [29]. At large temperatures we expect them to tend towards their perturbative values. This is indeed happening, however, we need higher order thermal perturbation theory. The one-loop Debye mass is

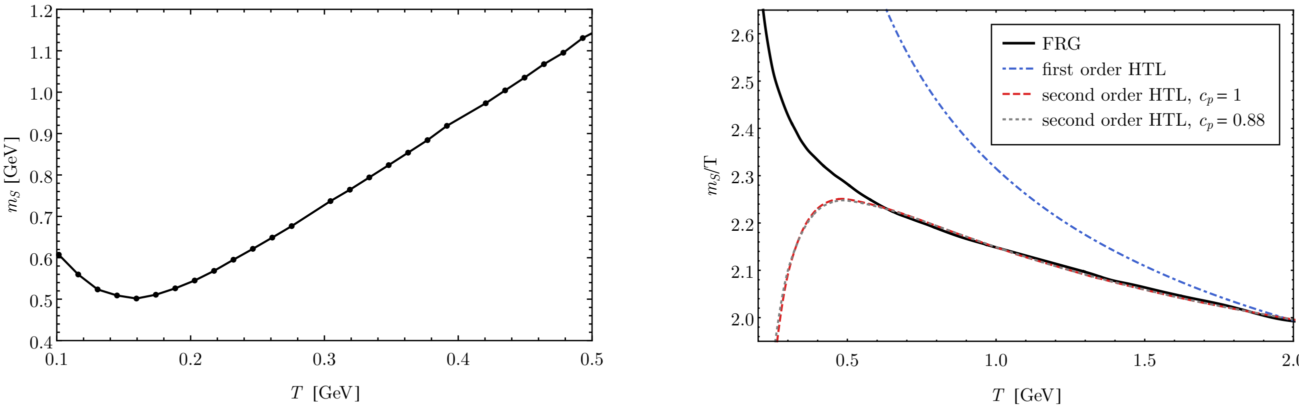

(a) Screening mass m_s in units of GeV at low temperatures. In the limit $T \to 0$ the screening mass smoothly tends towards its finite $T = 0$ value, see back curve in Fig. 25.

(b) Dimensionless Debye screening m_s/T mass at high temperatures in comparison with leading order perturbation theory (VII.103) and the Arnold-Yaffe prescription (VII.104) for accommodating beyond leading order effects [30].

FIG. 24: Debye screening mass m_s, plot taken from [29], for more details see there.

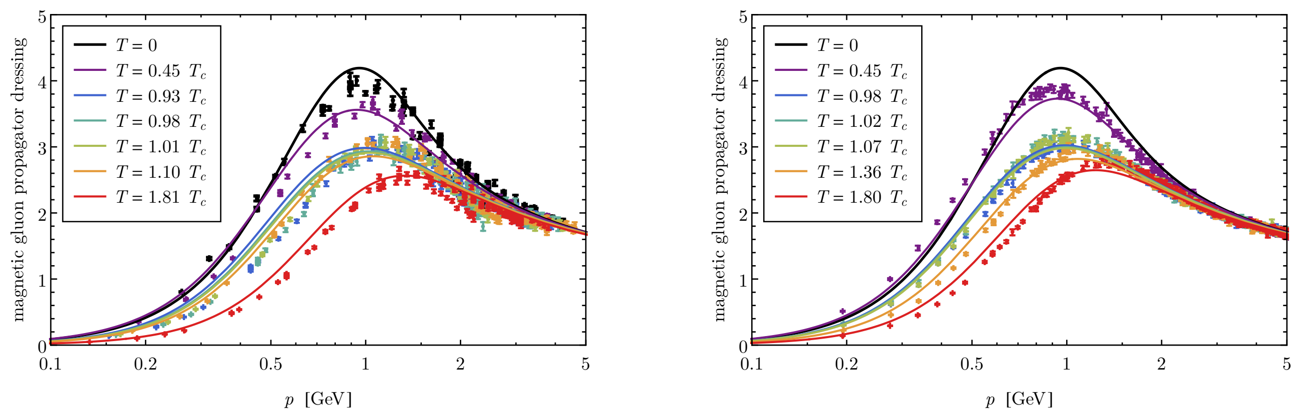

(a) Magnetic gluon dressing in $SU(2)$ from [29] in comparison with $SU(2)$ lattice results from [31, 32].

(b) Magnetic gluon dressing in $SU(2)$ from [29] in comparison with $SU(3)$ lattice results from [33].

FIG. 25: Magnetic gluon propagator dressing (VII.101).

given by

$$m_D^0 = \sqrt{\frac{N}{3}} g_T T + \mathcal{O}(g_T^2 T)\,, \tag{VII.103}$$

and is also displayed in Fig. 24. For the comparison, the temperature-dependent coupling is fully non-perturbative and has been also taken from [29] for internal consistency, for more details see there. In [30] higher order effects have been taken into account, leading to

$$m_D = m_D^0 + \left(c_D + \frac{N}{4\pi} \ln\left(\frac{m_D^0}{g_T^2 T}\right)\right) g_T^2 T + \mathcal{O}(g_T^3 T)\,. \tag{VII.104}$$

(VII.104) already leads to a very good agreement with the full result above 600 MeV. At low temperatures, the mass settles at its $T = 0$ value, indicated by the $1/T$ behaviour of m_d/T in Fig. 24b, and the perturbative prescriptions fail even with the full non-perturbative coupling. The Debye mass itself for low temperatures is depicted in Fig. 24a, from which it is evident that a temperature-independent (or decaying) additional part $\Delta m_D(T = 0) \approx 380$ MeV to m_D^0 would lead to agreement up to ≈ 150 MeV.

In conclusion a good semi-quantitative approximation to the thermal propagator (in particular the chromo-magnetic on) is the perturbative propagator with a temperature-dependent mass term. It goes beyond the scope of the present lecture notes to present a full computation, here we simply investigate the qualitative effect of such a mass gap, first done in [34], for a full, comprehensive analysis see [35]. We revisit (VII.92) for simple massive propagators

$$G_A \propto \frac{1}{(2\pi T)^2(n+\varphi)^2+\vec{p}^2+m_T^2}\,, \tag{VII.105}$$

even dropping the perturbative running. While the latter is important for the correct scaling (fixing $\Lambda_{\rm QCD}$ and hence for the correct T_c it is not important for the confining property. With the propagator (VII.105) we are led to

$$\begin{aligned} V_{\rm mode}(\varphi,m) &= \frac{T}{4\pi^2}\sum_{\pm}\sum_{n=1}^{\infty}\frac{1}{n}\,\left(e^{\pm 2\pi i\, n\varphi}-1\right)\int_0^\infty dp\, p^2\, e^{-\left(\beta\sqrt{p^2+m^2}\right)n} \\ &= \frac{T^4}{4\pi^2}\sum_{\pm}\sum_{n=1}^{\infty}\frac{1}{n}\,\left(e^{\pm 2\pi i\, n\varphi}-1\right)\int_0^\infty d\bar{p}\, \bar{p}^2\, e^{-\left(\sqrt{\bar{p}^2+\beta^2 m^2}\right)n}\,. \end{aligned} \tag{VII.106}$$

The momentum integration in (VII.107) cannot be performed analytically. However, in the zero temperature limit the terms in the sum decays with $e^{(-\beta m)n}$ up to polynomials. This is seen easily for the absolute value of the mode potential,

$$\begin{aligned} |V_{\rm mode}(\varphi,m)| &\leq \frac{T^4}{4\pi^2}\sum_{n=1}^{\infty}\frac{1}{n}\int_0^\infty d\bar{p}\,\bar{p}^2\, e^{-\left(\sqrt{\bar{p}^2+\beta^2m^2}\right)n} \\ &\leq \frac{T^4}{4\pi^2}\sum_{n=1}^{\infty}\frac{1}{n}\left[\int_0^{\beta m} d\bar{p}\,\bar{p}^2\; e^{-(\beta m)n}+\int_0^{\beta m} d\bar{p}\,\bar{p}^2\, e^{-\bar{p}n}\right] \\ &\stackrel{\beta m\to\infty}{\longrightarrow} T^4\,{\rm Pol}(\beta m)\, e^{-\beta m}\,, \end{aligned} \tag{VII.107}$$

with a polynomial ${\rm Pol}(\beta m)$. In summary the mode potential decays exponentially for gapped propagators. This entails that for sufficiently small temperatures the contributions of the chromo-electro and the two chromo-magnetic modes decay exponentially. The longitudinal gauge mode stays trivial and gives the contribution $2V_{\rm mode}(\varphi)$. Now we use that the ghost propagator keeps it $1/(-D^2)$ behaviour it already has perturbatively. In a covariant gauge this is already suggested from the ghost-gluon vertex which is linear in the anti-ghost momentum. Hence, all loop corrections to the inverse ghost propagator are proportional to p^2 from the onset. If no additional singularity is created from the propagators in the loops it stays this way. Since the gluon propagator is gapped this is only possible with a global non-trivial scaling.

Let us now study the case of a trivial ghost propagator and a gapped gluon propagator. In this case we conclude that

$$\begin{aligned} \lim_{T=0} V_{\rm Pol}(A_0) &\simeq \frac{1}{2}\lim_{T\to 0}{\rm Tr}\,\ln G_A^{-1}(A_0) - \lim_{T\to 0}{\rm Tr}\, G_c^{-1}(A_0) \\ &\simeq \frac{1}{2}{\rm Tr}\,\ln(-D_\rho^2)(A_0) - {\rm Tr}\,\ln(-D_\rho^2)(A_0) \end{aligned} \tag{VII.108}$$

$$= -\,{\rm Tr}\,\ln(-D_\rho^2)(A_0) = \sum_i V_{\rm mode}(\varphi_i)\,. \tag{VII.109}$$

With the mode potential (VII.89), see Fig. 23 this gives confinement. The present qualitative study can be extended to a fully non-perturbative one with the help of functional methods, leading to the $SU(2)$ and $SU(3)$ potentials depicted in Fig. 26 taken from [35]. The respective Polyakov loop expectation values $L[\langle A_0\rangle]$ are shown in Fig. 27.

The above considerations also hold in full Yang-Mills theory without approximations. This allows us to formulate a confinement criterion in Yang-Mills theory with (VII.83), (VII.94) and (VII.107):

Confinement criterion: *'In covariant gauges the gluon propagator has to be gapped relative to the ghost at low temperatures'*

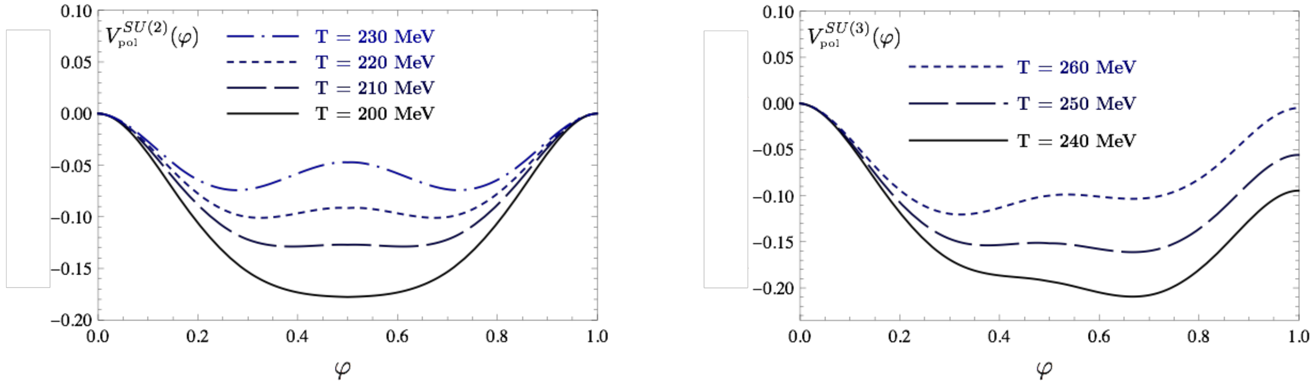

(a) $SU(2)$ Polyakov loop potential.

(b) $SU(3)$ Polyakov loop potential

FIG. 26: $SU(2)$ and $SU(3)$ Polyakov loop potential taken from [35] for different temperatures across the phase transition. The potentials exhibits the second and first order of the $SU(2)$ and $SU(3)$ transitions respectively.

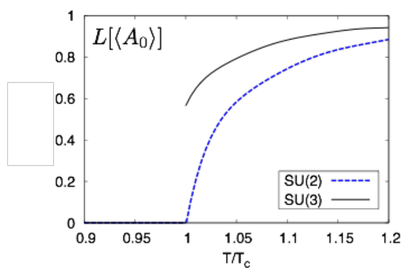

FIG. 27: Polyakov loop expectation values $L[\langle A_0\rangle]$ for $SU(2)$ and $SU(3)$ taken from [34].

put forward in [34]. Note that we have been led to this criterion in the one-loop resummed approximation with (VII.83). However, it can be proven in Yang-Mills theory without approximations on the basis of the functional renormalisation group, [34, 35], as well as Dyson-Schwinger equations and the two-particle irreducible (2PI) formalism [35]. It also extend beyond the covariant gauges, e.g. to the Coulomb gauge. In QCD with dynamical QCD -as expected- the quark contributions spoil the applicability of the confinement criterion as they introduce center-breaking terms to the potential, for a detailed discussion see [35].

We close this chapter with some remarks on the order parameter we introduced. We started with the Polyakov loop variable $\langle L[A_0]\rangle$, but computed the Polyakov loop potential $V_{\rm pol}[A_0]$ with the order parameter $\langle A_0\rangle$ or $L[\langle A_0\rangle]$. As both are order parameters for the same symmetry, this is not relevant for us. Still, one can investigate their relation: evidently they are not the same but only agree in a Gaußian approximation,

$$\langle L[A_0]\rangle \neq L[\langle A_0\rangle]\,, \tag{VII.110}$$

Dropping for the moment the necessary renormalisation of $\langle A_0\rangle$, they satisfy the Jensen inequality,

$$\langle L[A_0]\rangle \leq L[\langle A_0\rangle]\,, \tag{VII.111}$$

see [34]. We conclude that if $L[\langle A_0\rangle]=0$, so is $\langle L[A_0]\rangle$. In turn, one can show that $L[\langle A_0\rangle]$ vanishes if $\langle L[A_0]\rangle$ does, see [37]. While $L[\langle A_0\rangle]$ has so far only been computed with functional methods, we have a solid results for $\langle L[A_0]\rangle$ from the lattice, both in Yang-Mills theory and in QCD. More recently, $\langle L[A_0]\rangle$ has been also computed with the FRG on the basis of $L[\langle A_0\rangle]$ in quantitative agreement with the lattice results [36], see Fig. 29. Seemingly, their relation is rather non-trivial but is has been shown in [36] that most of the difference between $\langle L[A_0]\rangle$ and $L[\langle A_0\rangle$ comes from a temperature dependent normalisation of the former. In any case there is a relation

$$\langle L[A_0]\rangle(\varphi) \tag{VII.112}$$

that maps $\varphi = \beta g/(2\pi)\langle A_0\rangle$ to the Polyakov loop expectation value in a given background.

C. Phase structure of QCD

The preparations in Section VII A and Section VII B allow us to access the phase structure of QCD at finite temperature and density. We emphasise that, while we draw from QCD computation, the approach set up in these Chapters (and also the Chapters before) is based on an (intricate) low energy effective theory. This class of low energy EFTs is called *Polyakov loop augmented/enhanced low energy EFTs*. They are based on the following observation that can be made already on a one-loop level (with resummed propagators). The full one loop resummed effective action of $N_f = 2$ flavour QCD including effective mesonic degrees of freedom is given by

$$\Gamma_{\mathrm{QCD}}[\Phi] = S_{\mathrm{QCD}}[\Phi] + \frac{1}{2}\mathrm{Tr}\,\ln\, G_A^{-1}[\Phi] - \mathrm{Tr}\,\ln\, G_c^{-1}[\Phi] - \mathrm{Tr}\,\ln\, G_q^{-1}[\Phi] + \frac{1}{2}\mathrm{Tr}\,\ln\, G_\phi^{-1}[\Phi]\,, \qquad \Phi = (A_\mu, c, \bar c, \psi, \bar\psi, \sigma, \vec\pi)\,, \tag{VII.113}$$

with the gluon and ghost propagators G_A, G_c carrying the physics and fluctuations of the glue sector of QCD, and the quark and meson propagators carrying the physics and fluctuations of the matter sector of QCD. Note that (VII.113) with the full propagators is a complicated non-perturbative equation where all different loops feed into each other. For example, taking the derivative of (VII.113) w.r.t. the gauge field, we get

$$\frac{\delta\Gamma - S}{\delta A_0} = \frac{1}{2}\mathrm{Tr}\,\left[\Gamma^{(3)}\,G\right]_{AA} - \mathrm{Tr}\,G_c^{-1}[\Phi]\left[\Gamma^{(3)}\,G\right]_{c\bar c} - \mathrm{Tr}\,\left[\Gamma^{(3)}\,G\right]_{q\bar q} + \frac{1}{2}\mathrm{Tr}\,\left[\Gamma^{(3)}\,G\right]_{\phi^*\phi}\,, \tag{VII.114}$$

where the mesonic part has been dropped and G is the full matrix propagator of all modes. This has to be compared with the A_0-DSE

$$\frac{\delta\Gamma}{\delta A_0} = \left\langle \frac{\delta S}{\delta A_0}\right\rangle\,, \tag{VII.115}$$

the QCD-version of (III.14). It is derived analoguously from the path integral representation of the QCD effective action Γ, see (C.1), by taking an A_0-derivative. It is depicted in Fig. 30. The vertices in the DSE (VII.115) are the classical ones while in (VII.114) they are the full quantum vertices. The other difference is the two-loop term in Fig. 30 that is not present in (VII.114) but can be understood as part of the dressed vertices, see e.g. [35]. In any case, the two-loop term in the DSE is typically dropped in explicit computations for technical reasons, and modern applications often use 2PI and 3PI (three-particle irreducible) approximations that feature dressed vertices.

Note also that the Wegner-Houghton RG, or more generally functional renormalisation group equations for QCD, are one loop excact, see chapter III G 3. Hence, they are given by a sum of gluon, ghost, quark and optionally meson

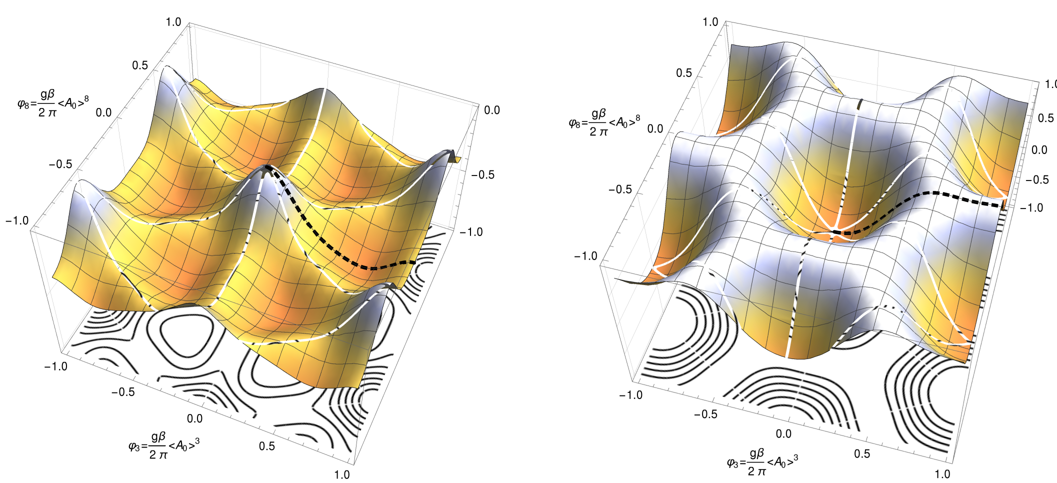

FIG. 28: The infrared glue potential, $V(\varphi_3, \varphi_8)$, is shown in the confined phase (left, $T = 236$ MeV) and in the deconfined phase (right, $T = 384$ MeV). We restrict ourselves to the line $\varphi_8 = 0$ and $\varphi_3 \geq 0$ (indicated by the black, dashed line), where one of the equivalent minima is always found, and where $L[\langle A0\rangle]$ is real and positive semi-definite.

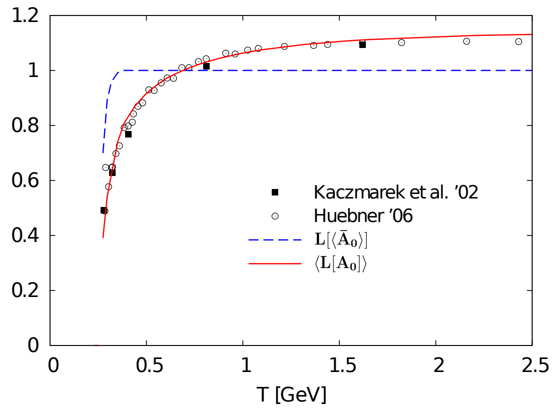

FIG. 29: Expectation value of $\langle L[A_0]\rangle$ versus $L[\langle \bar{A}_0\rangle]$ from [36]. Both observables are order parameters for the confinement-deconfinement phase transition. Moreover, $L[\langle \bar{A}_0\rangle] = 1$ entails $\langle \bar{A}_0\rangle = 0$.

diagrams, see Fig. 31. Note that the equation in Fig. 31 is exact, no two-loop or higher loop terms are missing.

1. *Glue Sector*

We conclude that (VII.113) provides a good qualitative approximation to full QCD, and the following formal arguments also go through beyond the current approximation: we are interested in the low energy limit of QCD, in which the gapped gluons do not drive the matter dynamics anymore. Since the ghost terms only couple to matter through the gluons, they also decouple even though they are massless. Hence, in a first qualitative approximation we can drop the dynamics of the glue sector. Still, the gluons, i.e. $\langle A_0\rangle$ serve as a background for the matter fluctuations. Its value is determined by the Polyakov loop potential in QCD, obtained by evaluating (VII.113) for constant A_0-background. The glue part of the potential,

$$V_{\rm glue}(A_0) = \frac{1}{2}{\rm Tr}\,\ln\,G_A^{-1}[A_0] - {\rm Tr}\,\ln\,G_c^{-1}[A_0]\,, \tag{VII.116}$$

The definition of $V_{\rm glue}$ is identical to that in pure Yang-Mills theory, (VII.83). In (VII.116), however, the QCD gluon and ghost propagator enter. A common procedure is now to use lattice results on the pressure and the Polyakov loop expectation value in pure Yang-Mills theory for an estimate of $V_{\rm glue}$. From the perspective of the correlation functions approaches discussed here this is justified if the Yang-Mills gluon and ghost propagators in an A_0-background are similar to those in QCD. This is indeed the case, the biggest difference coming from the RG-scaling that is reflected in the momentum-dependence at large and medium momenta $p^2 \gtrsim 2-5\,{\rm GeV}^2$. This can be made even more quantitative if simply comparing the two glue potentials (in terms of A_0) in QCD and Yang-Mills theory, see [38]. Apart from the different absolute temperature scale and the different RG-running the two potentials agree semi-quantitatively.

These results support in retrospect the low energy EFT approach with lattice-induced Polyakov loop potentials $V(L,\bar{L})$. On the lattice the Polyakov loop variables

$$L = \langle L[A_0]\rangle\,, \qquad\qquad \bar{L} = \langle L^*[A_0]\rangle\,, \tag{VII.117}$$

are computed. At vanishing density we have $\bar{L} = L^*$. At non-vanishing density this relation is not valid anymore as

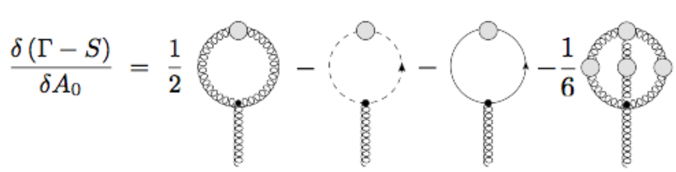

FIG. 30: Functional A_0-Dyson-Schwinger equation for QCD.

the chemical potential leads to a complex action in the path integral, and hence $\langle L[A_0]\rangle^* \neq \langle L[A_0]^*\rangle$. The respective potential is $U_{\rm pol}(L,\bar L)$. We emphasise that the potential $V_{\rm pol}(\varphi)$ is not simply $U(L(\varphi),\bar L(\varphi))$ due to (VII.110).

These potentials are derived as follows:

(1a) Compute the Yang-Mills pressure (zero-point function) and the Polyakov loop expectation value (one-point function)

$$p_{\rm A}(T) = \,, \qquad L = \langle L[A_0]\rangle(T), \qquad \bar L = \langle L[A_0]\rangle(T)\,. \tag{VII.118}$$

(1b) Further correlation functions of the Polyakov loop variable are computed. At present this approach only extends to the two-point functions of the Polyakov loop, [39]. The two-point function of the Polyakov loop is nothing but its propagator at large distances, which is given by the inverse of the second derivative of the Polyakov loop potential. We write schematically

$$\begin{pmatrix} \langle LL\rangle & \langle L\bar L\rangle \\ \langle \bar L L\rangle & \langle \bar L\bar L\rangle \end{pmatrix} \propto \begin{pmatrix} \partial_L^2 U_{\rm pol} & \partial_L\partial_{\bar L} U_{\rm pol} \\ \partial_{\bar L}\partial_L U_{\rm pol} & \partial_{\bar L}^2 U_{\rm pol} \end{pmatrix}^{-1}. \tag{VII.119}$$

(2) Construct a potential $V_{\rm YM}(L,\bar L)$ that leads to all the observables under (1a) and potentially (1b). We have

$$p_{\rm A} = -V(L_{\rm EoM},\bar L_{\rm EoM})\,, \qquad \left.\frac{\partial U(L,\bar L)}{\partial L}\right|_{\substack{L = L_{\rm EoM}\\ \bar L = \bar L_{\rm EoM}}} = 0\,, \qquad \left.\frac{\partial U(L,\bar L)}{\partial \bar L}\right|_{\substack{L = L_{\rm EoM}\\ \bar L = \bar L_{\rm EoM}}} = 0\,, \tag{VII.120}$$

and (VII.119), evaluated on the equations of motion.

Here we quote the standard form of the Polyakov loop potential. It reads

$$U(L,\bar L) = \frac{1}{2}a(T)\bar L\, L + b(T)\ln\, M_H(L,\bar L) + \frac{1}{2}c(T)\,(L^3+\bar L^3) + d(T)\bar(L\, L)^2\,, \tag{VII.121}$$

where M_H comes from the Haar measure of the gauge group

$$M_H = 1 - 6\,\bar L\, L + 4(L^3+\bar L^3) - 3(\bar L\, L)^2\,. \tag{VII.122}$$

Eq.(VII.121) is a variation of a Landau-Ginsburg-type phi^4-potential commonly used for describing phase transitions. The cubic terms proportional to $c(T)$ and in M_H carry the center symmetry $L\to zL$ where the cubic roots $z\in Z_3$ has the property $z^3=1$. Thse terms drives the phase transition. The parameters $a(T), b(T), c(T)$ are now adjusted to the temperature-dependent observables in (1). Examples can be found e.g. in [39–41]. The latter work also contains a detailed study of various model potentials. We close this discussion we a few remarks. Firstly, as it is not possible to compute the glue potential in QCD on the lattice, we have to rely on Yang-Mills potentials on the lattice extrapolated to the glue potential. Secondly, the direct computation of the Polyakov loop potential in Yang-Mills theory proves to be very costly and has not fully been resolved yet. For that reason one has to rely on potentials that only match a few but important observables. Thirdly, the Polyakov loop potential $U_{\rm pol}$ is not the natural input in the low energy EFTs, it is $V_{\rm pol}$ and the two only agree in the Gaußian approximations.

Alternatively one computes the glue potential directly in the continuum, but at present neither $U_{\rm pol}$ nor $V_{\rm pol}$ has been computed to a quantitative satisfactory precision. This task is left for future work.

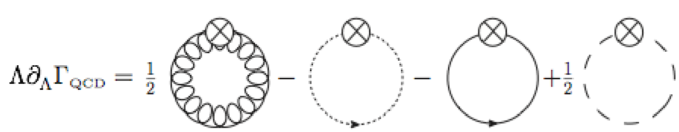

FIG. 31: Functional renormalisation group equation for QCD. In the Wegner-Houghton case the cross stands for the restriction of the loop integration to $p^2=\Lambda^2$.

2. Matter sector

It is left to discuss the matter sector. In (VII.113) it looks identical to the low energy EFT or the DSE/FRG in QCD we have discussed in the context of strong chiral symmetry breaking. However, now we have to consider also the glue background A_0 or $L, \bar L$ depending on the tratment of the glue sector. Since the mesons are color-neutral, they do not couple to the gluon and hence the meson loop stays the same as before.

However, the quark loop has to be taken in an A_0 background. We recall the one-loop expression in (VII.28), now in the presence of an A_0 background as well as a chemical potential μ. It reads

$$\begin{aligned}\Omega_{q,T}-\Omega_{q,T,\mu=0} &= -\,4\,T\sum_{n\in\mathbb{Z}}\int\frac{d^3p}{(2\pi)^3}\,\mathrm{tr}_{\mathrm{f}}\,\ln\frac{(2\pi T)^2\left(n+\frac12+\hat\varphi+i\,\mu\right)^2+\vec p^{\,2}+m_q^2}{(2\pi T)^2\left(n+\frac12\right)^2+\vec p^{\,2}+m_q^2}-p_{q,\mathrm{thermal}}\\ &= -\frac{2}{\pi^2}\,T\sum_{n\in\mathbb{Z}}\int_0^\infty dp\,p^2\,\mathrm{tr}_{\mathrm{f}}\left\{\ln\left(1+Pe^{-\beta(\epsilon_p^q-\mu)}\right)+\ln\left(1+P^\dagger e^{-\beta(\epsilon_p^q+\mu)}\right)\right\},\end{aligned} \tag{VII.123}$$

where $P(\vec x)=P(\beta,\vec x)$ is the untraced Polyakov loop, see (VII.44), and we recall the quark dispersion and the thermal distribution function from (VII.27)

$$\epsilon_p^q=\sqrt{\vec p^{\,2}+m_q^2}\,,\qquad\qquad n_F(\omega)=\frac{1}{e^{\beta\omega}+1}\,. \tag{VII.124}$$

In the present approximation $P, P^\dagger$ are $\vec x$-independent. The combinations $Pe^{\beta\mu}$ and $Pe^{-\beta\mu}$ reflect the relation of L and $\bar L$ to the creation operator of quark and anti-quark states respectively. The final expression in (VII.123) reduces to the quark contribution of the grand potential (VII.38) discussed in chapter VII A for $P=\mathbb{1}$. Due to the subtraction of the $T=0$ grand potential hidden in $p_{q,\mathrm{thermal}}$ is nothing but the negative thermal pressure in a given background. On the EoM for all fields it is the physical quark pressure of the system. The color trace in (VII.123) can be rewritten as a determinant with $\mathrm{tr}_{\mathrm{f}}\ln\mathcal{O}=\ln\det_{\mathrm{f}}\mathcal{O}$, and we are led to

$$\begin{aligned}\Omega_{q,T}-\Omega_{q,T,\mu=0} = -\frac{2}{\pi^2}T\int_0^\infty dp\,p^2&\left\{\ln\left[1+3(L+\bar L e^{-\beta(\epsilon_p^q-\mu)})\,e^{-\beta(\epsilon_p^q-\mu)}+e^{-3\beta(\epsilon_p^q-\mu)}\right]\right.\\ &\left.+\ln\left[1+3(\bar L+Le^{-\beta(\epsilon_p^q+\mu)})\,e^{-\beta(\epsilon_p^q+\mu)}+e^{-3\beta(\epsilon_p^q+\mu)}\right]\right\}.\end{aligned} \tag{VII.125}$$

For $L=\bar L=1$ and $\mu=0$ (VII.125) reduces to the one in (VII.38) in chapter VII A. This happens for large temperatures, $T/T_{\mathrm{conf}}\to\infty$ deep in the perturbative regime. Then we simply see the thermal distribution of single quarks. Note that (VII.125) only vanishes for $T\to0$ if $\epsilon_p>|\mu|$ for all p. For $\mu^2>m_q^2$ we have

$$\lim_{T\to0}\left(\Omega_{q,T}-\Omega_{q,T,\mu=0}\right)=-\frac{6}{\pi^2}\int_0^{\sqrt{\mu^2-m_q^2}}dp\,p^2\,\left(|\mu|-\epsilon_p^q\right)\,, \tag{VII.126}$$

reflecting the fact that for $\mu^2>m_q^2$ the level of the Fermi sea is rising accordingly and the part of the quark fluctuations below disappear from the fluctuation spectrum. As we have subtracted the grand potential at $T=0$ *and* $\mu=0$, this term is left in the $T\to0$ limit.

For $T/T_{\mathrm{conf}}\to0$ the Polyakov loop expectation value tends towards one, $L=\bar L=0$. Interestingly, for these values we have

$$\Omega_{q,T}-\Omega_{q,T,\mu=0}=-\frac{2}{\pi^2}T\int_0^\infty dp\,p^2\left\{\ln\left[1+e^{-3\beta(\epsilon_p^q-\mu)}\right]+\ln\left[1+e^{-3\beta(\epsilon_p^q+\mu)}\right]\right\}, \tag{VII.127}$$

the grand potential (or negative thermal pressure) of a gas of three-quark states, in our case the nucleons. This observation has been called *statistical confinement* as the confining value of the background Polyakov loop gives the thermal distribution of nucleons. If this property is investigated more carefully, the related distribution functions are given by

$$n_F(x,L,\bar L)=\frac{1+2\bar L\,e^{\beta x}+L\,e^{2\beta x}}{1+3\bar L\,e^{2\beta x}+3L\,e^{2\beta x}+e^{3\beta x}}\,,\qquad x=\sqrt{p^2+m_q^2}-\mu\,,\qquad \bar x=\sqrt{p^2+m_q^2}+\mu\,, \tag{VII.128}$$

for the quark and $n_F(\bar{x}, \bar{L}, L)$ for the anti-quark. As for the grand potential, the Polyakov-loop enhanced themral distribution functions tend towards the quark and anti-quark distribution functions for $L, \bar{L} \to 1$. For $L, \bar{L} \to 0$ (VII.128) gives the nucleon distribution function. However, this only happens if

$$\lim_{T/T_{\rm conf}\to 0} L\, e^{2\beta x} \to 0\,. \tag{VII.129}$$

It can be shown that the limit (VII.129) is not present in QCD, see [42]. This does not invalidate the above picture as the failure of (VII.129) orginates in mesonic contributions that indeed should be present. Moreover, the grand potential is that of nucleons.

This concludes our derivation of the low energy EFT that governs the phase structure of QCD. This specific type of low energy EFT has been constructed in [40]. On the one loop level its grand potential in $N_f = 2$ flavor QCD is given by the sum of the quark contribution (VII.125), the mesonic contribution and the Polyakov loop potential. This combination gives access to the two basic phenomena that governs the phase structure, confinement and chiral symmetry breaking.

3. *RG for the phase structure**

Here we simply repeat the steps for the derivation of the Wegner-Houghton equation done in chapter VII A 3 for finite temperature at finite temperature and density. The mesonic part is the same as in (VII.40) and we can just take it over here. The thermal quark part at finite density can be read off from (VII.127) while the vacuum part (at $\mu = 0$) of the integral is the same as before. In summary we get

$$\begin{aligned}\Lambda\partial_\Lambda\Omega_\Lambda(\psi,\bar\psi,\phi) = &-\frac{\Lambda^3}{2\pi^2}\Bigg\{\frac{1}{2}\left[\epsilon^\phi_\Lambda(m_\sigma)+\frac{3}{2}\epsilon^\phi_\Lambda(m_\pi)\right]-12\,\epsilon^q_\Lambda\\ &+T\left[\ln\left(1-e^{-\beta\epsilon^\phi_\Lambda(m_\sigma)}\right)+\ln\left(1-e^{-\beta\epsilon^\phi_\Lambda(m_\pi)}\right)\right]\\ &-4\,T\left\{\ln\left[1+3(L+\bar{L}e^{-\beta(\epsilon^q_\Lambda-\mu)})\,e^{-\beta(\epsilon^q_\Lambda-\mu)}+e^{-3\beta(\epsilon^q_\Lambda-\mu)}\right]\right.\\ &\left.\left.+\ln\left[1+3(\bar{L}+Le^{-\beta(\epsilon^q_\Lambda+\mu)})\,e^{-\beta(\epsilon^q_\Lambda+\mu)}+e^{-3\beta(\epsilon^q_\Lambda+\mu)}\right]\right\}\right.\,.\end{aligned} \tag{VII.130}$$

In (VII.130) the first line is the $T, \mu = 0$ part of the flow, the second line comprises the thermal part of the meson fluctuations, while the last two lines comprise the thermal and density fluctuations of the quarks. As has been discussed above, this term does not vanish in the limit $T \to 0$ but removes the infrared part of the vacuum fluctuations of the quark above the onset chemical potential $\mu^2 = m_q^2$, see (VII.126).

4. Results & discussion

Figure 32 contains the state of the art results from functional QCD for the phase structure of QCD. Further data are finite μ_B-extrapolations of lattice data at $\mu_B = 0$ and chemical freeze-out points obtained from experimental data with phenomenological freeze-out curves. While the functional QCD data have quantitative precision for $\mu_B/T \lesssim 4$, their systematic error increases successively for larger chemical potentials. This regime is the subject of current studies. For the sake of comparison we also show two different LEFT results in Figure 33.

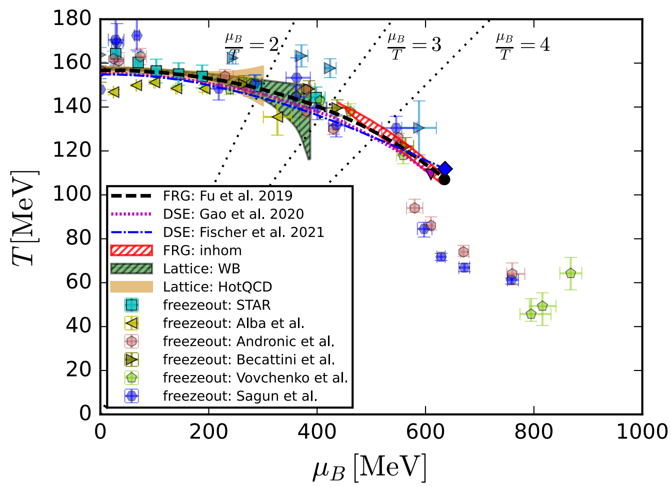

FIG. 32: Phase diagram in the plane of the temperature and the baryon chemical potential. The blue band denote the continuous crossover for the $N_f = 2$ and 2+1 flavor QCD, respectively; and the red star and circle is the CEP. The Functional QCD results refer to [43] (Fu et al. 2019), [44] Gao et al. 2020), and [45] (Fischer et al. 2021). The lattice results refer to [46] (WB), [47] (HotQCD).

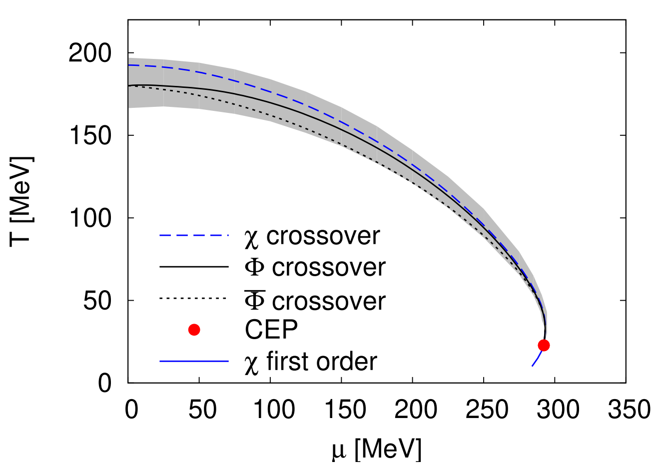

FIG. 33: Phase diagram from LEFTs [48] (two-flavour Polyakov-enhanced Quark-Meson Model, light constistuent quark mass $m_l = 298\,\mathrm{MeV}$. By now, improved LEFTs encode the same phase structure as full functional QCD, see e.g. [49]. This is achieved by augmenting them with correlation functions (scattering vertices) computed in full QCD (QCD-assisted LEFTs).

Appendix A: Feynman rules for QCD in the covariant gauge

In this Appendix we depict the Feynman rules for QCD in the general covariant gauge.

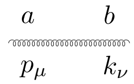

$$= \delta^{ab}\delta^{(4)}(p+k)\left(\delta_{\mu\nu} - (1-\xi)\frac{p_\mu p_\nu}{p^2}\right)\frac{1}{p^2}$$

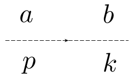

$$= -\delta^{ab}\delta^{(4)}(p+k)\frac{1}{p^2}$$

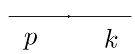

$$= \delta^{(4)}(p+k)\frac{1}{i\not{p}+m}$$

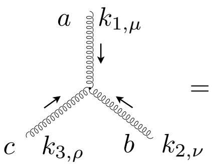

$$= i\,gf^{abc}(2\pi)^4\delta^{(4)}(k_1+k_2+k_3)\Big[(k_2-k_1)_\rho\,\delta_{\mu\nu} + (k_1-k_3)_\nu\,\delta_{\mu\rho} + (k_3-k_2)_\mu\,\delta_{\nu\rho}\Big]$$

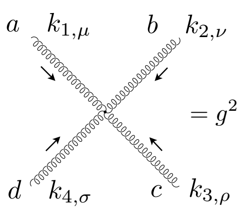

$$= g^2(2\pi)^4\delta^{(4)}\left(\sum_{i=1}^{4}k_i\right)\Big[f^{iab}f^{icd}\left(\delta_{\mu\rho}\delta_{\nu\sigma} - \delta_{\mu\sigma}\delta_{\nu\rho}\right) + f^{iac}f^{ibd}\left(\delta_{\mu\nu}\delta_{\rho\sigma} - \delta_{\mu\sigma}\delta_{\nu\rho}\right) + f^{iad}f^{ibc}\left(\delta_{\mu\nu}\delta_{\rho\sigma} - \delta_{\mu\rho}\delta_{\nu\sigma}\right)\Big]$$

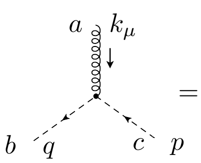

$$= -i\,gf^{abc}p_\mu(2\pi)^4\delta^{(4)}(p-q-k)$$

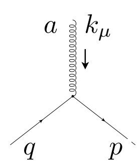

$$= -i\,g\gamma_\mu T^a\,(2\pi)^4\,\delta^{(4)}(p-q-k)$$

FIG. 34: Feynman rules.

Appendix B: Gribov copies

In Section I A we have derived the gauge-fixed path integral under the assumption that there is only one representative of the gauge orbit that satisfies the gauge fixing condition. However, there might be several (Gribov) copies, i.e. several physically equivalent solutions to the gauge fixing condition that are related by gauge transformations not yet fixed by the gauge fixing condition $\mathcal{F}=0$. Indeed, any sufficiently smooth gauge exhibits (infinite many) Gribov copies, $\sum_{\text{Gribov copies}} = \#_{\text{Gr}}$. As for the integration over the gauge group, $\#_{\text{Gr}}$ occurs in the numerator as well as the denominator in (I.18) and hence cancels. It is left to compute the Jacobian $J[A] = \Delta_{\mathcal{F}}[A]$. To that end we use the representation of the Dirac δ-function

$$\delta[\mathcal{F}[A^{\mathcal{U}}]] = \sum_{i=1}^{\#_{\rm Gr}} \frac{1}{|\det \frac{\delta \mathcal{F}}{\delta\omega}|}\delta[\omega-\omega_i] \quad \text{with} \quad \mathcal{U}=e^{i\omega}. \tag{B.1}$$

which leads to

$$\Delta_{\mathcal{F}}[A] = \left(\sum_{i=1}^{\#_{\rm Gr}} \frac{1}{|\det \mathcal{M}_{\mathcal{F}}[A^{e^{i\omega_i}}]\,|}\right)^{-1} \qquad \text{with} \qquad \mathcal{M}_{\mathcal{F}}[A] = \left.\frac{\delta \mathcal{F}}{\delta\omega}\right|_{\omega=0}[A^{e^{i\omega}}]\,. \tag{B.2}$$

In the QFTII lecture notes in chapter IV, Appendix A the occurance of the Gribov copies in gauge field reparameterisations due to gauge fixings is elucidated at the simple example of the reparameterisation of a two-dimensional intergal.

Appendix C: Some important fact of the background field approach

In the background field approach the effective action has the following integro-differential path integral representation which facilitates the access to important properties,

$$e^{-\Gamma[\bar A,a]} = \int D\hat a\, \Delta_{\mathcal{F}}[\bar A,\hat a+a]\,\delta[\bar D_\mu(\hat a_\mu+a)]\,e^{-S_{\rm YM}[A+\hat a]+\int_x \frac{\delta\Gamma[\bar A,a]}{\delta a_\mu}\hat a_\mu}\,, \qquad J=\frac{\delta\Gamma[\bar A,a]}{\delta a} \quad a=\langle\hat a\rangle\,. \tag{C.1}$$

where $\hat A = \bar A+\hat a$, $\bar D = D(\bar A)$, $D=D(A)$ and we restricted ourselves to *Landau-deWitt gauge* ($\xi=0$) with the background gauge fixing condition

$$\bar D_\mu \hat a_\mu = 0\,, \qquad \longrightarrow \qquad \mathcal{M}[\bar A,\hat a+a] = -\bar D_\mu D_\mu\,, \qquad \Delta_{\mathcal{F}}[\bar A,\hat a+a] = \det\mathcal{M}[\bar A,\hat a+a]\,. \tag{C.2}$$

see (VII.74). Inserting the relation between the a-derivative of Γ and the current J in (C.1) as well as using $\Gamma = \int_x J_\mu a_\mu - \log Z$ we arrive at the standard path integral expression for $Z[J]$ in the gauge (C.2). First we note that the effective action, evaluated on the equation of motion for the fluctuation field a,

$$\left.\frac{\delta\Gamma[\bar A,a]}{\delta a_\mu}\right|_{a=a_{\rm EoM}} = 0 \tag{C.3}$$

does not depend on the background field: the effective action $\Gamma[\bar A,a_{\rm EoM}]$ is given by (C.1) without the source term. Then the path integral in (C.1) reduces to

$$e^{-\Gamma[\bar A,a_{\rm EoM}]} = \int D\hat a_{\rm gf}\, e^{-S_{\rm YM}[A+\hat a_{\rm gf}]}\,. \tag{C.4}$$

Even though the measure depends on the background field via the gauge fixing, the intergration leads to $\bar A$-independent result as the action $S_{\rm YM}$ is gauge invariant. Accordingly we have

$$\frac{\delta\Gamma[\bar A,a_{\rm EoM}]}{\delta\bar A} = \left.\frac{\delta}{\delta\bar A}\right|_{a_{\rm EoM}}\Gamma[\bar A,a_{\rm EoM}] = 0\,. \tag{C.5}$$

The first relation in (C.5) follows with (C.3), the second from the $\bar A$-independence of the integration in (C.4). In conclusion, a solution to the EoM of a also is one of $\bar A$. Eq.(C.4) also entails that

$$\Gamma[\bar A,a_{\rm EoM}(\bar A)] = \Gamma[\bar A+a_{\rm EoM}(\bar A)]\,, \tag{C.6}$$

it only depends on the full gauge field A.

Appendix D: Wilson loop in QED

In this appendix we discuss the case of an electron-positron pair e^+e^-. Then the static potential is the standard Coulomb potential. Indeed in the static limit there is no self-interaction of the photon and the expectation value of the Wilson loop is simply given by the sum of boxes with n photon exchanges from positions x_i to y_i where one integrates over x_i and y_i on the contour $\mathcal{C}[L,T]$. This is depicted in Fig. 35.

In other words, we have

$$W[L,T] = e^{-\frac{e^2}{2}\int_{\mathcal{C}[L,T]} dx_\mu \int_{\mathcal{C}[L,T]} dy_\nu \langle A_\mu(x)A_\nu(y)\rangle_{\rm sub}}\,, \tag{D.1}$$

where we have used that $\langle A_{\mu_1}\cdots A_{\mu_{n+1}}\rangle = 0$. The subscript $\langle\cdots\rangle_{\rm sub}$ refers to the necessary subtraction of infinite selfenergies related to close loops with endpoints $x=y$. Moreover, all correlation functions decay in products of two-point functions (Wick-theorem), schematically we have $\langle A_1\cdots A_{2n}\rangle = \langle A_1A_2\rangle\cdots\langle A_{2n-1}A_{2n}\rangle+\cdots$, and there are $(2n-1)(2n-3)\cdots$ combinations. Upon contour integration all combinations give the same contribution and overall we have the nth order term in the propagator

$$\frac{(2n-1)(2n-3)\cdots}{(2n)!}2^n\left(-\frac{e^2}{2}\right)^n\left(\int_{\mathcal{C}} dx_\mu\int_{\mathcal{C}} dy_\nu\langle A_\mu(x)A_\nu(y)\rangle\right)^n = \frac{1}{n!}\left(-\frac{e^2}{2}\int_{\mathcal{C}} dx_\mu\int_{\mathcal{C}} dy_\nu\langle A_\mu(x)A_\nu(y)\rangle\right)^n\,, \tag{D.2}$$

for a general contour $\mathcal{C}$, leading to the Gaußian expression eq. (D.1). This leaves us with the task of computing

$$\begin{aligned}\int_{\mathcal{C}} dx_\mu\int_{\mathcal{C}} dy_\nu\langle A_\mu(x)A_\nu(y)\rangle &= \int_{\mathcal{C}} dx_\mu\int_{\mathcal{C}} dy_\nu\int\frac{d^4p}{(2\pi)^4}\frac{1}{p^2}\left(\delta_{\mu\nu}-(1-\xi)\frac{p_\mu p_\nu}{p^2}\right)e^{ip(x-y)}\\
&= \int_{\mathcal{C}} dx_\mu\int_{\mathcal{C}} dy_\mu\int\frac{d^4p}{(2\pi)^4}\frac{1}{p^2}e^{ip(x-y)}\\
&= \int_{\mathcal{C}} dx_\mu\int_{\mathcal{C}} dy_\mu\,\frac{1}{4\pi^2}\frac{1}{(x-y)^2}\,.\end{aligned} \tag{D.3}$$

To be explicit, we picked a covariant gauge in eq. (D.3). However, we have already proven that the *closed* Wilson line is gauge invariant which now is explicit as the ξ-dependent term drops out with the help of

$$\int_{\mathcal{C}} dx_\mu p_\mu e^{ipx} = -i\int_{\mathcal{C}} dx_\mu\partial^x_\mu e^{ipx} = 0\,, \tag{D.4}$$

which eliminates all longitudinal contributions for closed loops. Note that this is not valid for open Wilson lines. Finally we are interested in the large T-limit in (D.1), see also (VI.125), where we have

$$\begin{aligned}V_{e^+e^-}(L) = -\lim_{T\to\infty}\frac{1}{T}\log W[L,T] &= \lim_{T\to\infty}\frac{1}{T}\frac{e^2}{2}\lim_{T\to\infty}\int_{\mathcal{C}[L,T]} dx_\mu\int_{\mathcal{C}[L,T]} dy_\mu\left(\frac{1}{4\pi^2}\frac{1}{(x-y)^2}\right)_{\rm sub}\\
&= -\lim_{T\to\infty}\frac{1}{T}e^2\lim_{T\to\infty}\int_{t_0}^{t_1} dx_0\int_{t_0}^{t_1} dy_0\left(\frac{1}{4\pi^2}\frac{1}{(x_0-y_0)^2+L^2}\right)\\
&= -\lim_{T\to\infty}\frac{1}{T}\frac{e^2}{4\pi}\lim_{T\to\infty}\int_{t_0}^{t_1} dx_0\int_{t_0-x_0}^{t_1-x_0} dy_0\left(\frac{1}{\pi}\frac{1}{y_0^2+L^2}\right)\\
&= -\lim_{T\to\infty}\frac{1}{T}2\frac{e^2}{4\pi}\int_0^T dx_0\,\arctan\left(\frac{x_0}{L}\right)\\
&= -\frac{e^2}{4\pi}\frac{1}{L}\,.\end{aligned} \tag{D.5}$$

Equation (D.5) is the Coulomb potential as expected. This has to be compared with the lattice result in the strong coupling expansion that shows an area law.

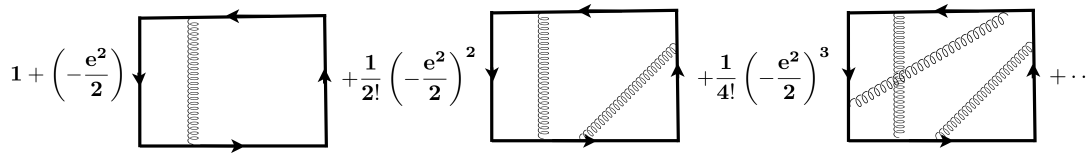

FIG. 35: Perturbative expansion of the Wilson loop expectation value for e^+e^-.

[1] W. Tung, *Group Theory in Physics* (World Scientific, 1985).
[2] L. Faddeev and V. Popov, Phys.Lett. **B25**, 29 (1967).
[3] S. Bethke, Progress in Particle and Nuclear Physics **58**, 351 (2007), arXiv:hep-ex/0606035.
[4] J. C. Collins, (1984).
[5] R. K. Ellis, W. J. Stirling, and B. R. Webber, Camb. Monogr. Part. Phys. Nucl. Phys. Cosmol. **8**, 1 (1996).
[6] R. Alkofer and L. von Smekal, Phys. Rept. **353**, 281 (2001), hep-ph/0007355.
[7] M. Buballa, Phys.Rept. **407**, 205 (2005), hep-ph/0402234.
[8] J. Braun, (2011), 1108.4449.
[9] A. K. Cyrol, M. Mitter, J. M. Pawlowski, and N. Strodthoff, (2017), 1706.06326.
[10] S. Klevansky, Rev.Mod.Phys. **64**, 649 (1992).
[11] F. J. Wegner and A. Houghton, Phys. Rev. **A8**, 401 (1973).
[12] K. Symanzik, Commun. Math. Phys. **18**, 227 (1970).
[13] C. G. Callan, Phys. Rev. D **2**, 1541 (1970).
[14] K. G. Wilson, Phys.Rev. **B4**, 3184 (1971).
[15] K. G. Wilson, Phys.Rev. **B4**, 3174 (1971).
[16] L. P. Kadanoff, Physics **2**, 263 (1966).
[17] E. C. G. Stueckelberg and A. Petermann, Helv. Phys. Acta **26**, 499 (1953).
[18] M. Gell-Mann and F. E. Low, Phys. Rev. **95**, 1300 (1954).
[19] Particle Data Group, C. Patrignani *et al.*, Chin. Phys. **C40**, 100001 (2016).
[20] J. R. Pelaez, Phys. Rept. **658**, 1 (2016), 1510.00653.
[21] O. Jahn and J. M. Pawlowski, Nucl.Phys. **B642**, 357 (2002), hep-lat/0205005.
[22] H. J. Rothe, *Lattice Gauge Theories : An Introduction (Fourth Edition)*volume 43 (World Scientific Publishing Company, 2012).
[23] C. Gattringer and C. B. Lang, *Quantum chromodynamics on the lattice* (Lect. Notes Phys., 2010).
[24] L. Fister and J. M. Pawlowski, Phys. Rev. **D92**, 076009 (2015), 1504.05166.
[25] A. Bazavov *et al.*, Phys. Rev. D **93**, 114502 (2016), 1603.06637.
[26] TUMQCD, A. Bazavov, N. Brambilla, P. Petreczky, A. Vairo, and J. H. Weber, Phys. Rev. D **98**, 054511 (2018), 1804.10600.
[27] D. J. Gross, R. D. Pisarski, and L. G. Yaffe, Rev.Mod.Phys. **53**, 43 (1981).
[28] N. Weiss, Phys.Rev. **D24**, 475 (1981).
[29] A. K. Cyrol, M. Mitter, J. M. Pawlowski, and N. Strodthoff, (2017), 1708.03482.
[30] P. B. Arnold and L. G. Yaffe, Phys. Rev. **D52**, 7208 (1995), hep-ph/9508280.
[31] A. Maas, J. M. Pawlowski, L. von Smekal, and D. Spielmann, Phys.Rev. **D85**, 034037 (2012), 1110.6340.
[32] A. Maas, private communication.
[33] P. J. Silva, O. Oliveira, P. Bicudo, and N. Cardoso, Phys. Rev. **D89**, 074503 (2014), 1310.5629.
[34] J. Braun, H. Gies, and J. M. Pawlowski, Phys.Lett. **B684**, 262 (2010), 0708.2413.
[35] L. Fister and J. M. Pawlowski, (2013), 1302.1373.
[36] T. K. Herbst, J. Luecker, and J. M. Pawlowski, (2015), 1510.03830.
[37] F. Marhauser and J. M. Pawlowski, (2008), 0812.1144.
[38] L. M. Haas, R. Stiele, J. Braun, J. M. Pawlowski, and J. Schaffner-Bielich, (2013), 1302.1993.
[39] P. M. Lo, B. Friman, O. Kaczmarek, K. Redlich, and C. Sasaki, Phys. Rev. **D88**, 074502 (2013), 1307.5958.
[40] B.-J. Schaefer, J. M. Pawlowski, and J. Wambach, Phys.Rev. **D76**, 074023 (2007), 0704.3234.
[41] B.-J. Schaefer, M. Wagner, and J. Wambach, Phys.Rev. **D81**, 074013 (2010), 0910.5628.
[42] W.-j. Fu and J. M. Pawlowski, Phys. Rev. **D92**, 116006 (2015), 1508.06504.
[43] W.-j. Fu, J. M. Pawlowski, and F. Rennecke, Phys. Rev. D **101**, 054032 (2020), 1909.02991.
[44] F. Gao and J. M. Pawlowski, Phys. Lett. B **820**, 136584 (2021), 2010.13705.
[45] P. J. Gunkel and C. S. Fischer, Phys. Rev. D **104**, 054022 (2021), 2106.08356.
[46] S. Borsanyi *et al.*, Phys. Rev. Lett. **125**, 052001 (2020), 2002.02821.
[47] HotQCD, A. Bazavov *et al.*, Phys. Lett. B **795**, 15 (2019), 1812.08235.
[48] T. K. Herbst, J. M. Pawlowski, and B.-J. Schaefer, Phys. Lett. B **696**, 58 (2011), 1008.0081.
[49] W.-j. Fu, X. Luo, J. M. Pawlowski, F. Rennecke, and S. Yin, (2023), 2308.15508.